NUI MAYNOOTH

Ollscoil na hÉireann Má Nuad

Pacemaking Neurons in the study of Parkinson's Disease

A dissertation submitted for the degree of
Doctor of Philosophy

by

Febe Francis

Under the supervision of
Prof. Richard H. Middleton
Dr. Míriam R. García (Co-supervisor)

Hamilton Institute
National University of Ireland Maynooth
Ollscoil na hÉireann, Má Nuad

October 2012

...

To the two wonderful people who joined me in the course of this journey,
Kripa and Dhruv
and
Our entire family for being our pillars of support.

...

In the loving memory of
Prof. George Thottappilly and Prof. Thomas M Varghese

...

Contents

List of Figures

List of Tables

Nomenclature

Molecules

ATP	adenosine triphosphate
Ca^{2+}	calcium ions
Calb	calbindin
CaCalb	calcium - calbindin complex
Cam	calmodulin
CaCam	calcium - calmodulin complex
cAMP	cyclic adenosine monophosphate
CaMK-II	calcium-calmodulin dependent protein kinase II
DHP	dihydropyridines
DNA	deoxyribonucleic acid
GABA	γ-aminobutyric acid
$InsP_3$	inositol trisphosphate
K^+	potassium ions
L-DOPA	levo-3,4-dihydroxyphenylalanine
NMDA	*N*-Methyl-D-aspartate
LRRK2	Leucine-rich repeat kinase 2
MPTP	1-methyl 4-phenyl 1,2,3,6-tetrahydropyridine
Na^+	sodium ions
PINK1	PTEN-induced kinase 1
PLC	phospholipase C
TEA	tetraethylammonium
TH	tyrosine hydroxylase
TTX	tetradotoxin

Terms

BMP	basal membrane potential
CICR	calcium induced calcium release
mtDNA	mitochondrial DNA
ER	endoplasmic reticulum
ERCA	endoplasmic reticulum calcium ATPase
ETC	electron transport chain
GHK	Goldman-Hodgkin-Katz current equation
HCN	hyper-polarization activated cyclic-nucleotide gated channel
HVA	high voltage activated channel
InsP_3R	InsP_3 receptor
LB	Lewy body
NaCax	plasma membrane sodium-calcium exchanger
NaCam	mitochondrial sodium-calcium exchanger
NaK	sodium-potassium
ODEs	ordinary differential equations
PD	Parkinson's disease
PMCA	plasma membrane calcium ATPase
PMP	peak membrane potential
PMU	the pacemaking unit
ROS	reactive oxygen species
RyR	ryanodine receptor
SNc	*substantia nigra pars compacta*
SNl	*substantia nigra pars lateralis*
SNr	*substantia nigra pars reticulata*
SOP	slow oscillatory potential
UPS	ubiquitin proteasome system
VTA	ventral tegmental area

Symbols

$A_{\mathbf{pmu}}$	Surface area of the pacemaking unit
$\mathcal{A}_{\mathbf{off}}$	Anionic offset
C_m	Membrane capacitance

C_{sp}	Specific membrane capacitance
$\mathcal{D}_s$	Diffusivity of species s
δ_x	Energy barrier position parameter for the process x
$\epsilon_{s,c}$	Permeability of the membrane for ion s through channel c
F	Faraday constant
$\mathcal{G}_{s,c}$	Channel conductance defined by the linear conductance relationship
$g_{s,c}$	Channel conductance defined by the electrodiffusion model
$\triangle G$	Free energy difference
I	Ionic current; $I_{s,x}$ is the current of ionic species s through the membrane protein x
J_s	Molar flux of species s
$J_{m,s}$	Molar flux of species s across membrane
k_{ij}	Rate of transition between states i and j
L	Membrane thickness
λ	Average cycle time
λ_m	Eigenvalue of the monodromy matrix
m_c, h_c	Fraction of activation and inactivation components of gating of channel c in the conductive state
$\mathcal{O}_c$	Open probability of channel c
$\mathcal{P}(X)$	Probability of the process considered to be in state X
ϕ_{cyt}	Volume fraction of cytosol
r	Universal gas constant
$\mathcal{S}_{\mathsf{pmu}}$	Surface to volume ratio of the pacemaking unit
s_c	Slope-factor in the Boltzmann-type equation for channel c
s_i	Intra-cellular concentration of ionic species s
s_e	Extra-cellular concentration of ionic species s
σ_λ	Standard deviation of λ
T	Physiological temperature in Kelvin
V	Transmembrane potential
$\mathcal{V}_\tau$	Voltage equivalent of temperature
$\hat{\mathcal{V}}_s$	Nernst potential of ionic species s
$V_{h,c}$	Half-activation voltage in the Boltzmann-type equation for channel c
$\mathcal{V}_{cyt}$	Cytosolic volume
z_s	Valency of ionic species s

Preface

Declaration

This thesis has not been previously submitted in whole or in part to this or any other University for any other degree and is the sole work of the author.

The thesis work was conducted from May 2008 to September 2012 under the supervision of Prof. Richard H Middleton in Hamilton Institute, National University of Ireland Maynooth. This work was supported by Science Foundation Ireland (SFI) grants 07/RPR/I1177 and 07/IN.1/I1838.

Febe Francis

Maynooth, Ireland

Abstract

Parkinson's disease is the second most common neurodegenerative disorder with a significant social cost. The disease that develops over years results in significant movement related problems for the affected. The pathogenesis however is partially understood.

Computational approaches are significant in the analysis of events that are multi-factorial. Parkinson's Disease results from a system failure that leads to severe degeneration in the *substantia nigra* , a locus in the mid-brain. Traditional approaches tend to focus on isolated sub-components of the pathogenic pathways. However, such an approach may be inadequate to describe the pathogenesis.

Substantia nigra neurons function on an expensive energy budget, due to a high level of arborisation and pacemaking activity. Spontaneous oscillations of these neurons are an important feature of motor control. Pacemaking involves the L-type calcium channel, and could impose long-term accumulation of calcium within its organelles. Modelling of this activity is an important part of developing an understanding of the pathogenic process. We develop a mathematical paradigm to describe this activity with a single compartment approach.

To develop the mathematical framework we initially identify the components that contribute to the process and investigate an appropriate mathematical representation for the respective components. In the next part, we bring together such representation to develop a model that can reproduce measured data. Global optimisation strategies are adopted to tune important parameters.

The model explicitly describes the dynamics of the transmembrane potential with changes in the levels of important cations. The model is verified for two major observations in literature regarding its response in the presence of channel blockers. The model is analysed for parameter bifurcation and stability of oscillations. Finally a framework is proposed to extend the model to include aspects of calcium homeostasis.

Acknowledgements

I owe gratitude to many more people than I mention here; the following is a very partial list of those who have been part and parcel of my life in the last four years.

First and foremost, I take the opportunity to thank my advisor, Prof. Richard H Middleton for everything he has done for me and for being the constant source of inspiration, information and support. The freedom and space that he provides in research is something that I greatly appreciate. Our research meetings would be something that I am going to miss for being one of the most interesting intellectual exercise laced with his sense of humour. Also, the care he gives have been evident in his support and understanding even in his absence. I am grateful for his influences.

I am eternally indebted to Dr. Míriam R. García for being the solid support that she was in these years. She has not only been very resourceful with many of my predicaments but has also remained a sister figure radiating optimism. I am grateful for her assistance, insights and encouragement.

I would like to thank Prof. Peter Wellstead for being a constant source of motivation. Equally encouraging has been the presence of Dr. Oliver Mason during my years in Hamilton. I am also indebted to the support from Prof. Douglas Leith and Prof. Robert Shorten during my time in Hamilton. I would fondly remember the interactions I had with Prof. Wilhelm Huisinga and Prof. Richard Abadi during their time in Hamilton.

As all students would agree, Hamilton would not have been such a great place to work without ample support from Rosemary Hunt, Kate Moriarty, Ruth Middleton and Yuriy Kuznetsov. They have been nice and cheerful with all of us and have made many of our official formalities a cakewalk.

I have had some of my best moments in the past few years in the Hamilton Institute thanks to a wonderful group of friends. Life would never have been the same without Vahid Samadi Bokharaie and his brand of humour. There are far too many names to remember from these four years but I would like to particularly name Buket Benek Gursoy, Fernando López-Caamal, Mark Readman,

Florian and Steffi Knorn, Arieh Schlote, Surya Shravan Kumar Sajja, Esteban Hernandez, Kfir Lavi, Mathieu Cloutier, Dimitris Kalamatianos, Tianji Li, Rade Stanojevich, Vijay Subramanian, Mark Verwoerd, Jane Breen, Magdalena Zebrowska, Yoann O'Donoghue and Ben-Fillippo Krippendorff.

A special mention to Dr. Venkataramana Badarla and his family for being a great support to me. There are numerous names that come to mind of people who have made my stay in Ireland a pleasant experience. A few among them that I would like to particularly name are Ricky Jacob, Fr. Koshy Vaidyan, Alex Abraham and family, Mathew Abraham and family, Honey George and family, Sanju John and Sminto Antony.

I would also like to thank my previous mentors whose advices have stood strong in my research. I would also like to thank my friends back in India for believing in me and would like to particularly name Karthik Mohan for the emotional support he gave and Dr. Ambili Mechoor for all those scientific discussions we had.

Finally, I am forever indebted to my family who have stood by me all throughout my life. I fondly remember the sacrifices that my parents have made for my benefit. I am also thankful to my in-laws for believing in me and facilitating an environment for my growth. My deepest appreciation for the efforts from Sobha during my final stage of writing. Words are not enough to express the role that Susan, my wife, played in my life these years. You have all instilled in me the confidence to pursue my goals and the desire to do something meaningful.

Part I

CHAPTER 1

Introduction

A story has no beginning or end; arbitrarily one chooses that moment of experience from which to look back or from which to look ahead.

Graham Greene (The End of the Affair)

For many of us who lead a 'normal' life, our perspective on diseases are mostly framed within the context of an infectious disease. However for people who are chronically debilitated with a condition like Parkinson's disease (PD), this framework is less useful in portraying their condition. The disease is more like a story which started randomly in their lives without any apparent cause.

Parkinson's disease involves progressive degeneration of neurons in the central nervous system. The diseased individuals are likely to have some or many of their movement-related (motor) activities restricted. PD as a clinical syndrome was first described by James Parkinson in his 1817 essay [Parkinson, 1817] and to date its etiology[1] remains elusive. Clinically, the disease is characterized by various motor and non-motor features that can have different influences on the person's normal functions. However, instances of resting tremors, rigidity, akinesia[2] (or bradykinesia[3]) and postural instability are considered fundamental in disease diagnosis. Additionally, flexed postures and motor freezing are also regarded as classic features of the disease.

[1] *Etiology* : The cause, set of causes, or manner of causation of a disease or condition
[2] *Akinesia* : Loss or impairment of the power of voluntary movement
[3] *Bradykinesia* : decreased bodily movement

It is difficult to assess the true prevalence of PD since it is often diagnosed at an advanced stage. Further, there is no consistent method to survey across the globe. Methods used range from medical records to door-to-door surveys. Incidentally, door-to-door surveys reveal a higher prevalence of the disease pointing to the fact that this condition often does not get recorded [Wirdefeldt et al., 2011].

Parkinson's disease is the second most common neurodegenerative condition after Alzheimer's disease and according to de Lau and Breteler [2006], an estimated 1% of the population in industrialised countries above the age of 60 are affected by PD. In the rest of the world it appears to be less prevalent. However, reasons suggested for such observed differences are varied, with population in Africa having shorter life spans and methods of survey not being standard. Some studies in different countries have suggested the prevalence of PD is comparable to that in industrialised countries contradicting some of the previous results showing low prevalence [Wirdefeldt et al., 2011]. This again questions the methodologies adopted in the different surveys.

The most prominent feature of PD that emerges from various surveys is that age of the patient is a major factor for the disease, with a mean age of onset around 60 years [Savica et al., 2012; Collier et al., 2011]. A small percent of the affected population (around 5%) can be classified as "early onset" cases. For such cases, symptoms appear between the age of 20 and 50 years. There have also been suggestions that males are more susceptible to PD than women. However, recent studies reveal a difference in risk factors associated with PD between men and women [Savica et al., 2012].

As with most brain diseases, the overall burden from PD is much more than that suggested by mortality figures alone. As a progressive chronic condition, the disabling effects persist over years affecting the lives and careers of the diseased. Disorders of the nervous system are considered amongst the highest contributors to global disease burden according to the estimates of the World Health Organisation[4] (WHO). The economic costs are correspondingly large,

[4]An index used by the WHO, to measure overall disease burden is the DALY (disability-adjusted life year), expressed as the number of years of healthy life lost due to ill-health, disability or early death. According to this survey, neurological disorders contributes to the global disease burden second only to psychological disorders and are prominent in high income coun-

not only with respect to the cost of treatment, but also as a loss of productivity of all who are concerned. The nature of the disease brings emotional concerns along with functional and financial difficulties, upsetting the lives and hence the productivity of patients, family and carers in various measures.

The extent of disability and deterioration varies among Parkinson's patients owing to the heterogeneous nature of disease progression. Some of the classical motor deficits tend to appear later in certain cases making an early diagnosis difficult. However, physicians to some extent use a number of rating scales to evaluate motor impairment and disability in PD. A few different rating scales exist in the clinical community. The Unified Parkinson's disease Rating scale (UPDRS) is among the most well received of them all due to its reliability [Goetz et al., 2007]. UPDRS based studies strongly suggest that the course of PD is non-linear and that the rate of deterioration is variable and more rapid in the early phase of the disease [Jankovic and Kapadia, 2001].

1.1 Context

Parkinson's disease has not been a major focus of medical research, however, it is becoming increasingly significant owing to the increased human life expectancy in general. Although less frequent than Alzheimer's disease and Dementia with Lewy body (LB); these neurodegenerative diseases have equally relevant social concerns. PD pathogenesis is a process that spans years and the most noticeable symptoms appear after a large number of neurons degenerate. For this reason, preventive measures are limited and the only option for patients are treatments for suppressing the disabling symptoms, rather than being remedial. For an effective therapy as well as for early preventive measures for susceptible individuals, it is thus necessary to have a deeper understanding of the pathogenic mechanism.

Infectious diseases are fairly easy to understand and analyse, with Koch's postulates guiding to establish a causal mechanism [Pelczar et al., 1993]. However, disorders like degenerative diseases are often difficult to comprehend and establishing their etiology is generally not a straightforward task. To some ex-

tries [Organization, 2004]

tent, genetic forms of the disease substantiate some of the molecular aspects of the pathology.

Experimental models have made major contributions to the understanding of some aspects of pathogenesis in PD. These models explore biochemical pathways important to the survival of neurons. The experiments are carried out in cell lines challenged with distress (chemical or genetic), to reproduce features of neurons that degenerate in the course of this disease [Blesa et al., 2012]. For example, animal studies in PD routinely use the neurotoxin 1-methyl 4-phenyl 1,2,3,6-tetrahydropyridine (MPTP) that can cause permanent symptoms of PD by destroying dopaminergic neurons in the *substantia nigra pars compacta (SNc)* of the mouse brain. The reductionist approach has unravelled different facets of pathogenesis, but the overall understanding remains incomplete. It seems difficult to develop a detailed mechanism of disease progression from animal models since these models do not naturally exhibit the disease. Also, the inherent multi-factorial nature of the disease limits such models as experiments most often focus on a specific aspect of the disease.

Development of cellular models is an effective method for investigating a complex pathological process. Sometimes referred to as the "system's approach", such models are established by means of identifying simple molecular events pronounced in the course of events and making connections between interacting components. By doing so, one has an overall view of the pathogenic process, and can identify distinct points of intervention with appropriate analysis of the flow and control that exist in the network.

1.2 Motivation

Being the second most prevalent neurodegenerative condition and with an increase in prevalence with age, PD becomes a significant burden to a society that has increasing life-spans. The disease, which is quite dynamic, develops in a very unmethodical way with varying time-scales and causative factors. Various mechanisms have been proposed for the degeneration of *SNc* neurons in PD, each with a different potential cause. These mechanisms proposed include factors such as mitochondrial dysfunction [Beal, 2006], misappropria-

tion of the protein α-synuclein [Goedert, 2001], dopamine toxicity [Lotharius and Brundin, 2002], genetic problems [Farrer, 2006], malfunction of protein homeostasis mechanisms [Matsuda and Tanaka, 2010], pathogens [Braak et al., 2003b], inflammatory responses [McGeer and McGeer, 2004], tau pathology [Wszolek et al., 2004], to environmental factors that impact the levels of reactive species [Przedborski and Ischiropoulos, 2005], ferric ions [Dexter et al., 2006] etc.

Although each of these postulated causes can contribute at various phases of the disease, their contribution to the pathogenesis is unclear. Some of the theories based on these postulates may be partial and and on their own, leave many missing links. In some instances the factors considered may not be really causative. For such cases we may need to make correlations of such factors to the disease perfectly clear. In any case, we need to have a fundamental idea about the disease progression.

Motor symptoms in PD become noticeable only after approximately 60% of a group of neurons are lost from the mid-brain [Bernheimer et al., 1973]. The selective degeneration of these neurons, the dopaminergic neurons of the *SNc*, corresponds to a 80% loss of dopamine in the striatum. The loss of these neurons results in the alteration of activity in the "basal ganglia" circuitry, leading to a reduced activity in the thalamus that facilitates the initiation of movement [Shulman et al., 2011]. Degeneration of these neurons comprise the principal pathology of PD. Pathological changes in these neurons are also thought to be involved in conditions of schizophrenia and depression [Swerdlow and Koob, 1987; Carlsson and Carlsson, 1990]. Animal models employed to study parkinsonism employ a method of killing these neurons using neurotoxins such as MPTP. The mechanism of *SNc* degradation is a primary focus of research into PD progression.

Dopamine release from *SNc* neurons is triggered by an intrinsic pacemaking activity that generates periodic spiking. The reliance of *SNc* neurons on the L-type calcium channel for this spontaneous activity is well documented. The engagement of these channels for the pacemaking activity is postulated to cause metabolic stress at various levels [Sulzer and Schmitz, 2007; Surmeier, 2007]. Theories that are developed to describe the degeneration of dopaminergic neu-

rons in PD now stress on a major role for calcium regulatory activities in the pathogenic process. One important discovery on this front is the preferential survival of *SNc* neurons that express the calcium binding protein "calbindin", at high levels [Yamada et al., 1990]. Also, decoupling the *SNc* neurons from the use of calcium channels for pacemaking has been suggested as a preventive measure for subjects prone to neurodegeneration [Ilijic et al., 2011]. A rise in cytosolic calcium concentration is a key activation signal in virtually all animal cells where it triggers a range of responses including neurotransmitter release, muscle contraction, cell growth and proliferation. *SNc* neurons function by an active interplay of calcium mobility in a high energy environment. However, this high energy demand results in lower tolerance of extra stresses. If energy demand rises due to factors involved in progressive neurodegeneration, *SNc* neurons become susceptible to damage in PD [Wellstead and Cloutier, 2011].

Environmental and genetic factors that predispose *SNc* neurons to degeneration have been associated with the activities of the mitochondria [Schapira et al., 1989; Ikebe et al., 1990, 1995; Bender et al., 2006; Beal, 2006; Henchcliffe and Beal, 2008]. Mitochondrial calcium uptake and release controls a large number of cellular events [Duchen et al., 2008]. The loss of mitochondrial calcium buffering has been attributed as a mechanism underlying cell damage and death [Kiselyov and Muallem, 2008]. Taken together, these observations indicate that there is an intricate arrangement of activities with respect to calcium handling and mitochondria. Since mitochondria are the powerhouse of the neuron, mitochondrial impairment has a critical influence on various neuronal functions by virtue of its energy metabolism. Also, many of the postulated causes of PD are metabolically linked to calcium homeostasis machinery and energy metabolism.

One of the primary aims of our research group is to facilitate the development of a framework that can relate miscellaneous cellular events pronounced in PD pathogenesis. The philosophy we adopt is that PD can be considered as an instance of "system failure". This assumption is supported by the lack of a unique identified cause as well as by the heterogeneity in time-scales for disease development. As discussed previously, traditional biological approaches are useful at a level of analysing events at the sub-cellular level. To understand the interactions between the various components at the cellular level, we require

a different approach that we would now refer to as the "system's approach". This approach involves the use of mathematical and engineering analysis principles developed for physical systems, in formulating methods to be applied for the analysis of living systems [Wellstead and Cloutier, 2012]. Along with the complexity of the problem, the difficulty to carry out *in vivo* experiments also support an approach that is non-invasive and rapid.

In the development of a systems biology design for understanding PD, we have a framework [Wellstead and Cloutier, 2011, 2012] based on an energetic viewpoint . By this design, the system is modularized into different components based on their energy properties. The design essentially compartmentalizes the whole system into units that may be individually analyzed. In this work, we are concerned with point of entry of Ca^{2+} in the system. The characteristics of *SNc* membrane enables these neurons to pacemake and as a result there is a constant flux of Ca^{2+} ions into the system. There exist various mechanisms that restricts the levels of Ca^{2+} within the neurons. However, it would be ideal to understand how this arrangement would fare under conditions of stress and what would be the price that these neurons pay for this arrangement.

1.3 Thesis Structure

The purpose of this dissertation is to develop a mathematical scheme to analyse the dynamics of membrane activities of *SNc* that give rise to the distinct electrophysiology in *SNc* neurons. The model developed should address the following aspects:

- Spontaneous oscillations stable against slow drift in intra-cellular ion concentrations.
- Role of calcium channel in pacemaking and energy stress.
- Demonstrate known responses to standard perturbations.
- Include features that would enable it to be used as a module in the larger energy systems framework for PD [Wellstead and Cloutier, 2012].

Pacemaking is an emergent phenomena mediated by the properties of the participating membrane proteins and also acts as the point of entry for neuronal calcium. Figure 1.1 gives a concise picture of components considered for the

membrane model. Prior to bringing together various component of the model

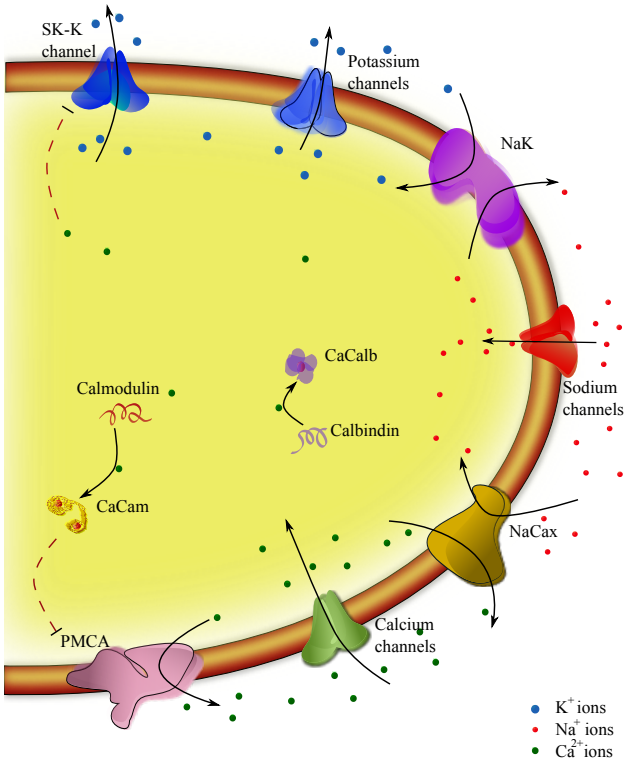

Figure 1.1: A cartoon representation of the scheme of events considered in the model

as a single model, it is necessary to under the mathematical interpretations of the component functions. The thesis is organised such that there is a logical progression of ideas that leads to the model.

This dissertation is outlined as follows: The next chapter reviews some of the key facets of PD detailed in literature. In addition, it examines the state-of-the-art with respect to electrophysiological models for neurons. In the third chapter we introduce the fundamentals of modelling ion-transport across biological membranes and discuss mathematical formulations of ion-channel activity. The fourth chapter compares various models of facilitated membrane transport. It also discusses some of the key mechanisms by which Ca^{2+} ions are handled inside a neuron. The fifth chapter brings together various concepts discussed in chapters two to four to develop a model for pacemaking in *SNc* neurons. The model is initially developed for a case of spherical geometry

and is later modified to a more realistic geometry. In each instance, the cost of active transport is calculated with respect to adenosine triphosphate (ATP) consumption. The model is later analysed for its dynamic properties. The final chapter discuss on various insights from the thesis and also proposes an extension to the model to incorporate various intracellular components relevant to Ca^{2+} handling within a neuron.

1.4 List of contributions

Given the need for a system to understand the complex pathophysiology in PD, mathematical models intended to describe the phenomena needs to elucidate them at a level greater than what can be achieved by current experiments. The results presented in this thesis are currently reported in peer-reviewed journals and attempt to bring together modeling *SNc* electrophysiology and modeling at the level of energetic requirements of these neurons.

Mathematical models of ion-channels have remained fundamental to neurophysiology, yet a model that is universally accepted has remained elusive. This has motivated us to study a model for voltage-gated ion channels and as preliminary step, we have developed a framework to describe the steady state conductance in chapter 3, section 3.3.3. This has been submitted to *Journal of Mathematical Biosciences* as,

> *Febe Francis, Míriam R. García, Oliver Mason and Richard H. Middleton, A Mathematical Model for Voltage Gated Ion-channel Stationary Conductance*

A model for pacemaking in *SNc* neuron was initially developed for a single compartment spherical geometry and is described in section 5.4. This work was published as a book chapter,

> *Febe Francis, Míriam R. García, and Richard H. Middleton. Energetics of ion transport in dopaminergic substantia nigra neurons. In P. Wellstead and M. Cloutier, editors, Systems Biology of Parkinson's Disease, pages 81-109. Springer New York, 2012*

The model is also submitted to the Physiome model repository,

A model for pacemaking in substantia nigra neurons (A simple model based on a spherical geometry), Francis et al. 2012, `http://models.cellml.org/e/c5/francis_garcia_middleton_2012_spherical.cellml/view`

The model is later refined for a more realistic geometry of the neuron and is discussed in section 5.5. The results of this section is reported in an article currently under review,

Febe Francis, Míriam R. García, and Richard H. Middleton. A single Compartment model of pacemaking in disassociated Substantia nigra neurons. Stability and energy analysis, ***Under review****, Journal of Computational Neuroscience, 2013*

CHAPTER 2

Prior Art

In this chapter we discuss observations in literature that testify the need for a system' approach in descring the pathogenic process in Parkinson's disease. We focus on the molecular pathways implied in the degeneration of substantia nigra neurons and their crosstalk with calcium homeostasis.

Parkinson's disease is not a rare disease. Even though it is the second most prevalent neurodegenerative disease in the European Union (EU) with an associated high social cost, the lack of public attention it receives is evident in the investments made towards research initiatives to understand and counter the condition. For example, a disease like cancer, which is less prevalent in the EU, receives many times the investment that is directed towards PD research [Wellstead and Cloutier, 2012]. One reason for this disinterest could be the general disregard for geriatric conditions in society. However, this perspective is gradually changing with longer lifespans achieved with modern healthcare systems.

The disability associated with the disease of the motor systems has been known since ancient times. One of the first report on this ailment is in the "*Charaka Samhita*" (Compendium of Charaka), an early encyclopaedia on *Ayurveda*, the Indian system of medicine. References to the symptom of the disease can also be found in the bible, some ancient Egyptian texts as well as in the writings of the Greek physician Galen who lived around the second century AD [García, 2004]. However, it was not until 1817 that a detailed medical description of the

disease was published [Parkinson, 1817]. The disease was later given the name of the author of this essay, James Parkinson, by the French neurologist Jean Martin Charcot who also made immense contributions to the understanding of PD. An account on the different milestones in the history of PD is provided in table 2.1.

PD is characterised by the loss of neurons and by the presence of LBs in different parts of the nervous system. Significant sites include the peripheral and enteric systems, olfactory bulb, hypothalamus, dorsal nucleus of the vagus, locus coeruleus and mid-brain dopaminergic neurons of the *substantia nigra*. Clinical analysis on post-mortem brain samples of PD patients indicates extensive damage of the mid-brain dopaminergic neurons (around 80 % cell loss) compared to other non-dopaminergic neurons (around 30-50 %) with most neuronal loss happening during the pre-clinical phase of the disease [Gonzalez-Hernandez et al., 2010]. Even among the different dopaminergic neurons of the mid-brain, *substantia nigra* shows higher vulnerability compared to other neurons in the same region. For instance, neurons of the ventral tegmental area (VTA) are relatively spared [Surmeier, 2007].

The selective degeneration of dopaminergic neurons of the *substantia nigra* is the hallmark of PD. The exceptionally high vulnerability of these neurons to degradation is consistent with both idiopathic[1] and genetic form of the disease [Sulzer, 2007]. To understand the mechanism of neuronal death in PD, it is essential to consider how these neurons function and how they interact with their environment.

Basic research to understand the pathophysiology in these neurons has yet to point out a single cause for this condition. There are many different factors and events thought to contribute to the pathogenesis. These include a range of factors within the following broad categories:

1. defects in common neuronal functions of metabolism and maintenance [McNaught et al., 2004; Henchcliffe and Beal, 2008; Abeliovich, 2010; Matsuda and Tanaka, 2010]
2. compounding extra neuronal factors such as inflammatory responses

[1] *Idiopathic* : A term used in medicine to indicate a disease or condition arising spontaneously or from an unknown cause

Year	Description	Reference
5000-3000 B.C.	Ayurveda literature records the condition including a herbal treatment that has contents of L-DOPA	Gourie-Devi et al. [1991]
1817	Clinical description of the shaking palsy by James Parkinson	Parkinson [1817]
1862	The disease formally named after Dr. Parkinson by the French neurologist Jean-Martin Charcot	Charcot and Vulpian [1862]
1906	Sherrington associates PD with disorders in the motor circuit	Sherrington [1966]
1912	Discovery of intra-neuronal inclusions	Lewy [1912]
1925	Foix and Nicolesco identify the loss of neurons in *substantia nigra pars compacta* critical to PD	Foix and Nicolesco [1925]
1953	Pathologic analysis of PD using brain stem lesions	Greenfield and Bosanquet [1953]
1958/59	Hypotheses on the role of dopamine loss in the pathogenesis of PD	Carlsson et al. [1958] Bertler and Rosengren [1959]
1961	L-DOPA therapy	Birkmayer and Hornykiewicz [1961]
1982	MPTP-induced Parkinsonism as a disease model	Drake [1983]
1987	Deep Brain Stimulation therapy	Benabid et al. [1987]
1989	Fibroblast graft therapy	Wolff et al. [1989]
1994	Gene therapy using viral vectors	Kaplitt et al. [1994]
1997	Association of α-synuclein andLBs	Polymeropoulos et al. [1997] Spillantini et al. [1997]
2002	Stem cell therapy in an animal model	Kim et al. [2002]
2003	Braak staging : a theory for the progression of PD.	Braak et al. [2003a]

Table 2.1: A brief history of Parkinson's disease indicating major milestones. A potential milestone in this timeline is the introduction of a Parkinson's vaccine. A candidate for the vaccine is already under clinical trial [Schneeberger et al., 2012]

[McGeer and McGeer, 2004; Beal, 2006; Whitton, 2009]

3. genetic factors [Polymeropoulos et al., 1997; Cookson, 2009; Hardy et al., 2006]
4. environmental factors [Priyadarshi et al., 2001]

As of now, Parkinsonian impairment is understood to be of heterogeneous origin, fostered by different pathogenic mechanisms, converging to a similar phenotype. This chapter will review the current understanding of various factors that contribute to the degeneration of *substantia nigra* neurons and hence to the progression of the disease.

2.1 Neurons of the *substantia nigra*

The *substantia nigra* is positioned in the *mesencephelon* (mid-brain) region of the brain and forms a part of the *Basal Ganglia* circuitry. The Basal Ganglia circuitry is important in functions such as coordination of movements, procedural learning and cognition. The neurons of the *substantia nigra* are dopaminergic, that is, they synthesise and release the neurotransmitter dopamine. Both synaptic and dendritic release of dopamine are reported for these neurons[2] [Bustos et al., 2004].

The mid-brain is also home to certain other groups of dopaminergic neurons like the neurons of the VTA and retrorubral area and many of these neurons remain intact until the final stages of PD. Although their distinction is not typically anatomical, the differences between these groups lie in their biophysical properties. For example, the dopaminergic neurons of these two regions show noticeable differences in the action potential waveform and duration [Klink et al., 2001] with respect to the dopaminergic *substantia nigra* neurons. While *substantia nigra* neurons exhibit strong activation with hyperpolarization and slow potential oscillations in the sub-threshold range, these are less pronounced for the neurons in the VTA. *Substantia nigra* neurons also show variations in the levels of some of the expressed proteins [Greene et al., 2005; Greene, 2006].

[2]Most neurons release neurotransmitters from their axons (synaptic release) and although unusual, select few neurons can release from their dendrites. Substantia nigra can release dopamine from axons and dendrites

Cyto-architecture of *substantia nigra* The *substantia nigra* is divided into three different parts [Di Giovanni et al., 2009] with the *substantia nigra pars compacta* (*SNc*) forming a horizontal sheet of densely packed neurons on the dorsal side. The neurons in this region are medium to large. The *substantia nigra pars reticulata* (*SNr*) is a division that is more diffuse and sparse with small and medium neurons, located between the *SNc* and cerebral peduncles. The *substantia nigra pars lateralis* (*SNl*) is a small cluster of neurons that extends along the lateral border of *SNc* and *SNr*. The neurons of *SNr* are medium in size. In this thesis we are concerned with the dopaminergic neurons of *SNc* that are the most affected in PD.

2.1.1 Phenotype and physiology

The *substantia nigra* forms the main regulatory nucleus of the basal ganglia network and mainly projects into the dorsal striatum. This nucleus was initially classified in to dorsal and ventral tier groups [Fallon and Moore, 1978; Fallon et al., 1978] with each group projecting to different areas of the striatum. According to Damier et al. [1999a], *substantia nigra* was classified according to the density of dopaminergic neurons. The dorsally located *SNc* contains dense clusters of dopaminergic cells (nigrosomes) and is surrounded by a nigral matrix that is a diffuse zone poor in dopaminergic neurons. The ventrally located

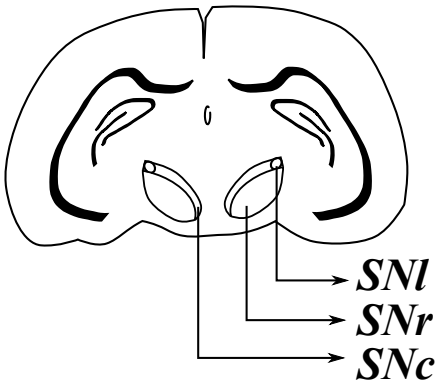

Figure 2.1: A sketch of brain cross-section showing different parts of *substantia nigra*

SNr neurons are mostly GABA-ergic[3] and forms one of the two primary output nuclei of the basal ganglia system projecting to the motor thalamus (see figure 2.2).

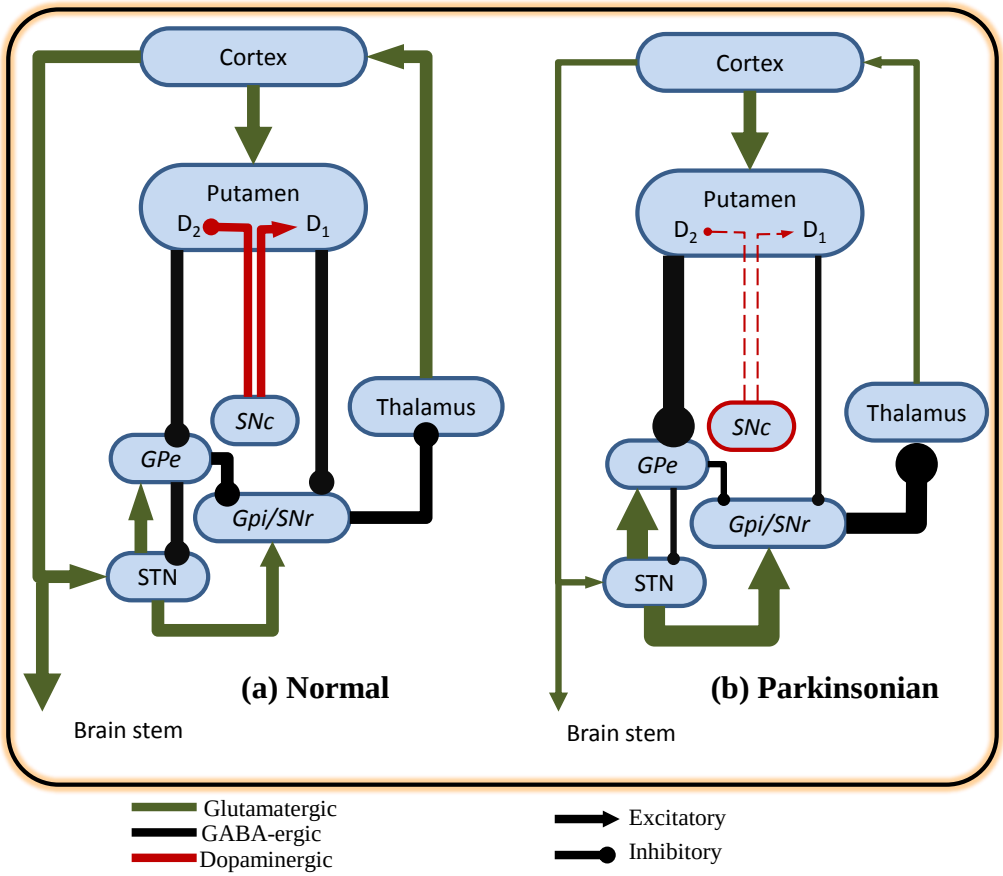

Figure 2.2: A connectivity diagram of the thalamocortical circuit that houses the basal ganglia circuitary. (Abbreviations: GPe: globus pallidus external; GPi: globus pallidus internal; STN: subthalamic nucleus; SNc: substantia nigra pars compacta; SNr: substantia nigra pars reticulata). With a reduction in the supply of dopamine from *SNc* of the Parkinsonian brain (broken red lines), there is a corresponding change in the strength of output from the different nuclei. Corresponding changes are reflected in the thickness of connecting lines of the circuit.

In this section we review some aspects of morphology and physiology of neurons of the *substantia nigra*. As cellular phenotype and physiology remains a function of expressed proteins, a dynamic environment can have tremendous influence on these characteristics. Ageing is one of the most prominent fac-

[3] *GABA* : γ-aminobutyric acid

tor affecting cellular physiology. Since PD is sometimes considered as a phenomenon of accelerated ageing, it is crucial to have an overview of associated changes in the disease phenotype.

Aspects of a regular healthy *substantia nigra* neuron

There are approximately 12,000 dopaminergic neurons in an adult rat's *SNc* [Nair-Roberts et al., 2008] with axons from a single neuron forming between 100,000 to 245,000 synapses[4] [Bolam and Pissadaki, 2012]. Morphological examination of rat *SNc* reveal neurons with 12-25 micron soma that are either fusiform or polygonal. The soma emits three to five major dendrites (see figure 5.2 a, b) that rapidly taper to approximately 1 μm [Tepper et al., 1987]. The dendrites that project dorsally are often shorter than the ones that project ventrally. The axon emerges from one of the major dendrites approximately 30 μm from the soma [Grace and Bunney, 1983b; Matsuda et al., 2009]. Visualization of *SNc* neurons using a combination of molecular techniques by Matsuda et al. [2009] revealed a highly arborised axon. The axon projects into the fore-brain providing massive unmyelinated innervations that supplies dopamine.

The activity of dopaminergic *substantia nigra* neurons is essential for voluntary movement control. An intrinsic pacemaker in these neurons generates spontaneous[5] activity, which triggers dopamine release. This low-frequency tonic[6] firing is the defining feature of *substantia nigra* electrophysiology and ensures a sustained background supply of dopamine to the brain areas these neurons are connected to. Even when isolated from the group, individual neurons exhibit this behaviour. Interestingly, the spiking is more regular in isolation implying that the spiking is modified by the cross-talk between different neurons in their

[4] Axons arborize or branch into numerous axon terminals and these axon terminals are connected to a neighbouring neuron by a structure called synapse, that permits the transmission of an electrical or chemical signal. Such an arrangement allows for the simultaneous transmission of messages to a large number of target neurons within a single region of the brain

[5] *Spontaneous oscillation* : Periodically varying state of a dynamic system in the absence of an external force, attained irrespective of initial conditions. Spontaneous oscillations only exist in non-linear dynamic systems and persist with finite amplitude.

[6] *Tonic activity* : Spiking of neurons at regular intervals that are sustained for long periods of time, to ensure a sufficient release of the neurotransmitter

natural environment. This notion is confirmed by the phenomenon of burst[7] firing, observed in response to an external stimulus. In brain-slice preparations, a molecule like *N*-Methyl-D-aspartate (NMDA) may be used to induce bursting. NMDA receptors are glutamate receptors at post-synaptic cites that opens an ion-channel when bound by an agonist. Bursting is observed *in vivo*, in response to reward-related stimuli, suggesting a role in reinforced learning and memory [Graybiel, 2005].

Diseased neurons

Even though the degeneration of dopaminergic *SNc* neurons remains the hallmark of PD, not all neurons in *SNc* show similar vulnerability to the disease. There is a specific pattern of progression of the disease starting from the ventrolateral and caudal regions spreading into the dorsomedial and rostral regions of *SNc* [Damier et al., 1999b; Braak et al., 2003a]. A quantitative analysis of cell loss based on calbindin and tyrosine hydroxylase immunostaining [Damier et al., 1999b] revealed a mean loss of 64% in dopaminergic neurons of the Parkinsonian brain with more loss in the caudal side compared to the rostral side. The average loss was maximum in *SNc* with the nigrosomes recording significant loss (95%) compared to the matrix (80%). Also, the extent of cell loss in *SNc* appeared to be closely related to disease duration. The pattern of cell loss so observed suggests a differential vulnerability of neurons in PD, also the spatio-temporal pattern suggests a definite progressive nature of the pathogenic process. Recent advances in imaging technology have been instrumental in both disease diagnosis, and understanding the changes in functional aspects of *SNc* neurons in PD [Brooks, 2010]. For example, PET[8] and SPECT[9] measurements show dopamine deficiency in both patients as well as subjects who are at risk of the disease.

A distinct feature of the pathogenic process that has appeared in a morphometric study of *SNc* is related to the volume of neurons of this area [Rudow et al., 2008]. In addition to the significant loss of pigmented neurons (28%), the surviv-

[7] *Bursting or phasic activity* : In this mode of firing, periods of rapid spiking are followed by silent periods.

[8] *PET* : Positron emission tomography

[9] *SPECT* : Single-photon emission computed tomography

ing neurons exhibited significant hypertrophy[10] in older controls compared to young controls. In the case of subjects with PD, the pigmented neurons rather exhibited atrophy[11] compared to all control groups. This observation suggested hypertrophy in *SNc* to be a compensatory mechanism whereby normal motor function is maintained despite the loss of neurons in normal ageing. However in PD, the loss of neurons is substantial and hypertrophy may not be sufficient to maintain normal motor activity. Such a condition would put the remaining cells of the *SNc* under immense stress prompting their degeneration.

One of the distinct features observable in neurons with PD, LBs are discussed in the following section.

2.1.2 Lewy Body

The typical histo-pathological hallmark of PD is the abnormal accumulation of insoluble fibrous material found in the neuronal soma. They are called Lewy bodies, after Friedrich Lewy who first described these entities in PD brains [Lewy, 1912; Galloway et al., 1992]. Although a characteristic feature of the disease, these intraneuronal intracytoplasmic inclusions are not pathognomonic[12]. LBs are formed by the aggregation of various proteins, with α-synuclein as a prominent component of the spherical core [Spillantini et al., 1997]. LBs are occasionally found together with thread-like Lewy neurites in the neuronal soma and neuroaxonal spheroids [Shults, 2006].

LBs as a pathological marker are generally observed in familial forms of PD that involve genes like α-synuclein [Polymeropoulos et al., 1997], LRRK2 [Zimprich et al., 2004] etc. Moreover, some PD animal models generated with the help of mitochondrial or ubiquitin proteasome system (UPS) inhibitors have demonstrated the development of LB-like inclusions [McNaught et al., 2004; Shults, 2006]. However, it must be noted that some reported cases of PD do not exhibit LBs [Takahashi et al., 1994] and this calls into question whether LBs are indeed causal or consequential in the pathogenic process. LBs have also been reported

[10] *Hypertrophy* : An increase in size of cells

[11] *Atrophy* : Wasting away or degeneration of cells

[12] *Pathognomonic* : Specifically characteristic or indicative of a particular disease or condition

Functional aspect	LB Components
Cellular structure related	α-synuclein, lipids, MAP-2, MAP-5, neurofilaments, Chromogranin, Sphingomyelin, Synaptic vesicle-specific protein, Synphilin-1, Synaptophysin, Tau-protein, tubulin,
Calcium binding related	*Cam kinase II*, Calbindin D_{28K}, $\alpha\beta-$ Crystallin
Cellular recycling related	Ubiquitin, Clusterin, heat-shock proteins, Torsin A, *Ubiquitin C-terminal hydroxylase*
Mitochondria related	Mitochondria, Cytochrome c, DJ-1, Dorfin, NEDD8, *SOD1, SOD2*
Signalling related	*cdk5*, Chondroitin sulfate, 14-3-3 protein, IκBα, NF-κB, *Tyrosine hydroxylase*

Table 2.2: Molecules and cellular components identified in Lewy bodies [Shults, 2006]

in a number of other neurological disorders such as LB dementia, Alzhimer's disease etc.. [Schmidt et al., 1996].

Microscopy with chemical or immunochemical staining techniques have been employed to understand the structure and composition of LBs [Shults, 2006]. They are typically 5 - 25 μm in diameter and appear to have a dense core of filamentous and granular material, surrounded by a fibrillar halo. They are a heterogeneous assembly of various cellular components with α-synuclein and ubiquitin being major components. Table 2.2 gives a list of different cellular components that constitute LBs, determined from different studies reviewed in Shults [2006].

Advances made in PD research using recent technological developments in molecular biology have also complimented the understanding of LBs. For example, stem cell technology has been employed in treating PD [Kim et al., 2002] and subsequent observations throw light into various facets of disease development. The routine was successful in developing grafts of functional dopaminergic neurons. Despite being healthy, these neurons showed a tendency to form LB. This suggests that it is the environment of the Parkinsonian brain that predisposes neurons for LB formation [Kordower et al., 2008; Li et al.,

2008].

Of particular interest with respect to the focus of this project is the association of calcium related pathways in the pathogenesis of PD. Since a few Ca^{2+}-binding proteins are detected on LBs by immunological studies (Table 2.2), we examine how some of these proteins may be associated with LBs.

Calbindin is one important calcium-binding protein whose presence in LBs is confirmed by immunoreactivity. Their presence in the LB core suggests an involvement in the early stages of LB formation. Calbindin is found to have a synergistic association with α-synuclein which would be discussed later and the association has a probable role in the pathology. Statistical studies also suggest *CALB1*, the gene associated with calbindin, to be a susceptibility gene for PD [Mizuta et al., 2008]. The susceptibility appears more to do with the expression levels of calbindin and its interaction with α-synuclein than any mutations in the gene.

One more relevant calcium-controlled protein observed in LBs are the Ca^{2+}-calmodulin dependent protein kinase II (CaM kinase II). CaM kinase II immunoreactivity was concentrated in the peripheral halos of LBs [Iwatsubo et al., 1991; Wakabayashi et al., 2007], suggesting a late role in the formation of LBs. Although their significance in LBs is still to be elucidated, they probably have a role in phoshorylating cytoskeletal proteins that accumulate into the LB, rendering them neutral.

2.2 Neurodegeneration

A facet common to neurodegenerative diseases is that there is a progressive loss of specific groups of neurons with disease progression. In most cases, symptoms appear to vary with the duration of the disease. During early stages of the disease, symptoms are difficult to diagnose and are often ignored or misinterpreted. Diagnosis usually occurs during the later stages of the disease, with the advent of noticeable symptoms, and by then earlier symptoms would have become inconclusive. This type of pathogenesis often leaves few clues to the underlying mechanisms.

The evolution of PD into a noticeable disease need not necessarily be a continuous process right from its inception. Being multi-factorial, PD is plausibly staged, requiring additional causative factors to come into effect for advancing to the next level. For instance, cases of incidental Lewy body disease (ILBD) are found in higher frequency among people older than 60 years compared to PD. Such cases of ILBD are in all probability pathologies that may not have advanced to the full clinical form of PD [Klos et al., 2006; Parkkinen et al., 2008; Savica et al., 2010]. A proper understanding of the pathogenesis would make way for an effective intervention of disease progression. This necessitates a framework to be developed that emphasises research that relates the different paths of the process.

A slow progressive loss of dopaminergic neurons is known to exist in neurologically normal population [Chu and Kordower, 2007]. However in PD, the damage is extensive and a substantial number of neurons are lost prior to detectable motor symptoms. For this reason, PD is sometimes seen as an accelerated ageing process [Thal et al., 2004; Chan et al., 2009; Cookson, 2009]. It was long assumed that the appearance of systemic failure in PD starts with degeneration of neurons in some brain regions including the mid-brain dopaminergic neurons. This view was ousted from common understanding when Braak brought forth his framework of staging the disease development

The development of PD into a clinical diagnosable condition is a process that spans years. It is the result of a damaging combination of various traits that pre-dispose an individual to PD. These traits, that vary to a great extent among individuals, start manifesting themselves in varying degrees during the *pre-physiological phase* of the pathogenic process. Over time they develop into marked physiological abnormalities giving rise to the *pre-clinical phase*. Such abnormalities may sometimes be rectified by life's adaptive mechanisms; sometimes persist unnoticed and in certain circumstances aggravate and join hands with other contributing traits to proceed into the *pre-motor phase* of the disease. The *pre-motor phase* is one of the longest in PD pathogenesis. As noted earlier, often, disease phenotypes that crop up during the pre-motor phase are ignored or go unnoticed. By the *pre-diagnostic phase* of the disease most of the associated motor symptoms are present, but not sufficient for a complete diagnosis. By the time motor symptoms are diagnosable PD is fully developed.

The Pre-motor phase of PD pathogenesis The pre-motor phase of PD is distinguished by the appearance of certain physiological anomalies that can be classified as 'non-motor' features of the disease. Clinically, the pre-motor phase is identified when LBs are observed in the autonomic nervous system [Probst et al., 2008; Braak and Del Tredici, 2008]. However, the presence of LBs need not be a prologue for PD pathogenesis, as the case is also observed as a part of normal ageing as well as in Incidental Lewy body disease, in which there is an absence of clinical Parkinsonism. In addition, some components of the peripheral nervous system (for example, *Stellate ganglia, Cardiac sympathetic neurons, Auerbach's plexus* and *Adrenal medulla*) exhibit LB formation during this pre-motor phase.

During this phase some symptoms do appear that are often disregarded as general autonomic dysfunction (Dysautonomia) often related to ageing. The symptoms may include problems with motility in the gastro-intestinal tract, urinary motility, erectile dysfunction and cardiac denervation. Among these, cardiac denervation is a significant symptom as around 40% of Parkinson patients are associated with the manifestation of this condition - orthostatic hypotension[13]. The denervation may be identified by MIBG (meta-iodobenzylguanidine) scans.

Olfactory deficits are an important symptom of PD that crops up during the pre-motor phase. However their low specificity, and being a common condition in general population, olfactory problems do not particularly raise any alarm for PD. Similar observations are also made with respect to other observed symptoms common to the pre-motor phase including anxiety, depression and sleep disorders.

Along with a definite pattern observed with respect to disease progression, observations show that there is a corresponding pattern with respect to neuronal loss in PD and this is discussed in the following section.

[13] *Orthostatic hypotension* : is a form of hypotension in which a person's blood pressure suddenly falls when standing up or stretching

2.2.1 Patterns of cell loss

Neurodegeneration in the *SNc* is heterogeneous with maximum damage in the ventro-lateral part. The dorsal regions of *SNc* is only partly damaged. The technique of calbindin D_{28K} immuno-staining has yielded an understanding of the regional specificity of neuronal damage in PD [Damier et al., 1999a,b]. The technique is based on the immunoreactivity of neurons against calbindin D_{28K}, that stains the calbindin rich neuropils and against tyrosine hydroxylase, that stains neurons producing dopamine. By this method, the *SNc* neuronal cluster is compartmentalised into a nigral matrix and nigrosomes (see 2.1.1). 60% of the neurons were distributed sparsely across the matrix that exhibited intense calbindin staining. The remaining neurons were densely packed into the nigrosomes embedded within the matrix. These five calbindin poor pockets are independent of the distribution of dopaminergic neurons. Maximum loss of dopaminergic neurons is observed in the nigrosomes (up to 98%) that are located in the caudal and mediolateral part of *SNc* [Damier et al., 1999b]. The loss appears to progress in the medial and rostral direction.

The seminal work of Braak and colleagues [Braak et al., 2003a] led to an understanding that PD begins as a synucleopathy outside the mid-brain in neurons that are non-dopaminergic. This work suggests that α-synuclein aggregation starts in the brain either in the brain-stem or the olfactory bulb and then spreads rostrally towards the mid-brain affecting the *substantia nigra* at a later stage of the disease. The disease, at a very late stage, progresses to other areas of the mid-brain, basal fore-brain, and finally reaches regions of the neocortex. The pathology is now understood to start much earlier with neuronal inclusion being visible in neurons of the enteric nervous system and progressing in a manner of anatomically interconnected regions [Braak and Del Tredici, 2008].

The theory of staging as proposed by Braak is still debated, based on various observations on post-mortem samples that lack correlations to the proposed concept [Burke et al., 2008]. However, there is a growing community that believes in a definite staging strategy that would help in early diagnosis of the condition [Probst et al., 2008].

2.3 Cellular Mechanisms leading to *SNc* neurodegeneration

Structural and functional aspects of *SNc* implied in PD pathogenesis The primary function of the *substantia nigra* neurons seems to be the constant supply of dopamine to the striatum. This supply of background dopamine is important for normal functioning of motor activities and its absence leads to the visible symptoms of PD. Moreover, restoration of this background level of dopamine often restores normal motor function.

To start with, we analyse possible reasons why these neurons are specifically affected in PD. From the structural perspective, neurons of the *substantia nigra* are one of the most arborised of all neurons [Matsuda et al., 2009]. The arborisation allows them to distribute dopamine over a wide area in the mid-brain. This arrangement apparently has an associated metabolic demand and the cellular machinery is therefore under constant metabolic strain. To compound this metabolic strain, the activity of these neurons is continuous, producing spikes at a frequency of 2-7 Hz.

There are other dopaminergic neurons in the mid-brain that are comparatively spared in PD [Damier et al., 1999b]. The observation that dopaminergic neurons of the VTA, that lies close to *SNc*, are comparatively spared in PD [Kish et al., 1988] has led to experiments investigating the molecular differences between these neurons. These neurons share similar physiological function, namely, dopamine production. However, they are functionally different, as they target separate regions of the brain. *SNc* neurons project to the striatum (nigrostriatal pathway) and VTA neurons project to cortex and forebrain. Experiments by Chan et al. [2007] differentiate the modus operandi of pacemaking in these two types of neurons. The spontaneous activity of *SNc* neurons is driven by Ca^{2+} currents originating in the somatodendritic L-type channels and to some extent by the Na^{+}currents from the hyper-polarization activated cyclic-nucleotide gated channel (HCN) channels; together with Ca^{2+} activated SK-K^{+}channels.

Chan's study also reviews developmental aspects of the pacemaking activity in mice. In newborn mice, the pacemaking is driven by Na^{+}ions in conjunction

with HCN channels. These channels are replaced by the L-type Ca^{2+} channel once the membrane potential becomes more negative with an increase in expression of Ca_v 1.3 α-subunit. Knock-out mice that do not express Ca_v 1.3 α continued pacemaking driven by the Na^+/HCN current all through their life. VTA neurons, on the other hand, exhibit pacemaking driven by the HCN channels.

The chemical agent used in Chan's experiment are a class of drugs given to patients with hypertension, called dihydropyridines (DHP). DHP function by binding to the Ca_v1.2 α-subunits of the cardiac calcium channels and reduce their activity. They are also found to be effective in suppressing L-type Ca^{2+} channels with the Ca_v1.3 α-subunit found in neurons of the mid-brain. This concept was successfully employed in Chan's experiment to halt pacemaking in mice *SNc*. Incidentally, they observed the return of pacemaking activity after a period of time, however the restoration of pacemaking was driven by Na^+/HCN currents.

It was also noted on an epidemiological basis that patients taking DHPs as a drug for hypertension had lower than usual incidence of PD [Becker et al., 2008; Ritz et al., 2010; Ilijic et al., 2011]. These observations led to an interpretation that high cytosolic Ca^{2+} levels contribute to PD pathology [Surmeier, 2007]. High levels of cytosolic calcium are known to induce oxidative stress and excitotoxicity in neurons, a plausible trigger for the pathogenic process. Moreover, the VTA neurons, and a few *SNc* neurons that are spared in PD and in animal models of PD using MPTP, are found to express higher levels of calbindin, a protein that buffers cytosolic Ca^{2+} [Sulzer and Schmitz, 2007]. However, there are studies that find no difference between the neurotoxic effect of MPTP in mid-brain dopaminergic neurons of a calbindin-deficient mice and their wild type variants [Airaksinen et al., 2006]. This result does not necessarily undermine the role of calcium in PD pathogenesis since this could also be explained as MPTP-toxicity in neurons having a distinct mechanism, with similar phenotype.

For a cellular system that is very active, oxidative stress is particularly common due to insufficient scavenging of reactive oxygen species (ROS) generated by an array of biochemical reactions. These species are habitually removed from

the cells by a system of anti-oxidants. However, the efficiency of this process depreciates with age [Mecocci et al., 2004]. In the case of nigral dopaminergic neurons, their involvement with dopamine and associated metabolites that are oxidative creates an additional burden in an environment that is increasingly oxidative [Lotharius and Brundin, 2002]. An increase in mtDNA oxidation is thought to decrease the efficiency of the electron transport chain (ETC) that provides the cell with energy. This can lead to a positive feedback loop with the inefficient ETC producing more ROS. Additionally, a corresponding reduction in energy production would prove detrimental to an already stressed *SNc* neuron.

The role of oxidative stress in the neuronal loss associated with PD is understood from the change in levels of molecular markers for oxidative stress. For instance, by products of lipid peroxidation, protein and DNA oxidation, and levels of iron, which are all used as markers for the presence of oxidation are found to be elevated in *substantia nigra* of the PD brain [Lotharius and Brundin, 2002]. Also, the neurotoxin 6-hydroxydopamine (6-OHDA) which is used to generate animal models of PD is understood to create conditions of oxidative stress and mimic early stages of the disease [Sauer and Oertel, 1994].

In addition to the energy and oxidative stresses, there are a number of factors playing important role in *SNc* neurons that are significant amongst the complex web of events leading to its pathological state. There are biomolecules found in the nigral cytosol that contribute to the stressful environment. There are elements in the nigral cellular machinery that impair the normal functioning of its mitochondrial system, protein handling machinery and also some features that become significant with age. Further, there are extra-neuronal factors like inflammatory pathways that contribute to this damaging process. These traits are discussed in the following sections.

2.3.1 Biomolecules from the nigral cytosol implicated in pathogenesis

α-synuclein

Neurodegenerative diseases are often characterised by the formation of protein aggregates in the neurons[14]. Neuritic plaques are rare in PD. However, formation of visible protein aggregates are mostly observed. The role of such aggregates in cognitive decline is as yet unclear, however the role of α-synuclein as the chief component of such aggregates [Spillantini et al., 1997] has fuelled studies of this protein.

α-synuclein is a soluble protein, characterised by a lipid-binding motif. These natively unfolded proteins are abundant in neural tissues, making up to 0.1 - 0.2 % of total proteins [Probst et al., 2008]. Although its function is yet to be identified, it is assumed to have a role in membrane associated processes. This assumption is motivated by its lipophilic nature and abundance in the neuropils, in close proximity to pre-synaptic terminals and synaptic vesicles. On the other hand, α-synuclein appears not to have an essential role in neurotransmission because α-synuclein knockout mice have not demonstrated any evident abnormalities [Cookson, 2009]. Recent studies suggest an activity dependent role for α-synuclein in the synaptic vesicle cycle, in the assembly and maintenance of SNARE complex[15] levels [Burre et al., 2010; Greten-Harrison et al., 2010].

Despite being known as a cytosolic protein, the presence of α-synuclein within neuronal nuclei [Yu et al., 2007] and mitochondria [Liu et al., 2009] in some brain regions adds to the mystery of its function. Interestingly, the name α-synuclein is based on observations that antibodies against the protein labelled both synapses and nuclei.

The association of α-synuclein with LBs, was first reported in the work of Polymeropoulos et al. [1997] based on clinical studies of an early onset familial form

[14]Protein aggregates are not always found within neurons, β-amyloid plaques in Alzheimer's Disease occur in the extra cellular space

[15]*SNARE* : derived from "SNAP (Soluble NSF Attachment Protein) Receptor". Relates to members of a large protein super-family that mediate vesicle fusion

of the disease. A point mutation in the α-synuclein gene was identified in reported cases, leading to an understanding of this protein's role in PD pathogenesis. In the same year, Spillantini et al. [1997] reported strong immunoreactivity of LBs for α-synuclein, confirming the link and bringing to focus a decisive role of α-synuclein aggregation in the disease development. α-synuclein was identified as the major protein component of LBs and Lewy neurites and further studies [Spillantini et al., 1997; Shults, 2006] confirm this notion.

Various molecular and genetic studies have brought out the different scenarios in which α-synuclein can become fatal. These include conditions of structural changes that may be caused by mutations in the α-synuclein gene [Polymeropoulos et al., 1997; Kim et al., 2000; Farrer, 2006], conditions of increased expression of the protein owing to extra copies of the gene [Zhou et al., 2000; Kirik et al., 2003] or by pathogenic transfer between neurons [Desplats et al., 2009]. A common mechanism among them, is the increased propensity of α-synuclein aggregation. If mutations contribute in creating more of the misfolded protein, higher expression levels of the protein pushes the cytosolic concentrations to a critical level that promote aggregation [Saha et al., 2008].

Ko et al. [2008] shows that α-synuclein aggregates are not particularly toxic. If not the product, the process itself may be responsible for the lethal turn of events. Dynamic light scattering experiments have been instrumental in revealing various stages of α-synuclein aggregation. α-synuclein is natively an unfolded monomer with long-range interactions. These soluble molecules can easily bind to membranes in an α-helical form, owing to their lipophilic nature. In the unfolded form, with the hydrophobic regions exposed, they tend to be aggregation-prone and form low-molecular weight oligomers that are structurally diverse. For example, a particular α-synuclein pentamer, forms an annular pore like structure and is known to interact with membranes to give a channel like structure.

α-synuclein lacks a stable structure and is thus natively unfolded [Uversky et al., 2001b]. This instability prompts it to adopt various partially folded conformations that are readily reversible. In addition, various chemical modifications of α-synuclein by oxidation, phosphorylation etc. and modifications because of mutation can lead to other conformational changes that are not

necessarily reversible. These partially folded molecules are unstable and can act as seeds for the nucleation process. Such molecules are routinely cleared by the activity of the UPS system.

The aggregation of α-synuclein is a complex process and modulated by various factors in the cellular environment. The formation of seeds or the nucleation phase is rate limiting and multi-factorial. We discuss in detail the influence of cytosolic calcium levels on the nucleation phase towards the end of this section. Figure 2.3 shows an approximate representation of the process of aggregation.

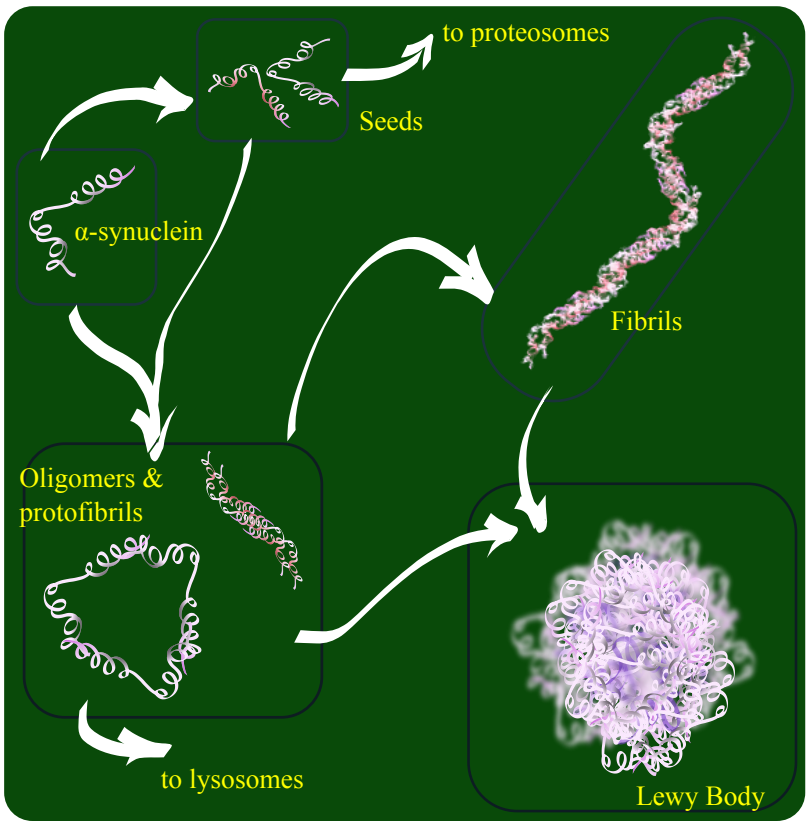

Figure 2.3: A cartoon representation of α-synuclein aggregation pathway: Fibril formation is initiated with the dimerization of partially folded monomers [Uversky et al., 2001a] followed by the formation of non-fibrillar oligomeric intermediates. Protofibrils are a set of β-sheet rich oligomers that are considered to be important in PD pathology [Lashuel et al., 2002; Volles and Lansbury, 2003]. Eventually, these β-sheet rich protofibrils gather to initiate fibrilization, and α-synuclein monomers are added to the assembly in an ordered manner. These insoluble fibrils pull in other fibrils, associated proteins and cellular structures to condense into a LB.

The tendency of α-synuclein to aggregate is often modified by various cellular processes. This is evinced by the presence of α-synuclein oligomers along

with membrane enriched fractions [Sharon et al., 2003; Welch and Yuan, 2003], suggesting an influence of the lipid environment which is frequently oxidized in PD. Such oligomers are also observed *in vitro* after conditions of oxidative stress [Ostrerova-Golts et al., 2000] or inflammations [Gao et al., 2008]. At the molecular level, this is seen as an enhanced tendency to aggregate following phosphorylation [Inglis et al., 2009], proteolytic truncation by enzymes like calpain [Dufty et al., 2007] or nitration by reactive nitrogen species that appear during an inflammatory response [Souza et al., 2000]. Formation of α-synuclein prefibrillar oligomers is presumed to be the primary affliction in a number of neurodegenerative pathways, although the exact nature of toxicity is yet to be understood [Souza et al., 2000; Welch and Yuan, 2003; Volles and Lansbury, 2003].

One factor influencing the steady state levels of α-synuclein in the cytosol is its relatively long half-life that tends to increase with age [Li et al., 2004]. The exact mechanism of α-synuclein degradation is yet to be elucidated despite the amount of research towards this end [Kim and Lee, 2008]. Proteolysis of α-synuclein seem to be a function carried out by both UPS machinery as well as lysosomes. Proteosomes appear to degrade monomeric units of the protein and as the oligomers need a larger system for their lysis, their lysis most likely falls to lysosomes. Vesicle mediated exocytosis is also understood to be one of the mechanisms employed by neurons to control levels of α-synuclein in the cytosol [Lee et al., 2005; Kim and Lee, 2008]. Even though exocytosis involves only a small fraction of the protein, the preferential aggregation of misfolded α-synuclein in vesicles [Lee et al., 2005] and the propensity for neuronal uptake of extracellular α-synuclein makes exocytosis a plausible mechanism for pathological progression of the disease among neurons [Desplats et al., 2009].

Calcium, calbindin and α-synuclein aggregation: The influence of Ca^{2+} levels on α-synuclein aggregation is a significant aspect of our study, as we are looking at some of the major influences of Ca^{2+} in PD pathogenesis. Interestingly, this aspect is not discussed much in the literature. However an *in vitro* study of the interaction between the Ca^{2+} binding protein calbindin and α-synuclein suggests an interaction that is noteworthy. The study by Zhou et al. [2010] involved fluorescent labelling of the two proteins, α-synuclein and

calbindin, to understand their interaction and co-aggregation. α-synuclein appeared to interact with calbindin in a Ca^{2+} dependent manner. Analysis of the experimental sample by electrophoresis supported the existence of an unstable complex of α-synuclein and calbindin and the formation of this complex appeared to hinder the fibrillation of α-synuclein. Addition of Ca^{2+} further strengthened the inhibition. However, the presence of Ca^{2+} in the absence of calbindin promoted fibrillation of α-synuclein. The experiment suggested that Ca^{2+}-bound calbindin functioned as a molecular chaperone that strongly inhibited the formation of α-synuclein fibrils. Also, calbindin was found to co-aggregate with α-synuclein, supporting observations of the presence of calbindin in Lewy Bodies.

Dopamine

Being dopaminergic, neurons of *substantia nigra* invariably handle dopamine metabolism. Dopamine is a neurotransmitter of the catecholamine family and is understood to be significant in reward-driven learning in the brain. It is synthesised from the amino acid 'tyrosine' in the cytosol by the action of enzymes tyrosine hydroxylase (TH) and 'DOPA decarboxylase' and is transported into the synaptic vesicles by means of a transporter protein. Dopamine remains in the vesicles until a neuron signal (action potential) forces the vesicles to merge with the cell membrane near to a synapse, thereby expelling the molecule into the synaptic space before it binds to a dopamine receptor.

Dopamine has been suspected to be causal in PD since the molecules generated by its catabolism are particularly oxidative and hence cytotoxic [Lotharius and Brundin, 2002].

An important feature of dopamine homeostasis is its regulation by intracellular Ca^{2+} [Mosharov et al., 2009]. The neurons of *SNc* seem to have higher cytosolic dopamine compared to VTA neurons because of the higher calcium influx during its pacemaking activity, mediated by the $Ca_v1.3$ channel. Intracellular Ca^{2+} appears to upregulate dopamine homeostasis through the enzyme 'aromatic L-amino acid decarboxylase' (AADC) and TH. Whether this upregulation raises the level of intracellular dopamine above critical toxic levels remains to be investigated.

Oxidative damage of *SNc* neurons by cytosolic dopamine is questionable. Regional variability in neuronal loss [Damier et al., 1999b], absence of pathological markers in certain disease phenotypes [Takahashi et al., 1994] and the fact that L-DOPA treatment do not advance the disease progression [Fahn, 2005] all suggest a minor role if any of dopamine as a source for oxidative damage. Mosharov et al. [2009] postulates that dopaminergic neurons are almost resistant to toxicity from cytosolic dopamine.

2.3.2 Mitochondrial Dysfunction

Mitochondria are an essential component of cellular functions with critical roles in ATP supply, calcium buffering and in the integration of cellular signals for apoptosis. As one of the most active sites of a cell, mitochondria often face assaults from within as well as outside. These assaults are mostly oxidative in nature and interferes with the proper functioning of mitochondrial proteins. Such events often result in toxic by-products which are usually kept in check. For example, inefficiency of mitochondrial protein can lead to further accumulation of oxidative species which are often controlled by the activity of the enzyme superoxide dismutase. However, continued assaults can accumulate such compounds leading to the malfunctioning of the organelle itself. Consequently it becomes important for the cell to have proper maintenance of the mitochondria and efficient disposal when they malfunction. Because of their key role in mediating cell death by apoptosis, mitochondrial well being is central to cell survival. In this section we review some aspects of the mitochondria important to nigral death in PD.

The involvement of mitochondrial dysfunction in Parkinson pathology became evident with the discovery that toxins such as MPTP and rotenone may be used to generate animal models of PD. These neurotoxins interfere with the activity of complex I of the ETC (NADH ubiquinone reductase) leading to reduced ATP levels, build up of free radicals and ultimately cell death. Post-mortem description of *SNc* neurons from PD patients confirms a decrease in complex I activity owing to oxidative damage [Schapira et al., 1989; Keeney et al., 2006; Chan et al., 2009]. Also, familial forms of the disease have been associated with proteins that are either mitochondrial or have a functional association with the

mitochondria. These include proteins like α-synuclein, parkin, DJ-1, PINK1 (PTEN-induced kinase 1), LRRK2 (Leucine-rich repeat kinase 2) [Thomas and Beal, 2007]. Further lines of evidence that suggest mitochondrial involvement in PD include increase in ROS in affected cells [Henchcliffe and Beal, 2008], variations with respect to mitochondrial fission and fusion [Yang et al., 2006; Poole et al., 2008], reduced mitochondrial membrane potential in animal models [Gandhi et al., 2009] as well as flaws with respect to mitochondrial trafficking [Weihofen et al., 2009]. Next we examine the relationships between mitochondria and the proteins implied in PD.

2.3.2.1 Protein - mitochondria interactions implicated in PD

With the identification of genetic mutations that can lead to loss of nigral dopaminergic neurons, a few different proteins have been found to have significant role in PD pathogenesis. We briefly describe some of the genes that have been associated with mitochondrial dysfunction in PD.

α-synuclein We have already discussed a major role that α-synuclein plays in *SNc* neurodegeneration (section 2.3.1). Experiments with a mice model harbouring human A53T α-synuclein mutant exhibited mitochondrial accumulation of the protein and thereon increased mtDNA damage and an increase in ETC complex IV activity was noted that led to mitochondrial dysfunction [Martin et al., 2006]. The effect seem to be complementary as use of neurotoxins that interfere with the ETC in rodents have resulted in α-synuclein aggregation (for example see Lee et al. [2002]). A few more effects of α-synuclein that creates a vicious interaction between α-synuclein, oxidative stress and mitochondrial dysfunction have been reviewed in Banerjee et al. [2009]. These observations suggest that both genetic and biochemical abnormalities with α-synuclein disturb the normal mitochondrial physiology.

Parkin The parkin gene (PARK2) is associated with an early onset juvenile form of PD [Kitada et al., 1998]. The parkin function as a component of the 'ubiquitin E3 ligase', a mediator of the polyubiquitination reaction that tags

aggregate prone proteins with ubiquitin, so that it is acted upon by the proteasome [Shimura et al., 2000]. The exact mechanism of how mutations in parkin lead to neuronal death is unclear, but it was presumed that their activity is critical in degrading one or more proteins that are toxic to these neurons.

PINK1 PTEN[16]-induced kinase 1 or PINK1 is a nuclear gene transcribing a mitochondrial serine/threonine-protein kinase. Mutations in this gene are found to cause an autosomal recessive form of PD which is rare, with nigral neuronal loss and LBs [Gandhi et al., 2006; Shulman et al., 2011]. In experiments these proteins are observed to be localised close to the mitochondria with its kinase domain facing the inter-membrane space. Loss of PINK1 function by mutation usually results in morphological defects in the mitochondria.

PINK1 also has a role in regulation of mitochondrial calcium efflux via the Na^{+}/Ca^{2+} exchanger [Gandhi et al., 2009]. Loss of PINK1 function limits calcium homeostasis resulting in a mitochondrial calcium overload. This in turn promotes higher ROS production and subsequent impairment of mitochondrial respiration.

PINK1, Parkin and Mitochondrial quality control The host of mitochondria present within a cell are known to undergo regular cycles of fusion and fission, the dynamics of which maintains a functional integrity among them. This process not only equilibrates the intra-mitochondrial contents, but also regularize the overall efficiency between them. Additionally, as mitochondria cannot be made *de novo*, the fission reaction is essential for mitochondrial biogenesis.

Lysosomes house the mitochondrial degradation process and any problems in lysosomal proteolytic pathways can lead to the accumulation of mitochondrial proteins. This process, often referred to as mitophagy is an important step that ensures the quality of mitochondria present in a cell. This is an important maintenance process of energy metabolism and thus, associated problems can add to the energy stress in a neuron like *substantia nigra*.

As neurons require efficient transfer of energy over longer distances compared

[16] *PTEN* : 'Phosphatase and tensin homolog' is a tumour suppressor gene

to other cells, mitochondrial dynamics become particularly relevant. This machinery is critically involved in the formation of synapses and dendritic spines. For instance, inhibition of fission proteins or over-expression of fusion proteins is known to reduce synapse formation [Arduíno et al., 2011].

PINK1 and Parkin are understood to cooperate in a common pathway involved in mitochondrial trafficking to the perinuclear region[17] [Vives-Bauza et al., 2010]. The accumulation of PINK1 in the mitochondria is understood to be a necessary step before Parkin is recruited onto the mitochondria and a selective accumulation of PINK1 on dysfunctional mitochondria is observed. This mechanism for *substantia nigra* neurons is relevant since both PD brains and animal models of PD exhibit mitochondria that are swollen with disrupted cristae and broken outer membrane [Arduíno et al., 2011].

DJ-1 DJ-1 or PARK7 is a protein reflected in early onset PD. It is a peptidase that works as a sensor for oxidative stress [Bonifati et al., 2003]. DJ-1 is considered to be neuroprotective as it tends to reduce the accumulation of hydrogen peroxide thereby reducing the damage resulting from ROS production [Chan et al., 2009]. In an experiment with DJ-1 knockout mice, it was proven that DJ-1 can be neuroprotective for *SNc* neurons by providing oxidation protection in a calcium stressed environment [Guzman et al., 2010]. Additionally, depending on its oxidation state DJ-1 functions as a molecular chaperone of α-synuclein that restricts the formation of aggregates [Zhou et al., 2006].

2.3.2.2 Implications of calcium homeostasis in mitochondrial dysfunction

Calcium is a global effector of mitochondrial function. Hence changes in cytosolic or mitochondrial calcium homeostasis are reflected in cell functions involving mitochondria, in particular ATP synthesis.

It has been well established that mitochondria have a huge capacity to accumulate calcium. Mitochondrial calcium uptake and release control how Ca^{2+} is handled within the cell. This includes the transport of Ca^{2+} across the cell membranes, management of Ca^{2+} concentration in cytoplasmic micro-domains,

[17] *Perinuclear region* : A sub-cellular area associated with autophagy-lysosomal degradation

frequency of oscillatory Ca^{2+} signals, rate of propagation of a Ca^{2+} signal across larger cells and the spatial distribution of a Ca^{2+} signal through the volume of a cell [Duchen et al., 2008]. This in turn influences events responsible for mitochondrial ATP synthesis via Kreb's cycle [Nelson and Cox, 2004]. Duchen et al. [2008] also discusses the proximity of mitochondria to cellular Ca^{2+} hotspots (In neurons mitochondria are clustered in active calcium signalling zones along axons and dendrites).

An extreme accumulation of Ca^{2+} within the mitochondria brings about the opening of a large channel in the inner mitochondrial membrane, called the permeability transition pore. Opening of the pore renders mitochondria incapable of ATP production and leads to severe damage of its ultra-structure.

Altered calcium homeostasis has also been associated with lysosomal storage diseases and bipolar disorder [Kiselyov and Muallem, 2008]. A search for a common mechanism underlying cell death in these conditions suggest a loss of mitochondrial Ca^{2+} buffering although the exact mechanism is yet to be experimentally validated.

Mitochondrial dysfunction and calpain activation Observations on enhanced levels of calpains in the *SNc* and *Locus coeruleus* of PD patients have revealed the involvement of these proteins in the pathogenic process. Calpains are family of calcium-dependent, non-lysosomal cysteine protease with a regulatory role in cellular activities. They have a significant part in apoptotic and necrotic pathways. Calpain inhibition seems to improve survival rates of *SNc* in animal models of PD [Esteves et al., 2010]. α-synuclein appears to be an important substrate of calpain. Esteves et al. [2010] demonstrates that calpains are capable of increasing the toxic soluble α-synuclein oligomers and their inhibition enhances the non-toxic insoluble α-synuclein fibrils, preventing caspase-3 activation.

2.3.2.3 Implications of oxidative stress in mitochondrial dysfunction

Reactive oxygen species (ROS) are routinely generated during mitochondrial metabolism and participate in cellular signalling and homeostasis. Cellular an-

tioxidant system guards against ROS toxicity, but some oxidative molecules escape and cause damage to cellular biomolecules like lipids, protein and nucleic acids. Such events tend to increase with increasing environmental stresses, as well as with inefficiencies in the ETC. Again, there exists a positive feedback loop between ROS generation and ETC inefficiencies (figure 2.4). ROS being a promoter of somatic DNA mutations can enhance ETC inefficiencies by the sheer proximity of its generation sites to mitochondrial DNA (mtDNA). Note that mtDNA encodes for around 13 proteins involved in mitochondrial respiration [Schapira, 2008].

Age seems to be the most important factor implied in oxidative damage of mtDNA. For instance, it is estimated that oxidative damage to mtDNA with age increases 15-fold compared to nuclear DNA damage increase with age [Mecocci et al., 2004].

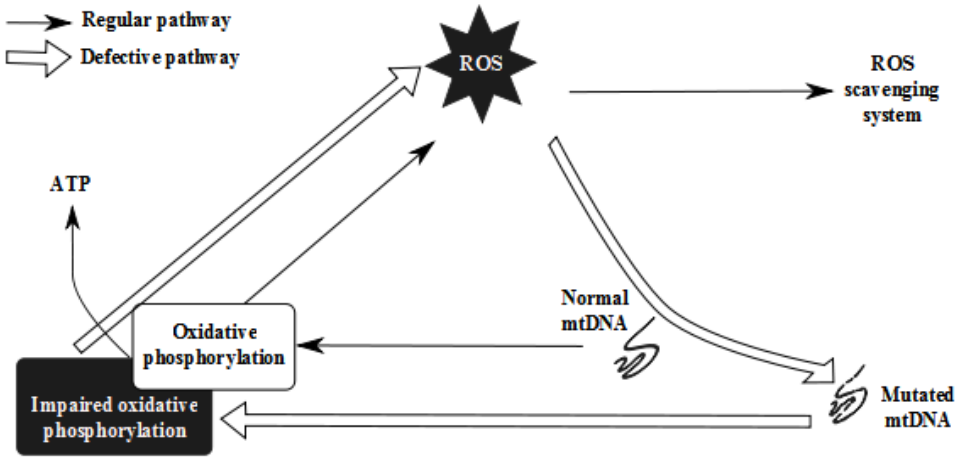

Figure 2.4: A positive feedback mechanism between mtDNA and ROS can arise when ROS-induced damaged mtDNA produce defective components of the ETC, thereby increasing electron leakage in the oxidative phosphorylation process. The electrons that leak from the ETC are captured by oxygen to form ROS. Steady state levels of ROS defines the system, and has important signalling role in establishing redox homeostasis in the cell. ROS levels are regulated by the action of molecular scavengers (antioxidants). Over time, the loop is expected to give an exponential expansion of mtDNA mutations, which eventually causes the loss of mitochondrial function in generating ATP.

2.3.3 Protein homeostasis and stress in the endoplasmic reticulum

Proteins function in a redox environment, making them susceptible to various types of chemical assaults. This makes it necessary for the system to break down the oxidised proteins to avoid process inefficiencies and effectively recycle the amino acids for producing fresh proteins. The proteasomes and endoplasmic reticulum (ER) are a major part of this maintenance process along with the golgi apparatus and lysosomes [Nelson and Cox, 2004]. However, this mechanism becomes less effective with age or when chronically stressed. The build up of proteins such as LBs in PD suggest the involvement of physiological stress in this machinery.

Genetic linkage studies have suggested that defects in the UPS contribute to the neurodegenerative process in PD [Betarbet et al., 2005]. For instance, the parkin gene (which encodes an E3 ubiquitin ligase) responsible for a juvenile and early onset parkinsonism [Kitada et al., 1998] has identified mutations implicating the involvement of aberrant UPS function in sporadic form of PD. α-synuclein aggregation was observed in a study of proteasome inhibition [Tofaris et al., 2001] and it was also noted that an over-expression of α-synuclein aggravates the toxic effects of proteasome inhibitors.

One major component of cellular state controlling protein homeostasis is the energy supply. Mitochondrial complex I damage, which could be a result of age, oxidation or environmental factors, results in decreased levels of cellular ATP. This has consequences in ubiquitination and protein degradation by the UPS [Beal, 2006; Wellstead and Cloutier, 2011]. Additionally, in dopaminergic nigral neurons, McNaught et al. [2004] observed a reduction in proteasomal α-subunits which are essential for proteasomal assembly, with age. These factors indicate an obvious compromise of UPS function in PD pathology. An increased instance of unwanted protein load because of a compromised recycling system will impact the function of ER and golgi complex that hosts most of the protein related activities.

A typical instance of association of ER stress with PD pathogenesis is the presence of protein dissulfide isomerase (PDI), identified to be an ER stress protein,

within LBs [Conn et al., 2004]. PDIs are chaperone proteins that are expressed during the UPR[18] phase of ER stress response. These ER-contained proteins are components of a quality-control system that ensures correct folding of proteins for cell viability, during conditions of stress.

Arduíno et al. [2009] demonstrates how an altered mitochondrial respiratory chain complex I activity (induced by neurotoxins such as MPTP), is linked with ER stress response. This correspondence is believed to be a result of an altered redox state of the cell, induced by an increased ROS level. Furthermore, ER stress response communicates back to the mitochondria mediated by Ca^{2+}. This feedback involves the release of Ca^{2+} from the ER, that finally ends up in the mitochondria. The resulting Ca^{2+} flux can reach alarming levels during conditions of extreme stress, and is thus a key signal in ER stress induced apoptotic pathway.

Accumulation of misfolded or over-expressed α-synuclein within the ER is also found to precede apoptotic events in experimental models of PD. Hoozemans et al. [2007] provides evidence for the activation of one of the three pathways of UPR, in LB laden dopaminergic *SNc* neurons from PD brains. Later, experiments by Bellucci et al. [2011] confirm this notion and suggest a role for α-synuclein as a neuronal sensor, whose misfolding, accumulation or aggregation resulting from a condition of cellular stress was translated in to ER stress related responses. Their results suggest that the activation of UPR in *SNc* can have early benefits, however, under conditions of extreme stress, as the response continues, apoptotic pathways are initiated.

Protein Aggregation Polypeptides fold to specific proteins as a means to achieve a state of minimum potential energy in physiological solution (conformational stability). The folding usually results in a characteristic three-dimensional structure that renders the molecule functional [Alberts et al., 2002]. Any flaw with the folding process (misfolding) produces an inactive protein that can be harmful to the system. Protein aggregation is an alternate to the

[18] *UPR* : The accumulation of misfolded proteins in the ER triggers the activation of a defence mechanism called the unfolded protein response (UPR). In this, three independent pathways are activated leading to the degradation of the associated protein and attenuation of protein translation [Høyer-Hansen and Jäättelä, 2007]

native folding process and can sometimes compete with the native process depending on the thermodynamic properties of the polypeptide. In addition to thermodynamic properties, factors that lead a protein to aggregate include concentration (which can be unusually high when over-expressed), mutations in the associated genes (thereby increasing the probability of misfolding), oxidation, inefficient protein maintenance pathway, etc.

The protein aggregation scenario in PD is reflective of aforementioned factors existing for the protein α-synuclein and we have already discussed various facets in some of the previous sections (see 2.3.1, 2.3.2.1). α-synuclein overexpression has been associated with both familial and sporadic forms of PD [Zhou et al., 2000]. Mutations in the α-synuclein gene is one of the earliest discoveries with respect to genetic links to PD [Polymeropoulos et al., 1997]. A dynamic interaction between ROS and α-synuclein is understood to exist in PD [Cloutier and Wellstead, 2012] and aspects of inefficiency in protein recycling machinery are discussed in this section. In addition, a pathogenic transfer of α-synuclein seeds is understood to exist between neurons [Desplats et al., 2009]. α-synuclein seeds can greatly influence the likelihood of protein aggregation for being the nucleation core of the process (see figure 2.3).

These studies point to a condition of α-synuclein aggregation and LB formation as a result of curtailed proteasome functioning. In an energy compromised state, a cell may divert its energy utilization to key cellular processes and protein recycling would be kept at bay. Hence an energy deficiency may be one of the prime reasons for LB build up in mammalian neurons.

2.3.4 Ageing

As mentioned in the previous chapter, the incidence of PD is age-related. In a study on non-human primates, Collier et al. [2011] report ageing to be the primary risk factor for the development of PD. The study reports that the degeneration of dopaminergic neurons in PD, follows the same cellular mechanisms as normal ageing. In PD, however, agents that pose cellular risk accumulate faster owing to environmental and genetic factors.

PD is often considered as a case of accelerated ageing. For instance, mtDNA

deletions tend to increase with age and among PD cases reported, mtDNA deletions are generally found to increase with time [Ikebe et al., 1990, 1995; Bender et al., 2006; Schapira, 2008].

2.4 Computational approaches for understanding PD etiology

The use of advances in molecular studies have enabled the scientific community to understand to some extent, various aspects of PD pathogenesis. However, these observations are often limited owing to the length of the disease process as well as the myriad variables influencing the process. Understanding the relationships of these variables is demanding and often requires computational support to test possible hypotheses.

Mathematical models are developed towards this end. However, mathematical models are often limited by the way they have been structured. Simple frameworks are often used by biologists, however they miss the bigger picture. For a disease like PD which can be seen as a failure of a cellular system, the corresponding mathematical model should be of a framework that includes analogs to the whole system involved in the pathogenesis.

In the previous sections, we have discussed various factors that contribute to cell death in PD. The spread of disease has been associated with the disease phenotype - the presence of LBs. This phenotype seems to exhibit a pathological spread starting from the enteric nervous system, to the brain-stem and ultimately into the mid-brain [Braak et al., 2003a]. The cardinal symptoms of the disease only seem to appear after a substantial number of the dopaminergic *SNc* neurons are lost. One of the most important question that needs to be answered in this scenario is what makes *SNc* neurons predestined to death and why is there a heterogeneity in vulnerability within the population?

The fact remains that most of the factors thought to contribute to the vulnerability, such as protein mishandling, oxidative stress, inflammation, mitochondrial dysfunction etc. are not unique to *SNc* neurons but are wide spread in the nervous system. In animal models, the use of a general mitochondrial

toxin like rotenone[19] leads to selective death of *SNc* neurons [Sherer et al., 2003]. Even with a genetic predisposition, the corresponding proteins like α-synuclein, LRRK2, PINK1 etc., are widely expressed in the brain and are not just unique to *SNc*. Similar arguments are valid for many other factors and together they suggest that the pathogenic process is complex.

Identifying some of the unique aspects of *SNc* implied in their vulnerability would help establish a framework that is significant for describing the pathogenesis. Some of the striking aspects of *SNc* that makes them vulnerable to degeneration have been discussed in section 2.3. The axons of these neurons are unmyelinated and immensely arborised with a large number of synapses. This feature makes the neurons highly stressed in terms of resources, specifically energy. Secondly, these neurons show an unusual reliance on the L-type calcium channel for its characteristic function of pacemaking creating a calcium stress within them. The pacemaking again is an activity that challenges the energy system of the neuron. Also, a limitation in available energy can compromise a few of the non-essential pathways that maintain the neuron. Any compromise of protein recycling can lead to conditions of material stress in compartments such as ER and further add to the existing stress. If we try to link the various factors implied in PD, they are directly or indirectly related to the energy pathways of the system and frequently cross paths with the calcium homeostasis network. We now look into one of the best approaches from engineering to link a system that has components that are partially defined.

2.4.1 A basis for model integration - metabolic energy

The metabolic activity of the brain accounts for about 20 % of the calories consumed by the body [Clarke and Sokoloff, 1999]. The energy spend by the brain mostly consists of energy produced as ATP from the breakdown of glucose molecules and its consumptions remains high even if the body is at rest or when there is an observable physical or mental activity. Despite varying activities of the brain, this rate of metabolism remain remarkably constant over time [Raichle and Gusnard, 2002].

[19]The use of MPTP is a markedly different scenario, as these molecules are taken in to the neurons depending on the activity of the dopamine transporter which are heavily expressed in *SNc* neurons [Lammel et al., 2008].

According to the estimates of Attwell and Laughlin [2001], a large component of energy used in the brain goes towards the propagation of neuronal signals; this includes the generation and propagation of action potentials, restoration of ionic fluxes and resting potential following and excitatory event, and cycling of neurotransmitter molecules. These estimates are comparable to experimental observations using magnetic resonance spectroscopy techniques [Sibson et al., 1998].

Neurons with their unique structure and physiology are by themselves hubs of energy consumption and by an inherent pacemaking activity *substantia nigra* neurons stand at the extreme upper end of the energy use spectrum. The competence of these neurons depends on an efficient energy production pathway by mitochondrial oxidative phosphorylation from chemical energy transported to or stored in these neurons. There are numerous factors affecting energy metabolism of these neurons that are as diverse as age, blood flow rate, redox environment, Ca^{2+} homeostasis etc. A central role for energy metabolism in cellular activities is evident from the fact that these pathways are the most preserved in living organisms.

Biological regulation of energy metabolism show essential features of basic control systems, including control components (proportional, derivative, integral) and control structures (feedback, feed-forward and cascade control) [Cloutier and Wellstead, 2010]. A systems analysis on a model developed for energy metabolism would be thus instrumental in identifying important mechanisms underlying the use of energy in a neuron. A system's framework with energy as the unifying components have been proposed [Wellstead and Cloutier, 2011]. This basis strikes as being appropriate because a cell metabolic state is intimately linked to its energetic state. Furthermore, defects in mitochondrial dynamics are one of the most observed feature in the disease phenotype.

2.4.2 Pacemaking models of *SNc*

Neurons are highly specialized cells that undergo unique challenges in carrying out their important physiological functions. The *substantia nigra* neurons are active cells and thus require large amounts of energy. Furthermore, these neu-

rons are extremely arborised as it projects into the striatum. One aspect that puts them in a permanent state of stress is their electrophysiology, the spontaneous pacemaking that ensures a continuous supply of dopamine to areas they project to. Pacemaking is also responsible for a continued entry of calcium ions into these neurons. Thus pacemaking becomes a subcomponent of a larger framework to analyse the energy and calcium stress of these neurons.

Mathematical models have been extensively used to describe the electrophysiology of *SNc* neurons [Amini et al., 1999; Canavier, 1999; Wilson and Callaway, 2000; Komendantov et al., 2004; Canavier and Landry, 2006; Kuznetsova et al., 2010; Drion et al., 2011]. These models have been instrumental in elucidating various components on the *SNc* membrane that work towards establishing its characteristic electrophysiology. An important aspect of the *SNc* pacemaker that these models discuss is how Ca^{2+} ions are significant in establishing its electrophysiology. L-type calcium channels have a central role in initiating membrane depolarisation that sets the pacemaking cycle [Takada et al., 2001; Chan et al., 2007]. This calcium driven mechanism of membrane oscillations has been reported to be present in all parts of *SNc* neuron [Wilson and Callaway, 2000], strongly coupled with membrane voltage.

For a cell that relies heavily on Ca^{2+}, the disposition of these ions become decisive. One of the major findings with respect to PD pathogenesis, is related to the calcium handling aspects of *SNc* neuron. We have discussed in section 1.2 about the relative sparing of dopaminergic *SNc* neurons that express the Ca^{2+} buffering protein calbindin at high levels [Yamada et al., 1990]. The study by Yamada strongly suggest a pivotal role of calcium stress in the neurodegenerative process and for this reason, mechanisms involved in Ca^{2+} disposal needs to be considered in models that aim to relate pathways leading to the degeneration of these neurons.

Some of the mathematical models previously presented do incorporate mechanisms of Ca^{2+} buffering [Wilson and Callaway, 2000] or removal by a calcium pump [Amini et al., 1999]. However, most often these steps are abstract, or at best simplified models are used with little attention to the dynamics of the Ca^{2+} pumps and/or buffers. These limitations are potentially serious in any study of Ca^{2+} mechanisms in the electrophysiology and functioning of these neurons.

Mathematical models for neuronal membrane dynamics are essentially a dynamical system describing various ion-transport proceeding across the plasma-membrane. A model would represent the system well when the model components and parameters are well identified. An outline of this process is to follow.

2.4.2.1 Representing ion transport across biological membranes

Living cells constantly require the exchange of molecules across their biological membrane for their extensive functions. Biological membranes are selectively permeable and they achieve this by means of phenomenological and structural features embedded within them. Materials exchanged across membranes include metabolites, ions, amino acids, nucleotides and gases implied in cellular metabolism. The distribution of the ions across the membrane (figure 2.5) defines such transport phenomena.

Depending upon the need for energy in such transports, they may be classified into the active or passive categories. The major transporters of ionic species found on a biological membrane are integral proteins, that may function as ion-channels, pumps or exchangers and are responsible for generating electrical responses to different stimuli. Electrical activity of excitable cells such as neurons are often represented by mathematical models of the functioning of these proteins. Such models are extensively used in the study and analysis of various brain functions including control and cognition.

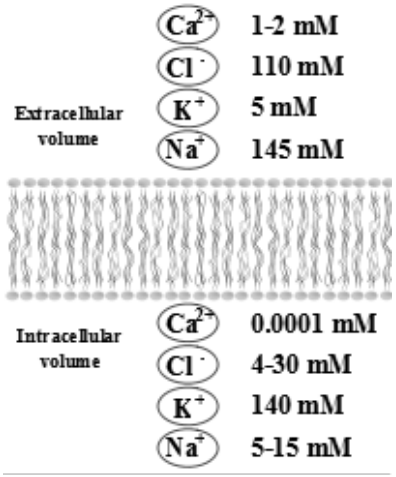

Figure 2.5: Typical distribution of ions across mammalian neurons

Passive transport may be considered as accelerated selective diffusion. Ion channels are the most diverse and prolific passive transporters found on the lipid membranes and they allow the passage of selected ions along respective concentration gradients, based on the given environmental conditions. The opening

of such channels, which is often termed 'gating', involves a change of the native channel conformation to a conductive conformation. This usually takes place under the influence of either a change in electric field or with respect to the binding of an agonist. The former category of ion channels are said to be voltage-gated and the later are known to be ligand-gated.

Active transport, on the other hand, involves the movement of solutes against their concentration gradient, by coupling to a process that provides the required energy. In primary active transport, the process is coupled to the hydrolysis of a high energy molecule such as ATP. In secondary active transport or co-transport, the process is usually coupled with one that utilises the electrochemical potential difference of another molecule that is transported simultaneously. Symport involves the co-transport of molecules in the same direction and antiport involves the co-transport in opposite directions of the membrane.

All pathways or processes of a living cell are directly or indirectly dependent on its energy metabolism. For an excitatory cell, many of its activities at the membrane are governed by the levels of intracellular ATP and cyclic adenosine monophosphate (cAMP). For instance, ATP has a direct influence on membrane functions via membrane cation pumps. These pumps are 'ATPases' and their function is critical in establishing electrochemical gradients and resting membrane potential. Transport through ion channels can continue as long as the electrochemical gradient persists. Also, there are certain ion-channels that are ATP sensitive and modulation of these channels, by changes in the level of cytosolic ATP, are reflected in the properties of action potentials produced along the length of the membrane. Thus, ATP has an indirect influence on the excitatory properties of these cells and consequently their energy metabolism. On these grounds, ion transport has been argued to be one of the most energy demanding processes in excitatory cells [Attwell and Laughlin, 2001].

Describing the mechanism of Ion-channel activity Ion channels are pore-forming transmembrane protein ensembles that are responsible for regulating or gating ion flows across the cell membrane. Gating arises from the conformational changes in the proteins that comprise the channel. These conformational changes are driven by changes in the electric field or by molecules

(ligands) that bind to them. For this reason, ion-channels are often classified into voltage-gated and ligand-gated categories.

Technological advances in the field of neuroscience have enabled recording of ion channel activities with increased precision. Patch-clamp techniques are extensively used to study ion-channel behaviour on excitable membranes. Ion-channel recordings by the patch-clamp are essentially of two kinds. In the first, known as 'whole cell recording', a macroscopic current which is the resultant of the combined activities of a large number of channels is recorded. The second method of 'single channel recording', records discrete changes in the conduction of a single channel over time.

In spite of all the advances in the field, experiments have yet to give a complete picture of ion channel structure and function. In the case of channel electro physiology, the large variability and plasticity of the channels makes it very complex to deduce a comprehensive model of the channel.

In chapter 3, we describe some of the popular modelling approaches used to describe ion-transport through a voltage gated ion channel.

Active transport across membranes From a thermodynamic perspective, transport is spontaneous when ions move down the overall gradient in free energy. Unlike in passive transport where this condition exists naturally, facilitated transport includes those processes in which the movement against the energy gradient is achieved by coupling with a process that provides surplus energy to overcome the free energy barrier. Carrier proteins found on biological membranes are sites of such energetic coupling.

The mechanism of active transport has its fundamental in the coupling of a free energy releasing process to the work done in moving the ions against its gradient. The energy required per transporter cycle, is the sum of work done in transporting the ions against their electrochemical gradients.

In chapter 4, we discuss different modelling approaches used to model the pumps and exchangers present on the *substantia nigra* membrane. In the fifth chapter we bring together appropriate representations of ion-transport discussed in chapter 3 and 4 to generate a model that reproduces spontaneous

pacemaking in a dissociated *substantia nigra* neuron.

Chapter Summary

In this chapter, we have made a review of important components and activities of the *substantia nigra* neuron that makes it vulnerable to degradation in PD. Rather than a single cause-single effect phenomena, PD appears to be a failure of an exquisite network of regulatory activities in a neuron burdened with its structure and function. The PD phenotype is a mixed bag and, despite this heterogeneity, research has brought forth some underlying themes of the pathophysiology. These include compromises made in cellular pathways that are involved with cellular maintenance and stress management and impairment of efficient metabolism owing to factors that are genetic or extra-neuronal.

The sheer vastness of cellular factors involved with the pathogenesis necessitates limitation of the discussion to a subset of events related to our theme. Our discussion has omitted some aspects implied in PD like the influence of inflammatory response, excitotoxicity and others. Discussions have been made from a platform of energy metabolism on the premises of Ca^{2+} homeostasis and since this theme encompasses many major landmarks of the pathological process, this chapter has illustrated circumstances regarding *substantia nigra* degeneration without much selective bias.

It is difficult to have a simple mathematical representation of disease progression in PD. Rather, it is appropriate to have a system with various subcomponents that may be connected by a few important variables. From the review in this chapter, we have argued that calcium is an important variable to consider and energy utilization could be the basis upon which the system is built. In the following chapters we build a mathematical description of a particular component of the *substantia nigra* metabolism, its characteristic electrophysiology and how it relates to the calcium stress in these neurons.

Part II

Dynamics of Ion-Transport

CHAPTER 3

Elements of membrane conduction : passive transport

This chapter discusses components of the model responsible for passive transport of ionic species across the membrane (ion channels)

Introduction One of the defining aspects of life on earth and its current diversity is 'specialization'. It is a fundamental characteristic of multi-cellular systems by which overall complexity has been distributed among its components, thereby making individual units simpler and their interactions complex. This specialization can be seen in all levels of life from within cells to the level of ecosystems.

An aspect of complex organisms that has co-evolved with specialization is 'communication' that enables the multi-cellular structure to function as a single unit. Communication in and among cells can be either chemical or electrical in nature. For faster communications over longer distances, life forms use electricity as a reliable mode. A cell is 'excitable' when it is capable of producing or responding to an electro-chemical signal and is distinguished by the presence of a membrane that is polarised[1]. Both excitable and non-excitable cells main-

[1]A cell membrane is polarised when there is a difference in the distribution of ions or charges across it creating a voltage gradient. At equilibrium, a resting membrane potential is established with the cell interior negative with respect to the exterior.

tain a resting potential by means of specialised membrane proteins that are ion pumps. Substantial perturbation of the voltage gradient in excitable cells can give rise to an electrical activity, by the activation of another set of membrane proteins that are voltage regulated ion-channels.

The electrical activity of a living system is thus a function of dynamic ionic transport that exists across biological membranes of its excitable cells. Neurons are the most distinctive among excitable cells and in this thesis we are concerned with the function of a specialised group of neurons (*SNc*) pronounced in PD. To understand how a neuron's electrophysiology transcribes into its function, it is important to understand the dynamics of its membrane ion-transport. In this chapter, we discuss the aspects of transport that are passive in nature, i.e. transport that takes place in the direction of the electro-chemical gradient and the following chapter will discuss active transport mechanisms, that is, those that work against the gradient.

3.1 Underlying physiology of neuronal membranes

The nervous system consists of billions of neurons that can conduct electrical impulses. The composition of its membrane, along with its structure, enables neuronal conduction of electrical pulses. As discussed, the particular classes of proteins embedded in the membrane play a major role in this function. The two key components of this are: (i) active transporters establishing the resting membrane potential, by mechanically translocating ions across the membrane; and, (ii) the regulated passive transporters giving rise to appropriate responses, by forming pores and facilitating ionic diffusion. The most visible form of this response is an action potential, which is a very rapid (milliseconds time scale) change in membrane potential from its resting state to a positive value.

An action potential involves the opening of a few different ion-channels for a short interval. These membrane proteins are usually specific to a particular type of ion and their opening allows a rapid passive diffusion of this ionic species. For example, opening of sodium channels allows a transient flow of Na^+ions into the cell, creating a Na^+current that depolarises the membrane. Simultaneous opening of potassium channels, creates a K^+current that repo-

larises the membrane. The transmembrane potential (V) is thus a dynamic variable depending on the flow of currents across the membrane and was originally described with a mathematical formulation based on Kirchoff's law [Hodgkin and Huxley, 1952]. According to this formalism of an "equivalent electrical circuit", the cell membrane is a capacitor (representing charge accumulation), connected in parallel with variable conductances (representing ion transport), with voltage sources to represent the driving forces [Hodgkin and Huxley, 1952; DiFrancesco and Noble, 1985].

The original modelling paradigm established by Hodgkin and Huxley, uses the net flow of ionic currents (I_s) to determine the transmembrane potential.

$$C_m \cdot \frac{dV}{dt} = \sum_{s \in S} \left[I - I_s \right], \tag{3.1}$$

where $s \in S = \{Na, Ca, K, A\}$, represents sodium, calcium, potassium and anions, respectively. C_m is the membrane capacitance and I, any external current injected into the membrane. In the sections to follow, we do not consider any injection of external currents, and therefore equation 3.1 is simplified to

$$C_m \cdot \frac{dV}{dt} = -\sum_{s \in S} \left[I_s \right], \tag{3.2}$$

The flow of ions across the cell membrane undeniably creates a change in the concentration of participating ionic species in the cytosol. Earlier modelling approaches did not consider the dynamics of cytosolic ionic concentrations and in most instances they were taken as constants. As modelling methods evolved, later models of excitable cells started to include the dynamic changes associated with intracellular cations (for example, see DiFrancesco and Noble [1985]; Luo and Rudy [1994]). However, in these models, the relationship between transmembrane potential and cytosolic concentrations was indirect. They were related through membrane currents, as

$$\frac{ds}{dt} = \frac{1}{z_s \cdot F \cdot \mathcal{V}_{cyt}} \cdot \sum_{x \in X_s} I_{s,x}, \tag{3.3}$$

where X_s includes all mechanisms by which species s are transported across the membrane. Here F represents the Faraday constant, $\mathcal{V}_{cyt}$ the cytosolic volume, and z_s the valency of ionic species s.

One difficulty with the above formulations concerns the behaviour of the model under prolonged simulations. Since there is no direct connection between ionic concentrations and membrane potential, numerical errors may accumulate giving rise to drifts of ion concentrations and membrane potential as well as the existence of multiple steady states [Guan et al., 1997; Endresen et al., 2000; Hund et al., 2001]. As an alternative, the voltage expression may be formulated using ionic charge conservation principles [Varghese and Sell, 1997]. According to Poignard et al. [2011], if we assume the cell volume to be constant because of an osmotic equilibrium, we have

$$C_m \cdot \frac{dV}{dt} = \mathcal{V}_{cyt} \cdot F \cdot \sum_{s \in S} z_s \frac{ds_i}{dt}. \tag{3.4}$$

The algebraic equation relating transmembrane potential to intracellular concentrations is simply the integrated form of equation 3.4 and this paradigm of representing the membrane dynamics is generally referred to as the "algebraic method" [Varghese and Sell, 1997; Endresen et al., 2000; Hund et al., 2001]. Thus, an explicit relation of the transmembrane potential in terms of ionic concentration is obtained by assuming that the cell shape is retained by an osmotic equilibrium,

$$V = \frac{F \cdot \mathcal{V}_{cyt}}{C_m} \sum_{s \in S} \left[z_s \cdot (s_i - s_e) \right]. \tag{3.5}$$

Assuming that outer ionic concentrations are constant, the membrane potential is a function of the intra-cellular ionic concentrations.

Ion flux and equilibrium The transport of ionic species across the membrane depends on the ionic concentration gradient and electrical field. This flux can be described by the Nernst-Planck equation in which, for a constant electric field along the width of the membrane, the flux of species s is influenced by both concentration gradient and electric field:

$$J_s = -\mathcal{D}_s \cdot \left(\frac{ds}{dx} + \frac{z_s \cdot F}{R \cdot T} \cdot s \cdot \frac{V}{L} \right), \tag{3.6}$$

where $\mathcal{D}_s$ is the diffusivity of species s and V is the voltage across the membrane of length L. The Nernst potential $\hat{\mathcal{V}}_s$, represents the equilibrium voltage at which the net transport of the species across the membrane is zero:

$$\hat{\mathcal{V}}_s = \frac{\mathcal{V}_\tau}{z_s} \cdot \ln \frac{s_e}{s_i} \qquad s \in S, \tag{3.7}$$

where $\mathcal{V}_\tau = {}^{R \cdot T}/_{F}$ is a temperature defined thermodynamic entity, the voltage equivalent of temperature.

3.2 Modelling ion conduction

The flow of species s through ion-channels is a passive diffusion process and thus is dependent on the difference in potential energy of s across the membrane. The expected rate of flow also depends on the probability that the channel remains open (see the note that follows). This may be represented as:

$$I_{s,c} = \mathcal{O}_c \cdot f_{s,c}, \tag{3.8}$$

where the sub-index c denotes the ion channels to be considered. Here, $f_{s,c}$ is a function that defines the transport of species s through an open channel, c, influenced by the given electrochemical field; and, $\mathcal{O}_c$ represents the probability of channel c being open at the given membrane potential or a given ligand concentration l in the given environment.

We describe the possible forms of both terms in equation 3.8 in this chapter. In the subsections to follow, we have the two different ways of describing the function f; the first is a linear relationship between current and voltage and later, is non-linear. In the next section, the different mathematical formalisms to model the open probability of a channel, $\mathcal{O}_c$, are described.

Note : The switch of ion-channels between their conducting state is generally observed to be a stochastic process, biased by the driving force. Physiologically, this stochastic nature becomes significant when the number of ion-channels are small. Models based on discrete stochastic ion channels are found to converge to continuous deterministic models when the ion-channel population is sufficiently large [Strassberg and DeFelice, 1993]. The use of the variable $\mathcal{O}$ in the thesis implies that we are looking at a statistically significant population of ion-channels contributing to important currents in our model and any individual stochastic events are ignored.

3.2.1 Current equation in the circuit model : linear conductance relationship

Hodgkin and Huxley [1952] observed that the electric current crossing a membrane could be described as a sum of ionic components, of which the currents carried by sodium and potassium were the most important. From their experiments over a limited range of voltage, they showed that the conductance can be approximated by a function linear in voltage as follows

$$f_{s,c} = \mathcal{G}_{s,c} \cdot (V - \hat{\mathcal{V}}_s), \tag{3.9}$$

where $\mathcal{G}_{s,c}$ is the channel conductance.

3.2.2 Goldman-Hodgkin-Katz (GHK) current equation

In the previous approach (subsection 3.2.1), Hodgkin and Huxley considered only the electrical drift associated with the transport of ions. However, molecular diffusion of the ionic species is a readily observable phenomenon and may be easily accounted for in an expression for the transmembrane ion flux (see equation 3.6). The model describing this phenomenon is commonly known as the Goldman-Hodgkin-Katz (GHK) current equation [Goldman, 1943; Eisenberg, 1998; Endresen et al., 2000; Clay, 2009], although it is occasionally also named the drift-diffusion equation or the electrodiffusion model. This model results in a more complete mechanistic representation of ion channel currents, though it has not yet been widely adopted in literature [Clay, 1984, 2009].

The GHK equation is generated by integrating the Nernst-Plank equation (3.6) as,

$$f_{s,c} = \epsilon_{s,c} \cdot z_s^2 \cdot F \cdot \frac{V}{\mathcal{V}_\tau} \cdot \frac{s_i - s_e \cdot \exp\left(-z_s \frac{V}{\mathcal{V}_\tau}\right)}{1 - \exp\left(-z_s \frac{V}{\mathcal{V}_\tau}\right)}. \tag{3.10}$$

Here $\epsilon_{s,c}$ represents the permeability of the membrane for ion s through channel c. This equation may also be expressed using the hyperbolic sine ($\sinh$)

function [2] as

$$f_{s,c} = g_{s,c} \cdot z_s \cdot \sqrt{s_i \cdot s_e} \cdot \frac{\sinh\left(z_s \cdot \frac{V-\hat{\mathcal{V}}_s}{2\mathcal{V}_\tau}\right)}{\text{sinhc}\left(z_s \cdot \frac{V}{2\mathcal{V}_\tau}\right)}. \tag{3.11}$$

The linear conductance relationship (equation 3.9) is a linear approximation of the electrodiffusion model around the Nernst potential [Herrera-Valdez, 2012] and is more commonly used in the literature . The GHK equation (equation 3.11) may be more appropriate when there are significant differences in the voltage and ionic concentrations inside the cell, that is, when V and or $\hat{\mathcal{V}}_s$ vary significantly compared with $\mathcal{V}_\tau$. For example, this is significant when calcium dynamics are considered.

3.3 Gating of voltage-gated ion channels

Voltage-gated ion channels have charged domains that make their structure sensitive to variations in the external electric field. For a particular range of membrane potentials they adopt a conformation with a central hole, forming a channel for the free movement of ions. Such an 'open' state is further defined by certain 'selectivity filters' (often amino acids) that render the protein specific to certain ions[Beyl et al., 2007]. At other membrane potentials, the flow of ionic current is blocked as a result of the 'closed' or 'inactive' conformations that the protein adopts. A channel protein can thus adopt various conformational states with varying degrees of conductance, and they can spontaneously switch between these states. The dynamics of such switches is central to any study that involves an ion channel.

Equation based kinetic models are useful to interpret the behaviour of a channel in a given situation. Starting with the model of Hodgkin and Huxley [Hodgkin and Huxley, 1952], several researchers have developed theoretical frameworks that partially explain observations made on channel activity. The Hodgkin-Huxley formalism relies on an underlying model of average channel conductance and their equations describe the changes of ionic permeability with membrane potential. The model makes use of hypothetical gating particles to bring about the channel's function, by forcing their motion with respect

[2] The cardinal hyperbolic sine is given by, $\text{sinhc}(x) = \frac{\sinh x}{x}$

to the electric field across the membrane. Although this model has been used in many instances, hypothetical gating particles do not appear to be consistent with underlying molecular mechanisms. The use of stochastic versions of the model was based on the understanding that ion-channels are essentially stochastic entities [Fox, 1997].

Further developments in the study of ion-channels made an attempt to give a mechanistic description to the gating phenomena. Such models consist of non-linear ordinary differential equations (ODEs): a current balance equation plus the dynamics of conformational transitions incorporated as a 'gating variable' that corresponds to the state of the ion channels. Discrete-state Markov models have been used to describe the different states of the ion channel [Kienker, 1989] and have found good acceptance in the literature for providing a mechanistic description for the otherwise abstract Hodgkin-Huxley formalism based models.

Markov chain models are developed on the assumption that ion channels exist in a finite number of significant energy states, with time - homogeneous rates of transition between them. The model consists of a topology of allowed transitions between these states, together with the rates for these transitions. Fitting single-channel recording data with a Markovian kinetic scheme has been standard in neurophysiology for quite some time [Kienker, 1989; Milescu et al., 2005; Sansom et al., 1989]. However, for a good agreement with experimental data, frequently the number of closed states needed varies with the experimental protocol. Markov models have advantages over the Hodgkin-Huxley formalism with the large degree of freedom in the model structure that brings it closer to experimental observations [Fink and Noble, 2009]. Thermodynamic models are a two state Markovian description of channel flipping, the rate kinetics of which are described by concepts in thermodynamics [Destexhe and Huguenard, 2000; Ozer, 2004].

Fractal models [Liebovitch et al., 1987; Liebovitch, 1989] of ion channel gating provide a different description of the underlying mechanism compared to Markov models. Such models are characterised by transition rates that depend on the amount of time that the channel has spent in a given state. The Diffusion models introduced by Millhauser, justify Fractal models at a micro-

scopic level [Millhauser et al., 1988]. Statistical analysis, however, has often favoured Markov models over Fractal models [Sansom et al., 1989; Nekouzadeh and Rudy, 2007].

A major hurdle in modelling ion-channel gating using a Markov-jump scheme is in the determination of an appropriate number of closed states. As the topology space expands with the number of states, generating appropriate kinetic schemes imposes ambiguity because it may be possible to come up with multiple schemes that are consistent with a given set of data. Moreover, numerical simulation of such models becomes increasingly CPU intensive. This limits the usefulness of the model during both parameter estimation and multi-cellular simulations [Fink and Noble, 2009].

An increasing complexity of the model topology thus calls for model reduction. Kienker [1989] discusses the existence of equivalence in topologies of models that are identifiable within the same data set. This would imply that models with a larger number of states are reducible. Keener [2009] illustrates the possibility of reducing the complexity to stable invariant manifolds. This approach would reduce the dimension of the system without suffering from large approximation errors. Furthermore, the time scale of the Markovian transitions are much faster than the main time scales involved in the aggregate cell voltage and ion behaviour [Aidley and Stanfield, 1996; Hille, 2001], which in turn offers options for model reduction.

Another difficulty in the acceptability of ion channel models is related to parameter identifiability. A model is said to have structurally unidentifiable parameters when multiple parameters are equally powerful in explaining observed data in noise-free perfect experiments [Bellman and Åström, 1970; Walter and Pronzato, 1997; Balsa-Canto et al., 2010]. Since it is well-known that a large segment of ion-channel models in the literature lack parameter identifiability in noise experiments [Fink and Noble, 2009], fundamental studies on structural identifiability are scarce due to the difficulty of solving the associated set of symbolic equations [Csercsik et al., 2010, 2012].

It should be noted that most experimental protocols optimised to better the signal-to-noise ratio [Beaumont et al., 1993; Willms et al., 1999], provide two sets of separated data: one used to characterise the steady-state, and the other

the time constants, when dynamics are not sufficiently fast to be disregarded. With this in mind, Hodgkin-Huxley models employ empirical expressions for both steps that are not always realistic [Willms et al., 1999]. On the other hand, estimation in models based on Markov chains often make use of other types of experimental protocols, and do not exploit the large range of data available using the standard protocols.

In this section, we describe some of the popular representations of ion-channel gating. We also give an approach to describe the stationary conductance of an ion-channel gate with a small number of parameters. Also, the current equation (equation 3.8) combines two distinct formulations, one for the channel gating and the second for the transport. The choice of a particular model can affect the response and we seek to identify the differences in using a particular transport expression (linear conductance or GHK equation) with a particular gating model described in this section.

3.3.1 The Hodgkin-Huxley Approach

In the Hodgkin-Huxley formalism the "channel gates" are of two types: those that activate the channels and those that inactivate them. The probability that the channels are open ($\mathcal{O}$) is thus a function of these gates:

$$\mathcal{O}_c(V) = [m_c(t)]^{a_c} \cdot [h_c(t)]^{b_c} \,,$$

where for channel c, a_c and b_c are respectively the numbers and m_c and h_c the fraction of activation and inactivation components in the conductive state. The dynamics of each of the gating variables (m_c, h_c) may be described by a first-order differential equation:

$$\frac{dy}{dt} = \frac{y_\infty - y}{\tau_y}, \quad y \in \{m_c, h_c\} \,.$$

The steady state values of these variables are modelled by a Boltzmann-type equation:

$$y_\infty = \frac{1}{1 + \exp\left(\frac{V_{h,y} - V}{s}\right)},$$

with the parameter $V_{h,y}$ satisfying $y_\infty(V_{h,y}) = 0.5$ and s being the slope factor. The slope factor is positive for activation gates and negative for inactivation

gates. The dependence of the time-constant, τ_y on voltage is mostly expressed empirically, and one popular way of approximating the time constant is by a Gaussian function [Izhikevich, 2007].

3.3.2 The Markov Approach

Background : Stable conformations of ion channels

The probability of a protein molecule adapting a particular conformation in space is largely influenced by the electrical force-field surrounding it. When subject to an electric field, charged groups within a protein will experience a force and may attain a new electrostatic equilibrium by incorporating angular changes in the dipoles associated with the peptide bond [Manna et al., 2007]. If the thermodynamic kinetic energy is large enough to overcome the energy barrier, the protein takes up a new conformational state. Proteins can hence take up a large number of conformational states separated by small energy barriers. Despite the continuum of intermediate states, this dynamical system would typically have only a few stable equilibria [Keener, 2009] and hence a limited number of experimentally observable states.

Transition velocities The rate at which a protein switches between such stable states is mainly determined by the driving forces that help in overcoming the thermodynamic energy barrier. However, there are some conformational changes that are not regulated by either electric field or ligands. They may be considered to have a constant energy barrier in the given environment, and hence may be thought to have a uniform rate. Classical thermodynamics identifies the rate of transition between two reaction states based on the free energy barrier between them [Hänggi et al., 1990], as

$$k = k_0 e^{-(\triangle G)/RT} \tag{3.12}$$

where, k is the rate of transition between the two states, k_0 is a constant, ΔG is the free energy barrier between the two states, R is the universal gas constant and T the absolute temperature.

Usually the free energy barrier may be dependent on the electric field, that is, the membrane potential V. In this case we have

$$k(V) = k_0 e^{-\Delta G(V)/RT}, \tag{3.13}$$

Here $\Delta G(V)$ is the free energy barrier between the two states defined by the voltage [Milescu et al., 2005].

In the case of voltage based transition, the activation energy can be approximated by using a Taylor series expansion [Destexhe and Huguenard, 2000; Ozer, 2004], as follows:

$$\Delta G(V) = a + bV + cV^2 + \cdots$$

and the rate of transition $k(V)$ may be written as,

$$k(V) = k_0 e^{-(a+bV+cV^2+\cdots)/RT}. \tag{3.14}$$

Here a corresponds to the free energy independent of the electric field and bV corresponds to interactions between electric field and isolated charges and rigid dipoles on the protein. The higher order terms correspond to the influence of polarization and deformation within the protein structure as well as mechanical constraints. These effects are usually negligible as the trans-membrane voltage variations are generally small [Destexhe and Huguenard, 2000].

In what follows, we are mainly interested in models where the free energy is linear in the membrane potential. The effect of temperature variations are not relevant to model the system under consideration and may be neglected. In this case, the following lemma, helps us derive a simple expression for voltage regulated conformational transitions.

Lemma 1 *Consider a set $\{\Delta G_1(V), \Delta G_2(V), \ldots, \Delta G_M(V)\}$ of activation energies, where each $\Delta G_i(V)$ is affine in V. Denote the corresponding transition rates by $\{k_1, k_2, \ldots, k_M\}$. Then any expression of the form $\prod_{p=1}^{P} \left(\frac{k_{i_p}(V)}{k_{j_p}(V)}\right)$ may be expressed as $e^{[(V-V_h)s]}$*

Proof: see A.1

Markov Models for conformation transitions A Markov process is a stochastic series of events satisfying the property that the probability of the process being in a particular state depends only on the state of the system at the time that immediately precedes the present state. By this property one can make predictions for the process solely based on the present state. Molecular changes associated with the opening of an ion channel has been popularly demonstrated with Markov models with discrete states [Kienker, 1989; Sansom et al., 1989; Keener, 2009]. Consider a simple form of transition between an open and closed state. Let O and C represent the probability that the molecule is in the corresponding open and closed state at a given time. The transition between the two states may be represented by a kinetic scheme, as follows

$$C \underset{k_{CO}}{\overset{k_{OC}}{\rightleftharpoons}} O$$

where, k_{ij} represents the rate of transition from state j to state i. The above kinetic scheme has a transition intensity matrix $\mathcal{K}$,

$$\begin{bmatrix} -k_{CO} & k_{OC} \\ k_{CO} & -k_{OC} \end{bmatrix}$$

and a corresponding steady state probability for the channel to be in an open state as

$$\mathcal{O}_{\text{ss}} = \frac{1}{1 + \frac{k_{OC}}{k_{CO}}}$$

and using Lemma (1) we obtain,

$$\mathcal{O}_{\text{ss}} = \frac{1}{1 + e^{[(V - V_h)s]}}. \tag{3.15}$$

The expression is the modified Boltzmann's expression used in modelling ion-channel gating [Beyl et al., 2007; Xu and Lipscombe, 2001]. This sigmoidal function of voltage is symmetric about the half-activation voltage, V_h. However, experimental data frequently show one or both of: (i) activation and inactivation behaviour; (ii) asymmetric behaviour. Hence it is hard to fit data with a single Boltzmann function. This implies that use of only two states to define the system with linear energy barriers, does not ably model experimental observations.

Several possible ways to resolve this divergence between observed data and the Boltzmann model are:

1. Model the system with several gates and different transition rates between the Markovian open and closed states. When there are enough channels so that the mean behaviour is very close to the deterministic model, this approach is equivalent to a class of Hodgkin-Huxley models.
2. Model the system as a single gate having more than two macro-states (stable conformational states)
3. Model the system as having transition rates that change with the dwell times, leading to a fractal model
4. Model one gate with Markovian open and closed states where the energy barrier includes non-linear terms with respect to voltage.

The third option is not considered as the system is being described as a time-homogeneous Markov process. For the final option, we show later that the use of higher order non-linear energy models (equation 3.27) does not appear to give simpler models, nor does it give more accurate fits to experimental data.

3.3.2.1 Markov models with multiple gates

The opening of an individual gate may also be represented as a simple Markov transition between two states, with voltage dependent transition rates $\alpha(V)$ and $\beta(V)$ in the forward and reverse direction, respectively. We can represent the dynamics of these transitions as,

$$\mathcal{O}_c(V) = \prod_{i=1}^{n_{c,m}} \left[m_c^{\{i\}}(V)\right] \cdot \prod_{j=1}^{n_{c,h}} \left[h_c^{\{j\}}(V)\right]$$

$$\frac{dy}{dt} = \alpha_y \cdot (1-y) - \beta_y \cdot y \qquad y \in m_c^{\{i\}}, h_c^{\{j\}}.$$

Here $n_{c,m}$ and $n_{c,h}$ represents the respective numbers of activation and inactivation gates considered for the channel c. Approximations for these rates of transition [Varghese and Boland, 2002] are,

$$\alpha = \alpha_0 \cdot \exp\left(-\frac{z\delta VF}{RT}\right) = \alpha_0 \cdot \exp\left(-z_a \frac{V}{\mathcal{V}_\tau}\right) \tag{3.16}$$

$$\beta = \beta_0 \cdot \exp\left(-\frac{z(1-\delta)VF}{RT}\right) = \beta_0 \cdot \exp\left(-z_b \frac{V}{\mathcal{V}_\tau}\right) \tag{3.17}$$

Here, δ is a parameter that represents the location of a transition energy barrier placed asymmetrically in the electric field of the membrane and thus, z_a and z_b

are charges associated with this barrier. For activation gates, $z_{am}, z_{bm} > 0$ and for inactivation gates, $z_{ah}, z_{bh} < 0$.

Note that this model would give an open probability equivalent to the Hodgkin-Huxley model for the condition, $\tau_y = 1/(\alpha + \beta)$.

3.3.3 A Multiple Conformation Extension of the 'Modified Boltzmann Function' for stationary conductance

Models developed on the basis of one Markov chain often have more than three states for a good agreement with experimental observations [Kienker, 1989; Milescu et al., 2005]. In such models the rate constant is often defined with an exponential or a Boltzmann function in voltage.

The simple two-state model involving the transition between the open and close conformation, may be extended into a network of macro-states for further analysis. Voltage-gated ion channels are characterised by a central pore formed from the union of four similar subunits or domains [Aidley and Stanfield, 1996]. Each of these domains contains six transmembrane α helical structures (S1 to S6), the segment S4 often acting as the voltage sensor [Bezanilla, 2000]. Such a three dimensional entity often provide options for parallel transitions among the various sub-states. In any case, transitions to the open-state are achievable.

The Master Equation and Transition Rates Here we consider the transition network of the ion-channel as a system with a set of $\mathcal{N}$ stable states, marked $i = 0, 1, ..., n$; with $n = \mathcal{N} - 1$ closed or inactive states and 0 being the open state. In the sections that follow, we consider models with only a single open state, as it is logical with respect to the molecular structure of ion channels and reflects fine details in experiments [Liebovitch, 1989]. If S_i denotes the probability for the protein to be in state i at any time t, the system obeys the *master equation*,

$$\dot{S} = \mathcal{K}S \tag{3.18}$$

where, $S = (\mathcal{O}, S_1, S_2, ..., S_n)$ and $\mathcal{K} \in \mathbb{R}^{\mathcal{N}\times\mathcal{N}}$ is a transition matrix with $k_{ij} \geq 0$ giving the rate of transit from state j to state i. The diagonal elements satisfy, $k_{ii} = -\sum_{i:i\neq j}^{\mathcal{N}} k_{ij}$, to ensure the system evolves on the probability

simplex. The entry $k_{ij} \neq 0$ if and only if there is a transition from state j to state i. The stationary probability distribution S satisfies $\mathcal{K}S = 0$, $\mathbb{1}_{\mathcal{N}}^T S = 1$, where $\mathbb{1}_{\mathcal{N}}$ is the column vector of size $\mathcal{N}$ with all entries equal to one.

As is standard, we associated a directed graph with the Markov process described by (3.18) consisting of the nodes $\{0, 1, \ldots, n\}$ with an edge from state j to state i ($i \neq j$) if and only if $k_{ij} \neq 0$.

In what follows, we derive explicit formulae for the form of the stationary vector in some simple cases; emphasising that in these cases the open state probability $\mathcal{O}$ takes a particularly simple form. We also describe a general condition on the structure of the graph associated with the Markov process that is sufficient for this simple form to hold.

3.3.3.1 Examples with similar form of solution

Solution for a special case: A three state linear system with reversible transitions A three state transition diagram for channel opening is given below

$$C_1 \underset{k_{12}}{\overset{k_{21}}{\rightleftarrows}} C_2 \underset{k_{20}}{\overset{k_{02}}{\rightleftarrows}} O \,.$$

Here O represents an open state and C_1 and C_2 represent closed or inactive conformations. The steady-state probability for the channel to be in the open state may be deduced as

$$\mathcal{O}_{\text{ss}} = \frac{1}{\left(1 + \frac{k_{12}}{k_{21}} + \frac{k_{12}}{k_{21}}\frac{k_{20}}{k_{02}}\right)}.$$

By using lemma 1, there exist $V_{h_1}, s_1, V_{h_2}, s_2$ such that

$$\mathcal{O}_{\text{ss}} = \frac{1}{1 + e^{\left[(V - V_{h_1})s_1\right]} + e^{\left[(V - V_{h_2})s_2\right]}} \tag{3.19}$$

In the case of a slightly different topology,

$$C_1 \underset{k_{10}}{\overset{k_{01}}{\rightleftarrows}} O \underset{k_{02}}{\overset{k_{20}}{\rightleftarrows}} C_2$$

the probability of the channel to be in an open conformation would be

$$\mathcal{O}_{\text{ss}} = \frac{1}{\left(1 + \frac{k_{10}}{k_{01}} + \frac{k_{20}}{k_{02}}\right)}$$

and once again, using lemma 1, the stationary probability of being open can be represented in the form of equation 3.19.

Linear Networks The scheme above, can be generalized for n macrostates depending on the position of the open state in the entire topology. A topology involving the open state on the network extremum,

$$O \underset{k_{01}}{\overset{k_{10}}{\rightleftarrows}} C_1 \underset{k_{12}}{\overset{k_{21}}{\rightleftarrows}} C_2 \cdots\cdots C_i \cdots\cdots C_{n-1} \underset{k_{n-1,n}}{\overset{k_{n,n-1}}{\rightleftarrows}} C_n$$

would have an open state stationary probability,

$$\mathcal{O}_{\text{ss}} = \frac{1}{\left(1 + \sum_{j=1}^{n} \prod_{i=1}^{j} \frac{k_{i,i-1}}{k_{i-1,i}}\right)}$$

and a topology,

$$C_1 \underset{k_{12}}{\overset{k_{21}}{\rightleftarrows}} C_2 \underset{k_{23}}{\overset{k_{32}}{\rightleftarrows}} \cdots C_{p-1} \underset{k_{p-1,0}}{\overset{k_{0,p-1}}{\rightleftarrows}} O \underset{k_{0,p+1}}{\overset{k_{p+1,0}}{\rightleftarrows}} \cdots C_{n-1} \underset{k_{n-1,n}}{\overset{k_{n,n-1}}{\rightleftarrows}} C_n$$

would yield,

$$\mathcal{O}_{\text{ss}} = \frac{1}{\left(1 + \sum_{j=1}^{p-1} \prod_{i=1}^{j} \frac{k_{i,i+1}}{k_{i+1,i}} + \sum_{j=p}^{n} \prod_{i=1}^{j} \frac{k_{i+1,i}}{k_{i,i+1}}\right)}$$

In either case, with respect to the argument in lemma (1), the open state probability can be reduced and, in general, a linear system with N macro-states related in order of their conformational transitions would have an open state stationary probability,

$$\mathcal{O}_{\text{ss}} = \frac{1}{1 + \sum_{i=1}^{n} e^{(V - V_{h,i})s_i}}$$

where, $n = \mathcal{N} - 1$, is the number of transitions in the linear network.

Remark For the networks considered so far, rendering one of the transitions irreversible, would make the network absorbing in nature. In other words, the system would reach and never leave a fixed conformation. Since such a possibility is not physically reasonable for ion-channels under consideration, this case is not considered further.

Other networks :

More generally, consider a transition network in which a unique simple path exists from every stable state to the open state; so in the directed graph associated with the matrix $\mathcal{K}$, there is a unique path from every $j \neq 0$ to the node 0. We also assume that the matrix $\mathcal{K}$ is irreducible [Horn and Johnson, 1985].

The celebrated Markov Chain Tree Theorem [Leighton and Rivest, 1986] allows us to characterise the form of the steady state probability of the open state in this case. This result is usually stated for column stochastic matrices or discrete Markov chains; however, it is trivial to see that an exact analogue also holds for continuous chains with matrices of the form $\mathcal{K}$. We state a restricted version of this result below but first introduce some notation.

For the directed graph G associated with $\mathcal{K}$, a rooted spanning tree T_i at $i \in \{0, \ldots, n\}$ consists of the vertices $\{0, 1, \ldots, n\}$ and has the following properties:

1. T_i is acyclic
2. for every $j \neq i$, there exists exactly one outgoing edge from j
3. there exist no edge outgoing from i

We denote by $w(T_i)$ the weight of T_i, which is given by the product of the entries of $\mathcal{K}$ corresponding to the edges in T_i. For $0 \leq i \leq n$, let $\mathcal{T}_i$ denote the set of all directed spanning trees rooted at i, and define $w_i = \sum_{\mathcal{T}_i} w(T_i)$. Note that each w_i will be a sum of terms of the form

$$k_{i_1 j_1} k_{i_2 j_2} \cdots k_{i_n j_n} \tag{3.20}$$

The following result is now a simple re-wording of the Markov Chain Tree Theorem as presented in Leighton and Rivest [1986] and elsewhere.

Theorem 1 *Assume the matrix $\mathcal{K}$ is irreducible. The unique stationary probability vector associated with $\mathcal{K}$, π is given by*

$$\pi_i = \frac{w_i}{\sum_j w_j}$$

where w_i is defined as above for $0 \leq i \leq n$.

If there is a unique path from every node $j \neq 0$ back to the node 0, then it follows immediately that there is exactly one directed spanning tree T_0 rooted at 0 (which represents the open state). It then follows that the steady state probability of the channel being in the open state is of the form

$$\mathcal{O} \quad = \quad \frac{w(T_0)}{\sum_j w_j}. \tag{3.21}$$

As there is only a single term of the form (3.20) in the numerator, it follows readily by combining (3.21) with Lemma 1 that $\mathcal{O}$ can will take the form

$$\mathcal{O} = \frac{1}{1 + \sum_{i=1}^{N} e^{(V - V_{h,i})s_i}}. \tag{3.22}$$

A few examples of network topologies for which this form is guaranteed by this analysis are illustrated in figures (3.1) and (3.2).

3.3.3.2 Numerical analysis and low order approximation

We have observed so far that, in many cases of interest, open-state probabilities of ion-channels may be expressed in a similar form to the modified Boltzmann equation, but with a sum of exponentials replacing the single exponential term as in equation 3.22. The value of N is generally not less than the number of transition macro-states. The ambiguity in the value of N (which is mainly dependent on the network structure) together with computational and identifiability issues for large N motivate us to consider models with small N. Of course, when considering such approximations, we potentially open up inaccuracies in the model [Liebovitch, 1989], and it is therefore important to check that any such reduction still accurately captures the observable behaviour of the system.

A good way of approximating the model would be to search for the minimum number of exponential terms that yields a good fit for experimentally observed ion channel current-voltage characteristic data. Let us denote the M-vector of ionic currents obtained from patch clamp experiments on a certain channel by $\mathrm{I}^{\mathrm{m}} \in \mathbb{R}^M$. Let $\mathrm{V}^{\mathrm{m}} \in \mathbb{R}^M$ be the corresponding voltage vector. In order to fit these data to equation 3.22, the distance between the experimental data and the

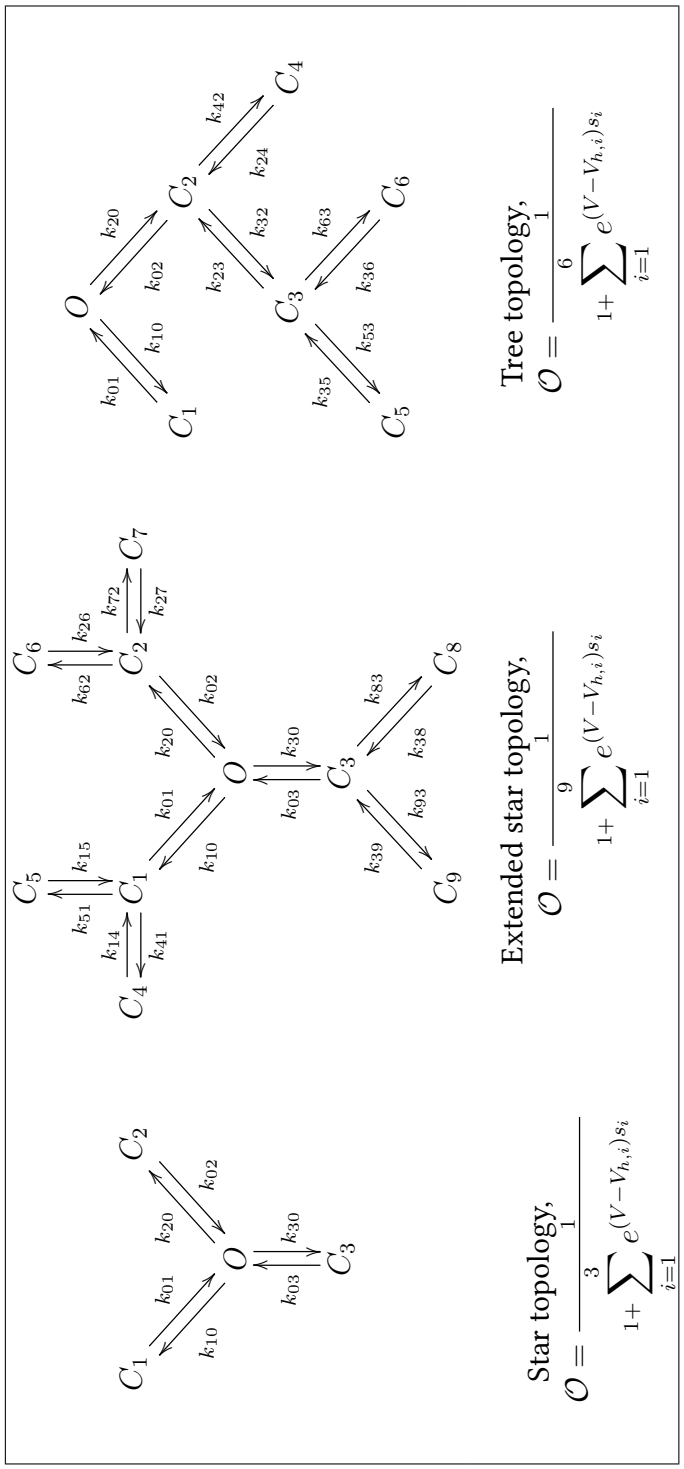

Figure 3.1: Examples of ion-channel topologies that satisfy the criteria of a unique simple path to the open state

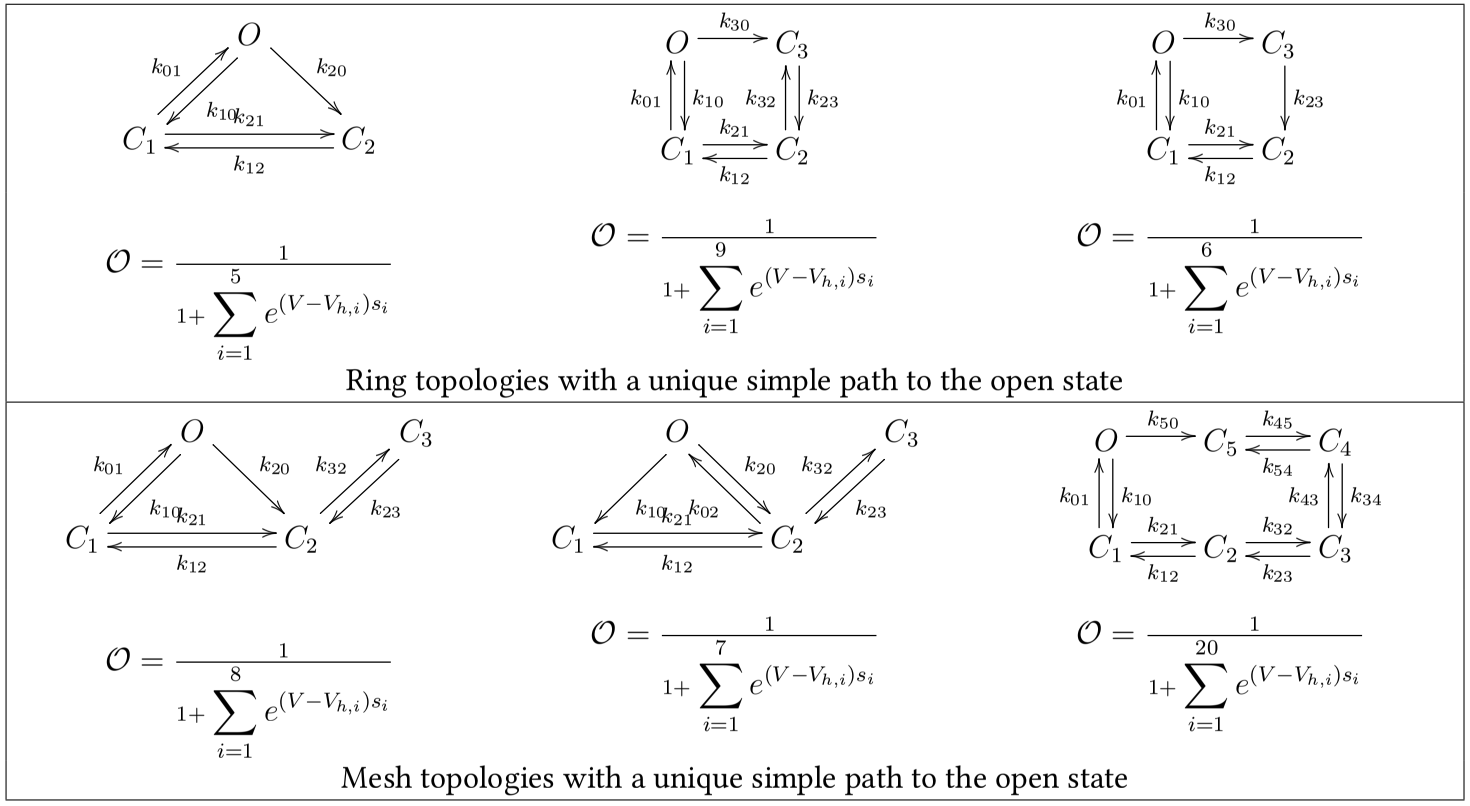

Figure 3.2: Examples of ion-channel topologies that satisfy the criteria of a unique simple path to the open state, continued

model needs to be minimized. The distance may be measured as square of the L_2 norm:

$$J(\mathrm{I^m}, \mathrm{I}(\mathrm{V^m})) = \|\mathrm{I^m} - \mathrm{I}(\mathrm{V^m})\|_2^2 = \sum_{j=1}^{m} \left(I_j^m - I(V_j^m)\right)^2$$

where $\mathrm{I}(\mathrm{V^m}) \in \mathbb{R}^M$ is the vector of ionic current predicted by the model, given membrane potentials in the vector $\mathrm{V^m}$. I_j^m and V_j^m are respectively the j^{th} position in vectors $\mathrm{I^m}$ and $\mathrm{V^m}$. Let g_{max} be the maximal conductance of the channel and V^*, the equilibrium potential of the ion transported by the channel. Mathematically, this optimization problem can be formulated as follows:

$$\min_{\{V_{h,i}\}_{i=1}^N, \{s_i\}_{i=1}^N, g_{max}} J(\mathrm{I^m}, \mathrm{I}(\mathrm{V^m})) \tag{3.23}$$

subject to the conductance expression:

$$I(V_j) = \frac{g_{max}(V_j - V^*)}{1 + \sum_{i=1}^{N} e^{(V - V_{h,i})s_i}} \quad \forall j = 1, .., m \tag{3.24}$$

and with bounds that are physiologically justified.

In this context, there are two significant facets of this optimization problem (i) Although the cost function is convex in $I(V_j)$, the voltage-dependence is non-linear and this can bring forth a possibility for non-convexity. (ii) The number of dominant conformations that the protein adopts is usually unknown and hence the order of the exponentials, N is unknown.

To guarantee that the global best fit to the data is achieved, an initial guess at the unknown constants should be carefully selected. It is possible to give an initial estimate of V_h values from the current-voltage characteristics, positioned centrally over the range of values at which the curve shows steady activation or inactivation. The steepness of the tangent drawn at this estimated voltage may be used as an initial estimate of the slope value. Alternatively, the recently developed global optimization Scatter Search based methodology, SSm GO [Egea et al., 2009], can be used. This algorithm combines a population-based metaheuristic method with a local optimization.

Regarding the number of exponentials, the aim is to curtail the number of conformational transitions so that it leads to minimum parameters to fit the data.

For this purpose an algorithm was implemented which calculates the global optimum for several order of exponentials until an accurate fit is obtained. As the problem is ill-posed, we impose a numerical restriction as the stop criteria for the optimizer. The algorithm starts at $N = 1$ and progressively increases until the best fit between the model and the data has a relative error less than ϵ times the original data. The measure considered is again the square of the L_2 norm and mathematically, this criterion may be formulated as:

$$J(\mathrm{I}^{\mathrm{m}}, \mathrm{I}(\mathrm{V}^{\mathrm{m}})) < \|\epsilon \mathrm{I}^{\mathrm{m}}\|_2^2$$

The choice of ϵ is subjective[3] and for all the cases we have considered, a good fit is obtained by setting $\epsilon = 0.10$.

Interestingly, for all these cases we have examined, a maximum of two exponentials, i.e. $N = 2$ was required. The data could be accurately fitted by using a two dimensional state space ($N = 1$) for simple symmetric data-plots, and for all other cases, a three dimensional state space ($N = 2$) could accurately explain the data (see figure 3.3). This would imply that, to a large extent, voltage gated ion-channels can be adequately modelled as dwelling predominantly among three different macro-states even if they are able to change between several conformations. The time that the protein dwells in some of these states may be considerably smaller than that of the three dominant conformations. The three macrostates may incorporate some of the effects of the minor conformations rather than completely negating their influences; as reflected from the data-fits.

With the above argument we propose the following equation for the open state probability corresponding to a three state system,

$$\mathcal{O}_{\mathrm{ss}} = \frac{1}{1 + e^{\left[(V - V_{h_1})s_1\right]} + e^{\left[(V - V_{h_2})s_2\right]}} \tag{3.25}$$

as a good approximation to represent the stationary probability of voltage gated ion-channels to remain open. The channel current may hence be calculated with the following equation:

[3]The optimizer included a global stochastic optimization, and a stop criteria was required on the basis of a "reasonable behaviour" with respect to our objectives. Since the problem that we pose to solve here poses uncertainty, the "reasonable behaviour" is quite subjective and we choose to stop the optimization by providing a numerical target.

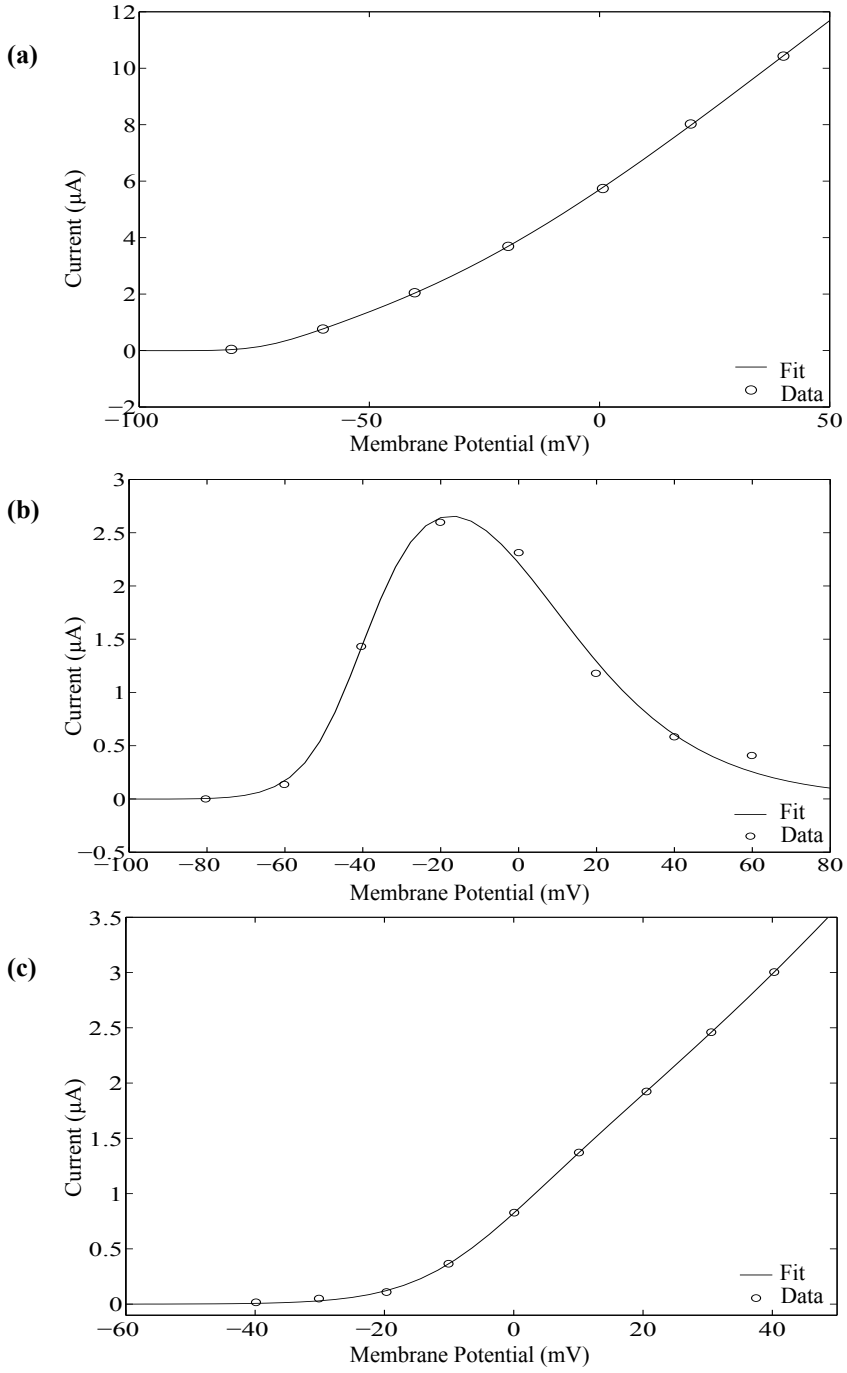

Figure 3.3: Steady state Current-voltage relations for KCNH5 (a), KCNH7 (b) and KCNB1 (c) class of potassium channels expressed in oocytes, from the study by Zou et al. [2003] fitted with equation 3.24

$$I_i = \frac{g_{max,i}(V - V_i^*)}{1 + e^{\{V - V_{h,1}(i)\}s_1(i)} + e^{\{V - V_{h,2}(i)\}s_2(i)}} \tag{3.26}$$

where, I_i is the channel current; V_i^*, the reversal potential of ion i; V, the membrane potential; $g_{max,i}$, the maximal conductance of the channel for the ion i and $V_{h,1}(i)$, $s_1(i)$, $V_{h,2}(i)$, $s_2(i)$ being the parameters for the activation function as defined by equation 3.25.

Fitting of experimental data to the model Most papers in the literature follow the voltage step protocol where steady-state voltage-current characteristics are obtained independently of the ion channel dynamics. Several were selected for utilizable data on single channel studies. We collect data from both, stationary conductance obtained from peak currents (with improved signal-to-noise ratio Beaumont et al. [1993]) or from raw steady-state measurements. Data were extracted from the published curves using the Enguage Digitizer 4.1. The digitized data sets were fit by equation 3.26. The global scatter search algorithm, SSm GO [Egea et al., 2009], implemented in MATLAB, was used for making the fits. The resulting data fits are presented in figures 3.3 and summarized in table 3.1. In all cases, with $N \leq 2$, we are able to represent the observed data using the model structure proposed.

Table 3.1: Parameters of current-voltage characteristics of a few ion-channels from Zou et al. [2003], fitted using equation 3.25

Figure	Channel type	V_{h_1} (mV)	s_1 (mV)	V_{h_2} (mV)	s_2 (mV)	g_{max} $(\mu A/mV)$
3.3a	$K_v10.2$	-64.5494	-0.17538	-29.4952	-0.02195	0.1009
3.3b	$K_v11.3$	-41.6897	-0.11727	-6.79872	0.053344	0.0630
3.3c	$K_v2.1$	40	-0.021769	3.51185	-0.13161	0.0476

Model Identifiability A mathematical model implemented for a biological phenomenon is assured to have uniquely estimated parameters if the model structure ensures identifiability [Walter and Pronzato, 1997]. Conventionally, ion-channel data has limited interpretations by producing indistinguishable models [Kienker, 1989]. In-silico representation of ion-channel dynamics has yet to come up with a model for the reason that the model structure needs to be tweaked each time to incorporate experimental observation. This indeed is a question of parameter identifiability. The model presented in this thesis, is

found to have *structurally output locally identifiable (s.o.l.i)* parameters (see A.2 for formal definition), according to the following lemma.

Lemma 2 *The model for ion channel open state probability described by means of a Markov chain with three macro-states [equation (3.25)] is s.o.l.i by the Taylor approximation of fourth order.*

Proof: see A.2

3.3.4 The Thermodynamic Approach

The estimation of the open-state probability of voltage-gated ion channels to an equation of the form (3.22) is equivalent to a steady-state approximation of the Hodgkin-Huxley formalism. However, as we seek to look beyond the Hodgkin-Huxley formalism for a good mechanistic description, the given model need to be compared with efforts made to represent the system on a realistic perspective. A thermodynamic formalism comes close to this requirement. Although the fundamentals are in place, such models [Destexhe and Huguenard, 2000] show very poor performance in even small extrapolations from the given data (Figure 3.4). We would also argue that the biophysical basis of the multiple conformation model is much clearer than that of a Taylor's series dual conformation model used in the thermodynamic formalism [Destexhe and Huguenard, 2000; Ozer, 2004].

Ozer [2004, 2007] modified the non-linear model to a functional form by lumping the different transitions in the protein to a single event. The model, which uses a sum of Gaussian distributions, seems to give the best fit for experimental data. The steady-state open probability of ion-channels, written with respect to this model, may be arrived using equation (8) of Ozer [2007] as,

$$\mathcal{O} = \frac{1}{1 + \frac{\sum_{i=1}^{n} \alpha_{0,i} e^{[(V - V_{\alpha,i}) s_{\alpha,i}]^2}}{\sum_{i=1}^{n} \beta_{0,i} e^{[(V - V_{\beta,i}) s_{\beta,i}]^2}}} \tag{3.27}$$

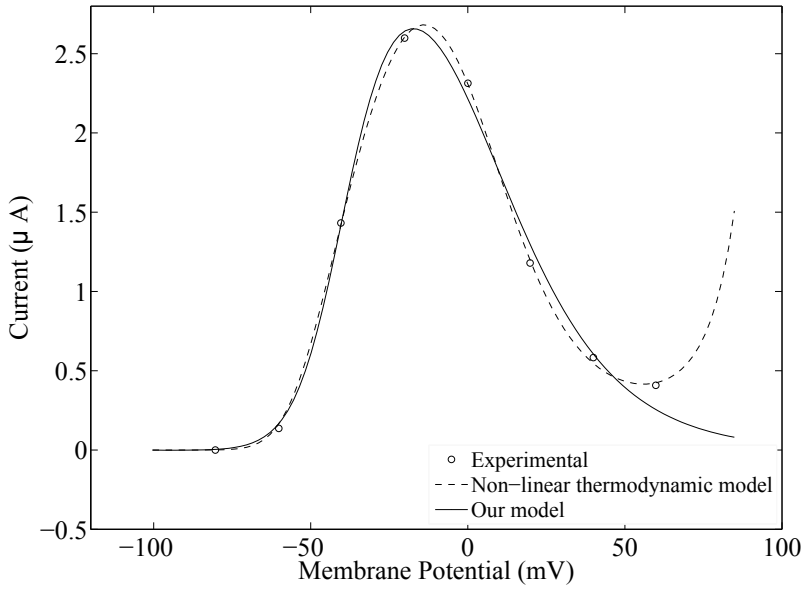

Figure 3.4: Current-voltage relationship of ion-channels obtained from the studies of Zou et al. [2003] fitted with a third order non-linear model and our model presented in equation 3.24. The non-linear model appear to overfit the data. On extrapolation the non-linear model behaves worse because in this particular case, the channel is not expected to conduct at higher membrane potentials.

where, n was defined as the number of distinct transitions defined by different energy barriers. It should be noted that Ozer [2007] was also able to get acceptable fits with two transitions. The problem with this model, however, seems to be in the existence of practically unidentifiable parameters, as is the case with majority of the existing Markov Models [Fink and Noble, 2009]. Further, if no manipulation is carried out to collect groups of parameters that are not identifiable only with stationary data, the model requires the fitting of a minimum of twelve parameters (provided two macro-transitions ($n = 2$) gives an acceptable fit).

3.3.5 A different approach towards modelling membrane ion-conduction

The different modelling paradigms in the literature that are popular with electrophysiologists have their basis in the equivalent circuit representation popu-

larised by Hodgkin and Huxley. But there are certain observations with respect to neuronal electrophysiology that these models do not explain [Heimburg, 2010b]. This includes

- Mechanical activation of neurons [Heimburg, 1998].
- Changes in membrane dimension observed with an action potential [Iwasa et al., 1980].
- Axonal propagation of action potential [Heimburg and Jackson, 2005].
  - These models assume that in unmyelinated axons a steadily propagating solution exists, in which the shape of the voltage spike is preserved in time
- Reversible Heat:
  - According to Hodgkin-Huxley, there should always be heat dissipation (Ions moving from a region of high energy to low energy), which is much larger than the capacitive energy of the pulse. Experimentally the net heat release is found to be negligible [Ritchie and Keynes, 1985].
- Effect of anaesthetics on neuronal transmission [Overton, 1901].

These observations suggest several questions with respect to the modelling of neuronal activity: (a) Does a constant membrane capacitance make sense? (b) Is the transport of ions across the membrane fast enough to account for the speed of nerve pulse propagation (c) Is the Hodgkin-Huxley formalism consistent with the underlying thermodynamics? (d) Is neuronal activity really an ion-channel phenomenon?

The last question is based on an observation that the lipid membrane itself can conduct, subject to mechanical and electrical perturbations. Furthermore, this conduction shows quantized current events, which is typical of ion-channels. Also, the ionic permeability is observed to increase greatly at the melting temperature of the membrane [Papahadjopoulos et al., 1973], as well as by doping the membrane with a few different proteins such as gramicidine A [Ivanova et al., 2003].

These observation have led Heimburg [2010a], to a totally different paradigm for modelling ion-channels. According to this theory, ion-channels are formed by the physical changes observed in the lipid membrane in response to changes in a few different thermodynamic variables around its melting transition. This observation is based on the fact that lipid membranes have transition temper-

atures close to physiological temperatures. Protein-lipid interfaces are regions experiencing high fluctuations and the hydrophobic interactions between the proteins and membrane can influence the melting behaviour in these interfaces. Accordingly, a protein with a large hydrophobic matching length gives maximum likelihood of channel formation.

The theory is yet to gain ground in the area of membrane electrophysiology. However, it remains a fact that no experiments have ever been conducted on protein ion-channels in the absence of lipid membrane. If further experimental work confirms this model of condution, it will take some time to develop a proper mathematical model for this type of ionic conduction.

3.4 A model for channel conduction appropriate for describing the neuronal membrane system

From what we have seen so far, the transmembrane potential remains the most significant determinant of ion channel activity. The relationship of voltage and the dynamics of ion-channels is complex and for this reason, there have been numerous interpretations of this activity by different approaches. The predominant approach for modelling ion-channels in the past years have been based on the Hodgkin-Huxley approach. Although several models that were developed since this model had better description of the mechanisms involved, the Hodgkin-Huxley model remains the primary choice for many in the study of neuronal physiology. This is essentially due to its ease of use and the relatively small number of unknown parameters needed to describe the channel behaviour.

Suggested alternatives for the Hodgkin-Huxley model also involve similar kinetic formalisms. Although there are other approaches emerging in this area of study (for example, the lipid-ion channel model, see 3.3.5), they are yet to reach maturity and need experimental validation. The utility of these models depend on their predictive capabilities, as a good model with its estimated parameters should describe the channel dynamics well, even outside the range in which the experiments are conducted. Thus experimental conditions along with model formulation dictate the parameters estimated and in most cases,

limit the model's ability to predict channel dynamics. From this perspective, single-channel recordings have been considered as the best approach to explore channel kinetics [Sakmann and Neher, 2009]. However, the recordings and analysis of this method is found to be extremely difficult. Further, as discussed previously, when there are sufficiently large number of channels on the membrane, continuous deterministic models can easily approximate such phenomena which otherwise require a stochastic model.

To develop a typical representation for the activity at a neuron's membrane, we need to consider many different ion-channels. Since it remains an ambitious procedure to experimentally determine the kinetic parameters for the activity of a single type of ion-channel, determining the same for a set of channel types becomes very complex. As a result, when models are developed to represent neuronal activity, investigators frequently tend to use established models of channel gating for that particular channel type from the literature. Hodgkin-Huxley gating models appear to be the most popular in this respect on account of vast data that has been generated with experiments designed on this concept. In spite of the fact that the experiments need not necessarily be on the same tissue type or physiological condition, such adaptations have given reasonable representation of the electrophysiology in many neuron types. For our case, of developing a model for *SNc* membrane electrophysiology, as we do not have access to wet lab experiments, appropriate models and data in the literature are used for the respective ion channels.

In our model for *SNc* neurons, we aim to have a model which gives an appropriate abstraction of the dynamics of ions involved in its characteristic electrophysiology. For the current equation, we prefer the use of the electrodiffusion equation (equation 3.11) of ionic conduction, since it is a more realistic representation of ion flow dynamics than the linear conductance relationship (equation 3.9). However, most models in the literature for various ion-channels have their models for channel gating parametrised using the linear conductance relationship. It is therefore important to know if the use of such parameters with the electrodiffusion model yields some advantage.

Figure 3.5 shows the difference in the response of models with the same gating equations and parameters, but with the two different current equations, in the

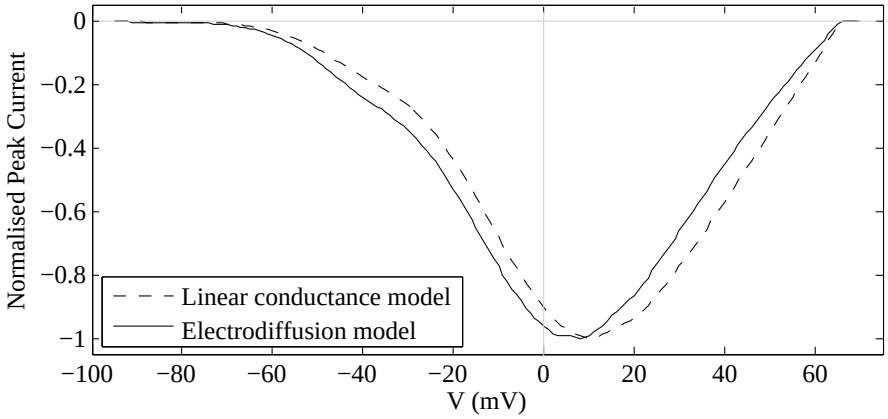

Figure 3.5: Comparisson of responses when two different forms of the current equation was used along a gating scheme of the Hodgkin-Huxley model. Normalised peak inward currents of sodium channels are plotted against the applied test potential, for a command voltage involving a holding potential of -100 mV and depolarizing voltage pulses at the test potential of 5 ms duration.
The gating of this fast transient Na^+channel is described by the Hodgkin-Huxley approach with,
$m_\infty = \frac{1}{1+\exp(-(V+40)/15)}$
$\tau_m = 0.04 + 0.46\exp\left(-(V+38)^2/900\right)$
$h_\infty = \frac{1}{1+\exp((V+62)/7)}$
$\tau_h = 1.2 + 7.4\exp\left(-(V+67)^2/400\right)$ [Izhikevich, 2007]

same physiological environment. The gating parameters have supposedly been estimated with the linear conductance relationship. There is an apparent difference in the response between the two current expressions and it would require a different set of parameters with the electrodiffusion equation to get a similar response of the linear relationship. Consequently, in the larger model that we develop for the dynamics at the *SNc* membrane, for channels using gating parameters estimated with the linear conductance relation, the same relation (equation 3.9) is used for obtaining the channel current. For all other cases, we employ the electrodiffusion relationship (equation 3.11).

3.5 Gating of Ligand-gated ion channels

Ligand gated ion-channels are transmembrane allosteric proteins that respond to the binding of an activator molecule (often a neurotransmitter or Ca^{2+} ion)

by opening a pore that enables the free diffusion of a selected ion. In neurons, such channels are mostly localised near synapses and play an important role in neurotransmission.

Although there are a few different types of ligand gated channels found on neuronal membranes, we concentrate on channels that have a role in the generation and sustenance of spontaneous oscillations. Ligand gated channels on the dendrites, such as the NMDA receptor, have a major role in neuron to neuron synaptic transmission. In this thesis, we aim to develop a model for the spontaneous pacemaking in *SNc* neurons and for this we use recordings obtained from an experiment with an acutely isolated neuron. As the *SNc* neurons are isolated they tend to lose minor dendrites and thus are free from the influence of above mentioned ligand gated channels found at the synapses. Hence, such ligand gated channels are not considered further.

3.5.1 Calcium gated channels

Calcium-activated potassium channels are gated by intracellular calcium ions, thereby coupling intracellular calcium levels and membrane potential. During the refractory period, the slow afterhyperpolarization that follows an action potential is driven by the activation of calcium-activated potassium channels. Afterhyperpolarization limits the firing frequency of repetitive action potentials (spike-frequency adaptation) and is essential for normal neurotransmission [Xia et al., 1998].

SNc dopaminergic neurons have at least two forms of potassium currents that are controlled by intra-cellular calcium [Silva et al., 1990; Moran et al., 2006]: (i) the apamin - sensitive, small-conductance (SK), calcium - activated potassium current and (ii) the apamin - insensitive large-conductance (BK) calcium - activated potassium current that is blocked by tetraethylammonium. The BK channel current is less important for producing the slow underlying oscillations as they are less sensitive to cytosolic calcium and are hence excluded from our model.

SK channels are voltage-independent and activated by sub-micro molar concentrations of intracellular calcium, and are not gated by calcium binding di-

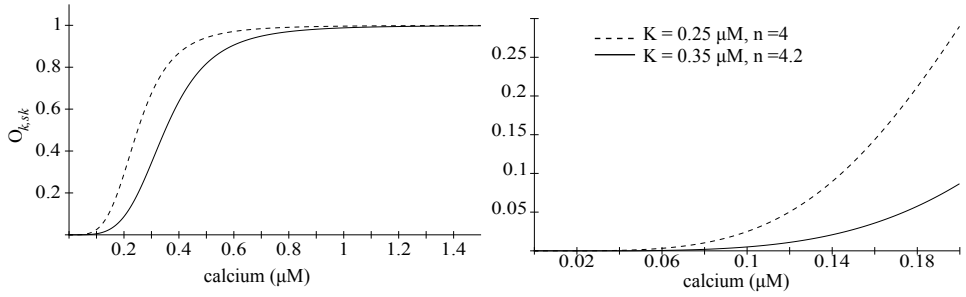

Figure 3.6: Comparison of the steady state response of the SK-type potassium channel using the parameters from two different observations. Broken lines represent response using parameters from Kuznetsova et al. [2010] and straight lines represent response using parameters from Xia et al. [1998]. The figure on the right is an expanded view of the region of interest.

rectly to the channel α-subunits. Instead, the functional SK channels are heteromeric complexes with calmodulin, which is associated with the α-subunits in a calcium-independent manner [Xia et al., 1998]. These two components are thought to have been structurally and functionally paired at an early stage of eukaryotic evolution. Hence it can be reasonably assumed that calcium indirectly controls the functioning of these channels via calmodulin.

A popular way of modelling SK-channel gating is by using the Hill expression [Wilson and Callaway, 2000]:

$$\mathcal{O}_{k,sk} = \frac{Ca_i^n}{K_{0.5}^n + Ca_i^n} \tag{3.28}$$

Prior attempts to model the pacemaking of dopaminergic neurons [Wilson and Callaway, 2000; Kuznetsova et al., 2010] have employed $K_{0.5}$ of 0.25 μM and a Hill coefficient (n) of 4. An experiment conducted on SK channels co-expressed with calmodulin [Xia et al., 1998], suggests parameters of $K_{0.5}$ = 0.35 μM and a Hill coefficient = 4.2. A comparison of response generated by using these parameters are given in figure 3.6. Although the model show similar response at high Ca^{2+} concentration, at the expected range of Ca^{2+} concentration (0.01μM - 0.15μM) the picture is different. The model with parameters obtained in the presence of calmodulin responds slowly to increasing Ca^{2+}, which is expected of a secondary influence.

Chapter Summary In this chapter, we have presented aspects of modelling passive ion transport on neuronal membrane, through ion-channels. From the seminal work of Hodgkin and Huxley [1952], ion-channel research has evolved to diverse paradigms of representing this protein activity. However, a representative model incorporating major characteristics is still elusive. Despite being mechanistically limited the Hodgkin-Huxley models traditionally enjoy wide acceptance and a huge knowledge-base has been developed for different ion-channels based on this approach. In this chapter, we have also attempted at developing a reduced Markov representation of ion-channel dynamics, but needs actual experiments to analyse its utility. Some of the concepts discussed in this chapter shall be put to use in subsequent chapters for developing a framework to describe the pacemaking activity of *SNc* neurons.

CHAPTER 4

Elements of facilitated transport and calcium metabolism

This chapter discusses components of the model that are responsible for facilitated and active transport across the membrane (pumps and exchangers) as well as cellular elements responsible for handling calcium

In the previous chapter we discussed ion-channels, that is, passive transporters of ionic species. When materials are transported in and out of the cell, it is important to retain a functional state that is characteristic to the cell. In particular, when the transport of ions has been the result of a stimulus, it is essential to transfer back some of the ions to allow the cell to revert to the original operating state. Again, when the ionic species in question is an entity like calcium, which has an important signalling role within cells; there should be mechanisms by which concentrations are restricted to levels required for normal functioning. In this section, we consider some of the important carrier proteins significant to our model. We also examine some of the mechanisms that are important in calcium homeostasis.

Facilitated transport in excitable cells Extrusion of cations from cells against their gradient eventuates essentially by two transport mechanisms. Calcium ATPases of the plasma membrane (PMCA) and endoplasmic reticulum (ERCA

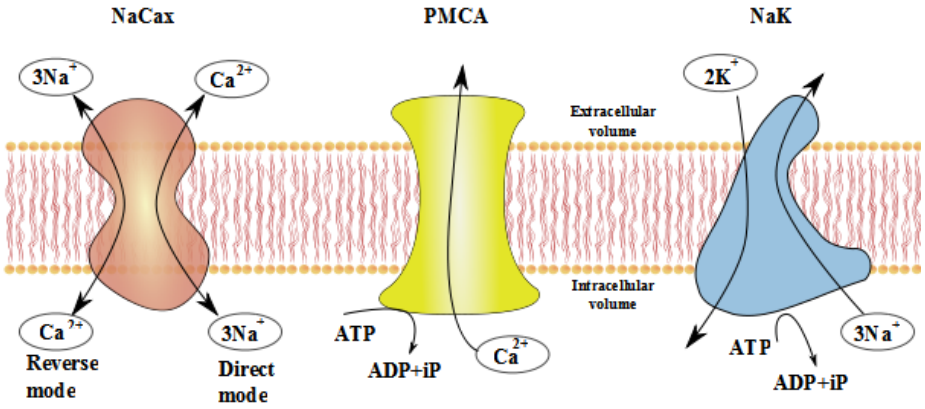

Figure 4.1: A cartoon illustrating transporters on the plasma membrane.

or SERCA[1]) are active transporters which expel calcium from the cytoplasm with energy from the hydrolysis of ATP (figure 4.1). Likewise, the sodium-potassium (NaK) uses the energy from ATP hydrolysis to transport sodium and potassium ions against their gradient. On the other hand, plasma membrane sodium-calcium exchanger (NaCax) and mitochondrial sodium-calcium exchanger (NaCam) are 'anti-porters' which utilize the gradient of sodium to extrude calcium. A third mechanism exists in the mitochondria to transport calcium released from the endoplasmic reticulum into its inner matrix. The mitochondrial uniporter opens in response to a stimulus and allow the free flow of calcium along its gradient.

The PMCA are a high-affinity calcium removal system that makes up for small and moderate changes of calcium concentration from its control level. Excessive changes in calcium levels are however handled by the low affinity NaCax. Again, the activation of PMCA is comparatively slow and hence the relative contribution of NaCax to calcium removal is more important during the early stages of calcium increase [Sedova and Blatter, 1999]. Further in this section, we detail the functional aspects of these transport processes from an energetic perspective.

[1]SERCA is the calcium pump on the sarcoplasmic reticulum (SR), the ER found in smooth and striated muscles, which mostly function as a Ca^{2+} handling organelle. The calcium ATPases of the ER are conventionally named SERCA as they were first studied in muscle cells.

4.1 Energetics of exchange

The free energy changes in a system are directly related to the changes in its molecular components. The first derivative of the Gibbs free energy with respect to the molar concentration of component 'n_i' at constant temperature and pressure $\left(\left[\frac{\partial G}{\partial n}\right]_{T,p}\right)$, is called its chemical potential μ_i (for neutral species) or the electrochemical potential, $\bar{\mu}_i$ (for charged species). In the presence of an electric field of potential Φ, the electrochemical potential of an ionic species 's' is given by [Schultz, 1980],

$$\bar{\mu}_s = \mu_s^0 + RT \ln[s] + z_s F \Phi$$

where μ_s^0 represents the standard chemical potential, R the gas constant, T the ambient temperature, z_s the valency of s, $[s]$ the concentration of s and F Faraday's constant. Electrochemical potential is a measure of energy and its difference acts as the driving force for the transport of molecules across a given cross-section. Ionic transport across a membrane [Nelson and Cox, 2004] is driven by the electrochemical gradient that exist along its thickness and a transport against this gradient requires energy.

The energy required to translocate any ion s, from the cytosol (i) to the extracellular environment (e) is given by the difference in the electrochemical potentials of the species across the membrane, or

$$\Delta G_s = \bar{\mu}_{s,e} - \bar{\mu}_{s,i} = RT \ln \frac{s_e}{s_i} - z_s F V.$$

The term V is the membrane potential, which is the difference in electrical potential between the interior and the exterior of a biological cell. The first term can be written in terms of the Nernst potential of the ion ($\hat{\mathcal{V}}_s$) and hence we have,

$$\Delta G_s = z_s F \left(\hat{\mathcal{V}}_s - V\right). \tag{4.1}$$

For the case of co-transport, consider the transport of the ion s_1 coupled to the transport of a second ion, s_2. The transport of the ion s_1 is against its gradient, say from the interior to the exterior of the cell where there is a higher concentration of s_1. The energy that this process requires is gathered from the free energy gain associated with transport of s_2 in the direction of its gradient.

For the transport to be favourable the energy gradient for s_2 should be greater than the gradient of s_1, or,

$$n_{s_2}\Delta G_{s_2} > n_{s_1}\Delta G_{s_1},$$

where n_s represents the moles of s transported. If "$\Gamma_{s_1 s_2}$" is the coupling coefficient for the exchange (moles of s_2 exchanged per mole of s_1 transported), we have

$$z_{s_2}\Gamma_{s_1 s_2}(\hat{\mathcal{V}}_{s_2} - V) > z_{s_1}(\hat{\mathcal{V}}_{s_1} - V).$$

For transporters that are molecular pumps (ATPases), the energy consumed per pump cycle is determined from the ratio of the concentrations of MgATP[2] to its hydrolysis products:

$$\Delta G_{\text{MgATP}} = \Delta G^0_{\text{MgATP}} + RT \ln \frac{[MgADP][Pi][H^+]}{MgATP}. \tag{4.2}$$

$\Delta G^0_{\text{MgATP}}$ the free energy under standard conditions, is related to the equilibrium constant for the hydrolysis reaction according to

$$\Delta G^0_{\text{MgATP}} = -RT \ln K_{\text{MgATP}}.$$

Under normal physiological conditions of living cells ΔG_{MgATP} is negative, implying a release of energy.

Most often the transport of cations by ATPases is a co-transport. For example, the sodium pump co-transports both $Na^+$and K^+ions against their gradient. Calcium ATPases antiport a proton

$$\Delta G_{\text{pump}} = \xi_1 \Delta G_{s_1} + \xi_2 \Delta G_{s_2}$$

where ξ_1/ξ_2 is the coupling ratio of transport. Under normal physiological conditions when $[-\Delta G_{\text{MgATP}} < \Delta G_{\text{pump}}]$, the pump runs in the forward direction. When the free energy of hydrolysis drops such that $\Delta G_{\text{MgATP}} + \Delta G_{\text{pump}} = 0$, transport ceases as equilibrium is reached. When this total energy become negative, the pump reverses and the electrochemical gradient of the ions can be used to generate ATP. This is a condition that exists for ATP production

[2]ATP is mostly ionized in solution and in cells they exist mostly as a complex with Mg^{2+}. MgATP is the biologically active form of ATP.

in the proton pumps of the mitochondria. For the plasma membrane ATPases this may be achieved only by manipulating the ion concentrations to abnormal levels. This has been demonstrated for the sodium-potassium pump in an experiment on erythrocytes [Glynn and Lew, 1970].

Factors influencing the rate of transport Although the rate of transport is often dictated by the energy limits imposed by thermodynamics, there may be other factors that need to be accounted for. Most mathematical models are limited by the experiments they are based on, and no model to date accounts for all the phenomena relevant to transporter kinetics. Some of the key features that may influence a transporter model include:

- The affinity of the cations and counter-ions to the binding site
- The voltage dependent transition : Kinetic models developed for transporters using Markov jump schemes usually lump the voltage dependence on select transitions
- The sequence of binding
- Presence of secondary modifiers that alter the binding rate (eg. Ca^{2+} binding on PMCA is modulated by calmodulin)
- Allosteric modulation of these enzymes by the cations themselves (eg. intracellular Ca^{2+} modulate NaCax)
- Modulation by metabolites (eg. Glucose modulates NaK)
- Modulation by pH

In the following sections, we discuss the three transporters (NaCax, NaK and PMCA) with a major role in the electrophysiology of neuronal membranes. The functioning of these proteins have been described by a few different mathematical formalisms that are either empirical or mechanistic. We give a basic comparison of these models and look for an apt representation that may be used in our model for *SNc* pacemaking.

4.2 The sodium calcium exchanger

NaCax is an antiporter responsible for transporting calcium across a membrane against its gradient by using the electrochemical gradient of sodium. In the

calcium exit mode, the exchange is defined as an external sodium (Na_e) dependent calcium efflux, which implies a process of Ca^{2+} extrusion constrained by the binding of $Na^+$to the outward facing side of the protein. The hydrolysis of ATP is not required to power the calcium extrusion directly, although it is necessary to maintain sodium gradient. Moreover, cytosolic ATP seems to slightly influence the kinetics by phosphorylating the exchanger and altering its affinity for the ions [Blaustein and Lederer, 1999].

Scheme of events for NaCax exchange : Structural studies of the exchanger suggests the existence of two major conformational states for the protein [Liao et al., 2012]. In the first state, the calcium binding site faces the interior of the cell and in the second state, the calcium binding site faces the exterior. Such observations suggest a cyclic, ping-pong-like enzyme mechanism in which extracellular sodium and intracellular calcium bind alternatively as the exchanger cycle progresses [Kappl et al., 2001; Fujioka et al., 2000].

Coupling ratio : It has been long understood that the efflux of Ca^{2+} was activated by the cooperative action of more than two Na^+ions [Blaustein, 1974]. Further experiments on cardiac cells confirmed that the coupling ratio between $Na^+$and Ca^{2+} was greater than 2, suggesting the exchange to be electrogenic [3]. Various experiments aimed at establishing the stoichiometry have suggested a coupling ratio of 3 Na^+:1 Ca^{2+}. In some rare cases a ratio of 4 Na^+: 1 Ca^{2+} has been observed [Mullins, 1979].

Total change in the Gibb's free energy. For a coupling ratio of 3 Na^+:1 Ca^{2+}, we have $\Delta G_{\text{exchanger}} = 3\Delta G_{\text{Na}} - \Delta G_{\text{Ca}}$ and hence by equation 4.1, we have

$$\Delta G_{\text{naca}} = F(3\hat{\mathcal{V}}_{Na} - 2\hat{\mathcal{V}}_{Ca} - V) = F(\hat{\mathcal{V}}_{\text{naca}} - V). \tag{4.3}$$

Here, $\hat{\mathcal{V}}_{\text{naca}}$ is the effective reversal potential, a resultant of the gradient of sodium in the forward direction and the gradient of calcium in the reverse

[3] A transport of cations is said to be electro-neutral when the flow of charges in one direction is balanced by the counterflow of an equal number of charges in the opposite direction. Otherwise the transport is said to be electrogenic

direction and the difference, $\hat{\mathcal{V}}_{\text{naca}} - V$, gives the apparent driving force for transport. Calcium efflux would be favoured when $\hat{\mathcal{V}}_{\text{naca}} > V$ and in the opposite case, calcium entry to the cell would be favoured. When a neuron is not excited, $\hat{\mathcal{V}}_{\text{naca}}$ is more positive than the resting membrane potential; the exchanger will work in calcium extrusion/ sodium influx mode in resting neurons. During an action potential NaCax briefly works in calcium entry/ sodium exit mode, as the membrane potential changes significantly.

Voltage Dependence : The binding of the individual cations to the exchanger is generally considered voltage independent (although mobility of cations, along with the binding and associated changes in protein conformation, are to some extent influenced by the changes in the voltage across the membrane) and these steps are mostly defined by the ion-protein affinity. Models of the exchanger that use the Markov scheme, usually assign the voltage dependence to steps that involve a major conformational change of the protein.

For a full elementary charge crossing the electric field with a single-rate limiting transition, the voltage dependence of Na^+-Ca^{2+} exchange currents have been observed to be less steep than one would expect from Eyring's transition-state theory [Eyring, 1935],

$$\text{rate} \propto \exp\left(\frac{eV}{RT}\right).$$

Most models of the exchanger incorporate a parameter δ, to accommodate this observation.

$$\text{rate} \propto \exp\left(\frac{\delta eV}{RT}\right).$$

The parameter δ has been best explained as an entity that represents the position of the energy-barrier located asymmetrically in the electric field of the cell membrane. Based on their experimental observations, Niggli and Lederer [1993] notes a difference in values for the energy-barrier position parameter δ, in the forward and reverse directions. Accordingly the report indicates that a single asymmetrically located energy barrier is not sufficient to explain the molecular mechanism of the exchanger. This suggests a need for having distinct voltage dependent steps in the conformational change of the protein and

strongly supports the existence of a cyclic mechanism, which we later adopt in the ping-pong model.

Dependence on intracellular Ca^{2+}: The concentration of Ca^{2+} within the cell is quite small, and hence it is quite possible that the net rate of transport is limited by the binding of intracellular calcium to the transporter. Further, there is evidence for the transporter being activated at an allosteric site by intracellular Ca^{2+} [Bers et al., 2003]. This allosteric activation[4] to some extent biases the exchanger to operate in the forward mode. Also recent evidence (e.g. [Beaugé and DiPolo, 2009]) points to the significance of this regulatory mechanism in establishing the ping-pong exchange scheme.

Dependence on extracellular Ca^{2+} and Na^{+}: At the extracellular facing side of the protein the existence of competitive binding between Ca^{2+} and Na^{+}has been reported in Blaustein and Lederer [1999].

Dependence on intracellular Na^{+}: Na^{+}seems to inhibit the exchanger at high concentration at the intracellular side as noted in some experiments [Blaustein and Lederer, 1999]. However, in these experiments concentrations used are way beyond what would be observed in normal physiology. For this reason, this effect need not be considered for modelling the exchanger under the normal physiological range of Na^{+}.

4.2.1 Mathematical models of sodium-calcium exchange

Research on ion-transport across membranes is dominated by studies on ion-channels and for this reason, the standards of experimenting and modelling are based on the research on these entities. Modelling facilitated transport of antiporters, such as sodium-calcium exchangers, is a little more complicated, and experiments on the lines of ion-channels that are conducted for such proteins offer limited insights to their function. The various features that we have

[4] Allosteric activation refers to the activation of a protein by an effector molecule at a site other than its active site.

discussed above cannot easily be incorporated in such models. For this reason, the functioning of these proteins are expressed in different ways. Such models are often an outcome of attempts at modelling cardiac pacemaking and may be typically empirical such as the popular model of Luo and Rudy [1994] or phenomenological as the Kyoto model [Matsuoka et al., 2007]. In this section, we discuss some of the popular attempts to represent exchanger function.

Quantitative models of sodium calcium exchange predict the exchanger current to be the difference between the unidirectional calcium fluxes or

$$I_{\text{naca}} = \kappa_{\text{naca}} \left(\text{Calcium influx - Calcium efflux}\right).$$

For the exchanger, with a transport stoichiometry,

$$3Na_e^+ + Ca_i^{2+} \underset{\beta}{\overset{\alpha}{\rightleftharpoons}} 3Na_i^+ + Ca_e^{2+},$$

the transport is defined by the concentration differences of $Na^+$and Ca^{2+} across the membrane. Most models of NaCax takes into account the dependence of such transitions on the electric field, represented by the membrane potential V. In general, we may relate the activation energy for this transition to voltage based on Eyring's rate theory [Eyring, 1935] and thus, rates of calcium transport are represented as,

$$\begin{aligned}\left[\frac{dCa}{dt}\right]_{\text{entry}} &= \beta Na_i^3 Ca_e \\ &= \lambda Na_i^3 Ca_e \exp\left[\frac{\delta V}{\hat{\mathcal{V}}_\tau}\right]\end{aligned}$$

and

$$\left[\frac{dCa}{dt}\right]_{\text{efflux}} = \lambda Na_e^3 Ca_i \exp\left[\frac{(\delta-1)V}{\hat{\mathcal{V}}_\tau}\right],$$

where δ is a factor due to the position of the energy barrier located asymmetrically in the electric field of the membrane. An approximate value for δ is 0.35 [Luo and Rudy, 1994].

Hence,

$$I_{\text{naca}} = k_{\text{naca}} \left(Na_i^3 Ca_e \exp\left[\frac{\delta V}{\hat{\mathcal{V}}_\tau}\right] - Na_e^3 Ca_i \exp\left[\frac{(\delta-1)V}{\hat{\mathcal{V}}_\tau}\right]\right). \tag{4.4}$$

DiFrancesco-Noble model This popular model is a simplification of an earlier model by Mullins [1977]. In Mullins' model, an analytical expression for the exchange is developed from a model that requires binding of Na^+onto the carrier protein, to induce Ca^{2+} binding and subsequent translocation. The expression provides a quantitative description of the Ca^{2+} fluxes for the system at equilibrium.

The elaborate mathematics of the Mullins model is simplified by DiFrancesco and Noble [1985] for their model on cardiac pacemaking. In this model, with a coupling ratio of 3, the exchanger current may be represented by,

$$I_{\text{naca}} = \kappa_{\text{naca}} \frac{\exp\left(\delta \frac{V}{\mathcal{V}_\tau}\right) Na_i^3 Ca_e - \exp\left((\delta - 1)\frac{V}{\mathcal{V}_\tau}\right) Na_e^3 Ca_i}{\left(1 + \mathcal{D}_{\text{naca}}\left[Na_i^3 Ca_e + Na_e^3 Ca_i\right]\right)\left(1 + \frac{Ca_i}{0.0069}\right)}. \tag{4.5}$$

In these equations δ (approximately 0.35) is the position of the energy barrier that controls the voltage dependence of the exchanger. $\mathcal{D}_{\text{naca}}$, the denominator factor for sodium-calcium exchange current, has a value of 0.001 in the model.

Luo-Rudy model According to Luo and Rudy [1994], DiFrancesco and Noble model does not correctly represent the dependence on external $Na^+$and Ca^{2+}. Furthermore, it does not consider the saturation of the exchanger current at very negative potentials. Their modification of the D-N model is as follows,

$$\begin{aligned} I_{\text{naca}} = \kappa_{\text{naca}} & \frac{1}{K_{\text{m,Na}}^3 + Na_e^3} \frac{1}{K_{\text{m,Ca}} + Ca_e} \frac{1}{\left(1 + \mathcal{K}_{\text{sat}} \exp\left((\delta - 1)\frac{V}{\mathcal{V}_\tau}\right)\right)} \\ & \left[\exp\left(\delta \frac{V}{\mathcal{V}_\tau}\right) Na_i^3 Ca_e - \exp\left((\delta - 1)\frac{V}{\mathcal{V}_\tau}\right) Na_e^3 Ca_i\right], \end{aligned} \tag{4.6}$$

where the parameters $K_{\text{m,Na}}$ and $K_{\text{m,Ca}}$ are the respective dissociation constants of external $Na^+$and Ca^{2+} (87.5 mM and 1.38 mM respectively); $\mathcal{K}_{\text{sat}}$ is a saturation factor and δ is the position of the energy barrier.

The saturation effects observed by Luo and Rudy are later critiqued by Niggli and Lederer [1993] as an error in conclusion made from experimental observations. They account for the saturating effects observed in these experiments by correlating it with changes in sub-sarcolemmal calcium concentrations due to physical diffusion limits.

Endresen model Endresen et al. [2000] put forth a model that is derived directly from free energy considerations. His model may be derived from the general equation (equation 4.4) for the sodium-calcium exchange with a value of $\delta = 0.5$

In this case, the equation 4.4 may be written as

$$\begin{aligned} I_{\text{naca}} &= k_1 \sqrt{Na_e^3 Na_i^3 Ca_e Ca_i} \left[\frac{Na_e^{\frac{3}{2}} Ca_i^{\frac{1}{2}}}{Na_i^{\frac{3}{2}} Ca_e^{\frac{1}{2}}} \exp\left(\frac{0.5V}{\hat{\mathcal{V}}_\tau}\right) - \frac{Na_i^{\frac{3}{2}} Ca_e^{\frac{1}{2}}}{Na_e^{\frac{3}{2}} Ca_i^{\frac{1}{2}}} \exp\left(-\frac{0.5V}{\hat{\mathcal{V}}_\tau}\right) \right] \\ &= k_1 \sqrt{Na_e^3 Na_i^3 Ca_e Ca_i} \left[\exp\left(\frac{V - 3\hat{\mathcal{V}}_{Na} + 2\hat{\mathcal{V}}_{Ca}}{2\hat{\mathcal{V}}_\tau}\right) - \exp\left(-\frac{V - 3\hat{\mathcal{V}}_{Na} + 2\hat{\mathcal{V}}_{Ca}}{2\hat{\mathcal{V}}_\tau}\right) \right] \\ &= k_{\text{naca}} \sqrt{Na_e^3 Na_i^3 Ca_e Ca_i} \sinh\left(\frac{V - 3\hat{\mathcal{V}}_{Na} + 2\hat{\mathcal{V}}_{Ca}}{2\hat{\mathcal{V}}_\tau}\right). \end{aligned}$$

Kyoto model The Kyoto model [Matsuoka et al., 2007] of transport of Ca^{2+} and Na^+ions across the exchanger involves the transition of the protein among six different protein binding states. States E_1 and E_2 correspond to the two different conformation of the protein. State $E_2^\dagger$ is achieved with the binding of Na^+on E_2 at the extra-cellular binding site. With sufficient activation by the external electric field, the protein changes conformation to $E_1^\dagger$ exposing the bound $Na^+$to the intra-cellular space. Dissociation of the bound Na^+yields state E_1. Intracellular Ca^{2+} attaches to E_1 to form state E_1^*. This state can revert back to the original conformation by a voltage dependent transition and dissociation of bound Ca^{2+} on the extra cellular side.

This six state model can be easily be lumped into a two state model as seen in figure 4.2. The following equations describe the model.

Let e_1,e_1^*,$e_1^\dagger$,e_2,e_2^* and $e_2^\dagger$ represent the fraction of exchanger proteins in the respective states. We have

$$y = e_1^* + e_1 + e_1^\dagger, \qquad 1 - y = e_2^* + e_2 + e_2^\dagger.$$

If $k_{\text{d,cai}}$, $k_{\text{d,cae}}$, $k_{\text{d,nai}}$ and $k_{\text{d,nae}}$ represent the dissociation constants of the corresponding ions, we have

$$k_{\text{d,cai}} = \frac{e_1 Ca_i}{e_1^*}, \qquad k_{\text{d,cae}} = \frac{e_2 Ca_e}{e_2^*}, \qquad k_{\text{d,nai}} = \frac{e_1 Na_i^3}{e_1^\dagger}, \qquad k_{\text{d,nae}} = \frac{e_2 Na_e^3}{e_2^\dagger}.$$

If $P(e_1^*)$ represent the fraction of lumped conformation, y in the E_1^* state, we have

$$P(e_1^*) = \frac{e_1^*}{e_1^* + e_1 + e_1^\dagger} = \frac{\frac{Ca_i}{k_{\text{d,cai}}}}{\frac{Ca_i}{k_{\text{d,cai}}} + 1 + \frac{Na_i^3}{k_{\text{d,nai}}}}$$
$$= \frac{1}{1 + \frac{k_{\text{d,cai}}}{Ca_i}\left(1 + \frac{Na_i^3}{k_{\text{d,nai}}}\right)} = \frac{1}{1 + \frac{k_{\text{d,cai}}}{Ca_i}\left(1 + \left[\frac{Na_i}{k_{\text{d,nai}}}\right]^3\right)},$$

similarly, we have

$$P(e_1^\dagger) = \frac{1}{1 + \left[\frac{k_{\text{d,nai}}}{Na_i}\right]^3\left(1 + \frac{Ca_i}{k_{\text{d,cai}}}\right)},$$

$$P(e_2^*) = \frac{1}{1 + \frac{k_{\text{d,cae}}}{Ca_e}\left(1 + \left[\frac{Na_e}{k_{\text{d,nae}}}\right]^3\right)},$$

$$P(e_2^\dagger) = \frac{1}{1 + \left[\frac{k_{\text{d,nae}}}{Na_e}\right]^3\left(1 + \frac{Ca_e}{k_{\text{d,cae}}}\right)}.$$

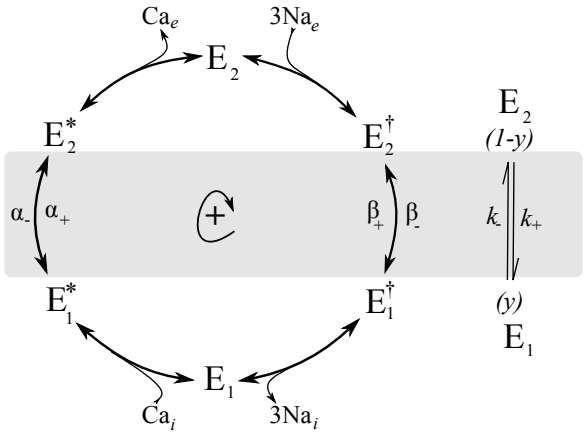

Figure 4.2: Sodium-calcium exchanger transport scheme according to the Kyoto model. The six state model of Na^+-Ca^{2+} exchange (left) was lumped into a two state model (right) assuming that the ion-binding steps are fast and the trans-membrane steps are rate limiting.

parameter	value	units
k_{dne}	87.5	mM
k_{dni}	8.75	mM
k_{dce}	1.38	mM
k_{dci}	0.00138	mM
δ	0.32	-

Table 4.1: Parameters for the reduced two-state Kyoto model for sodium calcium exchanger from Matsuoka et al. [2007]

The apparent rates of transitions between the two states of the lumped model is given by

$$k_+ = \alpha_+ P(e_1^*) + \beta_- P(e_1^\dagger),$$
$$k_- = \alpha_- P(e_2^*) + \beta_+ P(e_2^\dagger),$$

where α and β are transition rates between the two major conformations The subscript '$+$' signifies the Ca extrusion /Na influx mode and vice-versa. The model attributes the charge carrying step to the transport of Na^+ions and hence the transport rates and current is written as

$$\alpha_+ = 1, \quad \alpha_- = 1,$$
$$\beta_+ = exp\left(-\delta\frac{V}{\mathcal{V}_\tau}\right) \quad \beta_- = exp\left((1-\delta)\frac{V}{\mathcal{V}_\tau}\right),$$
$$I_{\text{naca}} = k_{\text{naca}}\left[\beta_- e_1^\dagger - \beta_+ e_2^\dagger\right] = k_{\text{naca}}\left[\beta_- P(e_1^\dagger)y - \beta_+ P(e_2^\dagger)(1-y)\right]. \quad (4.7)$$

The different parameters of the model are given in table 4.1

The modified Kyoto Model The original Kyoto model employs the rates in such a way that both α_+ and α_- are both assigned a value of 1. This would only be true if these rates were voltage-independent. However various experiments suggest that Ca^{2+} translocation is indeed voltage dependent Kappl et al. [2001]. For this reason, for a realistic consideration, the rates are modified by assigning the voltage dependence of the transport on these rates as well [Francis et al., 2012]. Thus,

$$\alpha_+ = exp\left(-\delta_\alpha\frac{V}{\mathcal{V}_\tau}\right), \quad \alpha_- = exp\left((1-\delta_\alpha)\frac{V}{\mathcal{V}_\tau}\right),$$

$$\beta_+ = exp\left(-\delta_\beta \frac{V}{\mathcal{V}_\tau}\right), \quad \beta_- = exp\left((1-\delta_\beta)\frac{V}{\mathcal{V}_\tau}\right),$$

where the parameters δ_α and δ_β denote the position of the free energy barrier located asymmetrically in the electric field.

Kyoto model modified with Ca_i^{2+}allosteric effects The Markov model described above may be modified to incorporate the allosteric regulation of the exchanger by intracellular Ca^{2+} [Fujioka et al., 2000]. According to this model, which is modified for a coupling ratio of 3:1, we have two additional inactive states I_1 and I_2. The exchanger enters the inactive state I_1 from state $E_2^\dagger$. The exchanger may enter the I_2 state from any of the E_2 states but not from the E_1 states (see figure 4.2). With these additional states, the equations are modified as follows:

$$\frac{dI_1}{dt} = a_1 \cdot P(e_2^\dagger) \cdot (1 - y - I_1 - I_2) - b_1 \cdot I_1,$$
$$\frac{dI_2}{dt} = a_2 \cdot (1 - y - I_1 - I_2) - b_2 \cdot I_2,$$

where the allosteric binding rates are given by

$$f = \frac{Ca_i}{Ca_i + 0.004},$$
$$a_1 = 0.002 \cdot f + 0.0015 \cdot (1 - f),$$
$$b_1 = 0.0012 \cdot f + 0.0000005 \cdot (1 - f),$$
$$a_2 = 0.00003 \cdot f + 0.01 \cdot (1 - f),$$
$$b_2 = 0.09 \cdot f + 0.0001 \cdot (1 - f).$$

4.2.2 A comparison between the different models of sodium-calcium exchange

A basic comparison between the models discussed in this section are provided in table 4.2.

The differences in the response of these models to the control variables i.e. the voltage and the concentrations of the participating cations are understood from

Model	1	2	3	4	5
Voltage dependence	yes	yes	yes	yes	yes
Influence of cations *					
Ca_i^{2+}	(a)	(a)	(a)	(b)	(b)
Ca_e^{2+}	(a)	(b)	(a)	(b)	(b)
Na_i^{+}	(a)	(a)	(a)	(b)	(b)
Na_e^{+}	(a)	(b)	(a)	(b)	(b)
Allosteric effect of Ca_i^{2+}	yes**	no	no	no	yes
Saturation at higher voltages	no	yes	no	no	no

* The dependence of exchanger current on the respective cations is based on their concentration. Additionally their binding onto the protein can have an influence on the model. Here models are classified based on how model incorporates these concepts. (a) suggest that the model has a concentration term alone, (b) suggests that model includes an affinity parameter in addition to the concentration term

** One of the terms in the DiFrancesco-Noble equation can be considered as a representation of the allosteric effect of Ca_i^{2+}

Table 4.2: A comparison between different models for NaCax (1) DiFrancesco-Noble model (2) Luo-Rudy model (3) Endresen model (4) Kyoto model/modified Kyoto model (5) Kyoto model with allosteric calcium inhibition

the responses of these variables to a step change in voltage. For a step change of voltage in the physiological range, we find comparable responses from these models (figure 4.3a). There is a notable difference in the response from the model of Endresen and the original Kyoto model. The exchanger is expected to exhibit a change of operating direction at positive potentials. However, the Endresen model does not exhibit this. The original Kyoto model displays a dramatic response to change in voltage and has relatively smaller current compared to rest of the models around the resting potential (which may be a numerical issue with respect to the scaling, but if appropriately scaled that would make the exchanger have large currents at positive potentials or in other words this model would work heavily in the opposite direction at an action potential overshoot). However the modified Kyoto model, which includes all the voltage dependencies, appears to behave reasonably with respect to changes in the membrane potential.

All models are comparable with changes in the concentration of intracellular Na^+, extracellular Ca^{2+} and Na^+, in the expected physiological range (figures

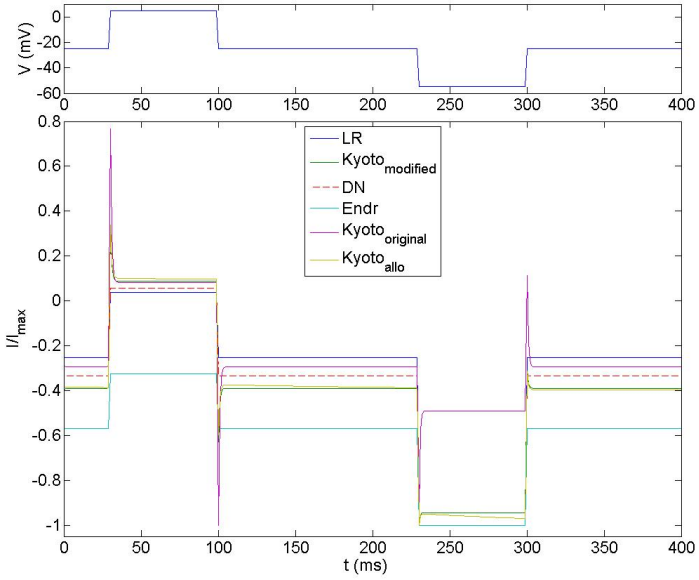

(a) Influence of membrane potential

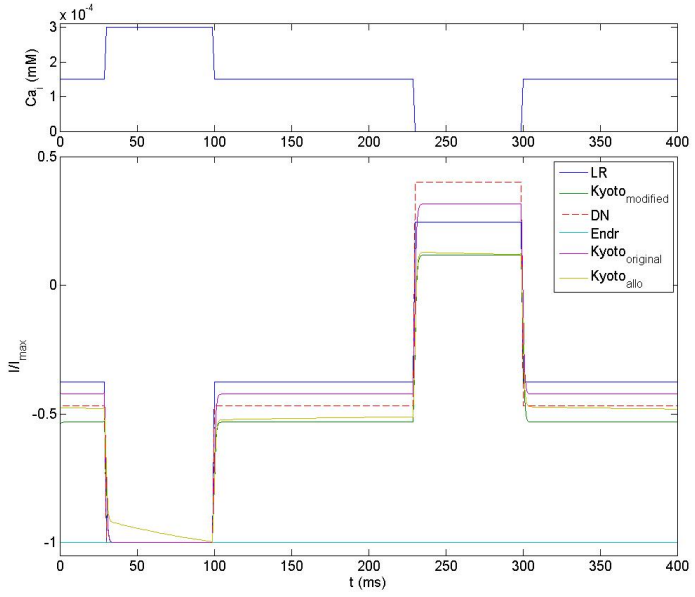

(b) Influence of intracellular Ca^{2+}

Figure 4.3: Comparison of models for sodium-calcium exchanger : Influence of voltage and ionic-concentrations on the response from the different models of the sodium-calcium exchanger. The different models considered include the Luo-Rudy exchanger model (LR), DiFrancesco-Noble model (DN), Endresen model (Endr) and the Kyoto model ($\text{Kyoto}_{\text{original}}$) as well as its modified version used in our chapter ($\text{Kyoto}_{\text{modified}}$) and the modification with the allosteric activation of Ca_i ($\text{Kyoto}_{\text{allo}}$)

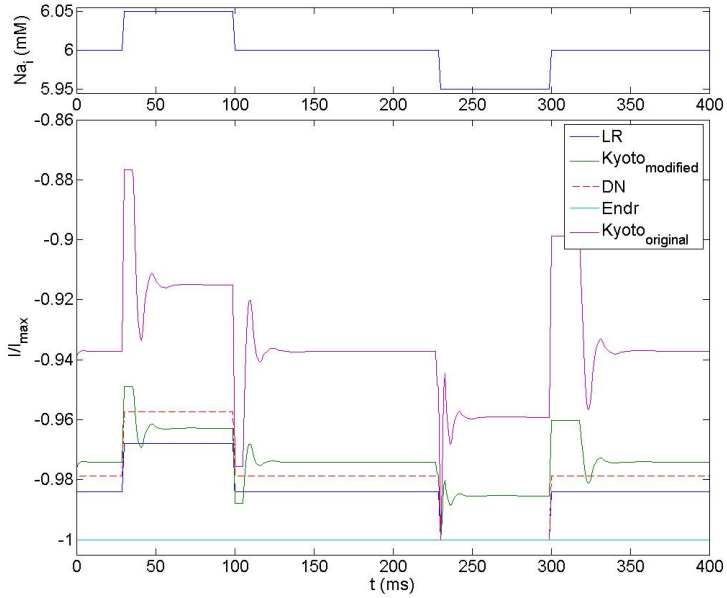

(c) Influence of intracellular Na^+

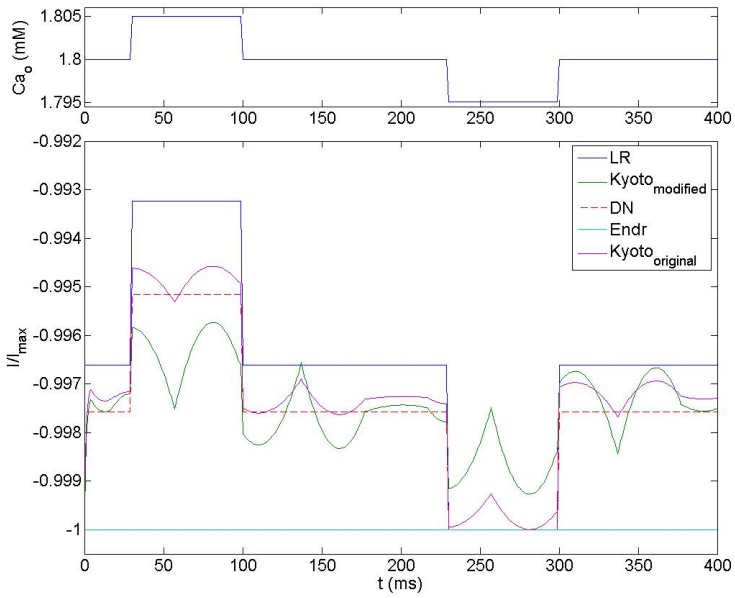

(d) Influence of extracellular Ca^{2+}

Figure 4.3: Comparison of models for sodium-calcium exchanger - continued

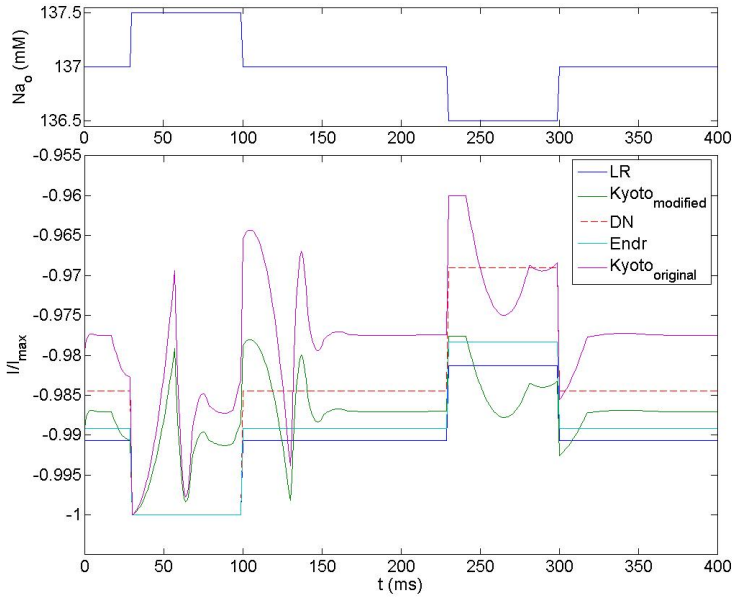

(e) Influence of extracellular Na^+

Figure 4.3: Comparison of models for sodium-calcium exchanger - continued

4.3c,4.3d and 4.3e). In the case of intracellular Ca^{2+} (figure 4.3b), the Endresen model displays little effect. The rest of the models are comparable, however the dynamics involved make the Markov models slower than the rest. This can prove detrimental when Ca_i^{2+}goes to zero, as the steady state models instantly reverse direction whereas the Markov model continues the exchange numerically, leading to negative concentrations. The allosteric modification of the Kyoto model of the exchanger does not seem to give any distinct advantage in this situation. Moreover, the exchangers are expected to work more rapidly than pumps and hence it would be ideal to have a model that shows instantaneous response to changes in concentrations.

The selection of a suitable model of NaCax to be included in developing a model for membrane pacemaking in *SNc* neuron has to be made based on the maximum mechanistic criteria it would satisfy and minimum modelling and dynamic problems it would impose. The Endresen model is ruled out because it does not bring about the reversal of direction of the protein's operation at positive potentials. The Luo-Rudy model has an unwanted saturation criteria, the original Kyoto model has a problem with voltage dependence and the al-

losteric Kyoto model does not seem to add any distinct advantage other than making the modelling more complex. The DiFrancesco-Noble model has the advantage of having a faster response, a feature that is expected of NaCax, compared to the modified Kyoto model, in spite of its mechanistic detailing. The DiFrancesco-Noble model will therefore be considered later in the full model of neuronal electrochemical dynamics.

4.3 The sodium-potassium ATPase

The sodium pump or the Na^+/ K^+ATPase is responsible for the formation and maintenance of electrochemical gradient in animal cells. The enzyme transports three molecules of $Na^+$from and two K^+into the intracellular space for every molecule of ATP hydrolysed. Experiments indicate that the rate of transfer of this ATPase shows very little dependence on voltage. The main step in the chain that shows some voltage dependence is the dissociation of Na^+into the external space Rakowski et al. [1997].

Scheme of events Rakowski et al. [1997] gives a good picture of the mechanism by which these pumps function. The sodium pump exists in two conformational states characterized by differences in their interactions with the ions and ATP. Sodium and ATP bind with very high affinity to the E1 conformation. Equilibrium binding of two sodium ions facilitates the electrogenic binding of the third sodium ion. The phosphorylation of the enzyme in this bound state leads to a conformational change, which renders the sodium ions open to the external space. Unbinding and release of sodium ions leads to the binding of potassium ions on to the E2 conformation. This then leads to the dephosphorylation of the enzyme and a conformational change. The equilibrium binding of the ATP molecule to this structure promotes the release of the potassium ions and completes the cycle (see figure 4.4).

In this cycle, the rate limiting step is the release of the first sodium ion into the extracellular space. This is mostly because release of this first ion is based on the prevailing electro-chemical forces. The release of next two Na^+ions

are typical dissociation. For this reason, the voltage dependence of the pump function is mostly assigned with the first step.

Coupling ratio A coupling ratio of 3 Na^+:2 $K^+$is well accepted.

Total change in the Gibb's free energy If $\hat{\mathcal{V}}_{atp}$ represents the voltage equivalent of free energy change associated with ATP hydrolysis (see equation 4.2), we have $\Delta G_{\text{atp}} = F\hat{\mathcal{V}}_{atp}$. Therefore, for a coupling ratio of 3:2, the total change in Gibbs free energy is

$$\Delta G_{\text{nak}} = \Delta G_{\text{atp}} + 3\Delta G_{\text{Na}} + 2\Delta G_{\text{K}} = F(\hat{\mathcal{V}}_{atp} + 3\hat{\mathcal{V}}_{Na} - 2\hat{\mathcal{V}}_{K} - V).$$

For the normal levels of molecules implied in ATP hydrolysis within the cells, ΔG_{nak} is usually negative and favours the spontaneous operation of this pump.

4.3.1 Mathematical models of the sodium-potassium pump

D'Francesco-Noble model The model of DiFrancesco and Noble [1985], provides a Michaelis - Menten type dependence on the extracellular potassium and

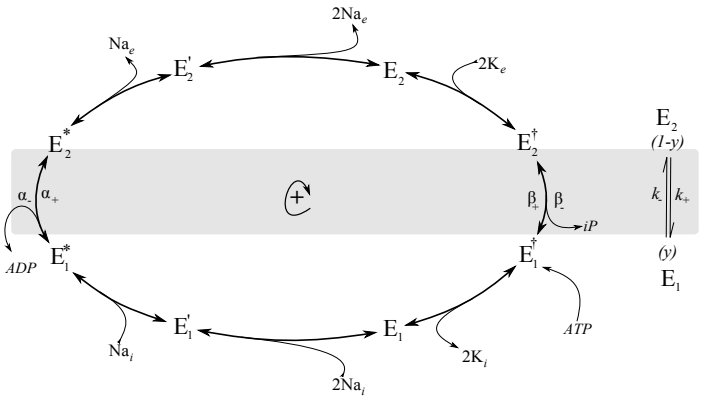

Figure 4.4: Functioning of sodium-potassium ATPase captured as an eight state Markov model. The scheme of events may be lumped into two-states that reflect the major conformational change of the protein

intracellular sodium. The current is given by the equation

$$I_{\text{nak}} = K_{\text{nak}} \frac{1}{1 + \left(\frac{k_{\text{m,ke}}}{K_e}\right)} \frac{1}{1 + \left(\frac{k_{\text{m,nai}}}{Na_i}\right)}. \tag{4.8}$$

The parameters are given in table 4.3

Luo-Rudy model This model considers only the forward functioning of the pump and uses a coupling ratio of 3 Na^+: 2 K^+. The model is an improvement over the DiFrancesco and Noble [1985] model by including a function that is voltage dependent.

$$I_{\text{nak}} = K_{\text{nak}} \cdot f_{\text{nak}} \frac{1}{1 + \left(\frac{k_{\text{m,nai}}}{Na_i}\right)^{1.5}} \frac{1}{1 + \left(\frac{k_{\text{m,ke}}}{K_e}\right)}. \tag{4.9}$$

Here, f_{nak} is a function that gives the fraction of functioning pumps at the given voltage,

$$f_{\text{nak}} = \frac{1}{1 + 0.1245 \exp\left(-0.1\frac{V}{\mathcal{V}_\tau}\right) + 0.0365 \cdot \sigma_{\text{nak}} \exp\left(-\frac{V}{\mathcal{V}_\tau}\right)},$$

and σ_{nak} is a factor that relates the influence of voltage dependence on the external sodium concentration,

$$\sigma_{\text{nak}} = \frac{1}{7}\left[\exp\left(\frac{Na_e}{67.3}\right) - 1\right].$$

The different parameters of the model are given in table 4.3.

Endresen model The model of Endresen et al. [2000] considers only the free energy changes associated with the transport. According to this model the pump current is given by

$$I_{\text{nak}} = K_{\text{nak}} \tanh\left(\frac{V + 2\hat{\mathcal{V}}_K - 3\hat{\mathcal{V}}_{Na} - \hat{\mathcal{V}}_{atp}}{2\mathcal{V}_\tau}\right). \tag{4.10}$$

parameter	value	units
DiFrancesco and Noble [1985] model		
$k_{\text{m,nai}}$	40	mM
$k_{\text{m,ke}}$	1	mM
Luo and Rudy [1994] model		
$k_{\text{m,nai}}$	10	mM
$k_{\text{m,ke}}$	1.5	mM
Endresen et al. [2000] model		
$\hat{\mathcal{V}}_{atp}$	-450	mV

Table 4.3: A list of parameters used in different models of the sodium-potassium pump

Kyoto model The Kyoto model for NaK may be derived similar to the way in which the sodium-calcium exchanger has been done in the previous section. The important equations for this model (figure 4.4) are given below

$$I_{\text{nak}} = K_{\text{nak}}[\alpha_+ \mathcal{P}(E_1^*)y - \alpha_- \mathcal{P}(E_2^*)(1-y)], \tag{4.11}$$

$$\begin{aligned}
\tfrac{dy}{dt} &= k_-(1-y) - k_+ y, \\
k_+ &= \alpha_+ \mathcal{P}(E_1^*) + \beta_- \mathcal{P}(E_1^\dagger), \qquad k_- = \alpha_- \mathcal{P}(E_2^*) + \beta_+ \mathcal{P}(E_2^\dagger), \\
\mathcal{P}(E_1^*) &= \tfrac{1}{1+\frac{4.05}{Na_i}\left(1+\frac{K_i}{32.88}\right)}, \qquad \mathcal{P}(E_1^\dagger) = \tfrac{1}{1+\frac{32.88}{K_i}\left(1+\frac{Na_i}{4.05}\right)}, \\
\mathcal{P}(E_2^*) &= \tfrac{1}{1+\frac{69.8}{Na_{\text{eff}}}\left(1+\frac{K_e}{0.258}\right)}, \qquad \mathcal{P}(E_2^\dagger) = \tfrac{1}{1+\frac{0.258}{K_e}\left(1+\frac{Na_{\text{eff}}}{69.8}\right)}, \\
Na_{\text{eff}} &= Na_e \exp(-0.82\tfrac{V}{\mathcal{V}_\tau}), \\
\alpha_+ &= \tfrac{0.37}{1+0.0.094/[atp]}, \qquad \alpha_- = 0.04 \quad (ms^{-1}).
\end{aligned}$$

Smith-Crampin model Smith and Crampin [2004] made use of a lumping scheme to produce a 4-state model from a 15-state model (figure 4.5) while maintaining the thermodynamic properties in the original model of Läuger and Apell [1986]. The pump current according to this model can be summarised as follows

$$I_{\text{nak}} = K_{\text{nak}} \cdot v_{\text{cyc}} \tag{4.12}$$

where the clockwise pump rate v_{cyc} is given by

$$v_{\text{cyc}} = \frac{\alpha_1^+ \alpha_2^+ \alpha_3^+ \alpha_4^+ - \alpha_1^- \alpha_2^- \alpha_3^- \alpha_4^-}{\Sigma}$$

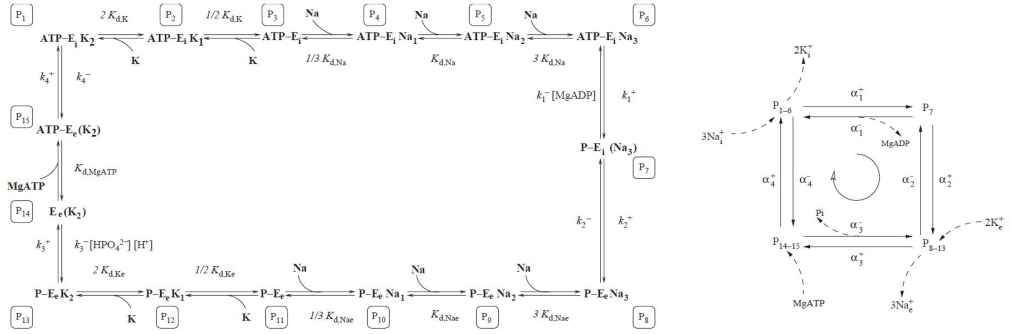

Figure 4.5: The Smith-Crampin model of sodium-potassium ATPase. The 15 state model on the left and the reduced 4-state model on the right

$$\begin{aligned}\Sigma \;&= \alpha_1^-\alpha_2^-\alpha_3^- + \alpha_1^+\alpha_2^-\alpha_3^- + \alpha_1^+\alpha_2^+\alpha_3^- + \alpha_1^+\alpha_2^+\alpha_3^+ \\ &+\alpha_2^-\alpha_3^-\alpha_4^- + \alpha_2^+\alpha_3^-\alpha_4^- + \alpha_2^+\alpha_3^+\alpha_4^- + \alpha_2^+\alpha_3^+\alpha_4^+ \\ &+\alpha_3^-\alpha_4^-\alpha_1^- + \alpha_3^+\alpha_4^-\alpha_1^- + \alpha_3^+\alpha_4^+\alpha_1^- + \alpha_3^+\alpha_4^+\alpha_1^+ \\ &+\alpha_4^-\alpha_1^-\alpha_2^- + \alpha_4^+\alpha_1^-\alpha_2^- + \alpha_4^+\alpha_1^+\alpha_2^- + \alpha_4^+\alpha_1^+\alpha_2^+ .\end{aligned}$$

The different rates are given by

$$\alpha_1^+ = \frac{k_1^+\overline{Na}_i^3}{(1+\overline{Na}_i)^3+(1+\overline{K}_i)^2-1} \qquad \alpha_2^- = k_1^-[MgADP]$$

$$\alpha_2^+ = k_2^+ \qquad \alpha_2^- = \frac{k_2^-\overline{Na}_e^3}{(1+\overline{Na}_e)^3+(1+\overline{K}_e)^2-1}$$

$$\alpha_3^+ = \frac{k_3^+\overline{K}_e^2}{(1+\overline{Na}_e)^3+(1+\overline{K}_e)^2-1} \qquad \alpha_3^- = \frac{k_3^-[Pi][H^+]}{1+\overline{MgATP}}$$

$$\alpha_4^+ = \frac{k_4^+\overline{MgATP}}{1+\overline{MgATP}} \qquad \alpha_4^- = \frac{k_4^-\overline{K}_i^2}{(1+\overline{Na}_i)^3+(1+\overline{K}_i)^2-1}$$

and the dimensionless concentrations are given by

$$\overline{Na}_i = \frac{Na_i}{K_{\text{d,nai}}} \quad \overline{Na}_e = \frac{Na_e}{K_{\text{d,nae}}} \quad \overline{K}_i = \frac{K_i}{K_{\text{d,ki}}} \quad \overline{K}_e = \frac{K_e}{K_{\text{d,ke}}} \quad \overline{MgATP} = \frac{[MgATP]}{K_{\text{d,mgatp}}}.$$

The voltage dependence is contained within the sodium transport function of the pump as,

$$K_{\text{d,nae}} = K^0_{\text{d,nae}}\exp\left(\frac{(1+\triangle)V}{3\mathcal{V}_\tau}\right) \qquad K_{\text{d,nai}} = K^0_{\text{d,nai}}\exp\left(\frac{\triangle V}{3\mathcal{V}_\tau}\right),$$

where $\triangle$ is the voltage dependence partition factor. The parameters of this model are given in table 4.4

parameter	value	units	parameter	value	units
Smith and Crampin [2004] model			Oka et al. [2010] model		
k_1^+	1.05	ms^{-1}	k_1^+	1.253	ms^{-1}
k_1^-	0.172	$ms^{-1}mM^{-1}$	k_1^-	0.139	$ms^{-1}mM^{-1}$
k_2^+	0.481	ms^{-1}	k_2^+	0.139	ms^{-1}
k_2^-	0.04	ms^{-1}	k_2^-	0.014	ms^{-1}
k_3^+	2	ms^{-1}	k_3^+	6.96	ms^{-1}
k_3^-	79.3	$ms^{-1}mM^{-2}$	k_3^-	13920	$ms^{-1}mM^{-2}$
k_4^+	0.32	ms^{-1}	k_4^+	0.522	ms^{-1}
k_4^-	0.04	ms^{-1}	k_4^-	0.348	ms^{-1}
$K^0_{\text{d,nai}}$	2.49	mM	$K^0_{\text{d,nai}}$	5	mM
$K^0_{\text{d,nae}}$	15.5	mM	$K^0_{\text{d,nae}}$	26.8	mM
$K_{\text{d,ki}}$	0.5	mM	$K^0_{\text{d,ki}}$	18.8	mM
$K_{\text{d,ke}}$	0.213	mM	$K^0_{\text{d,ke}}$	0.8	mM
$K_{\text{d,mgatp}}$	2.51	mM	$K_{\text{d,mgatp}}$	0.6	mM
$\triangle$	-0.031	-	$\triangle_{Na_i}$	-0.14	-
			$\triangle_{Na_e}$	0.44	-
			$\triangle_{K_i}$	-0.14	-
			$\triangle_{K_e}$	0.23	-

Table 4.4: A list of parameters used in two different Markov models of sodium-potassium pump

Oka model The Smith and Crampin [2004] model has been modified by Oka et al. [2010] to include the dependence of voltage on both the internal and external binding rates of ions as,

$$K_{\text{d,nae}} = K^0_{\text{d,nae}} \exp\left(\frac{\triangle_{Na_e} V}{\mathcal{V}_\tau}\right) \quad K_{\text{d,nai}} = K^0_{\text{d,nai}} \exp\left(\frac{\triangle_{Na_i} V}{\mathcal{V}_\tau}\right)$$

$$K_{\text{d,ke}} = K^0_{\text{d,ke}} \exp\left(\frac{\triangle_{K_e} V}{\mathcal{V}_\tau}\right) \quad K_{\text{d,ki}} = K^0_{\text{d,ki}} \exp\left(\frac{\triangle_{K_i} V}{\mathcal{V}_\tau}\right)$$

The parameters of this model are given in table 4.4

4.3.2 A comparison between the different models of sodium-potassium pump

A basic comparison between the models discussed in this chapter is provided in table 4.5. As in the case of NaCax, the response of the different models for NaK is made from step changes of the control variables (Figure 4.6). The models exhibit significantly different behaviours in response to changes in extracellular

Model	1	2	3	4	5
Voltage dependence	no	yes	yes	yes	yes
Influence of cations *					
K_i^{2+}	-	-	(a)	(b)	(b)
K_e^{2+}	(b)	(b)	(a)	(b)	(b)
Na_i^{+}	(b)	(b)	(a)	(b)	(b)
Na_e^{+}	-	(b)	(a)	(b)	(b)
Voltage dependence on Na_e	no	yes	no	yes	no
Effect of ATP	no	no	no	yes	yes
Effect of pH	no	no	no	no	yes

* The dependence of pump current on the respective cations is based on their concentration. Additionally their binding onto the protein can have an influence on the model. Here models are classified based on how model incorporates these concepts. (a) suggest that the model has a concentration term alone, (b) suggests that model includes an affinity parameter in addition to the concentration term

Table 4.5: A comparison between different models of NaK (1) DiFrancesco-Noble model (2) Luo-Rudy model (3) Endresen model (4) Kyoto model (5) Smith-Crampin model/Oka model

$Na^+$and $K^+$and intracellular K^+. The Smith-Crampin model is largely independent of membrane potential but has larger response to changes in intracellular Na^+compared to the other models. Being a Markov model, the Kyoto model exhibits reasonable dynamics with respect to the changes in variables.

Unlike exchangers, pumps are not expected to have a rapid response for small changes in the concentration of the molecules they transport. Moreover, for a model that is aimed at understanding the energetics of transport in makes more sense to a model that includes the mechanistic details and one that is influenced by ATP. For these reasons, we use the Kyoto model for the NaK ATPase in our model of *SNc* pacemaking.

4.4 The Plasma membrane calcium ATPase

The PMCA is a membrane protein responsible for the efflux of calcium ions against their gradient, powered by the energy associated with the hydrolysis of an ATP molecule. It binds tightly to calcium ions (has a high affinity, with a K_m of 100 to 200 nM) but does not remove calcium at a very fast rate.

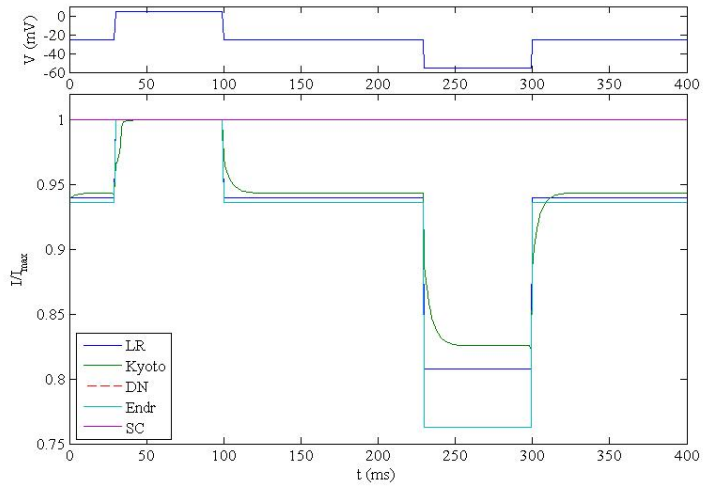

(a) Influence of membrane potential

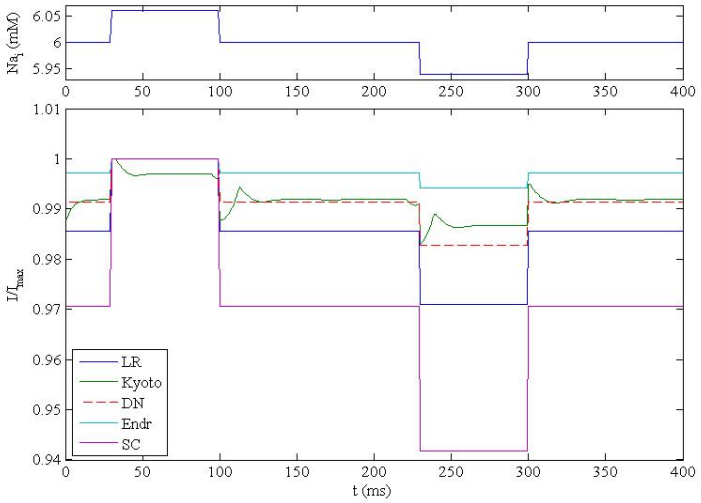

(b) Influence of intracellular Na^+

Figure 4.6: Comparison of models for the sodium-potassium pump : Influence of voltage and ionic-concentrations on the response from the different models of the sodium-potassium pump. The different models considered include the Luo-Rudy exchanger model (LR), DiFrancesco-Noble model (DN), Endresen model (Endr), the Kyoto model ($\text{Kyoto}_{\text{original}}$) and the Smith-Crampin Model (SC)

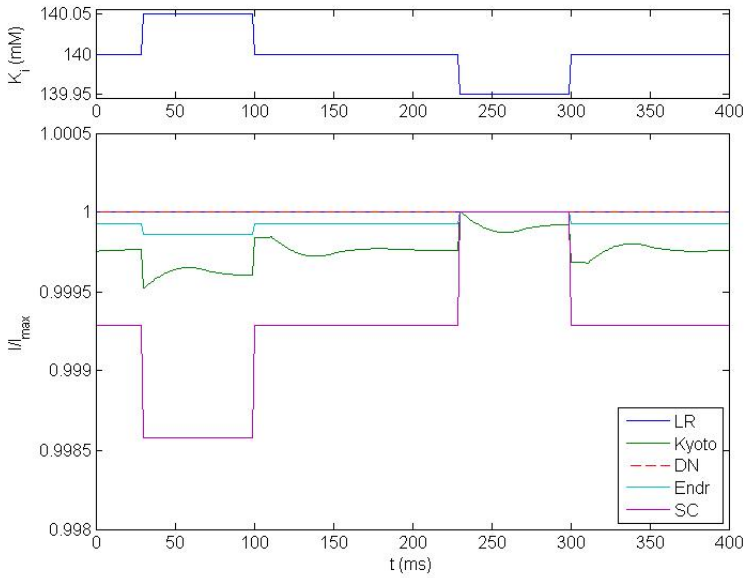

(c) Influence of intracellular K^+

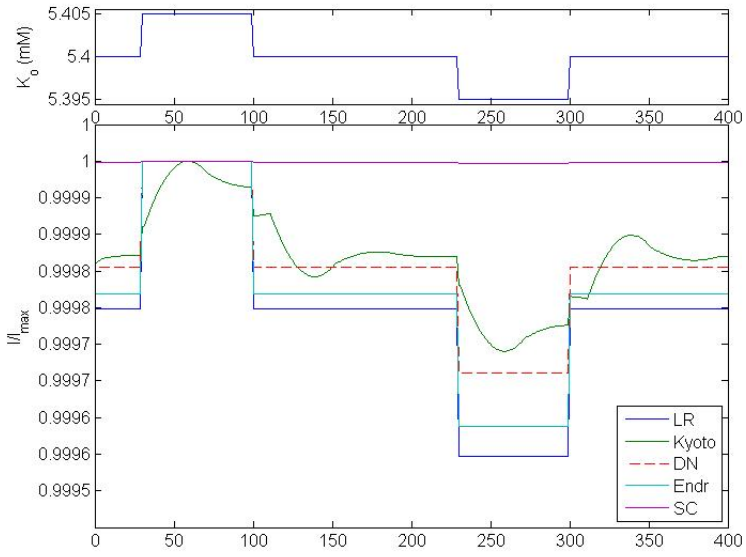

(d) Influence of extracellular K^+

Figure 4.6: Comparison of models for the sodium-potassium pump - continued

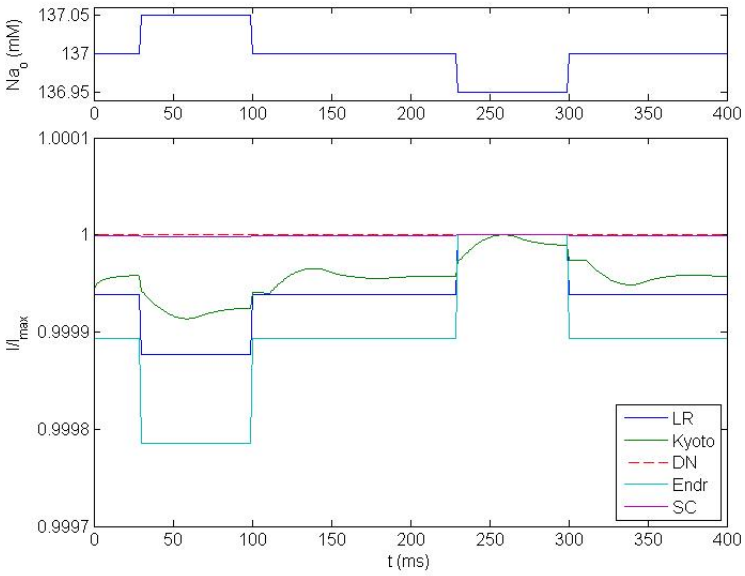

(e) Influence of extracellular Na^+

Figure 4.6: Comparison of models for the sodium-potassium pump - continued

The active transport of calcium ions mediated by these proteins may be approximately represented as,

$$Ca_i^{2+} \xrightarrow{\alpha} Ca_e^{2+}$$
$$ATP \xrightarrow{Mg^{2+},H_2O} ADP + iP$$

The free energy changes significant to this transport are

$$\Delta G_{Ca} = RT \ln \frac{Ca_e}{Ca_i} - z_{Ca}FV = z_{Ca}F(\hat{\mathcal{V}}_{Ca} - V) \tag{4.13a}$$

$$\Delta G_{atp} = -RT \ln(\kappa_{atp}) = RT \ln \frac{[Mg.ADP][iP]}{[Mg.ATP]} = FV_{atp} \tag{4.13b}$$

where κ_{atp} is the equilibrium constant for ATP hydrolysis (approximately 10^5 M). V_{atp} is a voltage equivalent of the hydrolytic energy. The ATP to ADP ratio is around 1000 [Nicholls and Ferguson, 1992] in the cytoplasm and the Mg.ATP/Mg.ADP ratio around 2300 [Manchester, 1980]. The inorganic phosphate concentration is assumed to be around 10 mM (An experiment in cardiac cells by Wu et al. [2008] shows that it varies between $0.3mM$ to $18mM$). Accordingly, the value of V_{atp} is roughly $-330mV$ at normal physiological tem-

peratures. (The value used in Endresen et al. [2000], is around $-450mV$, which would imply a very high ATP/ADP ratio).

Transport is feasible when it is favourably coupled to the energy from ATP hydrolysis, or when $\Gamma_{\text{pmca}}\Delta G_{atp} > \Delta G_{Ca}$; Γ_{pmca} being the coupling co-efficient (Γ_{pmca} = 1 mole of ATP per mole of calcium transported). For the condition of feasibility (see section 4.1), the apparent driving energy is

$$\Delta G_{\text{pmca}} = F(V_{atp} + 2\hat{\mathcal{V}}_{Ca} - 2V).$$

Since V_{atp} is much larger than other terms in the equation, the voltage dependence of the pump is apparently small. There are only two ways that net transport can be voltage dependent. Either a rate-limiting step in the transport cycle is itself voltage dependent or a voltage dependent step controls the level of an intermediate enzyme entering the rate-limiting step.

An important feature of PMCA activity is its regulation by the calcium signalling protein calmodulin (CaM). CaM reversibly binds and activates PMCA in a calcium dependent manner. This association is understood to stimulate the release of an auto-inhibitory domain from the ATP-binding site of PMCA [Osborn et al., 2004], thereby increasing its affinity and turnover rate.

4.4.1 Mathematical models of PMCA

Hill-equation type models One of the most popular way of representing calcium pump activity is to use the Hill-equation/ Michaelis-Menten formulation. The mathematical representation of PMCA's function has often been with such simple equations similar to the one in the Luo-Rudy model [Luo and Rudy, 1994]. These models represent the pump in terms of a binding process between the ions and the protein. According to such a model,

$$I_{\text{pmca}} = K_{\text{pmca}} \frac{Ca_i^n}{Ca_i^n + k_{\text{pmca}}^n}. \tag{4.14}$$

K_{pmca} is the maximal amplitude of the pump current, n is the Hill coefficient: number of calcium molecules bound, k_{pmca} is the affinity (half maximal concentration). PMCA has an apparent Hill coefficient of ~ 2 and the affinity factor is influenced by the presence of calmodulin.

Model derived from Endresen model The concepts used in Endresen et al. [2000] for developing a model for the Na^+/K^+pump may be extended to arrive at a model for PMCA. Accordingly, the PMCA current equation becomes

$$I_{\text{pmca}} = K_{\text{pmca}} \cdot \tanh\left(\frac{2V - 2\hat{\mathcal{V}}_{Ca} - \hat{\mathcal{V}}_{atp}}{2\mathcal{V}_\tau}\right). \tag{4.15}$$

Kyoto model Models using Markov principles can explain the binding process, incorporate voltage dependence if needed and can incorporate finer details of the mechanism, such as influence of calmodulin on PMCA activity. The Kyoto model [Matsuoka et al., 2007] is a four-state illustration of the transport mechanism of PMCA. This is further reduced to a two-state model by assuming fast binding of calcium ions (Figure 4.7). This model also includes the dependence of the pump on the presence of calmodulin. The model is as follows:

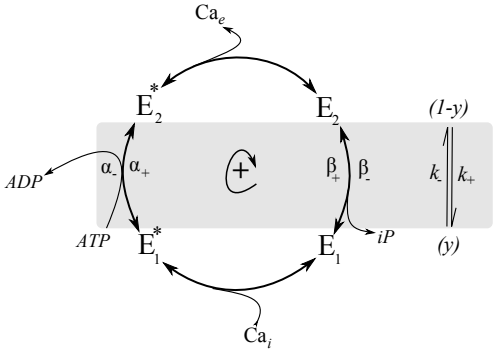

Figure 4.7: PMCA transport scheme

$$I_{\text{pmca}} = k_{\text{pmca}}.A_{\text{pmca}}\left[\frac{\alpha_+ y}{1 + \frac{k_{\text{pmca,cai}}}{Ca_i}} - \frac{\alpha_-(1-y)}{1 + \frac{2}{Ca_e}}\right] \tag{4.16}$$

$$\begin{aligned}
\frac{dy}{dt} &= k_-(1-y) - k_+ y \\
k_+ &= \frac{\alpha_+ - \beta_-}{1 + k_{\text{pmca,cai}}/Ca_i} + \beta_- \qquad k_- = \frac{\alpha_- - \beta_+}{1 + 2/Ca_e} + \beta_+ \\
\mathcal{P}(E_1^*) &= \frac{1}{1 + k_{\text{pmca,cai}}/Ca_i} \qquad \mathcal{P}(E_1) = 1 - \mathcal{P}(E_1^*) \\
\mathcal{P}(E_2^*) &= \frac{1}{1 + 2/Ca_e} \qquad \mathcal{P}(E_2) = 1 - \mathcal{P}(E_2^*)
\end{aligned}$$

$$A_{\text{pmca}} = 10.56\frac{[cacam]}{[cacam]+0.00005} + 1.2 \quad (pA)$$
$$k_{\text{pmca,cai}} = \frac{(180-6.4)\times 10^{-5}}{1+[cacam]/0.00005} + 6.4 \times 10^{-5} \quad (mM)$$

4.5 Cytosolic systems involved in calcium metabolism

The efficient management of the temporal and spatial intracellular calcium is critical to living systems and involves the effective collaboration of all participating components. The network of metabolic activity involved in handling calcium may be categorized into (a) calcium entry systems (b) cytosolic compartments involved with calcium release and uptake, referred to as the calcium stores, (c) buffers of calcium, and (d) calcium extrusion systems.

The calcium entry system involves a group of membrane proteins that aid in the entry of Ca^{2+} along its gradient when appropriately stimulated. This includes a group of voltage gated calcium channels, ligand gated calcium channels, store operated calcium channels and Ca^{2+} mobilizing networks. Ca^{2+} can be sourced either from extra-cellular space or internal membrane bound stores, predominantly the endoplasmic reticulum (ER) and to a small extent the mitochondria. Release from these store is primarily activated by Ca^{2+} itself and often termed *calcium-induced calcium release* (CICR) and is central to the mechanism of intra-cellular calcium signalling. This pathway involves the activation of various channels including the $InsP_3$ receptor ($InsP_3R$) and ryanodine receptor (RyR) families by the corresponding stimuli, a system of Ca^{2+}-mobilizing messengers regulated by various factors. Ca^{2+} itself can be a major regulating factor for these messengers.

On the other hand, the calcium extrusion system involves membrane proteins that are calcium-ATPases or exchangers. This include PMCA, ERCA, NaCax as well as NaCam.

Cytosolic calcium transients evoked by the concerted activity of entry and exit systems are effectively handled by entities that aid in buffering the concentration of calcium. These buffers include calcium binding proteins such as calbindin that act as mobile buffers and organelles such as the ER and mito-

chondria that operate as calcium stores. The ratio of free to bound calcium in the cytosol is characteristic to a cell and is influenced by the expression levels of the mobile buffers. This is important to determine the amplitude and duration of calcium signals, as well as in limiting the spatial spreading of local signals.

4.6 Buffering of intracellular calcium

Calcium - dependent signalling pathways control several cellular processes [Nelson and Cox, 2004]. Hence, it is essential for the cell to regulate the levels of intra-cellular calcium. In addition to being spatially limited, the response of the calcium extrusion apparatus to a sudden upsurge of calcium, is very slow. For this reason, cells require calcium buffering mechanisms to cushion such effects. These buffers are categorized as either mobile or stationary. The mobile buffers constitute a group of proteins such as calbindin with molecular weights of the order of 15 kDa. The Ca^{2+} they carry are taken up ultimately by organelles such as the endoplasmic reticulum and mitochondria, which act as fixed buffers.

The mobile buffers bind Ca^{2+} with a time constant estimated to be in the millisecond range or less and for this reason, free Ca^{2+} concentrations can be easily related to the association and dissociation constants of the buffer. Calcium buffers affect both fluxes and diffusion of free Ca^{2+} in the cytosol and consequently, have a significant role in cells whose functioning is subject to the dynamics of free cytosolic Ca^{2+}. In spite of this, calcium binding proteins are an often neglected constituent of the cytosolic network involved in calcium homeostasis. A large number of studies on the pathogenesis in PD [Surmeier, 2007] show the importance of calcium within neurons of the *SNc* neuron. Accordingly, we argue that models developed for relating activities in the *SNc* to its degeneration should include calcium handling.

The dopaminergic neurons of the *SNc* do not have a high intrinsic calcium binding capacity. According to observations of Foehring et al. [2009], up to 1% of Ca^{2+} entering the neuron remains free at steady state. These neurons are known to express traditional calcium binding proteins and data suggests that

neurons of the *SNc* that express high levels of calbindin are less vulnerable to damage in PD [Yamada et al., 1990; Damier et al., 1999b].

Pacemaking models of the *SNc* have often taken into account the influence of buffers. Amini et al. [1999] takes into account a single representative buffer and assume linear binding dynamics. Wilson and Callaway [2000] assumes that buffers are non-saturable and adopts a simple representation for the effect of both mobile and fixed buffers. Kuznetsova et al. [2010] implicitly model calcium buffering by defining a control parameter that gives the fraction of free Ca^{2+} in the respective compartments.

In our model we employ the binding dynamics of two calcium-binding proteins that appear to be significant in the generation of spontaneous membrane activity. Calbindin is a fast buffer of Ca^{2+} and its significance in these neurons is evident. Calmodulin, which is the primary decoder of Ca^{2+} levels within the cell, is also taken into account, as levels of the calcium-calmodulin complex define other calcium dependent mechanisms in the cell.

4.6.1 Calbindin

Calbindin D_{28k} is a member of the EF-hand family of Ca^{2+} binding proteins, characterised by a binding motif formed by twelve amino acids brought together by the spatial arrangement of fifth (E) and sixth (F) α - helix of the polypeptide chain. This protein is capable of binding up to four Ca^{2+} in the EF-hands of the respective loops. These proteins are widely expressed in tissues transporting Ca^{2+} such as the epithelial-absorptive cells of the intestine and the distal tubular epithelial cells of the kidney [Christakos et al., 1989]. They are also expressed widely in neurons. The nomenclature Calbindin D_{28k} indicates its vitamin D dependence and its apparent molecular weight [Wasserman et al., 1968]. In the brain however, its synthesis is found to be independent of Vitamin D.

Calbindin molecules are predominantly distributed in the cytosol, even though their size does allow them to passively diffuse into the cell nucleus. The resistance to their diffusion is mostly because they are anchored close to Ca^{2+} hotspots by strong chemical gradients. Calbindin's exact role in Ca^{2+} dependent

processes is yet to be unravelled. It is not sure if it does have a signalling role in metabolic pathways. However, their association with cytoskeletal structures [Sayer et al., 2000] and the existence of calbindin-binding proteins [Leathers and Norman, 1993] prove that they function more than just as a fast Ca^{2+} buffer.

Calbindin in PD pathogenesis A central role of Ca^{2+} in pathways leading to degeneration of *SNc* neurons in PD was ascertained with the report on neurons that are spared from degeneration in this disease. In a landmark study by Yamada et al. [1990], it was discovered that a sub-population of *SNc* neurons that was calbindin rich survived in PD. One mechanism by which calbindin would help the neurons survive would be by buffering excess intracellular Ca^{2+}, thereby limiting Ca^{2+} induced toxicity in these group of neurons. A second way calbindin enhances neuronal viability is by having a direct impact on metabolic activities specific to PD, such as α-synuclein aggregate formation.

Although the report by Yamada et al. [1990] brought to light the involvement of Ca^{2+}- pathways in the disease, the involvement of calbindin was not explored in detail. Recently, genetic analysis using Single-nucleotide polymorphism (SNP) revealed a statistically significant identification of *CALB1*, the gene involved with calbindin synthesis, as a susceptibility gene for the disease [Mizuta et al., 2008]. This analysis also suggested that *CALB1* is associated with PD independently of the gene *SNCA*, the gene involved with α-synuclein expression.

Later, *in vivo* studies suggested an altogether different dynamics between calbindin and α-synuclein [Zhou et al., 2010]. This study discussed in 2.3.1 showed that calbindin acts as a molecular chaperone that suppress the formation of α-synuclein fibrils. The study describes the dynamics that exist between α-synuclein, Ca^{2+} and calbindin in the formation of aggregates. Free Ca^{2+} was found to enhance fibrillation rates of α-synuclein, in the absence of calbindin. However, with calbindin in its vicinity, fibril forming tendency of α-synuclein was greatly reduced with increase in free Ca^{2+}. It was also noted that the fibrillation inhibition capacity of calbindin was Ca^{2+}-dependent.

Ca^{2+} binding dynamics The dynamics of binding of calcium to the fast buffer calbindin, is modelled using mass action kinetics. Although the protein has

four different binding sites for Ca^{2+}, due to their fast binding rates, it is assumed that the binding sites act independently of one other.

$$Ca + Calb \underset{k_{\text{calb,b}}}{\overset{k_{\text{calb,d}}}{\rightleftharpoons}} CaCalb,$$

with $CaCalb$ representing the bound complex. The kinetic parameters for the high affinity binding is adapted from Nagerl et al. [2000] (Table 4.6),

$$J_{\text{calb}} = k_{\text{calb,b}} \cdot Ca_i \cdot Calb - k_{\text{calb,d}} \cdot CaCalb. \tag{4.17}$$

4.6.2 Calmodulin

Calmodulin is the primary sensor of intracellular Ca^{2+} variations in eukaryotes and is involved in many regulatory Ca^{2+}-dependent signalling pathways. This 17 kDa acidic protein acts as an intermediate messenger that decodes Ca^{2+} signals, by virtue of its structural change upon sequestering Ca^{2+} [Symersky et al., 2003]. The binding of four Ca^{2+} ions reveals two hydrophobic patches that specifically bind to calmodulin binding domains[5] on target proteins, allowing the molecule to wrap around its target. The significance of calmodulin in metabolism can be realized if we look at the diversity of cellular events it mediates, including a number of metabolic pathways, ion transport, cell maintenance and apoptosis, memory, immune response etc.

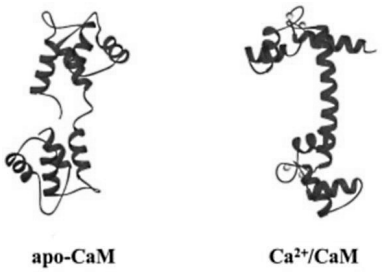

Figure 4.8: The role of calmodulin as a calcium sensor has to do with its conformational change. Note how the backbone of calmodulin is extended when Ca^{2+} binds to it. Figure from Vetter and Leclerc [2003].

[5]The calmodulin binding domains show a propensity to form a basic amphiphilic α-helix, that have hydrophobic regions complimentary to the one on the Ca^{2+}-calmodulin complex

Structure and its significance Calmodulin is a protein whose structure has been highly conserved among eukaryotes [Catalano and O'Day, 2008]. Ca^{2+}-free apo-calmodulin is made of two globular domains each containing two Ca^{2+}-binding sites that are EF-hand motifs. These domains are connected by a flexible α-helix. This compact apo-form is converted to an extended dumb-bell shaped form on binding with Ca^{2+} [Zhang et al., 1995] (see figure 4.8). The hydrophobic patches that lie buried between the α-helical segments in the apo-conformation, are revealed with the binding of Ca^{2+} and makes the molecule ready for Ca^{2+}-signal transduction. Although the four binding regions are formed from homologous sequences, there is a noticeable difference in the binding rates at the carboxy- (C) and amino- (N) terminal of the protein. The C-terminal lobe appears to have a higher affinity to Ca^{2+} Vetter and Leclerc [2003]. The high affinity site binds Ca^{2+} at lower concentrations, whilst the low affinity site binds only with a higher surge in cytosolic Ca^{2+} levels.

Calmodulin in PD pathogenesis Unlike calbindin, which has been directly implicated in PD development, calmodulin does not seem to have a direct affect on the pathogenic pathways. However, as the immediate effector of Ca^{2+} in calcium-signalling cascade, it is heavily involved in mechanisms leading to the degeneration of the neurons. Again, with a direct influence on membrane proteins like PMCA, ER CA and SK-type K^+channel, they are involved with the membrane electrophysiology of these neurons.

Another instance when calmodulin was possibly implicated in PD pathogenesis came from an immunoreactivity study on Lewy body [Iwatsubo et al., 1991]. A protein positioned downstream of calmodulin in the calcium - signalling cascade, calcium-calmodulin dependent protein kinase II (CaMK-II) was reported to be present on halos of LBs. However, since they were found on the periphery of LBs, it is hard to decipher their exact role in the process. This peripheral location of CaMK-II suggests a possible neuroprotective role. Martinez et al. [2003] had identified α-synuclein as a potential substrate of calmodulin, with the activated form accelerating the fibrillation rates of α-synuclein *in vitro*. However, it remains to be seen whether activated CaMK-II promotes fibrillation *in vivo*. Furthermore, this seems highly unlikely as Ca^{2+}-calmodulin immunoreactivity has not been observed in the core of a LB.

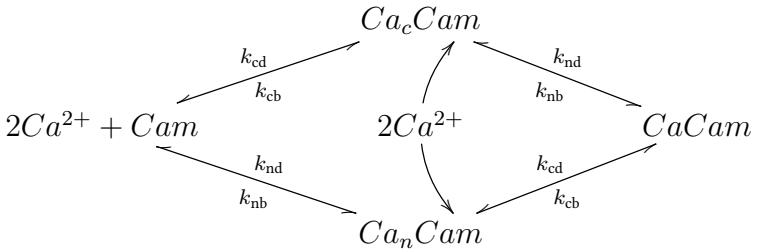

Figure 4.9: Dynamics of calcium - calmodulin buffering

Parameter	Value	Unit	Source
$k_{\text{calb,b}}$	10	1/mM.ms	Nagerl et al. [2000]
$k_{\text{calb,d}}$	2×10^{-3}	1/ms	Nagerl et al. [2000]
k_{cb}	12,000	1/mM^2.ms	Tadross et al. [2008]
k_{cd}	0.003	1/ms	Tadross et al. [2008]
k_{nb}	3.7×10^{-6}	1/mM^2.ms	Tadross et al. [2008]
k_{nd}	3	1/ms	Tadross et al. [2008]

Table 4.6: Kinetic parameters for calcium buffering

Calcium binding dynamics Ca^{2+} has four binding sites on calmodulin. Of these two are located on the C-terminal lobe and the remaining two on the N-terminal. However, the binding and dissociation rates to each of these lobes are different. We model the binding of calcium [Tadross et al., 2008] as a four state Markov process involving the simultaneous association of Ca^{2+} at each lobe. The model is further reduced to two states, assuming quasi-steady state for the intermediary states (Figure 4.9). The flux may be defined as,

$$J_{\text{cam}} = \alpha_{\text{cam}} \cdot Cam - \beta_{\text{cam}} \cdot CaCam, \tag{4.18}$$

where the rate constants, α_{cam} and β_{cam} are defined by cytosolic Ca^{2+} concentration as follows:

$$\begin{aligned}
\alpha_{\text{cam}} &= k'_{\text{cb}} \cdot k'_{\text{nb}} \cdot \left(\frac{1}{k'_{\text{cb}} + k_{\text{nd}}} + \frac{1}{k'_{\text{nb}} + k_{\text{cd}}} \right), \\
\beta_{\text{cam}} &= k_{\text{cd}} \cdot k_{\text{nd}} \cdot \left(\frac{1}{k'_{\text{cb}} + k_{\text{nd}}} + \frac{1}{k'_{\text{nb}} + k_{\text{cd}}} \right), \\
k'_{\text{cb}} &= k_{\text{cb}} \cdot [Ca_i]^2, \\
k'_{\text{nb}} &= k_{\text{nb}} \cdot [Ca_i]^2.
\end{aligned}$$

Table 4.6 gives the values of the kinetic parameters of calcium buffering.

4.7 Organelles implied in calcium homeostasis

The system of proteins on the neuronal membrane involved in pumping back calcium from the cytosol to the extracellular space has limited capacity. Also, having a large number of ATPases on the membrane adds to the metabolic burden of the cell. The same argument holds for the case of having a controlled level of mobile calcium buffers within the cytosol, in addition to some of them having important signalling roles. Any additional Ca^{2+} needs to be sequestered into near neutral spaces wherein the Ca^{2+} would have limited metabolic impact. ER and mitochondria assume this role of removing Ca^{2+} from the cytosol and playing important roles in calcium homeostasis by its controlled release.

4.7.1 The Endoplasmic Reticulum

The endoplasmic reticulum (ER) together with the mitochondria forms an intracellular network of dynamic interactions that controls metabolic flow, protein transport and calcium homeostasis. The ER is an organelle involved with a wide range of cellular processes. One of its primary role is as a calcium store and is responsible for regulating calcium signals at local and global levels [Berridge, 2002]. Its physical spread and continuity as well as absence of fixed luminal calcium buffers, enable ER in disseminating Ca^{2+} quickly across the length and breadth of the neuron [Park et al., 2000]. In some cell types it acts as the most important source of calcium signals through the process of CICR. The release of Ca^{2+} from ER is often positioned close to the plasma membrane near a calcium transporter or in the close proximity of mitochondria or other sites significant in calcium controlled pathways. This makes ER a bridge that connects various calcium hotspots and prevents a larger diffusion of Ca^{2+} in the cytosol.

The Ca^{2+} stored within the ER (luminal calcium, Ca^{2+}_{er}) also have important regulatory roles. A basal level of Ca^{2+}_{er} is required for protein folding, as ER protein processing pathways involve a number of calcium-dependent chaperones responsible for the folding and packaging of proteins. Also, emerging results in the field of apoptosis research suggest an important regulatory role for Ca^{2+}_{er} in the susceptibility of a cell to apoptosis [Berridge, 2002].

In *SNc* neurons, the ER forms an extensive network throughout the somato-dendritic tree [Schwyn and Fox, 1974]. The involvement of ER activities with the degeneration of *SNc* neurons in PD came to focus with the discovery of an ER stress protein in the Lewy Bodies [Conn et al., 2004] (Also see Section 2.3.3). The involvement of the ER as a centre of cellular calcium homeostasis necessitates including the luminal mechanism of Ca^{2+} handling, in models aimed at understanding Ca^{2+}-regulated pathways of the disease. Even though there are various models developed for relating the electrophysiology and involvement of Ca^{2+} in neurons of the *substantia nigra*, there is apparently no model linking them to the internal calcium-handling aspects. In this thesis, we aim to develop a basic framework that involves this aspect.

4.7.1.1 Calcium uptake by the ER

The clearance of calcium from cytosol into intracellular stores is usually against the electrochemical gradient and therefore requires the system to expend energy. The calcium ATPases of the ER (ERCA) transports Ca^{2+} from the cytosol to the ER lumen by a coupled ATP hydrolysis. The molecular mechanism by which the ERCA act is similar to that of the PMCA, with a cyclic process of transformation between two major conformational states [Wuytack et al., 2002]. However, the rate at which ERCA moves Ca^{2+} is influenced by proteins found in the lumen and cytosol. For example, the buffering of Ca^{2+}_{er} by calsequestrin, a luminal Ca^{2+} binding protein, considerably reduces the effective concentration gradient against which this pump operates. As with PMCA, the Ca^{2+}- calmodulin complex has a positive impact on the pump kinetics [Pifl et al., 1984]. Immunocytochemical studies indicate an abundance of ERCA in *SNc* neurons [Patel et al., 2009].

The uptake of Ca^{2+} ions by ERCA may be modelled with a simple Michaelis - Menten type kinetics such as in Tiveci et al. [2005] or using a detailed dynamics akin to the Kyoto model for PMCA, given in Matsuoka et al. [2007].

4.7.1.2 Calcium release by the ER

The release of Ca^{2+} from the ER is brought about by two sub-families of ligand gated calcium channels. One of these channels are activated by levels of Ca^{2+} in the cytosol and is dubbed as the ryanodine receptor (RyR). The other channel is regulated by the levels of inositol trisphosphate ($InsP_3$) and is known as the $InsP_3R$. In addition to these, there is a notable mechanism responsible for steady state luminal Ca^{2+} levels and involves a leak of Ca^{2+} from the ER membrane surface. The exact mechanism behind ER leakage of Ca^{2+} is yet to be explored.

Mobilization of Ca^{2+} from ER has an important functional implication in the somatodendritic dopamine release in *SNc* neurons [Patel et al., 2009]. Both $InsP_3R$ and RyR have been observed in these neurons by immunocytochemistry and their functioning makes the neurons less dependent on extra-cellular Ca^{2+} for neurotransmitter release.

Luminal calcium leak The process of calcium leak from ER was revealed in an experiment following the inhibition of ERCA [Hofer et al., 1996]. The inhibitors of $InsP_3R$, RyR, and other known Ca^{2+} release mechanisms had no effect on the rate of this leak [Hofer et al., 1996; Lomax et al., 2002; Camello et al., 2002]. A few different molecules seem to have some effect on this phenomena including ATP, glutathione, Ni^{2+}. However these effects were not universally observed and varied between cell types [Camello et al., 2002].

The primary effector of leak of Ca^{2+} from the lumen appears to be the level of Ca^{2+}_{er} itself. In the majority of the cell types studied, even though this passive leak is capable of completely depleting the lumen within minutes, there seems to be a regulatory mechanism in place that apparently slows down the leak as Ca^{2+}_{er} level goes below 40 μM [Mogami et al., 1998]. The kinetics of luminal calcium leak seem to be influenced by the saturation of probable moderators by Ca^{2+}_{er}, that drive the mechanism at the ER membrane. Additionally, the maximum leak rate appears to be cell dependent [Camello et al., 2002].

Calcium induced calcium release (CICR) The mechanism of CICR is brought about by RyR and with this mechanism a small, but substantial release of calcium is observed into the cytosol from the ER . In neurons of the *substantia nigra*, RyR appears to be preferentially distributed at the margins of the neuronal body closer to the plasma membrane and to a smaller extent throughout the cytoplasm of the soma. The distribution of the surface RyRs also parallels the distribution of L-type calcium channels suggesting a positional coupling between the two [Patel et al., 2009] driven by strong calcium gradients. This positioning enables CICR by minimal calcium entry in the vicinity of the plasma membrane and the mechanism is thought to amplify cytosolic Ca^{2+} levels in conditions of insufficient transmembrane Ca^{2+} influx.

$InsP_3$ mediated calcium release $InsP_3$ is an important second messenger involved in the release of Ca^{2+} from intra-cellular stores. It is formed from the hydrolysis of a membrane phospholipid, phosphatidylinositol 4,5-bisphosphate by phospholipase C (PLC) as a result of a signalling cascade initiated by an external signal. The cytosolic Ca^{2+} has an effect on the activation of PLC by a positive feedback, enhancing the production of $InsP_3$ and in turn enhancing the release of Ca^{2+} from ER [Meyer and Stryer, 1991; Oancea and Meyer, 1998]. The dynamic interaction between $InsP_3$ and Ca^{2+} in ER and cytosol is capable of spontaneous calcium waves within the cytosol [Lavrentovich and Hemkin, 2008], however this is often regulated by events at the plasma membrane. Complex calcium oscillations in non-excitable cells are often described by means of this dynamic interaction [Marhl et al., 2000].

In *SNc* neurons, immunostaining for $InsP_3R$ displayed a homogeneous distribution of the protein throughout the cytoplasm in the soma and proximal dendrites and an absence of these proteins in the distal dendrites [Patel et al., 2009]. The Ca^{2+} released by the $InsP_3R$ mediated process, usually enters a region formed by a close association of ER and mitochondria, referred to as the micro-domain [Csordás et al., 2006].

4.7.2 A significant calcium micro-domain between ER and mitochondria

In a cell, the position of its organelles has important functional implications. Most often, the cellular constituents are placed in a manner that would impose minimum energy expenditure in the cell. With respect to the calcium handling system of a neuron, the participating elements are often brought together by strong calcium gradients as well as certain cytoskeletal structures. One of most noticed among these is an association between ER and mitochondria and is referred to as a quasi-synaptic organization [Csordás et al., 1999]. Although there were suggestions of a physical link between the two organelles, recent developments in the field has identified the presence of molecular structures responsible for this association [Hayashi et al., 2009]. This physical association has been termed 'mitochondria-associated ER membrane' (MAM) and has been implicated in various metabolic activities of the cell and in particular calcium homeostasis.

The micro-domain so formed is characterised by the presence of membrane proteins that transport Ca^{2+} on organelles that surround the micro-domain. The ER face of the domain is most often occupied by the $InsP_3R$ and at times by the RyR. The mitochondrial face of the domain is occupied with the calcium uniporter system. This functional arrangement is critical for the functioning of the uniporter, which requires μM levels of Ca^{2+} to activate. When $InsP_3R$ is activated, it creates a local transient upsurge in Ca^{2+}, sufficient to activate the uniporter. This arrangement is also critical in apoptosis, when molecules associated with apoptosis such as cytochrome c activate $InsP_3R$. This activation leads to a sustained Ca^{2+} surge at the micro-domain, overloading the mitochondria.

A set of proteins that act as molecular chaperones is understood to regulate this association and in turn modulate the Ca^{2+} uptake rate of the mitochondria with metabolic implications [Hayashi et al., 2009].

4.7.3 Mitochondria

The mitochondrion is an important component of the calcium handling cellular machinery, as it sequesters Ca^{2+} during an upsurge, stores it efficiently, and slowly releases Ca^{2+} to the cytosol when the cell recovers. This mitochondrial activity contributes in shaping both the amplitude and spatio-temporal patterns of the calcium signals [Werth and Thayer, 1994; Duchen, 1999; Duchen et al., 2008]. The mitochondria are often found in the proximity of ER and plasma membrane [Boldogh and Pon, 2007; Pizzo and Pozzan, 2007], creating a local hotspot of high Ca^{2+} that aid in transport of Ca^{2+} into its inner matrix through a calcium uniporter.

The ability of mitochondria to store large amounts of Ca^{2+} within its matrix arise from the fact that the ingested Ca^{2+} forms a precipitate with phosphate, which is co-transported along the uniporter system [Kirichok et al., 2004]. These precipitates are observable with electron microscopy and are thought to be formed by a nucleation process initiated by a mitochondrial protein. The detailed mechanism by which precipitation occurs is yet to be confirmed.

Calcium sequestered into the mitochondria has important physiological effects on the cell's energetics and survival. To begin with, an increase in the levels of mitochondrial calcium (Ca^{2+}_{mit}), stimulates Ca^{2+} sensitive dehydrogenases of the Kreb's cycle[6], thereby enhancing the rate of NADPH and ATP synthesis. However, an increase in Ca^{2+}_{mit} level above a certain threshold has a direct influence on the mitochondrial membrane potential. A reduction in mitochondrial membrane potential with increasing Ca^{2+}_{mit} reduces the effectiveness of the electron transport chain and lowers ATP production. An overload of Ca^{2+}_{mit} can disrupt the mitochondrial membrane potential leading to the release of proteins like cytochrome c from the inner mitochondrial membrane into the cytosol. This promotes events leading to apoptosis.

The mitochondrial membrane potential ($\Delta\psi$) is an important parameter that defines the physiological state of a mitochondria and in turn indicate a cell's

[6] Ca^{2+} sensitive dehydrogenases of the Kreb's cycle includes pyruvate dehydrogenase, isocitrate dehydrogenase amd α-ketoglutarate dehydrogenase. These enzymes are associated with the important rate limiting steps of the cycle and their activations controls the rate of ATP synthesis in the mitochondria [Nelson and Cox, 2004]

health or distress. It signifies a cell's capacity to generate ATP by oxidative phosphorylation. Along with the mitochondrial pH gradient, it imparts the required driving force to transport protons in to the mitochondria. The mitochondrial membrane potential also has a significant role in mitochondrial Ca^{2+} sequestration as well as in the regulation of ROS production. When this potential is upset by means of protonophores, Ca^{2+} is released from the mitochodria and further uptake of Ca^{2+} from the cytosol is disrupted [Werth and Thayer, 1994].

A mitochondrial membrane potential between 150 - 180 mV is typical in normal cells. However, under conditions of cellular stress, the mitochondrial membrane potential is usually altered by the perturbed levels of intracellular cations, thereupon leading to changes in ATP production. An extreme stress can bring about a complete collapse of this regulatory system leading to apoptosis.

As the ultimate store of cellular Ca^{2+}, mitochondria have a crucial role in calcium homeostasis. Mitochondria employ an electrogenic carrier called the calcium uniporter to transport exogenous Ca^{2+} into the mitochondrial matrix, across the inner mitochondrial membrane (IMM). This transport is usually coupled with a co-transport of inorganic phosphate that together with the accumulated Ca^{2+}, form osmotically inactive precipitates within the matrix. Ca^{2+} is eventually released back into the cytosol by the activity of antiporters (Na^{+}/Ca^{2+} or H^{+}/Ca^{2+} exchangers) found on the IMM.

4.7.3.1 Calcium uptake by the mitochondria

Mitochondrial uptake of Ca^{2+} involves a complex system of proteins spanning its two membranes. The system consists of a uniporter mechanism driven by the steep membrane potential that exists in the inner mitochondrial membrane. This low-affinity uniporter works more like an ion-channel that is highly selective and inwardly rectifying [Kirichok et al., 2004]. The system which remains in a deactivated state at low cytosolic Ca^{2+} levels, assembles at high Ca^{2+} upsurge enabled by the ER - mitochondrial micro-domain arrangement, promoting the uniporter proteins to form a Ca^{2+} conducting channel. This consists of a gated pore with a Ca^{2+} binding site on the cytosolic side of the inner mito-

chondrial membrane [Starkov, 2010].

The exact molecular identities of the uniporter system had remained elusive for some time. Recent advances in molecular techniques has enabled the identification of the proteins involved in the regulation of this process. A genome-wide search for authentic mitochondrial proteins that satisfied expected properties of the uniporter, has yielded the identity of important proteins contributing to the process [De Stefani et al., 2011; Raffaello et al., 2012]. The chief protein of this system, dubbed as MCU (for mitochondrial calcium uniporter), is a 40 kDa protein, and is found localized in the inner mitochondrial membrane. This protein tends to enhance mitochondrial Ca^{2+} uptake on over-expression [De Stefani et al., 2011].

Even before the molecular identities of major proteins involved in this system were established, ongoing research had outlined the dynamics of the uniporter. It is now understood that the calcium uptake system operates in two modes. In the calcium-uniporter mode (CU mode), the system is able to take in Ca^{2+} only when the concentrations rise to μM range. The existence of the micro-domain helps this mode of operation. However, mitochondria are also capable of quickly responding to calcium signals in the nM range even when isolated, in the absence of a micro-domain [Picard et al., 2011]. This response of mitochondria is attributed to a rapid mode of Ca^{2+} uptake (RaM mode). This mechanism postulates Ca^{2+} binding onto an external trigger site, initiating a short transient of high Ca^{2+} conductivity [Starkov, 2010; Bazil and Dash, 2011] (see figure 4.10). According to the scheme of events from this proposal, Bazil and Dash [2011] has developed a four state Markov scheme to describe the kinetics of the Ca^{2+} uptake system of the mitochondria.

4.7.3.2 Calcium release from the mitochondria

The Na^{+}/Ca^{2+} antiporter of the mitochondria functions as the primary exit point for Ca^{2+}_{mit} and has an important role in mitochondrial calcium homeostasis. Similar to the plasma membrane Na^{+}/Ca^{2+} exchanger, its mitochondrial counterpart is also found to be a cytosolic Na^{+}dependent Ca^{2+} exchange. Although its kinetics are not yet completely understood, it is thought to be highly

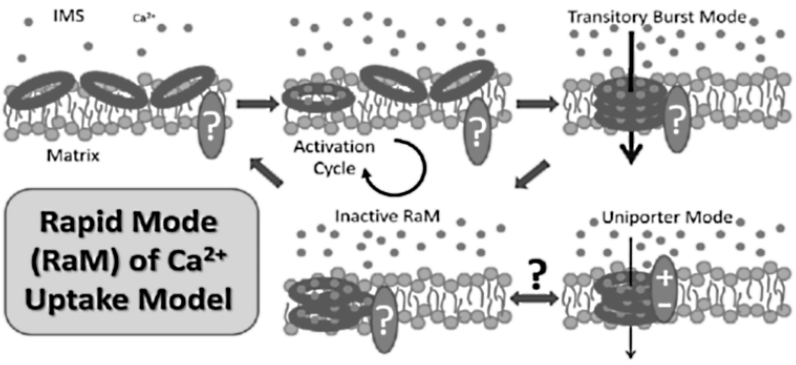

Figure 4.10: Scheme of events proposed by Starkov [2010] for the Ca^{2+} uptake mechanism of the mitochondrial Ca^{2+} uniporter system. According to this scheme, Ca^{2+} is required to initiate an activation cycle beginning with a transient high Ca^{2+} conductive state. This state achieved by the rearrangement of participating proteins, can undergo a conformational change eliciting a slow uptake mode or the uniporter mode, if the Ca^{2+} concentration remains elevated in the μM range. Once the external Ca^{2+} falls below a threshold, the complex dissociates to its original state. Image from Bazil and Dash [2011]

dependent on the environmental pH [Baysal et al., 1991]. As research is yet to uncover the facets of this exchanger, literature on the activity of this protein is limited. However, there are a few mathematical representations of its activity ranging from models based on the Hill function [Wingrove and Gunter, 1986], Kyoto model [Kim and Matsuoka, 2008] to detailed Markov models [Pradhan et al., 2010].

Concluding remarks In this chapter, we have discussed the different ways in which active and facilitated transport across membrane structures are mathematically described. In the literature, there is no single preference among these models. Some models are simple, and are used frequently in larger models. However, they do not completely describe the mechanism of the system. Models that incorporate mechanistic details are often larger and bring in computational and analytical complexities. We have done a basic comparison to understand how some of these models fare in a given situation. This has helped eliminate some models as not suitable for our purposes. However, with the remaining model choices there is no absolute winner. In chapter 6, we consider using some of these models for a larger framework of building a mathematical formalism to describe pacemaking in *SNc* neurons.

Part III

Towards a theory for *substantia nigra* neurodegeneration

CHAPTER 5

The *substantia nigra* pacemaker

In this chapter we bring together various concepts discussed previously, to develop a mathematical description of the pacemaking activity observed in SNc neurons. We initially discuss various facets of the electrophysiology in these neurons and identify membrane components that contribute towards these activites. As a first step, a model is developed by considering a simple geometric design of the neuronal soma. Later the model is improved upon by a change in design of the model geometry that is closer to the structure of these neurons. The model is analysed for its dynamics as well as implied energy usage.

Introduction Oscillations are an important feature of the functioning brain and are significant for information processing in the brain. Different brain regions often house neurons that are capable of pacemaking, that is, exhibit stable oscillations. The functioning of these neurons are defined by their phenotype, in other words, they express membrane proteins responsible for a variety of ionic membrane transport mechanisms.

The autonomous tonic pacemaking of *SNc* neurons is a unique feature that enables them to indirectly control motor activity. As each action potential prompts the release of dopamine from these neurons, the oscillations ensure a continual supply of dopamine to the striatum, significant for the normal functioning of such motor activities. These neurons are also known to switch from this pacemaking mode to a bursting mode, when stimulated. Such events are

often associated with rewarding stimulus and are associated with spatial learning and temporal processing [Da Cunha et al., 2003; Matell and Meck, 2000].

Conventionally, neuronal pacemaking is modelled as the result of events at the neuronal membrane. Although events within a cell play a role in the dynamics of membrane potential, the majority of models in the literature do not consider them within their framework. This is true even in the case of *SNc* neurons. With a few significant models developed for these neurons [Amini et al., 1999; Canavier, 1999; Wilson and Callaway, 2000; Komendantov et al., 2004; Canavier and Landry, 2006; Kuznetsova et al., 2010; Drion et al., 2011], there are few models that discuss how intracellular levels of participating cations are affected by the different membrane currents and vice versa. Although it is difficult to incorporate all cellular events contributing to the intracellular ionic dynamics, to model pacemaking activity, it may be sufficient to include the most significant events that contribute towards establishing the electrical rhythm in these neurons. We could do this by an extensive model that considers all major subcomponents that contribute or by a reduced model just by considering events closer to the membrane. We first attempt to model this activity based on the events that take place in the vicinity of the cell membrane.

In this chapter, we give a mathematical representation of the pacemaking activity of *SNc* neurons. Starting with a discussion on the observed electrophysiology of these neurons and elements contributing towards this, we start with a simple geometric design to develop the model. Later we switch to a realistic geometric design for the model and discuss different aspects of *SNc* pacemaking implied by the identified parameters of the model.

5.1 Ionic conduction at the *SNc* membrane

As for any neuron, the contribution of *SNc* towards the functioning of the animal brain, is characterised by its electrophysiology. *SNc* neurons have a characteristic pattern of spiking which is the result of a combination of its intrinsic membrane properties and extrinsic signals, through synaptic inputs. Ion-transport mechanisms present at the membrane, with its highly non-linear properties, result in a coordinated ensemble of ionic currents (Na^+, $K^+$and Ca^{2+}),

that underlies the changes in the membrane potential. In this section, we discuss the characteristics of *SNc* electrophysiology and different ion-channels that are understood to contribute to the dynamics.

5.1.1 Electrophysiology of *substantia nigra* neurons

Midbrain dopaminergic neurons including *SNc* neurons are characterised by broad action potentials and a spontaneous firing pattern [Komendantov et al., 2004]. The action potential generated has distinct components: (1) a *slow depolarization* involving a pacemaker like conductance, (2) a short *initial segment spike* which involves a low threshold spike probably originating at the axon hillock, (3) a longer *somatodendritic spike*, with a higher threshold , and (4) a long lasting *afterhyperpolarization* [Grace and Bunney, 1983a]. In extracellular recordings, the initial segment spike and the somatodendritic spike are seen as separate peaks.

In isolation (*in vitro*), *SNc* neurons fire at a highly regular pattern at low-frequency. However, this is rarely observed *in vivo* as the neurons fire at a less regular pattern, still at a similar frequency. Burst firing is also observed *in vivo* from time to time, in addition to this background firing. This mode of firing may be generated *in vitro* by stimulating the glutamate receptors with an agonist such as NMDA.

The background firing in *SNc* is a slow (1-8 Hz) process that is triggered from a high threshold of around -40 mV. To achieve this, the neuronal membrane needs to be depolarised from its resting potential (which is around -57 mV). The process of spike generation is considered to be comprised of both $Na^+$and Ca^{2+}- dependent conductances, as spiking is lost by blocking either of the currents by the administration of respective channel blocker. The background firing is thought to be driven by a sub-threshold oscillation that is observed when the spike generating conductances are blocked by pharmaceutical agents [Ping and Shepard, 1996]. This oscillation, which is commonly known as the slow oscillatory potential (SOP) is understood to be made up of a Ca^{2+}-K^+mechanism mediated by the L-type calcium channel and SK-type potassium channel [Harris et al., 1989; Wilson and Callaway, 2000]. A SOP is also observed in dendrites although at a slightly faster rate [Wilson and Callaway, 2000].

An increase in activity of the dopaminergic neuron is accompanied by a change in the pacemaking pattern, from a single-spike mode to burst firing [Grace and Bunney, 1984b,a]. One noticeable difference between burst firing in *SNc* and other neurons is that the burst is with respect to the interspike interval. This gap is comparatively longer in *SNc* and the burst cannot be generated easily unlike other neurons, *in vitro*, by somatic current injections [Richards et al., 1997]. On the other hand, intense bursting may be induced *in vivo*, with spikes that progressively decrease in amplitude and increase in spiking interval [Hyland et al., 2002]. Glutamatergic synaptic inputs play a major role in the generation of bursting activity [Grace and Bunney, 1984a] and may be mimicked in experiments with the help of NMDA. Also, interfering with GABA (γ-aminobutyric acid) receptors induce bursting [Tepper et al., 1995], suggesting a role for GABA in the inhibition of *SNc* neurons. Experiments to analyse bursting in these neurons achieve this by bath application of NMDA (for example, see Ibanez-Sandoval et al. [2007]).

The involvement of a Ca^{2+} and K^{+}currents in bursting has been demonstrated when bursting was suppressed with the application of a Ca^{2+} chelator and a SK-channel blocker [Grace and Bunney, 1984a]. However, Ca^{2+} does not appear to be critical, since Ca^{2+}-independent bursts have been demonstrated even with the chelation of cytosolic Ca^{2+}, *in vitro* with the application of an NMDA bath.

In essence, the electrical activity at the *SNc* membrane appears to be the result of a dynamic interaction of components responsible for the transport of ions across the membrane. Among the different ions, Ca^{2+}, $Na^{+}$and K^{+}appears to be the most significant. The alterations in the transport of these ions are based on the electrochemical properties of the respective transporter proteins and their concerted action is critical in defining the neuron properties. A model for these interactions would involve a good identification and description of these units. Also, it is important to understand the dynamic properties of the resulting system, that lends it the expected behaviour under a given perturbation. Such perturbations are discussed later in the chapter.

In tune with the theme of this thesis, we are concerned with how best we could relate the basal activity of these neurons to energy models that would be developed to understand PD pathogenesis. For this reason, we concentrate

on developing a model for the background firing activity and seek means to estimate the average energy use. For developing an electrophysiological model we need to understand the participating components that contribute to the characteristic electrophysiology. In the next section, we discuss on how these elements are elucidated.

5.1.2 Ion channels on *SNc* membrane contributing to its spontaneous activity

The development of mathematical models to represent neuronal activity, necessitates identification of the appropriate category of ion-channels involved. This identification process remains one of the biggest challenges in the development of electrophysiological models for neurons. Traditionally this is understood from studies involving channel blockers, but the resolving power of these experiments is not always good. The analysis can be limited for a variety of reasons, including problems with experimental design and set up, non-specificity of the blocker molecule towards a range of channel proteins, variability in the expression levels of target proteins in the region of interest etc.

In the case of *SNc* neurons, such experiments (for example, see Ibanez-Sandoval et al. [2007]) have revealed the involvement of various channels contributing to the pacemaking in these neurons. This includes tetradotoxin (TTX) sensitive sodium channels, high voltage activated calcium channels (sensitive to Calcicludine and dihydropyridines), T-type calcium channel (blocked by $NiCl_2$), Apamin sensitive SK-type calcium activated potassium channel, Tetraethylammonium (TEA) sensitive BK-type calcium activated potassium channel and ZD 7288 sensitive HCN channel.

Experiments with channel blockers have given rise to a number of mathematical models describing *SNc* electrophysiology. However, there exists a lack of agreement between these models on the formulation for the respective ion-channel activity. Apparently, only models coming from the same research group show some consistency in the kind of mathematical paradigms used. In table 5.1, we compare the different ion channels employed by some of the popular models in literature. As we can see from this comparison (table 5.1), there

Channel	Model number							
	1	2	3	4	5	6	7	8
Sodium conductance								
Transient	✗	✓	✓	✓	✓	✓	✓	✓
HCN (h-type)	✓	✗	✗	✓*	✓*	✗	✗	✗
Leak	✓	✓	✓	✓*	✓*	✓	✓*	✓*
potassium conductance								
SK-Type	✓	✗	✓	✓	✓	✓	✓	✓
BK-Type	✗	✗	✗	✗	✓	✗	✗	✗
Delayed rectifier	✓	✓	✓	✓	✓	✓	✓	✓
Inward rectifier	✓	✗	✗	✓	✗	✗	✗	✗
A-Type	✓	✗	✓	✓	✓	✓	✗	✗
HCN (h-type)	✓	✗	✗	✓*	✓*	✗	✗	✗
Leak	✓	✗	✓	✓*	✓*	✓	✓*	✓*
Calcium conductance								
L-Type	✓	✗	✓	✓	✓	✓	✓	✓
T-Type	✓	✗	✓	✗	✗	✗	✗	✗
N-Type	✓	✗	✓	✗	✗	✗	✗	✗
HVA-Type	✓	✗	✗	✓	✓	✗	✗	✗
Leak	✓	✗	✓	✗	✗	✓	✗	✗
Pumps and exchangers								
NaCax	✓	✗	✗	✗	✗	✗	✗	✗
NaK	✓	✓	✓	✗	✗	✓	✗	✗
PMCA	✓	✗	✓	✗	✗	✗	✗	✓
Others								
Electrode currents	✗	✓	✗	✗	✗	✓	✓	✗
Synaptic input currents	✗	✓	✓	✗	✗	✗	✓	✓

Table 5.1: List of ion-channels appearing in various models for *SNc* in literature (1) Amini et al. [1999] (2) Canavier [1999] (3) Komendantov et al. [2004] (4) Chan et al. [2007] (5) Guzman et al. [2009] (6) Kuznetsova et al. [2010] (7) Oster and Gutkin [2011] (8) Drion et al. [2011]. * In this case, the $Na^+$and K^+components are lumped for a mixed current

is no real consistency in the use of ion-channels among the different models. The conductances that appear in majority of the models include the transient sodium, L-type calcium, potassium delayed rectifier and SK-type potassium channels that are activated by Ca^{2+}. Most models avoid using pumps and exchangers, and since these models are mostly in the differential form, aspects of ionic charge conservation can be conveniently neglected.

Advances in the field of molecular biology has enabled the identification of proteins that are expressed by an organism. This provides an alternative to the rather indirect and tedious methods for assessing ion-channels expressed

in a neuron. Analysis of such expression profiles indicate that *SNc* neurons express a wide variety of cation channels, some of which play a significant role in its autonomous pacemaking behaviour. Based on the datasets of Moran et al. [2006] and Lesnick et al. [2007], Table 5.2 provides a comprehensive list of the type of cation channels expressed in the SN neuron on account of the α - subunits expressed.

Table 5.2: Channels of *substantia nigra*

A list of cation channel α sub-units expressed in Human *substantia nigra* based on the datasets of Moran et al. [2006] and Lesnick et al. [2007]

Channel type	Human gene	IUPHAR receptor
Family : Voltage-gated calcium channels		
L-type	CACNA1C	$Ca_v1.2$
	CACNA1D	$Ca_v1.3$
T-type	CACNA1G	$Ca_v3.1$
	CACNA1I	$Ca_v3.3$
P/Q-type	CACNA1A	$Ca_v2.1$
N-type	CACNA1B	$Ca_v2.2$
Family : Voltage-gated sodium channels		
	SCN1A	$Na_v1.1$
	SCN2A	$Na_v1.2$
	SCN3A	$Na_v1.3$
	SCN9A	$Na_v1.7$
	SCN11A	$Na_v1.9$
Family : Voltage-gated potassium channels		
Shaker-related delayed rectifier	KCNA1	$K_v1.1$
	KCNA6	$K_v1.6$
Shab-related delayed rectifier	KCNB1	$K_v2.1$
Shaw-related delayed rectifier	KCNC1	$K_v3.1$
	KCNC4	$K_v3.4$
Shal-related A-type channel	KCND2	$K_v4.2$
	KCND3	$K_v4.3$
Inward-rectifying channel	KCNH2	$K_v11.1$
	KCNH7	$K_v11.3$
Slowly activating outward rectifier	KCNH8	$K_v12.1$
Family : Inwardly rectifying potassium channels		
Inward-rectifier	KCNJ2	$K_{ir}2.1$

Continued on Next Page...

Table 5.2 – Continued

Channel type	Human gene	IUPHAR receptor
	KCNJ10	$K_{ir}4.1$
	KCNJ14	$K_{ir}2.4$
G protein-coupled	KCNJ6	$K_{ir}3.2$
inward-rectifier	KCNJ9	$K_{ir}3.3$
Family : Calcium-activated potassium channels		
BK channel	KCNMA1	$K_{Ca}1.1$
SK channel	KCNN2	$K_{Ca}2.2$
	KCNN3	$K_{Ca}2.3$
	KCNT2	$K_{Ca}4.2$
	KCNN2	$K_{Ca}2.2$
Family : Two-P potassium channels		
Tandem pore domain channel	KCNK1	$K_{2p}1.1$
	KCNK10	$K_{2p}10.1$
	KCNK12	$K_{2p}12.1$
	KCNK17	$K_{2p}17.1$
Family : Cyclic nucleotide-regulated channels		
Hyperpolarization-activated cyclic	HCN1	$HCN1$
nucleotide gated channel	HCN2	$HCN2$
	HCN4	$HCN4$
Other channels		
Voltage-independent, nonselective channel mostly responsible for sodium leak	NALCN	-
Two pore segment channel	TPCN1	$TPC1$
	TPCN2	$TPC2$

The protein expression profile results are quite consistent with the selection of ion-channels based on channel block studies. Although it is possible to model and connect all the different channels that are apparently expressed in a neuron, there are issues with such an approach. The first difficulty is in having a complex model with large number of components which, in turn, would make the model less comprehensible and appropriate for analysis. Next, a large number of parameters would likely result in identifiability problems. In such cases, even when a set of parameters are able to reproduce the experiments used for calibration, there can exist other families of parameter values that also

reproduce the data. Parameters identified may not necessarily have a physical meaning and in turn make the model limited in its predictive capabilities [Balsa-Canto et al., 2010].

Additionally, an important limitation of neuron models is the need for adaptation of electrophysiological characteristics of the ion-channels involved. Most often such characteristics are obtained from experiments that are not necessarily conducted with the same organism for which the larger model is developed (for example see Amini et al. [1999]). Even with these proteins being functionally conserved among species, there exist species to species differences in their post translational processing and variations in the choice of sub-units for their quaternary structure. Also, some of the post translational processing are tissue specific. Such differences, though subtle, are reflected in the dynamic response of these channels. Further, experiments on ion-channels are frequently conducted in conditions that are different from their native physiological environment. Parameters identified from such experiments when used in larger models, may lead to skewed interpretations of the phenomenon. On these grounds, mathematical models of neurons are necessarily simplifications that may represent some observable aspects of neuronal behaviour, but where many lower level details are treated in a simplified manner.

Thus, to develop our model we limit the selection of model components to a small number sufficient to reproduce the characteristic electrophysiology observed in *SNc*. Ion-channels were initially selected based on the criteria that they have been both used previously in modelling studies (table 5.1) as well as appear to be expressed in *SNc* neuron (table 5.2). Later in sections 5.4.2 and 5.5.2, when parameters were estimated , we eliminate some of these channels that do not appear to contribute significantly towards the measurable neuronal activity. The next type of components used in the model, membrane pumps and exchangers, are responsible for ionic charge conservation. We select only those proteins that contribute the most in the transport of cations considered in our model. The third type of model components are mobile calcium buffers that are understood to be present near Ca^{2+} entry points of the membrane. Details of selection made on type of transport components are discussed later, as we discuss the model. Figure 1.1 gives a sketch of components considered for the model and figure 5.1 is an extension showing the intricate relation of this

membrane system to the energy and calcium management in the neuron.

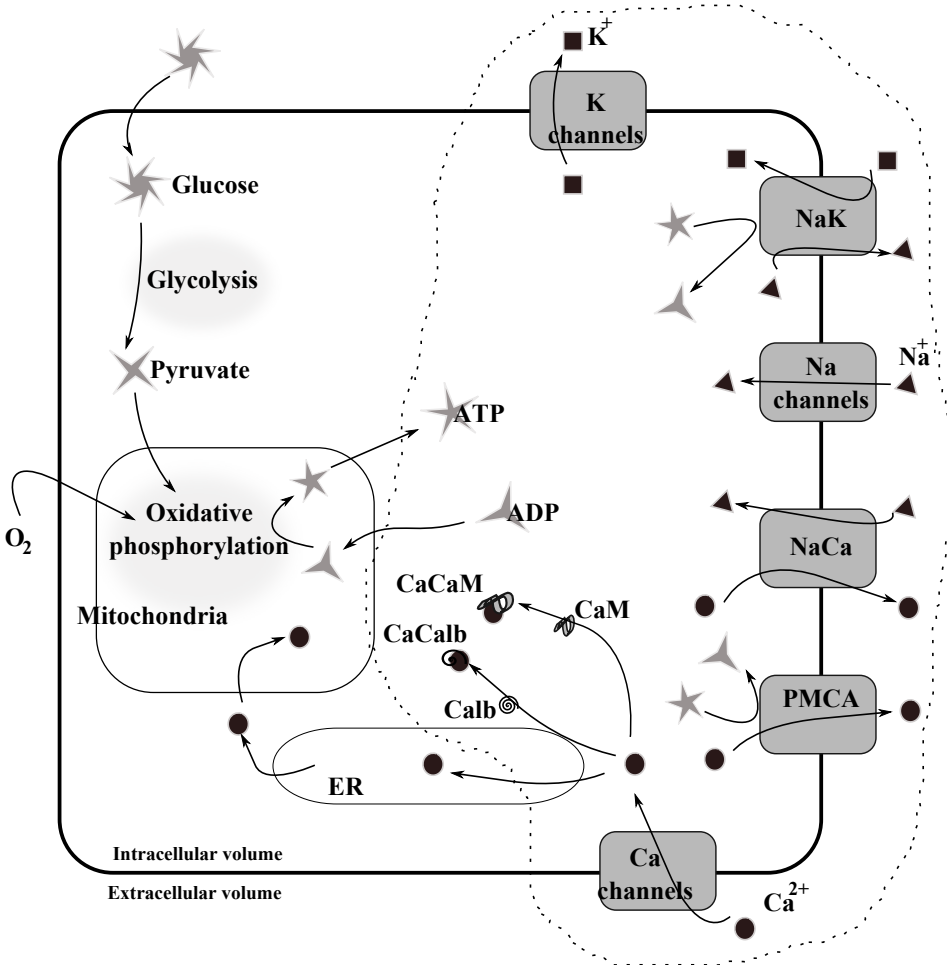

Figure 5.1: Schematic view showing the relationship of our model (marked off within dashed lines) with energy and calcium management system of the neuron

5.2 Theory of pacemaking

The very first attempt to analyse the electrophysiology of dopaminergic neurons took place 40 years ago [Bunney et al., 1973], in which a few different techniques were adopted to define the system of these neurons. Substantial research has taken place over the span of years to describe the different behavioural aspects of these neurons and a few attempts have been made to mathematically describe this system (see table 5.1). In this section we discuss the methodology that we adopt to develop a basic model to describe the back-

ground firing in *SNc* neurons and how we may roughly estimate the energy expenditure of this recurring process.

5.2.1 Modelling approaches

To develop a model for describing the pacemaking at the *SNc* membrane, we propose an approach that is technically a little different from many of the established models. One of the major differences with established models is in the use of the algebraic form of the voltage equation (see equation 3.5). By the use of algebraic form for calculating the membrane potential, in addition to having one dimension less in the state space, we also have a model which is more stable against slow drift in intracellular ion concentration often seen with the differential form (equation 3.2). Alternatively, we may use the modified differential form (equation 3.4) which incorporates ionic charge conservation principles and is stable against such drifts.

Next, owing to significant differences in the ion dynamics inside the cell, we prefer to use an electro diffusion model for channel conduction (equation 3.11) compared to the commonly used linear conductance relationship (equation 3.9). This is particularly important in the case of Ca^{2+} ions due to the large driving force of transport that exist for these ions across the membrane. Also, we use Markov models for the ionic pumps to incorporate the nuances of the limiting steps that control the dynamics of these proteins.

In the subsequent step, global optimisation strategies are used to identify important parameters of the model. The resulting model is then validated against observed behaviours for a set of perturbations.

5.2.2 Metabolic cost of membrane oscillations

A non-linear dynamic system is capable of spontaneous oscillations when it is an open system, i.e, there is a continuous flow of energy through the system from its environment [Strogatz, 2001]. In the case of neurons, oscillations at the membrane are driven by the energy supplied from its metabolic activities. Furthermore, neuronal oscillations are electrochemical in nature and they involve both the passive flow of ions with respect to the electrochemical gradient,

together with active (that is energy demanding) flows against the natural electrochemical gradient. The active transport mechanisms are demanding with respect to energy metabolism. In this section, we look for a simple mathematical formalism that can provide rough estimates of energy use at the membrane, owing to its spontaneous activity.

Estimates of energy use The transport and distribution of ions across the membrane, to maintain a functional state, involves proteins that use energy to transport ions against their gradient. The ATPase activity is directly coupled to ATP hydrolysis. The two ATPases in our model work towards maintaining the steady state levels of the cations and their activity is dependent on the availability of ATP for hydrolysis as well as their affinities for the respective cations. PMCA expels Ca^{2+} ions from the cytosol brought in by calcium channels at the membrane (as well as the intra-cellular stores, which is not included in the present model). NaK works to remove Na^{+}ions brought in by the action of sodium channels and NaCax. It also brings in K^{+}ions due to the coupled activity.

The energy-transduction associated with membrane excitation may be quantified according to the concepts laid down by Attwell and Laughlin [2001], in which such calculations are used to compare different functional aspects of neuronal signalling. Accordingly, we have

$$\frac{dATP_{\text{use}}}{dt} = \frac{[I_{\text{nak}} + I_{\text{pmca}}]}{F\mathcal{V}_{cyt}} \tag{5.1}$$

If ATP_{spike} represents the ATP consumed per spike by the *SNc* neuron, we have

$$ATP_{\text{spike}} = \frac{1}{F\mathcal{V}_{cyt}} \int_{0}^{t_{\text{spike}}} (I_{\text{nak}} + I_{\text{pmca}})\, dt \tag{5.2}$$

Note: If we consider the pacemaking oscillations to be stable, we have the transport of cations bound for a spike, i.e.

$$\int_{0}^{t_{\text{spike}}} d(S_i) = 0, S = \{Na^{+}, K^{+}, Ca^{2+}\}\,.$$

Accordingly, we may also calculate the energy use as ATP, from the corresponding current expressions.

5.3 Cellular geometry and relevance to mathematical modelling

Models developed for neuronal electrophysiology, predominantly use the differential form (equation 3.2) to described the variations in the membrane potential. The dynamics are then described by the variations in the current flow through the various channels considered for describing the membrane in the model. Most models assume fixed concentration of the participating cation species (or explicitly by assuming constant Nernst potentials for the corresponding ions). In some cases, when the dynamics of Ca^{2+} ions become significant to the model, the corresponding dynamics are included; but the rest of the ionic species are retained at a steady concentration. The advantage of this approach is that the cell geometry is irrelevant to the model, save that the surface area is often implicitly incorporated with the conductance parameter (for example, see Guzman et al. [2009]). In such cases, the conductance is often expressed as a density function (Siemens per square centimetre).

However, when it comes to having a model involving the dynamics of ionic concentration within the neuron, i.e. with the algebraic form of the voltage equation (equation 3.5) or the differential form that considers ionic charge conservation (equation 3.4), the geometry defined parameters become significant to the model.

One aspect that is least pronounced in established models of pacemaking is how the cell geometry influences the model. It is now an accepted fact that different regions of a neuron contribute distinctively towards the overall electrophysiology. For example, the significance of the axon hillock as the site for impulse-generation is widely accepted [Coombs et al., 1957]. Moreover, studies have shown that ion-channels are not uniformly distributed over neuronal membranes [Takada et al., 2001; Patel et al., 2009], instead, they are confined to specific locations along the neuronal membrane. This in turn has an impact on the electrophysiology of the neuron.

The simplest of mathematical approaches to represent neuronal function regards the whole neuron as a single geometrical unit or compartment. Although in most cases, the geometry is typically not mentioned, the model implicitly considers a spherical or cylindrical shape for this unit [Sala and Hernández-Cruz, 1990; Wilson and Callaway, 2000; Sterratt et al., 2011]. Only models that consider the contributions from the neuron's anatomical subdivisions, do incorporate additional structural features. In most cases this is achieved by multi-compartment models which include representations for dendritic trees, soma, axon hillock and axon. The use of equivalent cylindrical representations are very popular in this regard, in modelling neuronal electrophysiology [Komendantov et al., 2004; Wilson and Callaway, 2000; Kuznetsova et al., 2010]. A realistic compartmentalisation would call for a large number of compartments and the complexity may be compounded by the type of neuron and its intricate dendritic trees [Fohlmeister and Miller, 1997].

In the case of *SNc* neurons however, its profuse axonal arborisation, as detailed in Matsuda et al. [2009], would mean that it is nearly impossible to come up with a realistic multi-compartmental model. However, considering the fact that axonal processes have minimum contribution to the initiation of spikes, this may be ignored, akin to previous modelling attempts [Komendantov et al., 2004; Kuznetsova et al., 2010]. An interesting aspect of *SNc* spiking is the demonstrated ability to pacemake even without its dendritic components [Hainsworth et al., 1991; Puopolo et al., 2007]. This implies that the components responsible for the initiation and sustenance of regular spiking are found on the soma and its immediate extensions, including the axon hillock. This makes it possible to develop a model with essentially a single compartment, incorporating important channels responsible for pacemaking.

Again, in the sections to follow, we employ data obtained from spontaneous pacemaking recorded in an acutely dissociated neuron [Puopolo et al., 2007], to identify model parameters. For these reasons, we define this single compartment, called the pacemaking unit.

The Pacemaking Unit

We propose to initially build a single compartment model, the functioning unit of which would be termed as the pacemaking unit (PMU). The single compartment that we consider for our model does not necessarily include all the anatomical subdivisions observed in *SNc* neurons. However, it is assumed to have all the functional components (ion-channels) responsible to initiate and sustain the regular membrane oscillations. We initially build a model the traditional way, assuming the unit to be of a regular spherical geometry. Later on, we incorporate a more physiologically realistic geometry.

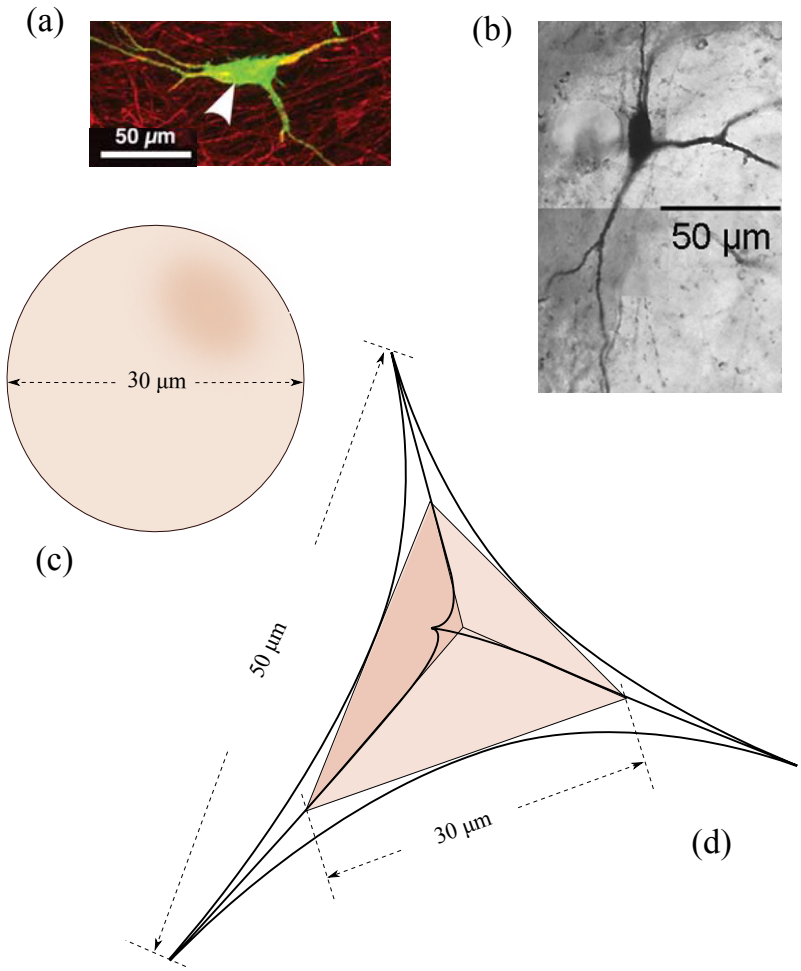

Figure 5.2: Geometrical aspects considered for the pacemaking unit of *SNc* (a) Micrograph of a immuno-stained *SNc* from Matsuda et al. [2009] (b) Micrograph of *SNc* neuron from Tepper [2010] (c) spherical geometry (d) Hyperbolic tetrahedral geometry

Case I : The classical geometry - sphere A preliminary approach to develop a simplified model for neurons, is to use a model with all its conductances lumped into a single spherical compartment that represents the neuronal soma. For our model we consider a spherical soma that is 30 microns wide and assume to be having all components necessary for the spontaneous activity.

Case II : The realistic geometry - hyperbolic tetrahedron Anatomical studies have established that the dopaminergic *SNc* neurons has a pyramidal shaped soma 12-30 microns in diameter with 3 to 6 major dendrites (figure 5.2 a,b). These dendrites extend 10 to 50 microns from the soma before they bifurcate [Grace and Bunney, 1983a]. The axon rises from one of these major dendrites. We define the geometry of PMU on this basis, as well as from various micrographs observed in literature [Matsuda et al., 2009; Tepper, 2010]. The unit which mostly comprised of the *SNc* soma, is a unique structure capable of spontaneous pacemaking.

The neuronal soma is assumed to be more of a tetrahedron than of other geometrical forms. As discussed before, it is difficult and impractical to include the entire dendritic tree to make an exact geometric construct for this neuron. However, it would be a good idea to include the dendritic regions in the immediate vicinity of the soma, so that it includes regions like axon hillock that has a high density of ion-channels responsible for the characteristic electrophysiology. Moreover, it is reasonable to assume that these regions are preserved on the neuron, even when it is acutely dissociated. This addition would now make the unit look more like a hyperbolic tetrahedron, with a high surface-to-volume ratio. A two-dimensional representation of this pacemaking unit is provided in figure 5.2 (d).

In the following sections we attempt to model the pacemaking activity of the *SNc* neuron. In the first stage, we develop a crude model based on a spherical geometry of the PMU, to understand the components contributing towards the dynamics at the neuron's membrane. In the second stage, we refine the model further using a more realistic geometry, the hyperbolic tetrahedron.

5.4 A mathematical model of *SNc* pacemaking with membrane components based on a spherical PMU

In the preliminary stage of modelling the pacemaker activity, the *SNc* PMU is considered to be a sphere of 30 microns, with its membrane comprising of component necessary for initiating the spontaneous activity. We base our model on the recorded data of pacemaking obtained by Puopolo et al. [2007], and its associated ionic currents quantified by voltage-clamp studies.

The results of this section appear in Francis et al. [2012].

5.4.1 Channels selected for the spherical model

For our model (see Figure 1.1), we select channels based on observed expression in *SNc* neurons (table 5.2) and their reported influence in generating the pacemaking current (Amini et al. [1999]; Wilson and Callaway [2000]; Puopolo et al. [2007]; Kuznetsova et al. [2010], also see table 5.1). These includes a representative sodium channel, three types of calcium channels (L-type, T-type and high voltage activated (HVA) type), a calcium dependent potassium channel (SK), three types of voltage-gated potassium channels (delayed rectifier, inward rectifier and A-type transient channel), HCN channel and a leak channel. A sodium-calcium exchanger, along with a calcium and sodium pump, works towards establishing ionic gradients across the membrane. We also include two mobile calcium buffers that are important for the calcium dynamics.

5.4.2 Parameter estimation

Puopolo et al. [2007] describes spontaneous firing in dissociated dopaminergic neurons of the *substantia nigra*, and provides useful information on sodium and calcium currents from dynamic clamp experiments. In particular, Puopolo's data can be put to use to estimate significant parameters for the corresponding ion-channels. In the work of Puopolo et al. [2007], experimental currents of sodium and calcium were measured from acutely dissociated dopaminergic

neurons of *substantia nigra*, capable of spontaneous pacemaking. It should be noted that both currents recorded are always negative, which implies a persisting inward flow of $Na^{+}$and Ca^{2+} respectively. From the perspective of dynamical systems, a biochemical arrangement exhibiting spontaneous oscillations involve stable limit cycles. For this to be realized, the sum of net current in a cycle should be zero. Since the data has only negative currents[1], we assume that data do not include the contribution of pumps and exchangers.

Estimation of parameters was carried out sequentially, beginning with the data on sodium current. As *SNc* neurons express a few different variants of proteins responsible for sodium conductance, it is not practical to have representations for each sub-type. Instead, we model a component representing the cumulative behaviour of these channel sub-types. The TTX sensitive sodium current observed by Puopolo et al. [2007] is modelled by using a Markovian gating scheme (equation 3.17) for this representative sodium channel.

Calcium channels, on the other hand, have varied voltage dependences and their specific contribution to the net calcium current needs to be accounted for separately. Again, the nature of the available data makes it difficult to estimate all parameters for calcium channels in an identifiable manner. Because of this, gating models of the T-type and HVA calcium channel were adopted from the literature. Parameters for the Hodgkin-Huxley gating of low voltage activated L-type channels ($Ca_v1.3$) were identified from experimental data. The HVA current is representative of the high voltage activated L-type channel ($Ca_v1.2$), and P/Q type channel.

In the next stage, parameters for the cation pumps, exchanger and potassium channels were estimated by fitting against the command voltage, which was used in the experiment of Puopolo et al. [2007] for generating the current characteristics. To avoid identifiability issues, the number of different Potassium channel types was kept to a minimum and their parameters adopted from the literature.

Although the use of a linear conductance model is more popular, the GHK equation is better suited when mass fluxes are concerned. Again, the same gat-

[1]Note that, in the data, currents of sodium and calcium are always negative. This would mean that, according to equation 3.3, there will be an accumulation of both cations.

ing parameters of a channel can evoke moderately different responses when used along with the two separate formulations for channel current. For this reason, we employ the linear conductance relation (equation 3.9) to express only those channel currents in our model for which the gating parameters correspond to models in the literature that employ the linear relationship. For the rest we employ the GHK equation (equation 3.11).

To optimise the parameters of the model that best fits the data, a global optimization algorithm, SSm GO [Egea et al., 2009] was put to use. This algorithm combines a population based meta-heuristic method with a local optimization. Parameter bounds were based on physiological grounds. As cost functions, we used a sum of common least square functionals with proper weight coefficients to force better solution in those experiments with less uncertainty [Walter and Pronzato, 1997]. Parameter bounds were based on physiological grounds.

On the design of cost functions Design of the cost function was a complex procedure as the modeling study was limited in available data and the weight coefficients often evolved with the selected objectives. Some of the objectives, based on which the cost functions were designed, include

- Oscillations are present in the desired range of frequency and amplitude
- There is minimum drift in the concentration of intracellular concentration
- By introducing a sodium channel block, the model gives oscillations with smaller amplitude
- The model stops oscillating with the block of L-type channels and resumes oscillations with an increase in cAMP concentration

Often the parameter search space had to be modified to have a balance between selected criteria and speed of optimization, however in most instances they were kept in a range that was physiologically justified. As an exception, we had to particularly extend the allowed range of variation in the intra-cellular calcium concentration, such that the model reproduced the electrical activity with enough detail. For instance, restricting the allowed variations of intracellular calcium in a range as observed experimentally by Wilson and Callaway [2000] (50-250 nM) kept us from a good solution. It was required to raise the

upper bound of calcium concentration to 1000 nM for an acceptable solution.

5.4.3 Model Outcomes

Currently available models of pacemaking in *SNc* have adequately represented experimental studies with pharmacological manipulations and reproduced significant features of the functioning of the neuron. However, the influence of molecular entities that balance the flux of important cations, namely the pumps, exchangers and buffers, are mostly ignored in these models (see table 5.1).

In addition, the electrical activity of an individual neuron is frequently represented by means of the dynamics of the membrane potential. However, this overlooks the fact that membrane potential is directly determined by the membrane capacitance and ionic concentrations. The response of the system is ultimately a function of prevailing electrical forces and molecular diffusion. For this reason, our model is based on the dynamics of the important ions involved, rather than dynamics of membrane voltage. As a result, in common with other electro-physiological models of membrane potential in the algebraic form [Endresen et al., 2000; Hund et al., 2001; Poignard et al., 2011], our model provides more representative insights into the processes involved.

5.4.3.1 Some important features of the model

The role of calcium as the major charge carrier for spontaneous pacemaking in *SNc* neurons has been demonstrated by various studies involving pharmaceutical blockers, as well as experiments involving calcium imaging [Wilson and Callaway, 2000; Ibanez-Sandoval et al., 2007]. Results (see Figure 5.3) that fit our model, confirm that L-type calcium channels that open at relatively depolarized membrane potentials ($Ca_v1.3$) are the most crucial in driving spontaneous pacemaking [Putzier et al., 2009].

From the calcium data fits, the contribution from the L-type calcium channel appeared to be the most important. The HVA calcium channels, however, seem to have a small role in supporting the somatic calcium spikes. The T-type cal-

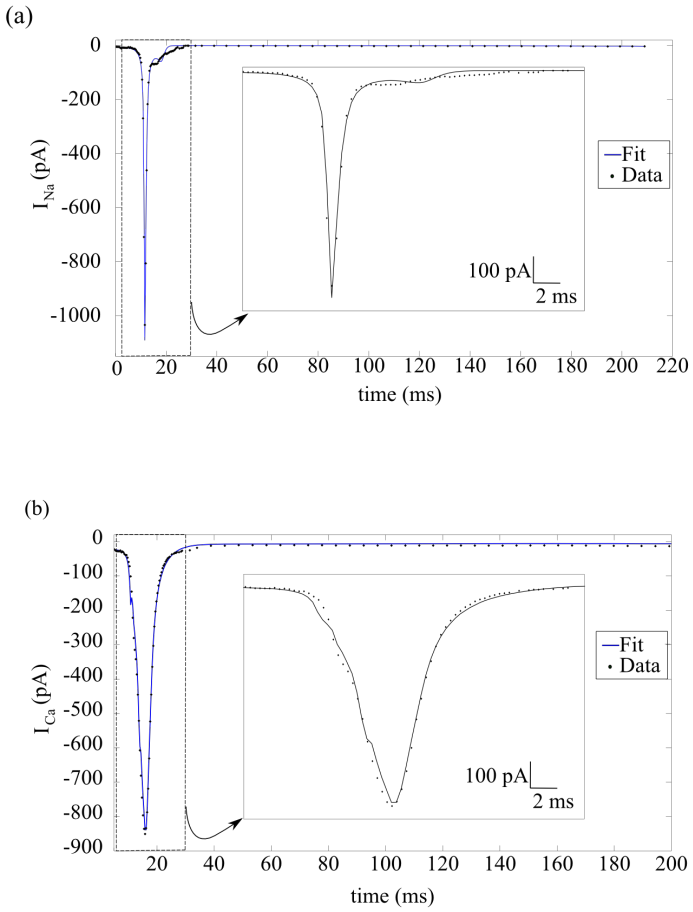

Figure 5.3: Data fits of currents in acutely dissociated *SNc* neurons determined using the action potential clamp technique (a) Fitting of the Tetrodotoxin-sensitive sodium current using Markovian gating dynamics and GHK current equation (b) Fitting of the cobalt-sensitive current by employing Hodgkin-Huxley type gating dynamics and GHK current equation

cium channels apparently have a limited role during spiking, however they were important in maintaining the levels of calcium during the inter-spike interval. According to Verkhratsky and Toescu [1998], among excitatory neurons, L-type calcium channels are predominantly harboured in the soma, whereas the high voltage activated N and P/Q calcium channels are mostly observed on dendrites and pre-synaptic terminals. Hence it is possible that the HVA current of the soma is mostly due to the high voltage activated L-type channel ($Ca_v1.2$) rather than P/Q type channels.

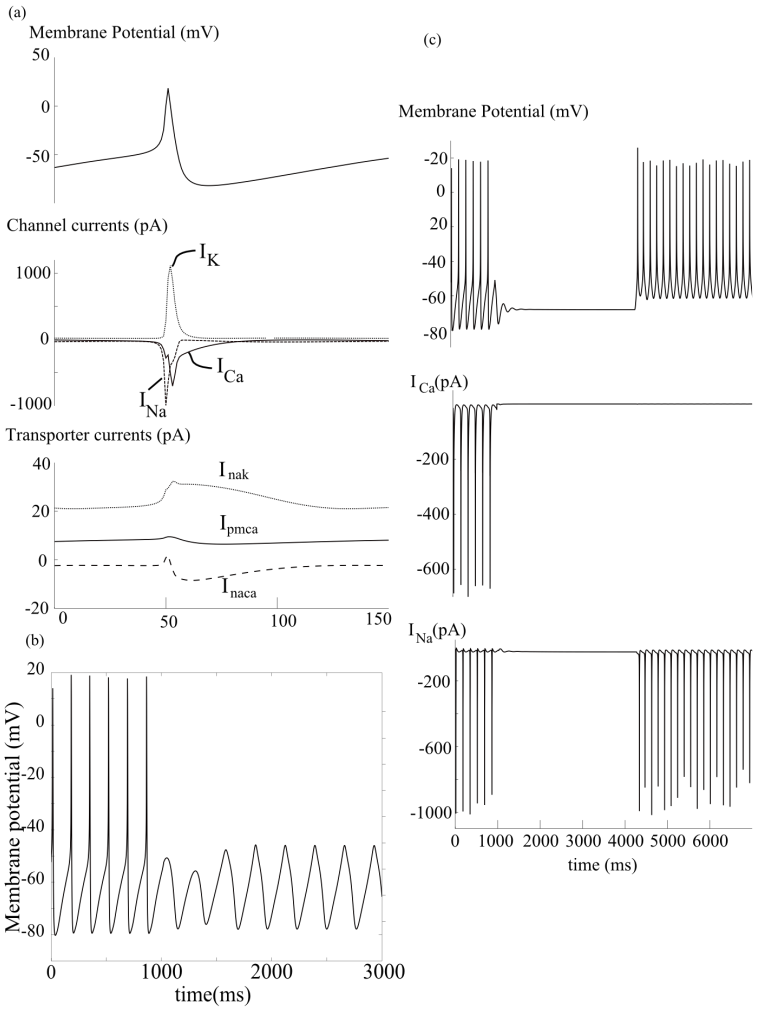

Figure 5.4: (a) Simulated response of the model with the spherical geometry of the PMU: Membrane potential, Channel currents contributing to the pacemaking for a single spike and Corresponding currents from the molecular transport mechanisms responsible for maintaining ionic fluxes. (b) Simulated block of fast sodium current by TTX (g_{na} is set to zero from 1000 ms). (c) Simulated block of L-type and HVA calcium channels. ($g_{\text{ca,l}}$ and $g_{\text{ca,hva}}$ are set to zero from 1000 ms, an increase in cAMP concentration from 4200 ms revives the pacemaking, now driven by sodium currents activated by the HCN channels).

The contribution of the different currents in generating the spontaneous pacemaking is shown in Figure 5.4 a. The role of calcium currents in the generation of oscillation has been demonstrated by blocking the fast sodium currents by the application of Tetrodotoxin (TTX) (Figure 5.4 b). The TTX blocking action is implemented in our model by setting the value of sodium conductance (g_{Na}) to zero. This leads to a dampening of oscillations from a spike-firing mode

as demonstrated in some of previous experiments [Amini et al., 1999; Ibanez-Sandoval et al., 2007].

Another important feature that may be noticed (see figure 5.4) and mentioned by Chan et al. [2007], is that *SNc* neurons can switch back to spontaneous pacemaking even without relying on the L-type channel. An increase in the level of cAMP activates the HCN channels to a higher degree and makes them drive pacemaking. As we shall see later, this switch could have important energy implications.

5.4.3.2 Energy implications

Figure 5.5 shows the variations of average ATP use by the pumps calculated from the model. In particular, it shows that there is a substantial reduction in the use of energy when the neurons switch from a Ca^{2+} dependent mode of pacemaking to a Na^{+}dependent mode. This reduction in energy requirement supports the recent proposal [Guzman et al., 2009; Chan et al., 2009] to employ drugs, that are used to treat hypertension by blocking L-type calcium channels, as a preventive measure against the progression of PD in prospective patients. Our energy budget predictions in Figure 5.5 suggest that this would reduce the energy stress on vulnerable *SNc* neurons through a reduced calcium entry. However, the reduced calcium entry may have other biochemical implications.

5.5 A mathematical model of *SNc* pacemaking with membrane components based on a realistic PMU

One of the striking feature of a neuron is its highly irregular geometric structure. But it is this structure that enables the unique physiological activities of these cells. However, mathematical models framed for describing their electrophysiology typically ignore the structure. As discussed before, use of the

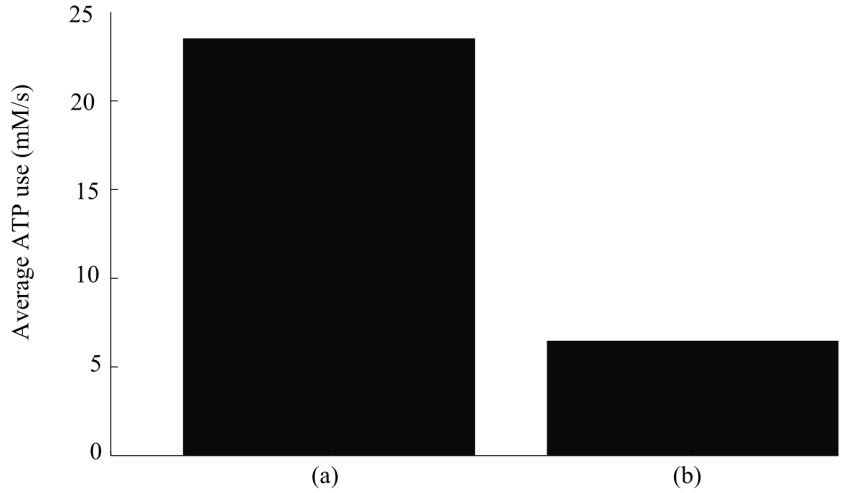

Figure 5.5: Average energy usage by membrane transport proteins calculated from the model (a) Normal pacemaking mode of *SNc* neurons when the L-type calcium current drives pacemaking (b) Pacemaking is driven by the HCN channels when the L-type calcium channels are blocked.

differential form of the voltage expression (equation 3.2), circumvents the need of considering structural aspects for describing the model.

In the previous section, we gave a model for *SNc* activity with a simple geometrical structure. However, a sphere of 30 microns implies a cell volume of 14.13 pl. This value of cell volume is significantly higher than expected for the neuronal perikaryon (If we consider the soma to be a regular tetrahedron of edge 30 microns, the volume would just be 3.2 pl). Further, neurons are known to have a high surface area to volume ratio and the sphere is the most regular structures with the lowest surface area to volume ratio. Also, our previous model did not consider the fact that the cytosol occupies only a fraction of the cell volume.

Hund et al. [2001] suggests that if charges are conserved, the choice of method (differential or algebraic) does not influence the behaviour of the system. In the case of using the algebraic form, we need to be cautious with the choice of initial conditions and the integration constant, as the model tends to be sensitive to this choice particularly during numerical simulation. With our

previous model with the spherical geometry, this particular aspect limited our parameter estimation procedure. For the model with the realistic geometry we adopt the modified differential form that explicitly relates the transmembrane potential to the dynamics of intracellular concentrations (equation C.1), in spite of having an additional state variable.

Keeping these aspects in mind we modify our existing model for a different PMU geometry, a hyperbolic tetrahedron with a characteristic dimension of 50 microns (see figure 5.2) and for the voltage expression we use the differential method with ionic charge conservation principles. As before, we assume the PMU to be in an osmotic equilibrium with its environment, so that cell dimensions are preserved in the course of the process. Membrane-bound sub compartments within the cell take up a substantial space of the cell. For this reason, we consider the cytoplasmic volume to be a fraction of the cell volume. Design parameters based on this geometry are provided in table 5.3.

Item	Symbol	Value (Units)	Reference
Characteristic dimension, soma	d_s	30 (μm)	Matsuda et al. [2009]
Characteristic dimension, PMU	d_{pmu}	50 (μm)	Tepper [2010]
Volume, PMU	$\mathcal{V}_{pmu}$	5 (pl)	approximated
Surface area-to-volume ratio, PMU	$\mathcal{S}_{\text{pmu}}$	16.667(μm^{-1})	fitted
Volume fraction, Cytosol	ϕ_{cyt}	0.5	Alberts et al. [2002]

Table 5.3: A list of parameters realted to the geometry of the realistic model

5.5.1 Channels selected for the HT model

We follow the same principle as described in section 5.4.1 in selecting the channels. However, we now eliminate a few of the channels that did not appear to contribute much to the electrical characteristics of our model. This includes both the T-type and HVA Ca^{2+} channels, A-type K^{+}channel as well as the potassium conductance through the HCN channel.

5.5.2 Parameter estimation

The parameters for the sodium and calcium currents were identified as in the previous section from the data of Puopolo et al. [2007]. As we have no change in

the model with respect to the TTX-sensitive sodium currents, the results of the previous section was used. In the case of calcium currents, experiments were initially repeated with both L-type and T-type current components to identify the respective parameters. However, the contribution from the T-type calcium channel was found to be insignificant towards the net calcium current. Hence, the T-type component was eliminated and parameters were fine tuned with only the L-type component for the calcium current.

In the final fitting, model tuning parameters were estimated from the data for command voltage, that was previously used for generating the current characteristics (Table C.2). These parameters include conductance parameters for channels and transporters on the membrane and concentrations of buffer proteins in the cytosol. They are a reflection of the density of different transport proteins and are bound to change according to the choice of design parameters, to match the expected behaviour of the system. Finally, the model was validated by blocking different ion channels and confirming that the model resembles the expected behaviour in a *SNc* neuron.

As in the previous case, we have used the global optimization algorithm, SSm GO [Egea et al., 2009], to identify the parameters of this model. Also, for the remaining channels, the parameters for their dynamic gating were adapted from literature. Although this is not the optimum routine for identifying various channel parameters for the model, for the reason discussed before, limitation in the data available to develop the model forces this measure to avoid identifiability issues.

5.5.3 Model outcomes

A model for *SNc* pacemaking was developed based on the recordings of Puopolo et al. [2007] on acutely dissociated neurons. The model includes a representative sodium channel that is sensitive to TTX. Ca^{2+} ions enter through L-type calcium channel and expelled by means of a sodium-calcium exchanger (NaCax) and a calcium pump (PMCA). The dynamics of K^+transport are controlled by three potassium channels, the delayed rectifier and internal rectifier being voltage controlled and the SK-type being calcium concentration controlled. The levels of $Na^+$and $K^+$are kept in check by the action of the sodium-

potassium pump (NaK). We have considered only transport of Na^+through the cAMP-dependent HCN channels as their range of activity is closer to the Nernst potential of K^+ions and we do not expect significant flow of K^+ions through this channel.

5.5.4 Dynamic behaviour

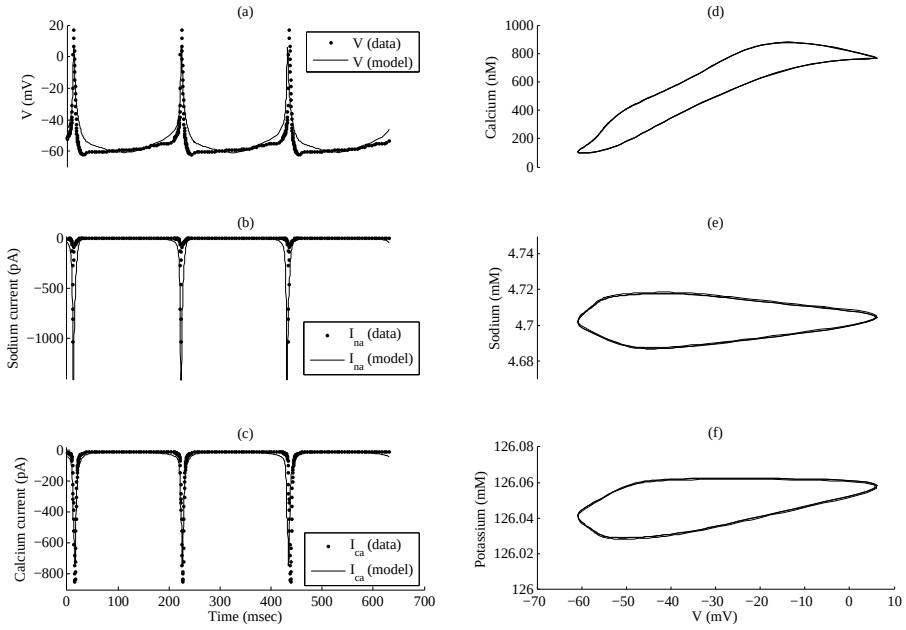

Figure 5.6: The response of the model with the realistic PMU geometry using estimated parameters. The tuning parameters of the model were fit from data on pacemaking in dissociated neurons by Puopolo et al. [2007] including the spontaneous spikes in its membrane potential, (a) TTX sensitive sodium currents (b) and cobalt sensitive calcium currents. The model shows stable limit cycles in the concentration of the cations involved (d,e,f)

The model was calibrated for obtaining normal pacemaking exhibited by *SNc* neurons. In order to assess the validity of the model, it was calibrated for obtaining behaviour expected of these neurons with respect to two different channel blockers. The presence of TTX, a sodium channel blocker has been reported to block the spiking currents and the neuron is expected to demonstrate slow oscillations driven by calcium currents [Amini et al., 1999; Ibanez-Sandoval et al., 2007]. Also, the presence of L-type calcium channel blockers like dihydropyridines is reported to abolish the pacemaking activity, but may

be reinstated with an increase in cytosolic cAMP levels [Chan et al., 2007]. These observations are experimented in the mathematical model by setting the corresponding channel conductance to zero.

Figure 5.6 shows the model simulation profiles generated using the estimated parameters and the experimental data used for the calibration: 5.6.a using pacemaking voltage that was later used as command voltage in the experiment of Puopolo et al. [2007] for analysing the $Na^+$and Ca^{2+} currents, 5.6.b TTX sensitive Na^+ion channel currents and 5.6.c cobalt sensitive Ca^{2+} ion channel currents. These figures show the goodness of the different estimations, where we note the correct match of the spiking frequency, as well as the main features of the spiking save for voltage, Na^+channel current and Ca^{2+} channel current. In the model, voltage is calculated as a function of ionic concentrations, where the intracellular cationic species (Ca^{2+}, $Na^+$and K^+) show the limit cycles in figures 5.6.d, 5.6.e and 5.6.f.

What we have in our model is only sodium conductances that are sensitive to TTX. The deactivation of sodium channels by TTX need not necessarily be equally effective on all subtypes of sodium channels [Goldin, 1999; Du et al., 2009]. There are reports on neuron to neuron variability for the extent of block in *SNc* neurons [Puopolo et al., 2007]. Studies involving blocking sodium conductance with TTX have shown a cessation of the spontaneous activity [Choi et al., 2003] and in many other cases a very slow oscillatory behaviour (SOP) was observed. On these grounds, sodium channels that are not blocked by TTX are in all probability contributing to SOPs.

SOPs were also observed when the TTX block study was carried out in an NMDA bath [Ibanez-Sandoval et al., 2007]. Since NMDA is applied to mimic glutamate input, for the neuronal soma this is equivalent to receiving dendritic inputs as Na^+ions. For this reason, a partial revival of sodium channel conductance from the blocked condition should lead to SOP. To analyse this our model was simulated by initially completely blocking the TTX sensitive Na^+current and later partially restoring this particular conductance. Figures 5.7, 5.8 and 5.9 shows the model behaviour when the sodium channels are inhibited in the presence of TTX and exhibits a slow oscillation in membrane potential with a partial revival of sodium channels.

These profiles support the observations made from some of the previous modelling studies on these neurons [Amini et al., 1999; Wilson and Callaway, 2000; Kuznetsova et al., 2010; Drion et al., 2011] and justifies the selection of ion-channels. Although the currents through the sodium channels (I_{na}) and potassium delayed rectifier ($I_{\mathrm{k,dr}}$) contribute to visible spikes, the underlying rhythm seem to be set by the concerted effort of currents through calcium channels ($I_{\mathrm{ca,l}}$) with the potassium SK-type channel ($I_{\mathrm{k,sk}}$) and internal rectifier ($I_{\mathrm{k,ir}}$), with ample support from membrane pumps and exchangers. This rhythm set by a pacemaker-like slow depolarisation was given the term 'slow oscillatory potential' (SOP) [Amini et al., 1999].

The SOP is calcium dependent and may be abolished by blocking the calcium currents (results not shown). Of particular interest is the dynamics of cation pumps during the SOP (Figure 5.8) which was not very pronounced in earlier models [Amini et al., 1999] which employed a simple Michaelis-Menten type expression for the pump's action or models that did not use them at all [Wilson and Callaway, 2000; Kuznetsova et al., 2010]. This experiment testifies to the role of calcium ions in initiation of pacemaking and the significance of membrane pumps and exchangers in establishing the background oscillations that underlie pacemaking.

The blockade of L-type calcium channel currents ($I_{\mathrm{ca,l}}$) by DHP is achieved by subjecting the channel conductance ($g_{\mathrm{ca,l}}$) to zero, in the model. DHP block keeps the system from spontaneous oscillations, and the pacemaking reappears with an increase in the levels of cAMP in the cytosol (figure 5.10). This is in accordance with the observation made by Chan et al. [2007] on mouse neurons. According to their theory, the block of L-type calcium channels brings about a drop in cytosolic Ca^{2+} levels, which in turn lifts the restriction imposed on the calcium-inhibited isoforms of the enzymes adenylyl cyclase. These enzymes catalyse the production of cAMP from ATP molecules at the membrane under the influence of G proteins as a part of the G protein signalling cascade. With reduced concentration of Ca^{2+} in the cytosol, an increase in cAMP would shift the voltage dependence of HCN channels that are allosterically regulated by these signalling molecules. This shift in voltage dependence re-establishes pacemaking, however with the help of Na^{+}ions.

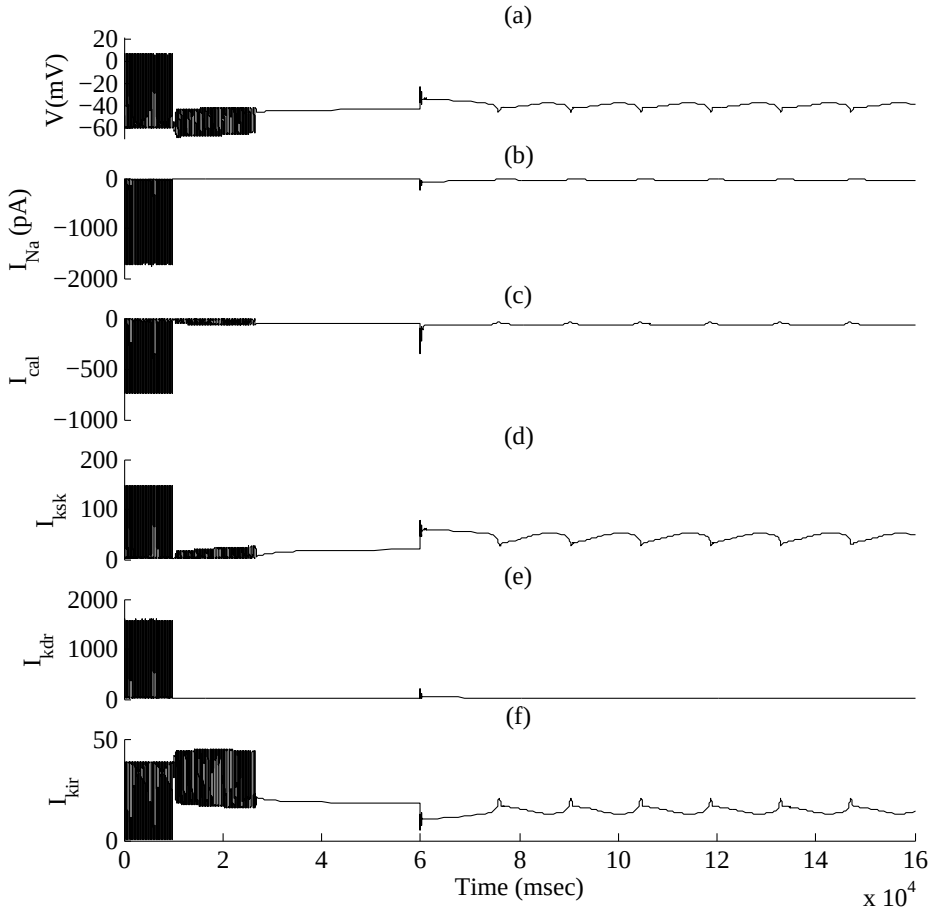

Figure 5.7: Blocking fast sodium channels by TTX brings forth the slow oscillatory activity that underlay the spontaneous pacemaking activity of *SNc* neurons (a) The TTX block was simulated by reducing the sodium channel conductance to zero at 10 seconds, the sodium currents were partially recovered from 60 seconds to simulate a partial block by TTX. The spiking wave is replaced by slow oscillations with a partial block. (b),(e) The currents responsible for spiking activity, the fast sodium and delayed rectifier potassium currents are silenced with the TTX block (c) The calcium channels have an important role in sustaining the oscillations. These channels are ably supported by the potassium channels (d,f).

The proposed model effectively links the energy allocation for ion concentration maintenance of *SNc* neurons with its pacemaker firing by means of the activity of ion-exchange proteins at the neuronal membrane. As discussed above, the switch from a calcium driven pacemaking mode to a sodium driven mode should effectively reduce the energy load on these neurons owing to the pre-

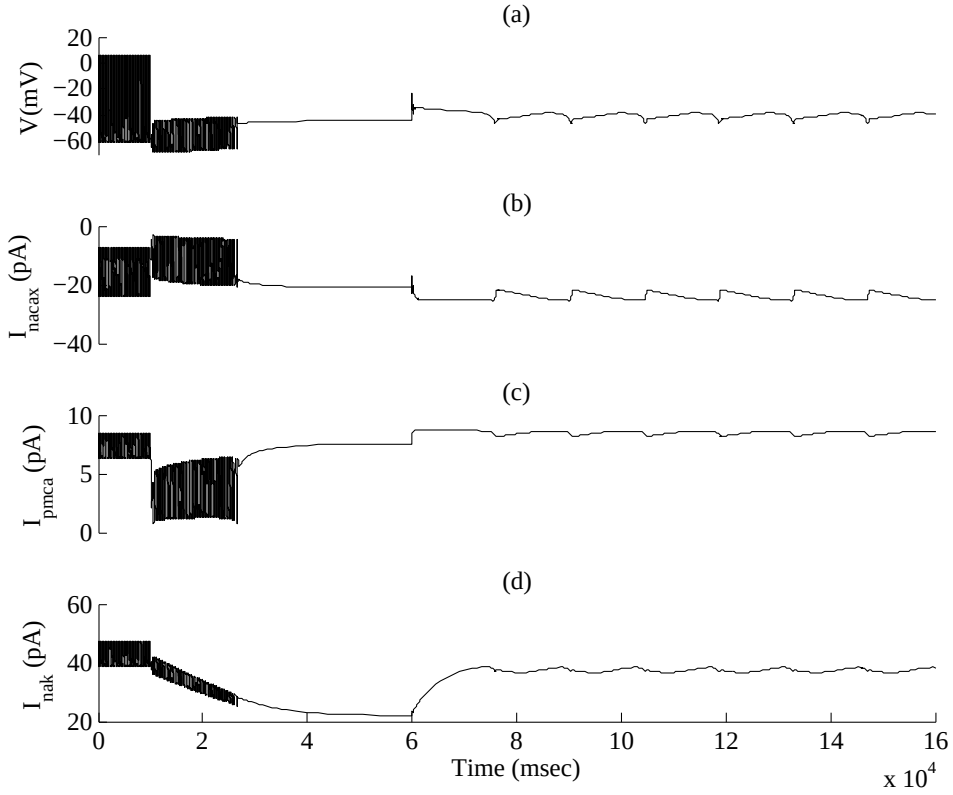

Figure 5.8: Contribution of membrane transporters observed with the block of fast sodium channels by TTX

vailing concentration gradients of these ions. Also, neuronal excitability is strongly dependent on cytosolic calcium levels with higher cytosolic calcium leading to lower excitability. This is mostly due to calcium dependent steps in the membrane electrophysiology that have larger response time. When the mode of pacemaking switches to the sodium-driven mode, there is a significant reduction in the intracellular Ca^{2+} levels (figure 5.10 f). This in turn makes the cell excitable and we see an increased spiking rate. In spite of increased firing rates, we see that the ATP use at the membrane is considerably less (figure 5.10 e, figure 5.11)

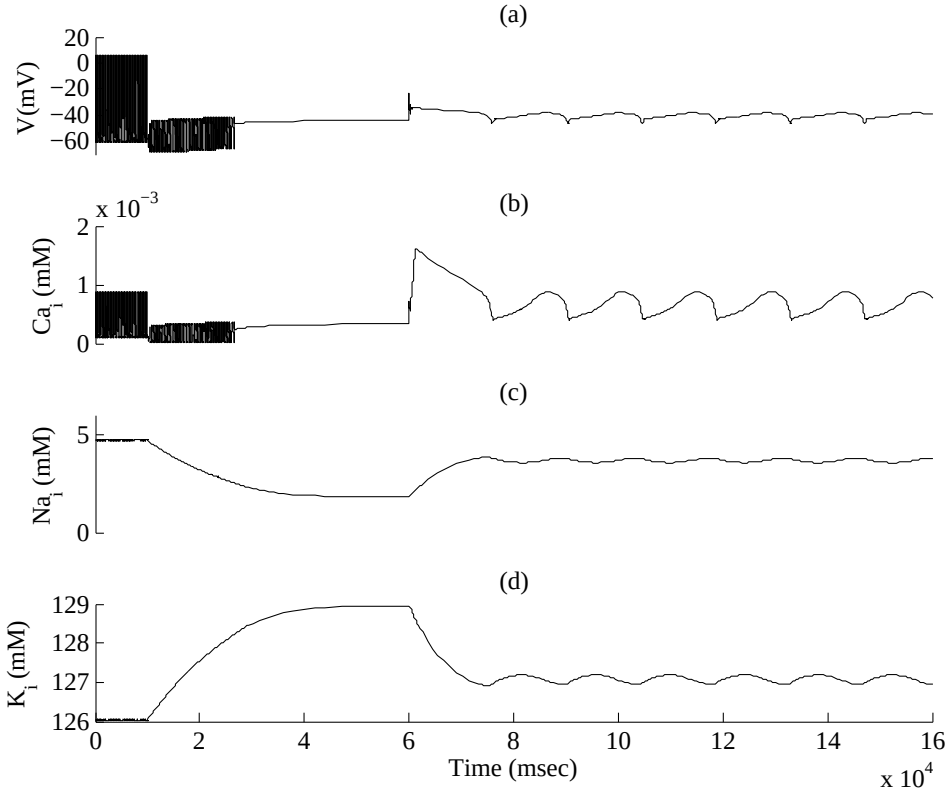

Figure 5.9: Oscillations in intracellular cation concentrations with the block of fast sodium channels by TTX

5.6 Model Analysis

5.6.1 Channel conductance parameters and oscillation dynamics : Bifurcation Analysis

In the model developed for describing the pacemaking in *SNc* neurons, we have a system of currents that control the membrane potential by their varied gating mechanisms that are, in turn, controlled by the changes in the intracellular ionic concentrations. As the magnitude of the ionic currents decides the extent of this synergy, the corresponding parameters, namely the channel conductances, defines the properties of this dynamic system. For this reason, we first aim to study how these parameters influence the oscillatory properties of

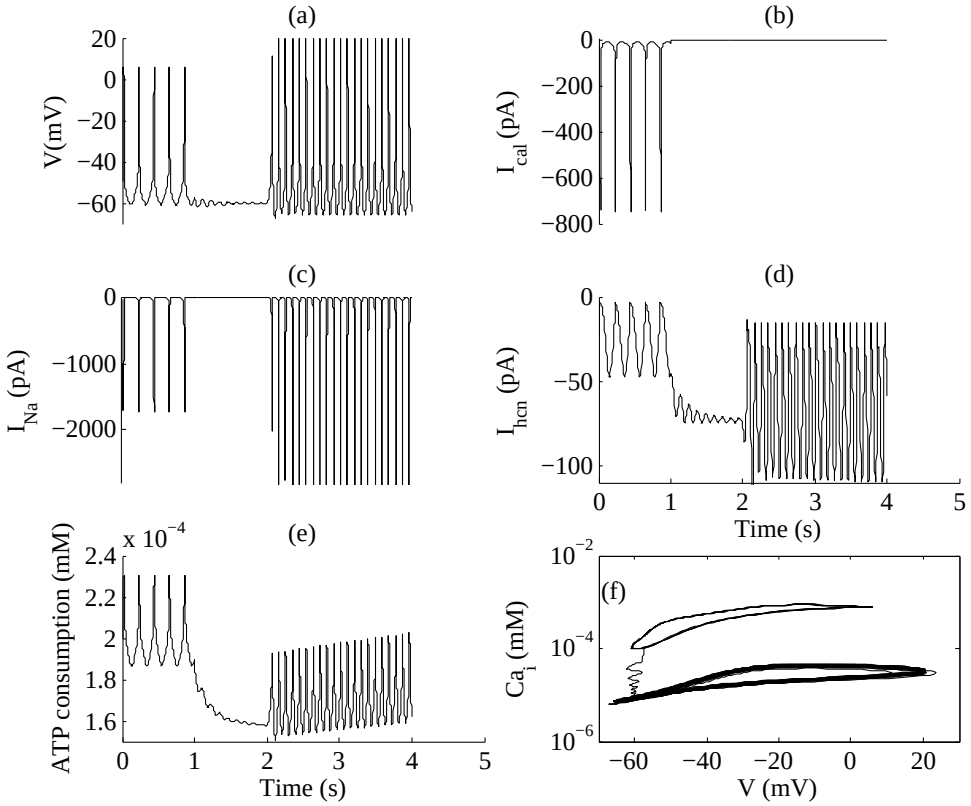

Figure 5.10: The response of the model with realistic PMU geometry when L-type calcium channels are blocked (a) The spontaneous pacemaking at the *SNc* membrane ceases with the introduction of L-type calcium channel blocker at 1 sec. In the simulations this is achieved by setting the L-type calcium channel conductance to zero. The pacemaking is re-established by an increase in cAMP concentration from 2 sec. (b) The L type calcium currents completely ceases with the block, however T type calcium channels are more active owing to a membrane that is more hyperpolarized. (c) There is higher sodium influx through sodium channels and the HCN channels (d). The HCN channels are activated by both hyperpolarization and increased cAMP levels. (e) The cell consumes less energy as ATP per spike however, at an increased spiking rate. (f) There is stable limit cycles in calcium levels in both cases, with the L-type channel blocked calcium levels are reduced by an order of magnitude.

the model and thereby, investigate the precise role of these currents in normal pacemaking.

Biologically speaking, the parameter describing the channel conductance combines two pieces of information, (a) the amount or number of proteins expressed by the neuron that comprise the channel and (b) the capacity or max-

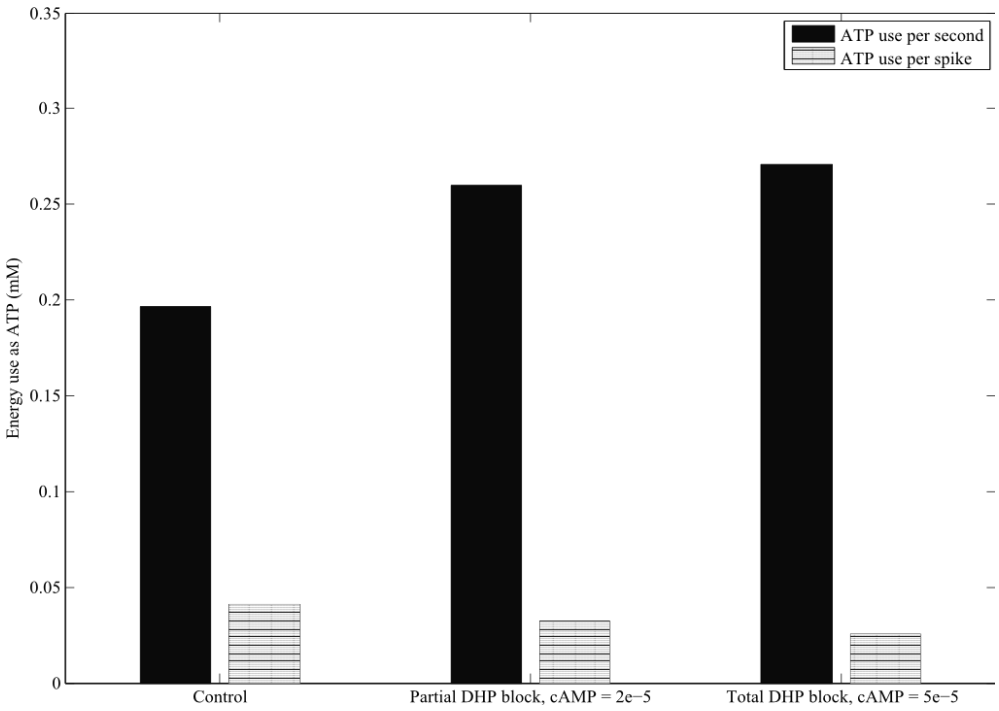

Figure 5.11: Difference in energy use patterns observed with the two modes of pacemaking in *SNc* neurons. In the control condition, the L-type calcium channels are active and the transport of Ca^{2+} ions drives the pacemaking. With the block of these channels by DHP, pacemaking is lost. However an increase in cytosolic cAMP revives pacemaking, driven by the Na^{+}ions transported through the HCN channel. Levels of cAMP modulate the pace and energy use associated with this continuous spiking.

imal conductance of each channel. Supposing that the capacity of a particular channel type is consistent in a neuron, the conductance parameter is essentially a measure of expression level of each channel. This is again consistent with the general view that protein abundance levels point to the cellular state, for being the functionary of cellular processes.

The expression of a particular protein is characteristic to a cell type and regulated at various levels of cellular metabolism [Alberts et al., 2002]. Further, the process of protein expression is not a continuous process within a cell, instead it is discrete with respect to the metabolic state of the cell. Simultaneously, there is a continued interaction of proteins with metabolites such as free-radicals that affect their viability. Cellular maintenance mechanisms are responsible for the degradation of proteins that are non-functional or beyond

their half-life. Such variability in the turnover of ion-channels have a role in variations of spiking rates of excitable cells and has been experimentally observed in myocytes [Ponard et al., 2007]. Hence, it is essential to understand how variations in the conductance parameter that are estimated would influence the properties of our model. Towards this, 1-dimensional bifurcation analysis with these parameters can be a useful tool to develop insights regarding such variations.

Bifurcation For a non-linear dynamical system, a bifurcation is a qualitative change in its dynamic behaviour when some system parameter is changed. For a n-dimensional dynamical system given by

$$\dot{x} = f(x, \varphi) \tag{5.3}$$

with state variables $x \in \mathbb{R}^n$ and parameters $\varphi \in \mathbb{R}^p$, a bifurcation occurs at some value of the bifurcation parameter $\varphi = \varphi_0$, when at the parameter value φ_1 close to φ_0, the system displays a markedly different dynamic behaviour. The change of behaviour is theoretically interpreted as a change in the number or type of attractors[2] of the dynamical system. A bifurcation can affect the stability of a periodic behaviour of the system.

Bifurcation observed in *SNc* neurons include cessation or generation of pacemaker activity as well as switching of pacemaker activity to bursting activity. In this section, we are mainly concerned with how the change of a few important conductance parameters affects the stability of the pacemaking activity. For this, we numerically search for properties that are representative of the dynamics of the system, at a given parameter value. This includes the peak (maximum) and basal (minimum) values of the membrane potential at steady state which are denoted PMP and BMP respectively, the average cycle time (λ) at the steady state as well as standard deviation of λ (σ_λ). The variations of these properties may be summarized as follows

[2] *Attractor* : An attractor is a region in state-space towards which a system variable evolves over time according to the dynamic properties of the system. A set that behaves the opposite is called a repeller. Equilibrium points and limit cycles are examples of attractors.

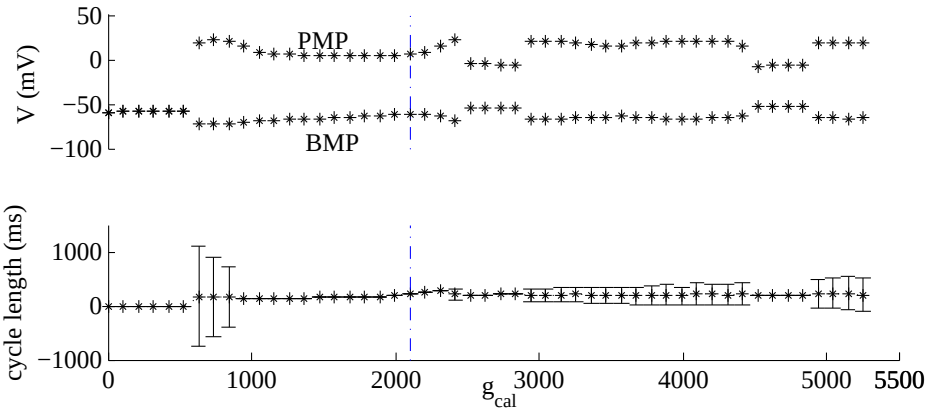

Figure 5.12: Bifurcation diagram : g_{cal}

Type	PMP and BMP	λ	σ_λ
Quiescence (equilibrium point)	Coalesce	0	0
Pacemaking (limit cycle)	Distinct	positive	small
Bursting (limit cycle)	Distinct	positive	large

5.6.1.1 Results

We explore the effect of changing some of the important channel conductances that have been pronounced important for the pacemaking activity in *SNc*. This includes the conductances of the Na^+channels, L-type Ca^{2+} channels as well as the SK-type K^+channels. We also look for the effect of changing the density of the membrane pumps and exchangers in the model.

Figure 5.12 shows an approximate bifurcation diagram constructed from the variables that represents system properties (PMP,BMP,λ and σ_λ), as functions of bifurcation parameters. From the diagram, we see that g_{cal} is a significant parameter for the neuron as a reduction in its value causes cessation of pacemaking activity when the other conductances are kept constant. An increase of the conductance g_{cal} appears to switch the mode to bursting. However, it is not straightforward to assess the dynamics with an increased conductance of the L-type channel as the dynamics of Ca^{2+} within the model is intricate.

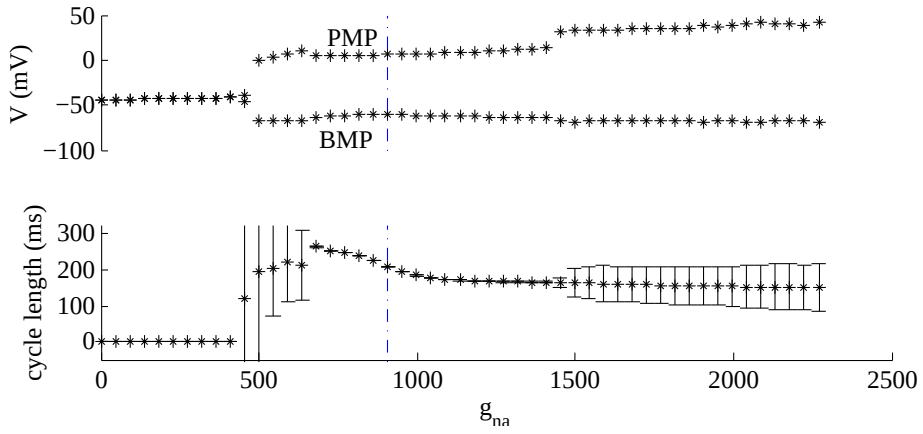

Figure 5.13: Bifurcation diagram : g_{na}

Figure 5.13 shows the bifurcation diagram constructed for the bifurcation parameter g_{na} We see that small changes in g_{na} from the nominal value (see table C.2) does not change the behaviour of the system and the system appears to be capable of generating stable oscillations between a range g_{cal} values $(700 - 1200nS)$, albeit at a different frequency. However, the pacemaking is ceased with a substantial reduction of this conductance, making it an essential component of the model. We see that in an intermediate range of this parameter (approximately between $400 - 500nS$), we see a different behaviour, in which we find a slow wave of reduced amplitude, corresponding to the SOP observed in a previous experiment. An increase in the density of these channels can result in bursting behaviour. This is comparable to the application of NMDA on these neurons that apparently increases the flow of Na^+into the PMU via dendritic inputs and change the mode of firing from pacemaking to bursting [Ibanez-Sandoval et al., 2007].

The conductance of the SK-type K^+channel is unimportant compared to the $Na^+$and Ca^{2+} channels. With the current value of this parameter in the model, small variations do not seem to significantly affect pacemaking (figure 5.14). Also, with the present configuration of ion-channels, removing this channel does not appear to cease pacemaking. The SK type K^+channels have been understood to have an important role in determining the frequency of pacemaking by mediating the calcium-dependent afterhyperpolarization [Surmeier

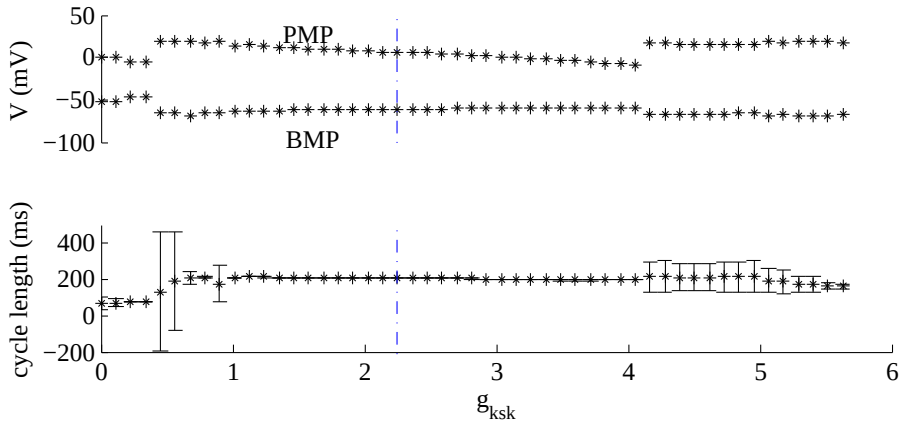

Figure 5.14: Bifurcation diagram : g_{ksk}

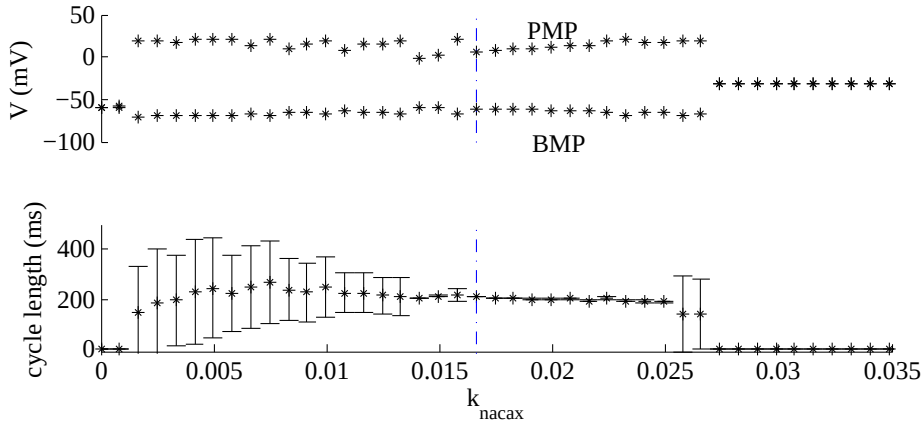

Figure 5.15: Bifurcation diagram : k_{naca}

et al., 2005].

The model behaviour appears to be highly sensitive to the value of the conductance of the sodium-calcium exchanger. The bifurcation diagram (figure 5.15) suggests that this transporter is significant for setting the mode and speed of the membrane spiking activity. At lower densities of this protein, the pacemaking is less regular. A critical level of the exchanger need to be reached before this irregular mode changes to the regular spiking mode, as evinced by the corresponding λ and σ_λ. Higher densities of the exchanger appear to destroy the

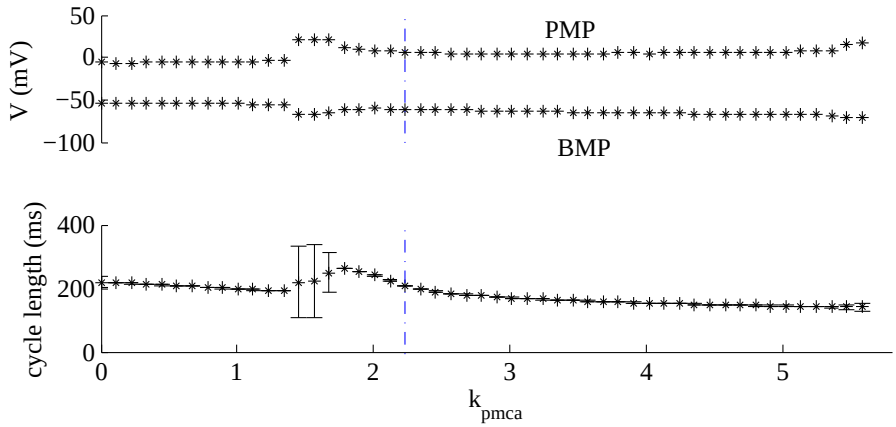

Figure 5.16: Bifurcation diagram : k_{pmca}

oscillations.

Much as the role of calcium exchanger is critical to the nature of oscillations, the calcium pump does not appear really critical for initiation of pacemaking. The system appears to be robust with regards to change in the density of PMCA as seen in the bifurcation graph, (figure 5.16). Again, being a Ca^{2+} handling machinery, it is a little difficult to asses the significance of this transporter from a single parameter bifurcation diagram. This is probably because the sodium-calcium exchanger have a faster response to changes in calcium concentration and it will require a drastic increase in calcium concentration to analyse the influence of PMCA. Also, the buffers of calcium act to maintain a steady level of Ca^{2+}. Taken together, calcium regulatory mechanisms work towards reducing the energy impact of calcium entering the system.

The sodium pump on the other hand contributes significantly to the activity of these neurons (figure 5.17). The neuron seems to be requiring a critical density of these transporters before it can switch to regular oscillations.

Remarks In this section we have investigated some of the dynamical properties of the pacemaker model with respect to some of the conductance parameters, by a 1-dimensional bifurcation analysis. We have examined the role of sodium currents, L-type calcium current and SK-type potassium current as well

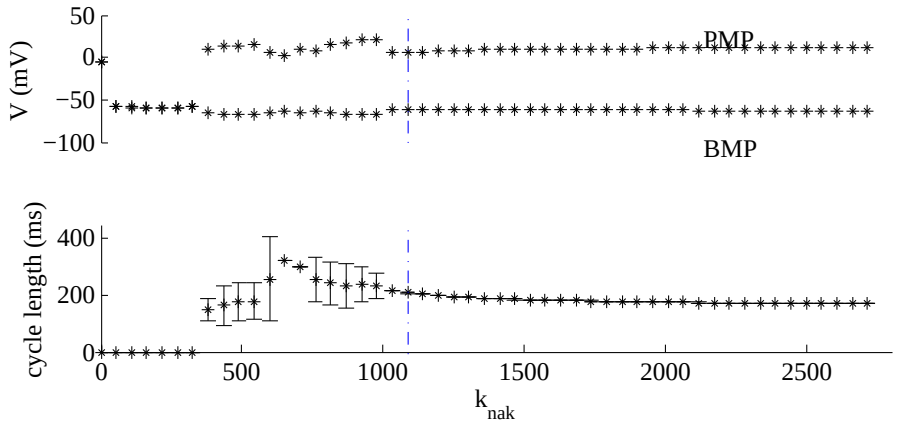

Figure 5.17: Bifurcation diagram : k_{nak}

as ionic currents across the pumps and exchanger. Most of these conductances were critical in the initiation of stable oscillations in these neurons. Given the fact that the bifurcation study handled only a single parameter at a time, the results are mostly suggestive of the impact of each component around the nominal value.

5.6.2 Limit Cycle Analysis

In the second part of this section we aim to understand the stability of our model with respect to its periodic oscillations. One of the defining aspect of *SNc* pacemaking is its spontaneous spiking and such self-sustained oscillations imply the existence of a stable limit cycle. Any perturbation to the model from the equilibrium must then make the system return to this limit cycle. For a complex model that we have at hand, a visual depiction of this process is not an easy task. Instead, we numerically find the monodromy matrix of the local time varying linearisation of a cycle and the eigenvalues of this matrix are employed to predict the stability and convergence of the limit cycle [Viswanath, 2001].

The monodromy matrix Consider a system of ODEs,

$$\dot{x} = f(x, \varphi), \quad x \in \mathbb{R}^n, \quad \varphi \in \mathbb{R}^p. \tag{5.4}$$

This system has a periodic solution if the solution is a closed trajectory, *i.e.*, $x(t+T) = x(t)$ for all real t and the smallest value of $T(T > 0)$, for which this holds is called the "period".

If $\psi_t(x_0)$ denotes the solution of (5.4) at time t starting from x_0 at time $t = 0$, then the Monodromy matrix is defined as,

$$M = \left.\frac{\partial \psi_T(x)}{\partial x}\right|_{x=x_0} \tag{5.5}$$

and may be obtained as the solution of the variation equation at time T. The variation equation is obtained by perturbing the system in the neighbourhood of a point ψ^* on the periodic solution $\psi(t)$ of the system. Upon linearisation we have, $\dot{y}(t) = A(t) \cdot y$, where $A(t)$ is the Jacobian of f around $x(t)$. If $Y(t)$ is the fundamental solution of this linear equation with $Y(0) = I$,

$$\frac{dY(t)}{dt} = \left.\frac{\partial f(x)}{\partial x}\right|_{x(t)} \cdot Y(t), \quad Y(0) = I, \tag{5.6}$$

then $M = Y(T)$.

The monodromy matrix and its eigenvectors depend on the choice of the initial conditions, whereas its eigenvalues (λ_m) does not depend on this and is invariant with respect to change of variables. The linear stability of the periodic orbit can be determined from the eigenvalues of the Monodromy matrix, which are also called the characteristic multipliers of the system. For a system exhibiting autonomous oscillations, one of the characteristic multipliers is always 1, and corresponds to perturbations along the periodic orbit. If $|\lambda_m| < 1$, the closed orbit is considered linearly stable and attracting [Hale and Lunel, 1993].

Thus, the spectral properties of the Monodromy matrix can provide information regarding the components of the system. For a periodic system close to a stable limit cycle (as a simple periodic orbit), the trajectories in state space should converge to the limit cycle. For a stable limit cycle, the largest eigenvalue is generically unity, and the magnitude of the second largest eigenvalue gives an estimate of the rate of convergence to the cycle. The magnitude of the eigenvector corresponding to the second largest eigenvalue can identify the components contributing to the fast and slow dynamics in the system. This

analysis is only valid for small deviations from the limit cycle, but is a useful numerical technique for studying stability.

From the numerical analysis, we observe that for our proposed model based on the realistic PMU geometry (see Appendix C), with the estimated parameters, the oscillations converge to a stable limit cycle. The results of this analysis is given in table 5.4.

Table 5.4: Limit Cycle stability

(a) Leading eigenvalues of monodromy matrix (estimated via numerical simulation)

i	$\lvert\lambda_i\rvert$
1	1
2	0.9868
3	0.9377
4	0.9258
5	0.4273
6	0.1101

(b)Properties from the second largest eigenvalue

State	Normalised eigenvector corresponding to the second largest eigenvalue
V	8.7e-7
Ca_i	-255.56
Na_i	-0.0005
K_i	-1.93e-6
Cam	42.608
$Calb$	88.4
m_{na}	0.0005
h_{na}	0.0072
$\mathcal{O}_{\text{hcn}}$	3.183
m_{cal}	0.0034
m_{kdr}	-0.0004
$\mathcal{O}_{\text{nk}}$	-0.0004
$\mathcal{O}_{\text{pc}}$	-1.153e-5

For our model, the largest eigenvalue is indeed at 1. However, the second largest eigenvalues is very close to one, which suggests that the rate of con-

vergence to the limit cycle would be very slow. The normalised magnitude of the eigenvector corresponding to the second largest eigenvalue (table 5.4 b) suggests the variables contributing to the slow dynamics involve components that correspond to the calcium dynamics, including the buffers, and the HCN channel.

Chapter summary We have presented an introduction to the characteristics of the *SNc* membrane that enable these neurons to pacemake. This activity ensures a continuous supply of dopamine to the striatum for its normal functioning. As an initial step towards modelling the membrane electrophysiology we set forth to identify important membrane proteins on the neuron's membrane that are crucial in the different ionic transports that contribute towards the membrane dynamics, by analysing protein expression profiles and comparing with various observations in the literature. The model is constructed based on a geometric approximation of the functioning unit and for this we consider two different approaches. In the first, we consider the unit to be a simple spherical entity that represent the neuron's soma and build our model on this assumption. Important parameters are identified with a global search algorithm to match with electrophysiological observations in the literature [Puopolo et al., 2007]. Since this geometry does not match that of a neuron, the model is a first step in identifying important components contributing to the electrophysiology.

In the second approach, we replace the spherical geometrical basis with an abstract representation of the neurons geometry which is closer to the volume and surface relationship of the functional module of a real neuron. Some of the components in the previous model were eliminated or changed, due to their behaviour and contribution to the overall response, and the parameters were re-estimated for the change in geometry and components. Both models were calibrated for expected behaviour of these neurons under a sodium channel blocker (TTX) as well as a L-type calcium channel blocker (DHP).

The dynamic properties of the final model was analysed with respect to some of the estimated parameters using a simple one dimensional bifurcation analysis. This analysis helped identify parameters contributing to the stable oscil-

lations and parameters that dictated the spiking rate. In the second analysis the model was examined for stability, by analysing the properties of emanant limit cycles using the spectral properties of the Monodromy matrix. The model was observed to be capable of producing stable and spontaneous oscillations, a property observed with the actual neurons.

Part IV

CHAPTER 6

Conclusion

In this chapter, we summarise the contributions made in this manuscript and give recommendations for possible extensions to those results.

6.1 Summary

In this thesis we developed a mathematical framework to study the mechanism of spontaneous oscillations in *substantia nigra* neurons with an emphasis on calcium regulation. Towards this end, important components of the model were identified and analyses were made on existing formulations to represent their mechanistic description in the best way possible.

Chapter 1 set the stage and discussed why systems research on PD is timely. A look at the economics of this disease and its increasing prevalence in today's world suggested a burden that society will have to handle in the near-future. The heterogeneity seen with respect to age, cause and symptoms, together with the multi-factorial nature of the disease, suggests that the use of computational tools and systems approaches are essential to understand its pathogenesis.

Although the objective of this research was to establish a mathematical scheme for the pacemaking activity of *substantia nigra* neurons that may be later incorporated into a larger framework of energy metabolism in these neurons, we need to have a fundamental idea about the pathogenic process. The literature regarding the molecular characteristics of *substantia nigra* neurons and its sig-

nificance in PD is broad and an all-encompassing review is very difficult. For this reason, we have examined and discussed literature directly relevant to our study. In chapter 2 we have presented this review on the molecular aspects of the pathogenic process and related various observations in the light of calcium homeostasis.

Chapter 3 was concerned with identifying an appropriate representation for the passive form of membrane ion-transport through ion-channels. Popular approaches to model ion-channels like the Hodgkin-Huxley models and Markov models were studied. A simple kinetic expression was developed for channel gating by defining this functional aspect from physical transitions in protein structure. The proposed model which works reasonably well for fast ion-channels and was found to be identifiable with a small number of parameters. Because of the difficulty to get good experimental data for the channels required for our model, it was decided to follow the conventional Hodgkin-Huxley formalism from the literature.

In chapter 4 different models for active ion-transport were compared with respect to their compliance with the expected behaviour. Although not very straight forward to express mathematically, Markov models on pumps and exchangers were found to work best with respect to the observations made in literature. The chapter also discussed about the different components in the cytosol, ER and mitochondria that work towards maintaining a steady level of calcium within the neuron.

The model for *substantia nigra* pacemaking was arrived at in two steps in chapter 5. Initially a simple geometry, capable of pacemaking spontaneously, was considered for the unit. Model components that are ion-channels were decided based on protein expression data and previous observations made in literature. Some of these channels were modelled and parametrised based on available data and for the rest appropriate models and parameters were adopted. The different components were brought together to generate the voltage profile expected of these neurons and the conductance parameters were tuned accordingly. A global search algorithm was used to identify the different tuning parameters to match the available data. In the second step the regular geometry of the pacemaking unit was replaced with a more realistic geometry to match

the dimensions of the *SNc* soma. The procedure was repeated but this time eliminating some of the components whose contribution to the model was observed to be minimal. A realistic model with the appropriate parameters was analysed first with a one dimensional bifurcation study for some of the conductance parameters. In the next analysis, numerical simulations were performed on the Monodromy matrix of the local time varying linearisation to predict the stability and convergence of the limit cycle.

In the following section 6.2 we present the framework for a model that may be employed to extend our model described in chapter 5 in such a way that it includes aspects on how Ca^{2+} is handled within the neuron and how the pacemaking may be linked to the energy metabolism. This multi-compartment model may be used for *in silico* experiments concerning the pathology.

6.2 Suggested extension for the membrane model with calcium dynamics

The flow of calcium across neuronal membranes and compartments is crucial for the normal functioning of a neuron. The efficiency of this system is compromised due to a range of natural events such as ageing and extrinsic cues such as toxins. Beyond a point, such perturbations to calcium homeostasis can lead to a tipping point beyond which the death of the neuron becomes inevitable. Understanding the different points of control in this system can lead to preventive as well as therapeutic interventions for a neurodegenerative disease like PD.

6.2.1 Calcium at the crux of neuronal survival

In chapter 2, we reviewed some of the important molecular aspects of PD pathogenesis. The wide range of biological factors implied in the process and the very slow nature of disease progression suggests that the neuron have more than a few regulatory points that need to be compromised before the disease state is established. An interesting observation is that many of these

pathogenic pathways interact with the calcium homeostasis machinery culminating in a calcium mediated apoptotic process.

The role calcium plays in neurodegeneration depends on the state of health of the neuron. As mentioned, calcium plays the role of a regulatory molecule of critical events. Disturbance of this equilibrium can see calcium changing tracks to be the facilitator of oxidative stress through a few different mechanisms. For instance, lipid peroxidation which is a common phenomena in neuronal damage impairs the ion-transport proteins leading to further influx of calcium. This in turn raises more ROS from the accumulation of calcium in the mitochondria. Elevated levels of calcium is also understood to interfere with the energy metabolism, activation of enzyme oxygenases etc. that enhances the oxidative environment inside the cell [Mattson and Chan, 2003]. Calcium can indirectly promote apoptosis by activating calpains that degrade a range of cytoskeletal structures and metabolic proteins. These proteins can mediate apoptosis by directly activating caspases in a cascade of events [Nixon, 2003]. Calcium can have also directly promote apoptosis by activating some of the pro-apoptotic proteins including caspases and by the release of cytochrome c from mitochondrial membranes [Fiskum et al., 2006].

In addition to the various molecular components that work to maintain control levels of Ca^{2+}, the design and arrangement of cellular space is in such a way that Ca^{2+} sparks are restricted within allocated sub-cellular spaces generally referred to a microdomains. Mitochondria lie at the farthest point of this cascade and the information passed on by the levels of calcium are integrated in the mitochondria with a specific cellular response. Since mitochondria are the source of energy for the cell, this response to Ca^{2+} influences many other pathways that may or may not be directly linked with Ca^{2+} homeostasis.

Most studies with regards to the pathophysiology of *SNc* neurons involves isolated sets of biochemical reactions/interactions which is a part of a larger network. There are significant crosstalk between the different pathways that constitute this network and this aspect is often ignored when experiments are designed. Mathematical modelling to some extent can overcome limitations of experiments that have been conducted on separate sub-networks. In our work we have developed a model for membrane events that contribute and interact

with a larger system of *substantia nigra* physiology. The immediate step to follow would be to connect it with the intracellular system that relate this activity to energy metabolism as well as cell degeneration. This could be carried out by extending the present model by including components of the neuronal machinery involved with the regulation of Ca^{2+} ions within its environment. In the following section, we describe the framework for a model that may be put to use to this end.

6.2.2 An extension of the pacemaking model detailing intracellular calcium dynamics

The model developed to describe the pacemaking (Appendix C) had a very basic representation of calcium handling closer to the membrane. In fact, the model considers only the fast buffers and did not consider aspects like calcium-induced calcium release described in section 4.7.1.2. Additionally as discussed in the previous section, accumulation of calcium in the mitochondria is critical to the survival of the cell. A detailed model that assimilates aspects of pacemaking and calcium handling would be the next step in understanding energetic constraints of the pacemaking process on *substantia nigra* neurons. In this section we bring forth a proposal for a model that can be build on the different concepts described previously.

6.2.2.1 Model description

Figure 6.1 gives a picture of the multi-compartmental model that may be developed towards this end. The model typically compartmentalises the cytoplasm into distinct regions on the basis of spatial restriction of Ca^{2+} in a typical neuron. "Compartment A" corresponds to sub-cellular space(s) existing between ER and the plasma membrane and is distinguished with the presence of membrane transporters of Ca^{2+} that are spatially tethered around a Ca^{2+} hotspot [Parekh, 2008]. "Compartment R" represents the ER that tunnels Ca^{2+} across the various sub-cellular locations. "Compartment M" represents mitochondria that function as the ultimate sink for Ca^{2+}. "Compartment D" applies to the microdomains formed as a result of the spatial arrangement of mitochondria

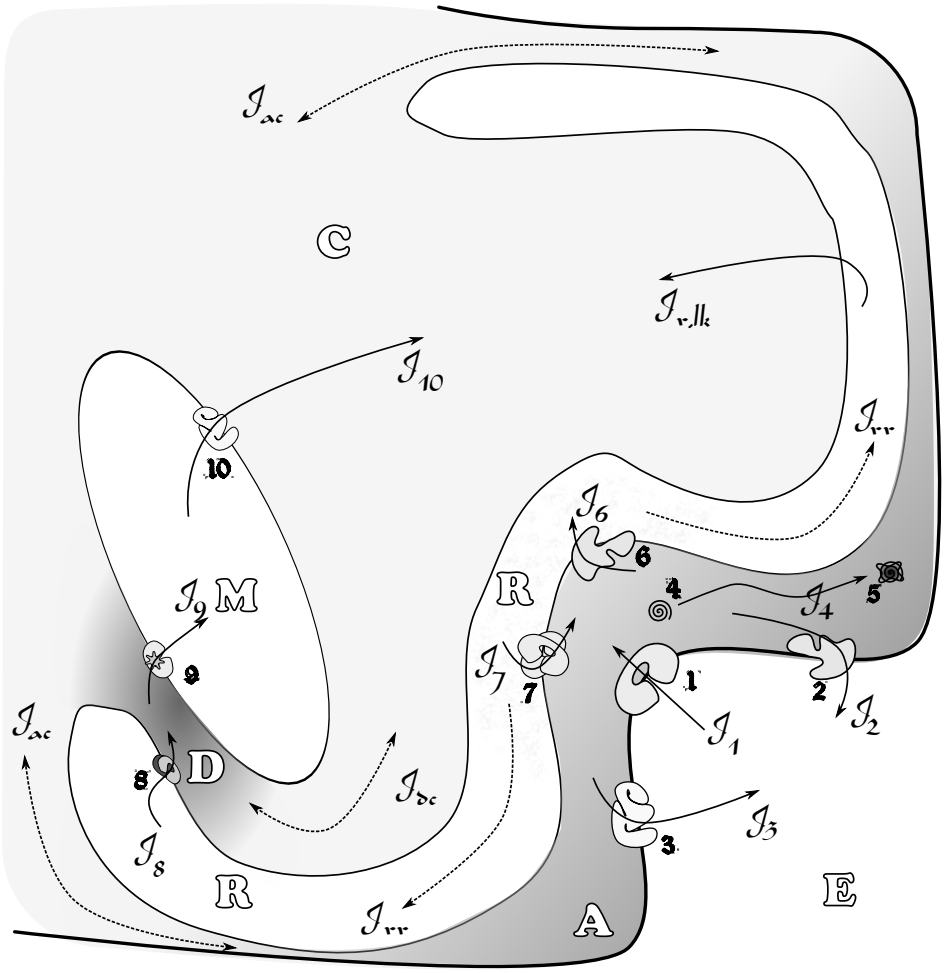

Figure 6.1: A cartoon representation of calcium related pathways presented on a cross-section of the neuronal soma. The model is constituted of the following compartments :
(A) microdomain formed between plasma membrane and ER, (R) ER, (C) cytosol, (M) mitochondria, (D) microdomain formed between ER and mitochondria and (E) extra-neuronal space
and the following components :
(1) calcium channels, (2) PMCA, (3) NaCax, (4) calcium buffers, (5) buffer-calcium complex, (6) ERCA, (7) RyR, (8) $InsP_3R$, (9) mitochondrial uniporter, (10) NaCam

along Ca^{2+} release points on the ER [Csordás et al., 1999, 2006]. "Compartment C" represents the bulk of the cytosol minus the microdomains.

There is a dynamic exchange of ions on the plasma membrane due to the action of the various ion transport proteins that we have discussed in the previous model. Figure only illustrates the fluxes associated with calcium considered for

the model. For the other cation species, sodium and potassium we follow the transport schemes that were employed in the previous model (Appendix C), with concentration terms appropriately subscripted for the compartment considered. We may well assume that there is a steady state in the concentrations of $Na^+$and K^+in compartment C and the membrane potential is the resultant of the dynamics of all ions in compartment A

$$\frac{dV}{dt} = \frac{F\mathcal{V}_{cyt}}{C_m}\left[2\frac{dCa_A}{dt} + \frac{dNa_A}{dt} + \frac{dK_A}{dt}\right] \tag{6.1}$$

and may be represented by modifying equations B.1.2 as

$$\begin{aligned}\frac{dCa_A}{dt} &= J_1 - J_2 - J_3 - J_4 - J_6 + J_7\\ \frac{dNa_A}{dt} &= J_{\text{m,Na}}\\ \frac{dK_A}{dt} &= J_{\text{m,K}}\end{aligned}$$

The fluxes $J_{\text{m,Na}}$ and $J_{\text{m,K}}$ has the same meaning as given in B.1.3.

We now describe the various calcium fluxes between the different compartments present in the model.

J_1: **calcium entry through the plasma membrane** Ca^{2+} enters the neuron mainly through membrane calcium channels and from the experience of the previous model we need consider only the voltage gated L-type channel. The dynamics are provided in table C.1.

J_2: **calcium exit through pumps** The dynamics of PMCA pumping Ca^{2+} in to the extra neuronal space may be described using the modified Kyoto model described in B.1.6.

J_3: **calcium exit through membrane exchanger** The co-transport of Ca^{2+} and Na^+along NaCax may be described with the DiFrancesco-Noble model given in C.1.5

J_4: **calcium buffering** Models for the fast buffering of Ca^{2+} in compartment A with proteins calbindin and calmodulin may be described with equations given in B.1.8 and B.1.9 respectively.

J_6: **calcium uptake by the ER** The effective sequestering of Ca^{2+} in to the inert luminal space is carried out by the Ca^{2+} ATPases on the ER membrane (ERCA) and may be modelled with a simple model provided in [Tiveci et al., 2005].

$J_{r,lk}$: **calcium leak from ER** As the primary effector of leak from ER is the luminal Ca^{2+} concentration, this flux may be modelled as

$$J_{r,lk} = k_{r,lk} \left(Ca_{er} - Ca_c \right)$$

J_7: **calcium induced calcium release** This flux is caused by the activation of RyR by the influx of Ca^{2+} into the sub-membrane space through the L-type calcium channel. This positive feedback should supplement the activity of the calcium channels in creating the transient Ca^{2+} surge. In the previous model, since this activity was not included, the estimated channel conductance is likely to have been over-estimated. The three state Markov scheme used in the Kyoto model [Matsuoka et al., 2007] may be employed to describe RyR activation.

J_{rr}: **calcium diffusion in the ER** This may be described with a simple diffusion expression.

J_8: **calcium release from the ER** The release of calcium from the ER by the $InsP_3R$ may be represented by the concepts used in Marhl et al. [2000].

J_9: **calcium uptake by the mitochondria** This flux may be modelled based on the four state Markov model described in Bazil and Dash [2011].

J_{10}: **calcium release by the mitochondria using an exchanger** A detailed model of NaCam is difficult to be implemented. For the sake of brevity a Hill type expression (for example Wingrove and Gunter [1986]), may be employed to represent this component.

J_{ac} **and** J_{dc}: **calcium diffusion into the cytosol from the microdomains A and D** The free diffusion of calcium from the microdomains into the bulk of cytosol may be described by a simple diffusion expression with corresponding driving forces, ($Ca_a - Ca_c$) and ($Ca_d - Ca_c$) respectively.

6.3 Suggestions for future work

In the previous section we have introduced a prospective model to augment the analysis on the pacemaking activity that would illuminate energy and calcium metabolism of *SNc* neurons. The existing model is a good starting point for this expanded model. However we need to re-estimate a few of the parameters to incorporate the nuances of the additional features that are being explored. One advantage of having the cytoplasm compartmentalised with respect to the calcium hotspots is that we can limit the larger variation in the intracellular Ca^{2+} observed with our model (figure 5.6) to a range that is comparable to observations made in this regard (for example Foehring et al. [2009]).

One of the primary objective with the model would be to troubleshoot a few different situations that are key to the understanding of the pathogenic mechanism. One of the important observation made in our review is regarding the significance of the Ca^{2+} binding protein calbindin in *SNc* cytoplasm. As a buffer they are neuroprotective in conditions of extreme calcium influx such as excitotoxicity or stroke [Mattson, 2007]. Zhou et al. [2010] suggests from an *in vitro* study, the existence of a synergy between α-synuclein and calbindin that prevents the formation of α-synuclein protofibrils in a Ca^{2+} dependent manner (see 2.3.1), which also appear neuroprotective.

But what we are interested in is an observation made in the same experiment regarding the propensity of calbindin to be co-aggregated with α-synuclein. Immunostaining experiments have also demonstrated the presence of calbindin

in LB core. Taking these observations together, there is a probability that accumulation of α-synuclein into LBs creates a transient condition of calbindin shortage in the *SNc* cytoplasm and alter the steady state levels of Ca^{2+} in different compartments of the neuron. α-synuclein accumulation, being a process that may be initiated by a few different factors, can continue for a longer period of time, pushing the mitochondrial Ca^{2+} levels to alter the regulatory role of this cation to a different level as mentioned in 6.2.1.

A second aspect is that we can have a better estimate of energy use with the extended model, as it incorporates a few more components that utilize energy to maintain the equilibrium. Additionally, with a calcium block study the new model becomes even more relevant as are a substantial number of components involved with Ca^{2+} homeostasis pathways with an appetite for energy. The model may be modified in a manner that it can communicate with the integrative dynamic model developed to study energy metabolism using *in vivo* experiments [Cloutier et al., 2009; Wellstead and Cloutier, 2012].

The model may also be extended in various manners to incorporate different aspects that are not incorporated in the model at the moment. Such extensions could include mitochondrial pathways pronounced in ATP generation, pathways relevant to the intracellular pH and osmotic aspects and so forth. Prior to such attempts it would be best to have an experimental design to work along with the model for hypotheses made.

6.4 To Conclude

Human civilization has flourished into what it is today from a fundamental instinct to expand its knowledge horizon. The pursuit of knowledge has always been a risky ride into the deep mysteries of existence, on a wave of available knowledge. For most parts, the boundaries have broadened owing to initiatives that add new perspectives to tried and tested theories and methods.

The road to a theory for PD pathogenesis is still being laid out. New intersections and diversions add to the knowledge base. However at times, they tend to burden the process by creating meandering flow of information, thereby diverting focus away from a wholesome picture. The ever-growing community

of seekers need means of correlating such staggered information, to coordinate their efforts to a meaningful end. An approach that accounts the whole system should be a rightful step towards this direction.

Appendices

APPENDIX A

Steady state open probability in Markovian Ion-channel Model

A.1 Proof of Lemma 1

Proof The proof is trivial and can be derived from the proprieties of the exponentials. If 'k_1' and 'k_2' are the rates of two separate transitions appearing in a transition network, their corresponding ratio could be written as,

$$\frac{k_1(V)}{k_2(V)} = \frac{k_{1,0}}{k_{2,0}} e^{-((a_2-a_1)+(b_2-b_1)V+\cdots)/RT} \tag{A.1}$$

This expression takes the form of equation 3.14. In conjunction with the reasoning provided in section (3.3.2), we may approximate equations (3.14) and (A.1) by neglecting higher order terms as:

$$k(V), \frac{k_1(V)}{k_2(V)} = e^{[(V-V_h)s]} \tag{A.2}$$

where s represents the slope at a voltage of V_h. The product of rate ratios may also be approximated as follows:

$$\begin{aligned} \prod \left[\frac{k_i(V)}{k_j(V)}\right] &= \left[e^{\left\{(V-\hat{V}_{h,a})\hat{s}_a\right\}} e^{\left\{(V-\hat{V}_{h,b})\hat{s}_b\right\}} \dots\right] \\ &= e^{\left[(V-\hat{V}_{h,a})\hat{s}_a + (V-\hat{V}_{h,b})\hat{s}_b + \cdots\right]} \\ &= e^{[(V-V_h)s]} \end{aligned}$$

A.2 Model Identifiability

To study the parameter identifiability of a model [given by equation 3.25], let us consider the following general mathematical structure:

$$M(\theta) : y(\theta) = f(\theta, x)$$

where $\theta \in \mathbb{R}^{n_\theta}$ is the set of parameters to be estimated and $y(\theta) \in \mathbb{R}$ and $x \in \mathbb{R}$ denote the output and input of the system, respectively. In addition, let us denote the search space of the parameter by $\Theta \subseteq \mathbb{R}^{n_\theta}$.

Definition 1 *The model $M(\theta)$ is said to be **structurally output globally identifiable** (s.o.g.i) , if for any $\widetilde{\theta} \in \Theta$, except for points on a subset of Θ of measure zero, and for all $x \in \mathbb{R}$:*

$$y(\theta, x) \equiv y(\widetilde{\theta}, x) \Longrightarrow \theta \equiv \widetilde{\theta}$$

*If the same conditions is fulfilled only in the neighbourhood of θ then the parameters will be **structurally output locally identifiable** (s.o.l.i.)*

This definition is quite general and is often difficult to put into practice. One of the usual approaches in such instances is the "Taylor approach" [Walter and Pronzato, 1997] where both outputs $y(\theta, x)$ and $y(\widehat{\theta}, x)$ are approximated by a Taylor expansion around a point $x^* \in \mathbb{R}$. If we denote by $\mathcal{U}_{x^*}^n$ the ball around x^*, where the Taylor approximation of order n holds; the general identifiability definition is therefore:

Definition 2 *The model $M(\theta)$ is said to be s.o.g.i in $x \in \mathcal{U}_{x^*}^n$ if the system of equations:*

$$\left[\frac{\partial^i y(\theta, x)}{\partial x^i}\right]_{x=x_0} = \left[\frac{\partial^i y(\widetilde{\theta}, x)}{\partial x^i}\right]_{x=x_0} \qquad \forall i = 1, ...n \tag{A.3}$$

has an unique solution. In the same way, the model will be s.o.l.i in $x \in \mathcal{U}_{x^*}^n$ if a finite number of solution is obtained.

Proof of Lemma 2 It has to be proved that, the ion channel open state probability represented by the equation,

$$G(\theta) = \frac{1}{1 + e^{(V-V_{h_1})s_1} + e^{(V-V_{h_2})s_2}} \tag{A.4}$$

is s.o.l.i for any $V \in \mathcal{U}^n_{V^*}$, by using the Taylor approximation of fourth order. It may be noted that studying the identifiability property for $G(\theta)$ with parameters

$$\theta = [V_{h,1}, s_1, V_{h,2}, s_2] \in \mathbb{R}^4 \qquad \widetilde{\theta} = [\widetilde{V}_{h,1}, \widetilde{s}_1, \widetilde{V}_{h,2}, \widetilde{s}_1] \in \mathbb{R}^4$$

is equivalent to studying this property for the model

$$M(\theta) = e^{(aV+b)} + e^{(cV+d)}, \quad \theta = [a, b, c, d]$$

where

$$a = s_1, \quad b = -V_{h_1}s_1, \quad c = s_2, \quad d = -V_{h_2}s_2$$
$$\widetilde{a} = \widetilde{s}_1, \quad \widetilde{b} = -\widetilde{V}_{h_1}\widetilde{s}_1, \quad \widetilde{c} = \widetilde{s}_2, \quad \widetilde{d} = -\widetilde{V}_{h_2}\widetilde{s}_2$$

Therefore, the system of equations built by using (A.3) leads to:

$$e^{aV_0+b} + e^{cV_0+d} = e^{\widetilde{a}V_0+\widetilde{b}} + e^{\widetilde{c}V_0+\widetilde{d}} \tag{A.5a}$$

$$ae^{aV_0+b} + ce^{cV_0+d} = \widetilde{a}e^{\widetilde{a}V_0+\widetilde{b}} + \widetilde{c}e^{\widetilde{c}V_0+\widetilde{d}} \tag{A.5b}$$

$$a^2e^{aV_0+b} + c^2e^{cV_0+d} = \widetilde{a}^2e^{\widetilde{a}V_0+\widetilde{b}} + \widetilde{c}^2e^{\widetilde{c}V_0+\widetilde{d}} \tag{A.5c}$$

$$a^3e^{aV_0+b} + c^3e^{cV_0+d} = \widetilde{a}^3e^{\widetilde{a}V_0+\widetilde{b}} + \widetilde{c}^3e^{\widetilde{c}V_0+\widetilde{d}} \tag{A.5d}$$

with the following two solutions obtained with Mathematica software [Wolfram Research, 2008]:

$$a = \widetilde{c}, \quad b = \widetilde{d}, \quad c = \widetilde{a}, \quad d = \widetilde{b}$$
$$a = \widetilde{a}, \quad b = \widetilde{b}, \quad c = \widetilde{c}, \quad d = \widetilde{d}$$

Therefore, the system is s.o.l.i in the neighbourhood of V^* where the Taylor approximation holds.

Corollary 1 *If the model (A.4) is constrained with the following condition:*

$$s_1 > s_2$$

it is trivial to see that the system (A.5)now has only one solution and the model is s.o.g.i. for almost all $V \in \mathcal{U}^n_{V^*}$.

APPENDIX B

Model equations and parameters for the spherical PMU geometry

B.1 Model equations

B.1.1 Membrane Potential

$$V = \frac{F\mathcal{V}_{cyt}}{C_m}[K_i - K_e + 2(Ca_i - Ca_e) + Na_i - Na_e + \mathcal{A}_{\text{off}}] \tag{B.1}$$

where, $\mathcal{V}_{cyt} = \phi_{\text{cyt}} \cdot \mathcal{V}_{pmu}$; $\quad C_m = C_{sp} \cdot A_{\text{pmu}}$.

B.1.2 Ion dynamics

$$\frac{dCa_i}{dt} = J_{\text{m,Ca}} - (J_{\text{calb}} + 4J_{\text{cam}})$$
$$\frac{dNa_i}{dt} = J_{\text{m,Na}} \qquad \frac{dK_i}{dt} = J_{\text{m,K}}$$

B.1.3 Membrane ion fluxes

$$J_{\text{m,Ca}} = \frac{1}{z_{\text{Ca}}\mathcal{V}_{cyt}}\left(I_{\text{Ca}} + 2I_{\text{pmca}} - 2I_{\text{nacax}}\right)$$

$$J_{\text{m,Na}} = \frac{1}{z_{\text{Na}} F \mathcal{V}_{cyt}} \left(3I_{\text{nak}} + 3I_{\text{nacax}} + I_{\text{Na}}\right)$$
$$J_{\text{m,K}} = \frac{1}{z_{\text{K}} F \mathcal{V}_{cyt}} \left(I_K - 2I_{\text{nak}}\right)$$

B.1.4 Membrane ion-channel currents

$$I_{\text{Ca}} = \left(g_{\text{ca,l}}\mathcal{O}_{\text{ca,l}} + g_{\text{ca,t}}\mathcal{O}_{\text{ca,t}} + g_{\text{ca,hva}}\mathcal{O}_{\text{ca,hva}}\right) \cdot \sqrt{Ca_e Ca_i} \cdot \frac{\sinh\left(\frac{V-\hat{\mathcal{V}}_{Ca}}{\mathcal{V}_\tau}\right)}{sinhc\left(\frac{V}{\mathcal{V}_\tau}\right)}$$

$$I_{\text{K}} = \left(g_{\text{k,sk}}\mathcal{O}_{\text{k,sk}} + g_{\text{k,hcn}}\mathcal{O}_{\text{hcn}}\right) \cdot \sqrt{K_e K_i} \cdot \frac{\sinh\left(\frac{V-\hat{\mathcal{V}}_K}{2\mathcal{V}_\tau}\right)}{sinhc\left(\frac{V}{2\mathcal{V}_\tau}\right)}$$
$$+ \left(\mathcal{G}_{\text{k,dr}}\mathcal{O}_{\text{k,dr}} + \mathcal{G}_{\text{k,a}}\mathcal{O}_{\text{k,a}} + \mathcal{G}_{\text{k,ir}}\mathcal{O}_{\text{k,ir}}\right) \cdot \left(V - \hat{\mathcal{V}}_K\right)$$

$$I_{\text{Na}} = \left(g_{\text{na}}\mathcal{O}_{\text{na}} + g_{\text{na,hcn}}\mathcal{O}_{\text{hcn}} + g_{\text{na,leak}}\right) \cdot \sqrt{Na_e Na_i} \cdot \frac{\sinh\left(\frac{V-\hat{\mathcal{V}}_{Na}}{2\mathcal{V}_\tau}\right)}{sinhc\left(\frac{V}{2\mathcal{V}_\tau}\right)}$$

The gating dynamics of the different channels are laid out in table B.1

Table B.1: Gating dynamics

Gating dynamics of different ion channels used in the spherical model

#	Channel type	Open probability	Source
	Voltage-gated calcium channels		
1	L type		fitted, based on Amini et al. [1999]
		$\mathcal{O}_{\text{ca,l}} = m_{\text{ca,l}} \cdot h_{\text{ca,l}}$	
		$\frac{dm_{\text{ca,l}}}{dt} = \frac{{}^{1}/\left(1+\exp\left(\frac{V+15}{-7}\right)\right) - m_{\text{ca,l}}}{10 \cdot \exp\left(-\left[\frac{V+86.4}{23.2}\right]^2\right)+0.943}$	
		$h_{\text{ca,l}} = \frac{0.00045}{0.00045+Ca_i}$	
2	T type		Amini et al. [1999]
		$\mathcal{O}_{\text{ca,t}} = m_{\text{ca,t}} \cdot h_{\text{ca,t}}$	
		$\frac{dm_{\text{ca,t}}}{dt} = \frac{{}^{1}/\left(1+\exp\left(\frac{V+63}{-1.5}\right)\right) - m_{\text{ca,t}}}{65 \cdot \exp\left(-\left[\frac{V+68}{6}\right]^2\right)+12}$	
		$\frac{dh_{\text{ca,t}}}{dt} = \frac{{}^{1}/\left(1+\exp\left(\frac{V+76.2}{3}\right)\right) - h_{\text{ca,t}}}{50 \cdot \exp\left(-\left[\frac{V+72}{10}\right]^2\right)+10}$	

Continued on Next Page...

Table B.1 – Continued

#	Channel type	Open probability	Source
3	high voltage activated (HVA) type	$\mathcal{O}_{\text{ca,hva}} = m_{\text{ca,hva}} \cdot h_{\text{ca,hva}}$ $\frac{dm_{\text{ca,hva}}}{dt} = \frac{1/\left(1+\exp\left(\frac{V+10}{-10}\right)\right)-m_{\text{ca,hva}}}{0.1\cdot\exp\left(-\left[\frac{V+62}{13}\right]^2\right)+0.05}$ $\frac{dh_{\text{ca,hva}}}{dt} = \frac{1/\left(1+\exp\left(\frac{V+48}{5}\right)\right)-h_{\text{ca,hva}}}{0.5\cdot\exp\left(-\left[\frac{V+55.6}{18}\right]^2\right)+0.5}$	Amini et al. [1999]
Voltage-gated sodium channels			
4	Representative	$\mathcal{O}_{\text{na}} = m_{\text{na}}^3 \cdot h_{\text{na}}$ $\frac{dm_{\text{na}}}{dt} = 1.965 \cdot e^{\left(\frac{1.7127\cdot V}{\mathcal{V}_\tau}\right)} \cdot (1 - m_{\text{na}})$ $-0.0424 \cdot e^{\left(\frac{-1.5581\cdot V}{\mathcal{V}_\tau}\right)} \cdot m_{\text{na}}$ $\frac{dh_{\text{na}}}{dt} = 0.0001 \cdot e^{\left(\frac{-2.4317\cdot V}{\mathcal{V}_\tau}\right)} \cdot (1 - h_{\text{na}})$ $-0.5296 \cdot e^{\left(\frac{1.1868\cdot V}{\mathcal{V}_\tau}\right)} \cdot h_{\text{na}}$	fitted
Calcium-gated potassium channel			
5	SK-type	$\mathcal{O}_{\text{k,sk}} = \frac{Ca_i^{4.2}}{Ca_i^{4.2}+0.00035^{4.2}}$	Xia et al. [1998]
Voltage-gated potassium channels			
6	Delayed rectifier	$\mathcal{O}_{\text{k,dr}} = m_{\text{k,dr}}^3$ $\frac{dm_{\text{k,dr}}}{dt} = \frac{1/\left(1+\exp\left(\frac{V+25}{-12}\right)\right)-m_{\text{k,dr}}}{18/\left(1+\exp\left(\frac{V+39}{8}\right)\right)+1}$	Amini et al. [1999]
7	A-type	$\mathcal{O}_{\text{k,a}} = m_{\text{k,a}}^3 \cdot h_{\text{k,a}}$ $\frac{dm_{\text{k,a}}}{dt} = \frac{1/\left(1+\exp\left(\frac{V+43}{-24}\right)\right)-m_{\text{k,a}}}{2\cdot\exp\left(-\left[\frac{V+50}{23.45}\right]^2\right)+1.1}$ $\frac{dh_{\text{k,a}}}{dt} = \frac{1/\left(1+\exp\left(\frac{V+56}{8}\right)\right)-h_{\text{k,a}}}{20}$	Amini et al. [1999]
8	Internal rectifier	$\mathcal{O}_{\text{k,ir}} = 1/\left(1+\exp\left(\frac{V+90}{12.1}\right)\right)$	Chan et al. [2007]

Continued on Next Page...

Table B.1 – Continued

#	Channel type	Open probability	Source
Family : Cyclic nucleotide-regulated channels			
9	HCN	$\frac{d\mathcal{O}_{\text{hcn}}}{dt} = k_{\text{f,hcn}}\mathcal{O}_{\text{hcn}} - k_{\text{r,hcn}}(1-\mathcal{O}_{\text{hcn}})$ $k_{\text{f,hcn}} = k_{\text{f,free}}\mathcal{P}(C) + k_{\text{f,bnd}}(1-\mathcal{P}(C))$ $k_{\text{r,hcn}} = k_{\text{r,free}}\mathcal{P}(O) + k_{\text{r,bnd}}(1-\mathcal{P}(O))$ $\mathcal{P}(C) = {}^{1}/_{[1+{}^{cAMP}/_{0.001163}]}$ $\mathcal{P}(O) = {}^{1}/_{[1+{}^{cAMP}/_{0.00145}]}$ $k_{\text{f,free}} = \frac{0.006}{1+\exp({}^{(V+87.7)}/_{6.45})}$ $k_{\text{r,free}} = \frac{0.08}{1+\exp(-{}^{(V+51.7)}/_{7})}$ $k_{\text{f,bnd}} = \frac{0.0268}{1+\exp({}^{(V+94.2)}/_{13.3})}$ $k_{\text{r,bnd}} = \frac{0.08}{1+\exp(-{}^{(V+35.5)}/_{7})}$	based on Chan et al. [2007]

B.1.5 Plasma membrane sodium calcium exchanger (NaCax)

The model uses the modified Kyoto model for Na^{+}- Ca^{2+} exchange (see figure 4.2)

$$
\begin{aligned}
I_{\text{nacax}} &= k_{\text{nacax}}\left[k_{3,\text{xm}}\mathcal{P}(E^{\dagger}_{1,\text{xm}})y_{\text{xm}} - k_{4,\text{xm}}\mathcal{P}(E^{\dagger}_{2,\text{xm}})(1-y_{\text{xm}})\right] \\
\frac{dy_{\text{xm}}}{dt} &= \beta_{\text{xm}}(1-y_{\text{xm}}) - \alpha_{\text{xm}}y_{\text{xm}} \\
\beta_{\text{xm}} &= k_{2,\text{xm}}\mathcal{P}(E^{*}_{2,\text{xm}}) + k_{4,\text{xm}}\mathcal{P}(E^{\dagger}_{2,\text{xm}}) \\
\alpha_{\text{xm}} &= k_{1,\text{xm}}\mathcal{P}(E^{*}_{1,\text{xm}}) + k_{3,\text{xm}}\mathcal{P}(E^{\dagger}_{1,\text{xm}}) \\
\mathcal{P}(E^{*}_{1,\text{xm}}) &= \left[1 + \frac{k_{\text{xm,cai}}}{Ca_i}\left(1 + \left[\frac{Na_i}{k_{\text{xm,nai}}}\right]^{3}\right)\right]^{-1} \\
\mathcal{P}(E^{\dagger}_{1,\text{xm}}) &= \left[1 + \left[\frac{k_{\text{xm,nai}}}{Na_i}\right]^{3}\left(1 + \frac{Ca_i}{k_{\text{xm,cai}}}\right)\right]^{-1} \\
\mathcal{P}(E^{*}_{2,\text{xm}}) &= \left[1 + \frac{k_{\text{xm,cae}}}{Ca_e}\left(1 + \left[\frac{Na_e}{k_{\text{xm,nae}}}\right]^{3}\right)\right]^{-1} \\
\mathcal{P}(E^{\dagger}_{2,\text{xm}}) &= \left[1 + \left[\frac{k_{\text{xm,nae}}}{Na_e}\right]^{3}\left(1 + \frac{ca_e}{k_{\text{xm,Cae}}}\right)\right]^{-1}
\end{aligned}
$$

$$k_{1,\text{xm}} = \exp\left(-\delta_{xm,ca}{}^{V}/\nu_{\tau}\right) \quad k_{2,\text{xm}} = \exp\left((1-\delta_{xm,ca})^{V}/\nu_{\tau}\right)$$
$$k_{3,\text{xm}} = \exp\left((1-\delta_{xm,na})^{V}/\nu_{\tau}\right) \quad k_{4,\text{xm}} = \exp\left(-\delta_{xm,na}{}^{V}/\nu_{\tau}\right)$$

B.1.6 Plasma membrane calcium ATPase (PMCA)

The model makes use of the Kyoto model for PMCA, to describe its activity (see figure 4.7)

$$\begin{aligned}
I_{\text{pmca}} &= K_{\text{pc}}\left[k_{1,\text{pc}}\mathcal{P}(E^{*}_{1,\text{pc}})y_{\text{pc}} - k_{2,\text{pc}}\mathcal{P}(E^{*}_{2,\text{pc}})(1-y_{\text{pc}})\right] \\
\frac{dy_{\text{pc}}}{dt} &= \beta_{\text{pc}}(1-y_{\text{pc}}) - \alpha_{\text{pc}}y_{\text{pc}} \\
\beta_{\text{pc}} &= k_{2,\text{pc}}\mathcal{P}(E^{*}_{2,\text{pc}}) + k_{4,\text{pc}}\mathcal{P}(E_{2,\text{pc}}) \\
\alpha_{\text{pc}} &= k_{1,\text{pc}}\mathcal{P}(E^{*}_{1,\text{pc}}) + k_{3,\text{pc}}\mathcal{P}(E_{1,\text{pc}}) \\
\mathcal{P}(E^{*}_{1,\text{pc}}) &= \left[1+\frac{K_{\text{pc,i}}}{Ca_i}\right]^{-1} \quad \mathcal{P}(E_{1,\text{pc}}) = 1-\mathcal{P}(E^{*}_{1,\text{pc}}) \\
\mathcal{P}(E^{*}_{2,\text{pc}}) &= \left[1+\frac{K_{\text{pc,e}}}{Ca_e}\right]^{-1} \quad \mathcal{P}(E_{2,\text{pc}}) = 1-\mathcal{P}(E^{*}_{2,\text{pc}}) \\
k_{1,\text{pc}} &= \left[1+{}^{0.1}/_{[\text{ATP}]}\right]^{-1} \\
K_{\text{pc,i}} &= \left[\frac{180-6.4}{1+{}^{CaCam}/_{0.000,05}}+6.4\right]\times 10^{-5} \\
K_{\text{pc}} &= \kappa_{\text{pmca}}\left[\frac{10.56\times CaCam}{CaCam+0.000,05}+1.2\right]
\end{aligned}$$

B.1.7 Plasma membrane sodium-potassium ATPase (NaK)

The model uses the modified Kyoto model to describe the dynamics of NaK (see figure 4.4)

$$\begin{aligned}
I_{\text{nk}} &= K_{\text{nk}}\left[k_{1,\text{nk}}\mathcal{P}(E^{*}_{1,\text{nk}})y_{\text{nk}} - k_{2,\text{nk}}\mathcal{P}(E^{*}_{2,\text{nk}})(1-y_{\text{nk}})\right] \\
\frac{dy_{\text{nk}}}{dt} &= \beta_{\text{nk}}(1-y_{\text{nk}}) - \alpha_{\text{nk}}y_{\text{nk}}
\end{aligned}$$

$$
\begin{aligned}
\beta_{\text{nk}} &= k_{2,\text{nk}}\mathcal{P}(E^{*}_{2,\text{nk}}) + k_{4,\text{nk}}\mathcal{P}(E^{\dagger}_{2,\text{nk}}) \\
\alpha_{\text{nk}} &= k_{1,\text{nk}}\mathcal{P}(E^{*}_{1,\text{nk}}) + k_{3,\text{nk}}\mathcal{P}(E^{\dagger}_{1,\text{nk}}) \\
\mathcal{P}(E^{*}_{1,\text{nk}}) &= \left[1 + \frac{K_{\text{nk,nai}}}{Na_i}\left(1 + \frac{K_i}{K_{\text{nk,ki}}}\right)\right]^{-1} \\
\mathcal{P}(E^{\dagger}_{1,\text{nk}}) &= \left[1 + \frac{K_{\text{nk,ki}}}{K_i}\left(1 + \frac{Na_i}{K_{\text{nk,nai}}}\right)\right]^{-1} \\
\mathcal{P}(E^{*}_{2,\text{nk}}) &= \left[1 + \frac{K_{\text{nk,nae}}}{Na_{\text{eff}}}\left(1 + \frac{K_e}{K_{\text{nk,ke}}}\right)\right]^{-1} \\
\mathcal{P}(E^{\dagger}_{2,\text{nk}}) &= \left[1 + \frac{K_{\text{nk,ke}}}{K_e}\left(1 + \frac{Na_{\text{eff}}}{K_{\text{nk,nae}}}\right)\right]^{-1} \\
Na_{\text{eff}} &= Na_e e^{\left(\frac{-0.82V}{\mathcal{V}_\tau}\right)} \quad k_{1,\text{nk}} = \frac{0.37}{1 + 0.094/[\text{ATP}]}
\end{aligned}
$$

B.1.8 Ca^{2+} Buffering by Calbindin

$$
\begin{aligned}
J_{\text{calb}} &= k_{\text{calb,b}} Ca_i Calb - k_{\text{calb,d}} CaCalb \\
Calb_{\text{total}} &= Calb + CaCalb \\
\frac{dCalb}{dt} &= -J_{\text{calb}}
\end{aligned}
$$

B.1.9 Ca^{2+} Buffering by Calmodulin

$$
\begin{aligned}
J_{\text{cam}} &= \alpha_{\text{cam}} Cam - \beta_{\text{cam}} CaCam \\
Cam_{\text{total}} &= Cam + CaCam \\
\frac{dCam}{dt} &= -J_{\text{cam}} \\
\alpha_{\text{cam}} &= K^{\text{cb}}_{\text{cam}} K^{\text{nb}}_{\text{cam}} \left[\frac{1}{K^{\text{cb}}_{\text{cam}} + k^{\text{nd}}_{\text{cam}}} + \frac{1}{k^{\text{cd}}_{\text{cam}} + K^{\text{nb}}_{\text{cam}}}\right] \\
\beta_{\text{cam}} &= k^{\text{cd}}_{\text{cam}} k^{\text{nd}}_{\text{cam}} \left[\frac{1}{K^{\text{cb}}_{\text{cam}} + k^{\text{nd}}_{\text{cam}}} + \frac{1}{k^{\text{cd}}_{\text{cam}} + K^{\text{nb}}_{\text{cam}}}\right] \\
K^{\text{cb}}_{\text{cam}} &= k^{\text{cb}}_{\text{cam}} Ca_i^2 \\
K^{\text{nb}}_{\text{cam}} &= k^{\text{nb}}_{\text{cam}} Ca_i^2
\end{aligned}
$$

B.2 Model parameters

Table B.2: Parameters used in the spherical model

Parameter	Symbol	Value (Units)	Reference
Physical and chemical constants			
Faraday's Constant	F	96485.31 (C/mol)	
Gas Constant	R	8314.472 $(J/Kmol.K)$	
Calcium valency	z_{Ca}	2	
Sodium valency	z_{Na}	1	
Potassium valency	z_{K}	1	
Common constants in literature			
Extracellular calcium	Ca_e	1.8 (mM)	Puopolo et al. [2007]
Extracellular sodium	Na_e	137 (mM)	Puopolo et al. [2007]
Extracellular potassium	K_e	5.4 (mM)	Puopolo et al. [2007]
Specific membrane capacitance	C_{sp}	0.9 $(\mu F/cm^2)$	Gentet et al. [2000]
Cytosolic calcium diffusivity	$\mathcal{D}_{\text{Ca}}$	5.3×10^{-6} (cm^2/s)	Donahue and Abercrombie [1987]
Other design parameters			
Characteristic dimension, soma	d_s	30 (μm)	Matsuda et al. [2009]
Volume, PMU	$\mathcal{V}_{pmu}$	14.14 (pl)	
Body temperature	T	37 (^oC)	
Cytosolic ATP	[ATP]	2 (mM)	
Fraction of cytosol considered	ϕ_{cyt}	1	
Na^+-Ca^{2+} exchanger			
Energy barrier parameter	$\delta_{xm,ca}$	0.68	Niggli and Lederer [1993]
	$\delta_{xm,na}$	0.32	Niggli and Lederer [1993]
Dissociation constants	$K_{\text{xm,nai}}$	8.75 (mM)	Matsuoka et al. [2007]
	$K_{\text{xm,nae}}$	87.5 (mM)	Matsuoka et al. [2007]
	$K_{\text{xm,cai}}$	0.00138 (mM)	Matsuoka et al. [2007]
	$K_{\text{xm,cae}}$	1.38 (mM)	Matsuoka et al. [2007]
Na^+- K^+ATPase			
Reaction rates	$k_{\text{2,nk}}$	0.04 (ms^{-1})	Matsuoka et al. [2007]
	$k_{\text{3,nk}}$	0.01 (ms^{-1})	Matsuoka et al. [2007]
	$k_{\text{4,nk}}$	0.165 (ms^{-1})	Matsuoka et al. [2007]
Dissociation constants	$K_{\text{nk,nai}}$	4.05 (mM)	Matsuoka et al. [2007]
	$K_{\text{nk,nae}}$	69.8 (mM)	Matsuoka et al. [2007]
	$K_{\text{nk,ki}}$	32.88 (mM)	Matsuoka et al. [2007]
	$K_{\text{nk,ke}}$	0.258 (mM)	Matsuoka et al. [2007]
Ca^{2+} ATPase			
Reaction rates	$k_{\text{2,pc}}$	0.001 (ms^{-1})	Matsuoka et al. [2007]
	$k_{\text{3,pc}}$	0.001 (ms^{-1})	Matsuoka et al. [2007]
	$k_{\text{4,pc}}$	1 (ms^{-1})	Matsuoka et al. [2007]
Dissociation constants	$K_{\text{pc,e}}$	2 (mM)	Matsuoka et al. [2007]
Buffer Dynamics			
Calbindin reaction rates	$k_{\text{calb,b}}$	10000 $(1/mM.s)$	Nagerl et al. [2000]
	$k_{\text{calb,d}}$	2 $(1/s)$	Nagerl et al. [2000]

Continued on Next Page...

Table B.2 – Continued

Parameter	Symbol	Value (Units)	Reference
Calmodulin reaction rates	$k_{\text{cam}}^{\text{cb}}$	1.2×10^7 $(1/mM^2.s)$	Tadross et al. [2008]
	$k_{\text{cam}}^{\text{cd}}$	3 $(1/s)$	Tadross et al. [2008]
	$k_{\text{cam}}^{\text{nb}}$	3.7×10^9 $(1/mM^2.s)$	Tadross et al. [2008]
	$k_{\text{cam}}^{\text{nd}}$	3000 $(1/s)$	Tadross et al. [2008]
Estimated parameters: Channel conductances			
L-type Ca^{2+} channel	$g_{\text{ca,l}}$	1158.2 (nS)	
T-type Ca^{2+} channel	$g_{\text{ca,t}}$	10 (nS)	
HVA Ca^{2+} channel	$g_{\text{ca,hva}}$	78.5 (nS)	
Na^+channel	g_{na}	395.14 (nS)	
SK-type K^+channel	$g_{\text{k,sk}}$	15 (nS)	
K^+delayed rectifier	$\mathcal{G}_{\text{k,dr}}$	10 (nS)	
K^+inward rectifier	$\mathcal{G}_{\text{k,ir}}$	5 (nS)	
K^+A-type channel	$\mathcal{G}_{\text{k,a}}$	0.2234 (nS)	
HCN channel, Na	g_{nahcn}	3 (nS)	
HCN channel, K	g_{khcn}	10 (nS)	
Na^+leak	$g_{\text{na,leak}}$	0.0039 (nS)	
NaCax	k_{nacax}	25 $(pA.ms)$	
NaK	k_{nak}	200 $(pA.ms)$	
PMCA	k_{pmca}	10 $(pA.ms)$	
Estimated parameters: Buffering			
Total cytosolic calmodulin	Cam_{total}	0.0489 (mM)	
Total cytosolic calbindin	$Calb_{\text{total}}$	0.002 (mM)	
Initial conditions			
Cytosolic Ca^{2+}	Ca_i	0.00015 (mM)	
Cytosolic Na^+	Na_i	6 (mM)	
Cytosolic K^+	K_i	140 (mM)	
Cytosolic calbindin	$Calb$	0.0011 (mM)	
Cytosolic calmodulin	Cam	0.0487 (mM)	

APPENDIX C

Model equations and parameters for the realistic PMU geometry

C.1 Model equations

C.1.1 Membrane Potential

$$\frac{dV}{dt} = \frac{F\mathcal{V}_{cyt}}{C_m}\left[2\frac{dCa_i}{dt} + \frac{dNa_i}{dt} + \frac{dK_i}{dt}\right] \tag{C.1}$$

where,

$$\mathcal{V}_{cyt} = \phi_{\text{cyt}} \cdot \mathcal{V}_{pmu}$$
$$A_{\text{pmu}} = \mathcal{S}_{\text{pmu}} \cdot \mathcal{V}_{pmu}$$
$$C_m = C_{\text{sp}} \cdot A_{\text{pmu}}$$

C.1.2 Ion dynamics

See equations in section B.1.2.

C.1.3 Membrane ion fluxes

See equations in section B.1.3.

C.1.4 Membrane ion-channel currents

$$I_{\text{Ca}} = (g_{\text{ca,l}}\mathcal{O}_{\text{ca,l}}) \cdot \sqrt{Ca_e Ca_i} \cdot \frac{\sinh\left(\frac{V-\hat{\mathcal{V}}_{Ca}}{\mathcal{V}_\tau}\right)}{sinhc\left(\frac{V}{\mathcal{V}_\tau}\right)}$$

$$I_{\text{K}} = (g_{\text{k,sk}}\mathcal{O}_{\text{k,sk}}) \cdot \sqrt{K_e K_i} \cdot \frac{\sinh\left(\frac{V-\hat{\mathcal{V}}_{K}}{2\mathcal{V}_\tau}\right)}{sinhc\left(\frac{V}{2\mathcal{V}_\tau}\right)} + (\mathcal{G}_{\text{k,dr}}\mathcal{O}_{\text{k,dr}} + \mathcal{G}_{\text{k,ir}}\mathcal{O}_{\text{k,ir}}) \cdot (V - \hat{\mathcal{V}}_K)$$

$$I_{\text{Na}} = (g_{\text{na}}\mathcal{O}_{\text{na}} + g_{\text{na,hcn}}\mathcal{O}_{\text{hcn}} + g_{\text{na,leak}}) \cdot \sqrt{Na_e Na_i} \cdot \frac{\sinh\left(\frac{V-\hat{\mathcal{V}}_{Na}}{2\mathcal{V}_\tau}\right)}{sinhc\left(\frac{V}{2\mathcal{V}_\tau}\right)}$$

The gating dynamics of the different channels used in the model are laid out in table C.1

Table C.1: Gating dynamics

Gating dynamics of different ion channels used in the spherical model

#	Channel type	Open probability	Source
Voltage-gated calcium channels			
1	L type	$\mathcal{O}_{\text{ca,l}} = m_{\text{ca,l}} \cdot h_{\text{ca,l}}$ $\frac{dm_{\text{ca,l}}}{dt} = \frac{1/\left(1+\exp\left(\frac{V+15}{-7}\right)\right)-m_{\text{ca,l}}}{7.68\cdot\exp\left(-\left[\frac{V+65}{17.33}\right]^2\right)+0.723}$ $h_{\text{ca,l}} = \frac{0.00045}{0.00045+Ca_i}$	fitted, based on Amini et al. [1999]
Voltage-gated sodium channels			
2	Representative	see table B.1, 4	
Calcium-gated potassium channel			
3	SK-type	see table B.1, 5	
Voltage-gated potassium channels			
4	Delayed rectifier	see table B.1, 6	
5	Internal rectifier	see table B.1, 8	
Family : Cyclic nucleotide-regulated channels			
6	HCN	see table B.1, 9	

C.1.5 Plasma membrane sodium calcium exchanger (NaCax)

The model uses the DiFrancesco-Noble concept for the Na^+-Ca^{2+} exchange instead of the modified Kyoto used earlier for a faster response

$$I_{\text{nacax}} = \kappa_{\text{nacax}} \frac{\exp\left(\delta_{\text{xm}} \frac{V}{\mathcal{V}_\tau}\right) Na_i^3 Ca_e - \exp\left((\delta_{\text{xm}} - 1) \frac{V}{\mathcal{V}_\tau}\right) Na_e^3 Ca_i}{\left(1 + \mathcal{D}_{\text{xm}} \left[Na_i^3 Ca_e + Na_e^3 Ca_i\right]\right) \left(1 + \frac{Ca_i}{0.0069}\right)}$$

C.1.6 Plasma membrane calcium ATPase (PMCA)

The model makes use of the Kyoto model as described before in section B.1.6.

C.1.7 Plasma membrane sodium-potassium ATPase (NaK)

The model uses the modified Kyoto model to describe the dynamics of NaK as described before in section B.1.7.

C.1.8 Ca^{2+} Buffering by Calbindin

The equations described in section B.1.8 is used.

C.1.9 Ca^{2+} Buffering by Calmodulin

The equations described in section B.1.9 is used.

C.2 Model parameters

Table C.2: Parameters used in the spherical model

Parameter	Symbol	Value (Units)	Reference
Physical and chemical constants			
Faraday's Constant	F	96485.31 (C/mol)	
Gas Constant	R	8314.472 ($J/Kmol.K$)	
Calcium valency	z_{Ca}	2	
Sodium valency	z_{Na}	1	
Continued on Next Page...			

Table C.2 – Continued

Parameter	Symbol	Value (Units)	Reference
Potassium valency	z_{K}	1	
Common constants in literature			
Extracellular calcium	Ca_e	1.8 (mM)	Puopolo et al. [2007]
Extracellular sodium	Na_e	137 (mM)	Puopolo et al. [2007]
Extracellular potassium	K_e	5.4 (mM)	Puopolo et al. [2007]
Specific membrane capacitance	C_{sp}	0.9 $(\mu F/cm^2)$	Gentet et al. [2000]
Cytosolic calcium diffusivity	$\mathcal{D}_{\mathrm{Ca}}$	5.3×10^{-6} (cm^2/s)	Donahue and Abercrombie [1987]
Design parameters : geometry			
Characteristic dimension, soma	d_s	30 (μm)	Matsuda et al. [2009]
Characteristic dimension, PMU	d_{pmu}	50 (μm)	Tepper [2010]
Volume, PMU	$\mathcal{V}_{pmu}$	5 (pl)	
Surface-to-volume ratio, PMU	$\mathcal{S}_{\mathrm{pmu}}$	16.667 (μm^{-1})	
Volume fraction, Cytosol	ϕ_{cyt}	0.5	Alberts et al. [2002]
Other design parameters			
Body temperature	T	37 (^oC)	
Cytosolic ATP	[ATP]	2 (mM)	
Anionic offset	$\mathcal{A}_{\mathrm{off}}$	15.2377 (mM)	
Na^+-Ca^{2+} exchanger			
Energy barrier parameter	δ_{xm}	0.35	DiFrancesco and Noble [1985]
Denominator factor	$\mathcal{D}_{\mathrm{xm}}$	0.001	DiFrancesco and Noble [1985]
Na^+- K^+ATPase			
Reaction rates	$k_{2,\mathrm{nk}}$	0.04 (ms^{-1})	Matsuoka et al. [2007]
	$k_{3,\mathrm{nk}}$	0.01 (ms^{-1})	Matsuoka et al. [2007]
	$k_{4,\mathrm{nk}}$	0.165 (ms^{-1})	Matsuoka et al. [2007]
Dissociation constants	$K_{\mathrm{nk,nai}}$	4.05 (mM)	Matsuoka et al. [2007]
	$K_{\mathrm{nk,nae}}$	69.8 (mM)	Matsuoka et al. [2007]
	$K_{\mathrm{nk,ki}}$	32.88 (mM)	Matsuoka et al. [2007]
	$K_{\mathrm{nk,ke}}$	0.258 (mM)	Matsuoka et al. [2007]
Ca^{2+} ATPase			
Reaction rates	$k_{2,\mathrm{pc}}$	0.001 (ms^{-1})	Matsuoka et al. [2007]
	$k_{3,\mathrm{pc}}$	0.001 (ms^{-1})	Matsuoka et al. [2007]
	$k_{4,\mathrm{pc}}$	1 (ms^{-1})	Matsuoka et al. [2007]
Dissociation constants	$K_{\mathrm{pc,e}}$	2 (mM)	Matsuoka et al. [2007]
Buffer Dynamics			
Calbindin reaction rates	$k_{\mathrm{calb,b}}$	10000 $(1/mM.s)$	Nagerl et al. [2000]
	$k_{\mathrm{calb,d}}$	2 $(1/s)$	Nagerl et al. [2000]
Calmodulin reaction rates	$k^{\mathrm{cb}}_{\mathrm{cam}}$	1.2×10^7 $(1/mM^2.s)$	Tadross et al. [2008]
	$k^{\mathrm{cd}}_{\mathrm{cam}}$	3 $(1/s)$	Tadross et al. [2008]
	$k^{\mathrm{nb}}_{\mathrm{cam}}$	3.7×10^9 $(1/mM^2.s)$	Tadross et al. [2008]
	$k^{\mathrm{nd}}_{\mathrm{cam}}$	3000 $(1/s)$	Tadross et al. [2008]
Estimated parameters: Channel conductances			
L-type Ca^{2+} channel	$g_{\mathrm{ca,l}}$	2101.2 (nS)	
Na^+channel	g_{na}	907.68 (nS)	
SK-type K^+channel	$g_{\mathrm{k,sk}}$	2.2515 (nS)	

Continued on Next Page...

Table C.2 – Continued

Parameter	Symbol	Value (Units)	Reference
K^+delayed rectifier	$\mathcal{G}_{\text{k,dr}}$	31.237 (nS)	
K^+inward rectifier	$\mathcal{G}_{\text{k,ir}}$	13.816 (nS)	
HCN channel	g_{nahcn}	51.1 (nS)	
Na^+leak	$g_{\text{na,leak}}$	0.0053 (nS)	
NaCax	k_{nacax}	0.0166 ($pA.ms$)	
NaK	k_{nak}	1085.7 ($pA.ms$)	
PMCA	k_{pmca}	2.233 ($pA.ms$)	
Estimated parameters: Buffering			
Total cytosolic calmodulin	Cam_{total}	0.0235 (mM)	
Total cytosolic calbindin	$Calb_{\text{total}}$	0.005 (mM)	
Initial conditions			
Cytosolic Ca^{2+}	Ca_i	0.00015 (mM)	
Cytosolic Na^+	Na_i	6 (mM)	
Cytosolic K^+	K_i	140 (mM)	
Cytosolic calbindin	$Calb$	0.0011 (mM)	
Cytosolic calmodulin	Cam	0.0487 (mM)	

Bibliography

A. Abeliovich. Parkinson's disease: Mitochondrial damage control. *Nature a-z index*, 463(7282):744–745, 2010.

D. J. Aidley and P. R. Stanfield. *Ion channels: molecules in action*. Cambridge University Press, 1996.

M. S. Airaksinen, H. Thoenen, and M. Meyer. Vulnerability of midbrain dopaminergic neurons in Calbindin-D28k-deficient mice: Lack of evidence for a neuroprotective role of endogenous calbindin in MPTP treated and weaver mice. *European Journal of Neuroscience*, 9(1):120–127, 2006.

B. Alberts, A. Johnson, J. Lewis, M. Raff, K. Roberts, and P. Walter. *Molecular biology of the cell*. Garland Science Taylor & Francis Group, 4 edition, 2002. ISBN 0815332181.

B. Amini, J. W. Clark Jr, and C. C. Canavier. Calcium dynamics underlying pacemaker-like and burst firing oscillations in midbrain dopaminergic neurons: a computational study. *Journal of Neurophysiology*, 82(5):2249, 1999.

D. M. Arduíno, A. R. Esteves, S. M. Cardoso, and C. R. Oliveira. Endoplasmic reticulum and mitochondria interplay mediates apoptotic cell death: relevance to Parkinson's disease. *Neurochemistry International*, 55:341–348, Sep 2009.

D. M. Arduíno, A. R. Esteves, and S. M. Cardoso. Mitochondrial fusion/fission, transport and autophagy in Parkinson's disease: when mitochondria get nasty. *Parkinson's Disease*, 2011, 2011.

D. Attwell and S. B. Laughlin. An energy budget for signaling in the grey matter of the brain. *Journal of Cerebral Blood Flow and Metabolism*, 21:1133–1145, 2001.

E. Balsa-Canto, J. R. Banga, and M. R. García. Dynamic model building using optimal identification strategies, with applications in bioprocess engineering. *Process Systems Engineering*, pages 441–467, 2010.

R. Banerjee, A. A. Starkov, M. F. Beal, and B. Thomas. Mitochondrial dysfunction in the limelight of Parkinson's disease pathogenesis. *Biochimica et Biophysica Acta (BBA)-Molecular Basis of Disease*, 1792(7):651–663, 2009.

K. Baysal, G. P. Brierley, S. Novgorodov, and D. W. Jung. Regulation of the mitochondrial Na+/Ca2+ antiport by matrix pH. *Archives of biochemistry and biophysics*, 291(2):383–389, 1991.

J. N. Bazil and R. K. Dash. A minimal model for the mitochondrial rapid mode of Ca^{2+} uptake mechanism. *PloS one*, 6(6):e21324, 2011.

M. F. Beal. Mitochondria, oxidative damage, and inflammation in Parkinson's disease. *Annals of the New York Academy of Sciences*, 991(1):120–131, 2006.

L. Beaugé and R. DiPolo. The squid axon Na^+ / Ca^{2+} exchanger shows ping pong kinetics only when the Ca_i-regulatory site is saturated. *Cellular Physiology and Biochemistry*, 23(1-3):037–042, 2009.

J. Beaumont, F. A. Roberge, and L. J. Leon. On the interpretation of voltage-clamp data using the Hodgkin-Huxley model. *Mathematical Biosciences*, 115 (1):65–101, 1993.

C. Becker, S. S. Jick, and C. R. Meier. Use of antihypertensives and the risk of Parkinson disease. *Neurology*, 70(16 Part 2):1438–1444, 2008.

R. Bellman and K. J. Åström. On structural identifiability. *Mathematical Biosciences*, 7(3):329–339, 1970.

A. Bellucci, L. Navarria, M. Zaltieri, E. Falarti, S. Bodei, S. Sigala, L. Battistin, M. G. Spillantini, C. Missale, and P. F. Spano. Induction of the unfolded protein response by α-synuclein in experimental models of Parkinson's disease. *Journal of Neurochemistry*, 116(4):588–605, 2011.

A. L. Benabid, P. Pollak, A. Louveau, S. Henry, and J. De Rougemont. Combined (thalamotomy and stimulation) stereotactic surgery of the VIM thalamic nucleus for bilateral Parkinson disease. *Stereotactic and Functional Neurosurgery*, 50(1-6):344–346, 1987.

A. Bender, K. J. Krishnan, C. M. Morris, G. A. Taylor, A. K. Reeve, R. H. Perry, E. Jaros, J. S. Hersheson, J. Betts, and T. Klopstock. High levels of mitochondrial DNA deletions in substantia nigra neurons in aging and Parkinson disease. *Nature Genetics*, 38(5):515–517, 2006.

H. Bernheimer, W. Birkmayer, O. Hornykiewicz, K. Jellinger, and F. Seitelberger. Brain dopamine and the syndromes of Parkinson and Huntington. Clinical, morphological and neurochemical correlations. *Journal of Neurological Sciences*, 20(4):415–455, 1973.

M. J. Berridge. The endoplasmic reticulum: a multifunctional signaling organelle. *Cell Calcium*, 32(5-6):235–249, 2002.

D. M. Bers, W. H. Barry, and S. Despa. Intracellular Na^+ regulation in cardiac myocytes. *Cardiovascular Research*, 57:897–912, Mar 2003.

Å. Bertler and E. Rosengren. Occurrence and distribution of dopamine in brain and other tissues. *Cellular and Molecular Life Sciences*, 15(1):10–11, 1959.

R. Betarbet, T. B. Sherer, and J. T. Greenamyre. Ubiquitin–proteasome system and Parkinson's diseases. *Experimental neurology*, 191:S17–S27, 2005.

S. Beyl, E. N. Timin, A. Hohaus, A. Stary, M. Kudrnac, R. H. Guy, and S. Hering. Probing the architecture of an L-type calcium channel with a charged phenylalkylamine. *Journal of Biological Chemistry*, 282(6):3864–3870, 2007.

F. Bezanilla. The voltage sensor in voltage-dependent ion channels. *Physiological Reviews*, 80:555–592, Apr 2000.

W. Birkmayer and O. Hornykiewicz. The L-3, 4-dioxyphenylalanine (DOPA)-effect in Parkinson-akinesia. *Wiener klinische Wochenschrift*, 73:787, 1961.

M. P. Blaustein. The interrelationship between sodium and calcium fluxes across cell membranes. *Reviews of Physiology, Biochemistry and Pharmacology*, 70:33–82, 1974.

M. P. Blaustein and W. J. Lederer. Sodium/calcium exchange: Its physiological implications. *Physiological Reviews*, 79(3):763–854, 1999.

J. Blesa, S. Phani, V. Jackson-Lewis, and S. Przedborski. Classic and new animal models of Parkinson's disease. *Journal of Biomedicine and Biotechnology*, 2012, 2012.

J. P. Bolam and E. K. Pissadaki. Living on the edge with too many mouths to feed: Why dopamine neurons die. *Movement Disorders*, 2012.

I. R. Boldogh and L. A. Pon. Mitochondria on the move. *Trends in Cell Biology*, 17(10):502–510, 2007.

V. Bonifati, P. Rizzu, M. J. Van Baren, O. Schaap, G. J. Breedveld, E. Krieger, M. C. J. Dekker, F. Squitieri, P. Ibanez, and M. Joosse. Mutations in the DJ-1 gene associated with autosomal recessive early-onset parkinsonism. *Science*, 299(5604):256–259, 2003.

H. Braak and K. Del Tredici. Invited article: Nervous system pathology in sporadic Parkinson disease. *Neurology*, 70(20):1916–1925, 2008.

H. Braak, K. Del Tredici, U. Rub, R. A. de Vos, E. N. Jansen Steur, and E. Braak. Staging of brain pathology related to sporadic Parkinson's disease. *Neurobiology of Aging*, 24:197–211, 2003a.

H. Braak, U. Rub, W. P. Gai, and K. Del Tredici. Idiopathic Parkinson's disease: possible routes by which vulnerable neuronal types may be subject to neuroinvasion by an unknown pathogen. *Journal of Neural Transmission*, 110: 517–536, 2003b.

D. J. Brooks. Imaging approaches to Parkinson disease. *Journal of Nuclear Medicine*, 51(4):596–609, 2010.

B. S. Bunney, J. R. Walters, R. H. Roth, and G. K. Aghajania. Dopaminergic neurons: effect of antipsychotic drugs and amphetamine on single cell activity. *Journal of Pharmacology and Experimental Therapeutics*, 185(3):560–571, 1973.

R.E. Burke, W.T. Dauer, and J.P.G. Vonsattel. A critical evaluation of the Braak staging scheme for Parkinson's disease. *Annals of Neurology*, 64(5):485–491, 2008.

J. Burre, M. Sharma, T. Tsetsenis, V. Buchman, M. R. Etherton, and T. C. Sudhof. Alpha-synuclein promotes SNARE-complex assembly *in vivo* and *in vitro*. *Science*, 329:1663–1667, 2010.

G. Bustos, J. Abarca, J. Campusano, V. Bustos, V. Noriega, and E. Aliaga. Functional interactions between somatodendritic dopamine release, glutamate receptors and brain-derived neurotrophic factor expression in mesencephalic structures of the brain. *Brain Research Reviews*, 47(1-3):126–144, 2004.

C. Camello, R. Lomax, O. H. Petersen, and A. V. Tepikin. Calcium leak from intracellular stores–the enigma of calcium signalling. *Cell Calcium*, 32(5-6): 355–361, 2002.

C. C. Canavier. Sodium dynamics underlying burst firing and putative mechanisms for the regulation of the firing pattern in midbrain dopamine neurons: A computational approach. *Journal of Computational Neuroscience*, 6:49–69, 1999. ISSN 0929-5313.

C. C. Canavier and R. S. Landry. An increase in AMPA and a decrease in SK conductance increase burst firing by different mechanisms in a model of a dopamine neuron *In Vivo*. *Journal of Neurophysiology*, 96(5):2549–2563, 2006. doi: 10.1152/jn.00704.2006.

A. Carlsson, M. Lindqvist, T. Magnusson, and B. Waldeck. On the presence of 3-hydroxytyramine in brain. *Science*, 127:471, 1958.

M. Carlsson and A. Carlsson. Interactions between glutamatergic and monoaminergic systems within the basal ganglia-implications for schizophrenia and Parkinson's disease. *Trends in Neurosciences*, 13(7):272–276, 1990.

A. Catalano and D. H. O'Day. Calmodulin-binding proteins in the model organism Dictyostelium: A complete & critical review. *Cellular Signalling*, 20 (2):277–291, 2008.

C. S. Chan, J. N. Guzman, E. Ilijic, J. N. Mercer, C. Rick, T. Tkatch, G. E. Meredith, and D. J. Surmeier. 'Rejuvenation' protects neurons in mouse models of Parkinson's disease. *Nature*, 447:1081–1086, 2007. doi: 10.1038/nature05865.

C. S. Chan, T. S. Gertler, and D. J. Surmeier. Calcium homeostasis, selective vulnerability and Parkinson's disease. *Trends in Neurosciences*, 32:249–256, 2009.

J. M. Charcot and A. Vulpian. *De la paralysie agitante: à propos d'un cas tiré de la clinique du professeur Oppolzer*. Masson, 1862.

Y. M. Choi, S. H. Kim, D. Y. Uhm, and M. K. Park. Glutamate-mediated Ca^{2+} dynamics in spontaneously firing dopamine neurons of the rat substantia nigra pars compacta. *Journal of Cell Science*, 116(13):2665–2675, 2003.

S. Christakos, C. Gabrielides, and W. B. Rhoten. Vitamin D-dependent calcium binding proteins: chemistry, distribution, functional considerations, and molecular biology. *Endocrine Reviews*, 10(1):3–26, 1989.

Y. Chu and J. H. Kordower. Age-associated increases of alpha-synuclein in monkeys and humans are associated with nigrostriatal dopamine depletion: Is this the target for Parkinson's disease? *Neurobiology of Disease*, 25(1): 134–149, 2007.

D. D. Clarke and L. Sokoloff. Circulation and energy metabolism of the brain. *Basic Neurochemistry*, 6:637–69, 1999.

J. R. Clay. Potassium channel kinetics in squid axons with elevated levels of external potassium concentration. *Biophysical Journal*, 45(2):481–485, 1984.

J. R. Clay. Determining K^+ channel activation curves from K^+ channel currents often requires the Goldman–Hodgkin–Katz equation. *Frontiers in Cellular Neuroscience*, 3, 2009.

M. Cloutier and P. Wellstead. The control systems structures of energy metabolism. *Journal of The Royal Society Interface*, 7(45):651–665, 2010.

M. Cloutier and P. Wellstead. Dynamic modelling of protein and oxidative metabolisms simulates the pathogenesis of Parkinson's disease. *Systems Biology, IET*, 6(3):65–72, 2012.

M. Cloutier, F.B. Bolger, J.P. Lowry, and P. Wellstead. An integrative dynamic model of brain energy metabolism using in vivo neurochemical measurements. *Journal of Computational Neuroscience*, 27(3):391–414, 2009.

T. J. Collier, N. M. Kanaan, and J. H. Kordower. Ageing as a primary risk factor for Parkinson's disease: evidence from studies of non-human primates. *Nature Reviews Neuroscience*, 12(6):359–366, 2011.

K. J. Conn, W. Gao, A. McKee, M. S. Lan, M. D. Ullman, P. B. Eisenhauer, R. E. Fine, and J. M. Wells. Identification of the protein disulfide isomerase family member PDIp in experimental Parkinson's disease and Lewy body pathology. *Brain Research*, 1022:164–172, 2004.

M. R. Cookson. alpha-Synuclein and neuronal cell death. *Molecular Neurodegeneration*, 4:9, 2009.

J. S. Coombs, D. R. Curtis, and J. C. Eccles. The generation of impulses in motoneurones. *The Journal of Physiology*, 139:232–249, 1957.

D. Csercsik, Szederkényi G., and K. M. Hangos. Identifiability of a Hodgkin-Huxley type ion channel under voltage step measurement conditions. *Proceedings of the 9th International Symposium on Dynamics and Control of Process Systems (DYCOPS 2010)*, MoAT3.4:318–323, 2010.

D. Csercsik, K. M. Hangos, and G. Szederkényi. Identifiability analysis and parameter estimation of a single hodgkin-huxley type voltage dependent ion channel under voltage step measurement conditions. *Neurocomputing*, 77: 178–188, 2012.

G. Csordás, A. P. Thomas, and G. Hajnóczky. Quasi-synaptic calcium signal transmission between endoplasmic reticulum and mitochondria. *The EMBO Journal*, 18(1):96–108, 1999.

G. Csordás, C. Renken, P. Várnai, L. Walter, D. Weaver, K. F. Buttle, T. Balla, C. A. Mannella, and G. Hajnóczky. Structural and functional features and significance of the physical linkage between ER and mitochondria. *The Journal of Cell Biology*, 174(7):915–921, 2006.

C. Da Cunha, S. Wietzikoski, E. C. Wietzikoski, E. Miyoshi, M. M. Ferro, J. A. Anselmo-Franci, and N. S. Canteras. Evidence for the substantia nigra pars compacta as an essential component of a memory system independent of the hippocampal memory system. *Neurobiology of Learning and Memory*, 79(3): 236–242, 2003.

P. Damier, E. C. Hirsch, Y. Agid, and A. M. Graybiel. The substantia nigra of the human brain. I. Nigrosomes and the nigral matrix, a compartmental organization based on calbindin D(28K) immunohistochemistry. *Brain*, 122 (Pt 8):1421–1436, 1999a.

P. Damier, E. C. Hirsch, Y. Agid, and A. M. Graybiel. The substantia nigra of the human brain. II. Patterns of loss of dopamine-containing neurons in Parkinson's disease. *Brain*, 122 (Pt 8):1437–1448, 1999b.

L. M. de Lau and M. M. Breteler. Epidemiology of Parkinson's disease. *The Lancet Neurology*, 5(6):525–535, Jun 2006.

D. De Stefani, A. Raffaello, E. Teardo, I. Szabò, and R. Rizzuto. A forty-kilodalton protein of the inner membrane is the mitochondrial calcium uniporter. *Nature*, 476(7360):336–340, 2011.

P. Desplats, H. J. Lee, E. J. Bae, C. Patrick, E. Rockenstein, L. Crews, B. Spencer, E. Masliah, and S. J. Lee. Inclusion formation and neuronal cell death through neuron-to-neuron transmission of α-synuclein. *Proceedings of the National Academy of Sciences*, 106(31):13010–13015, 2009.

A. Destexhe and J. R. Huguenard. Nonlinear thermodynamic models of voltage-dependent currents. *Journal of Computational Neuroscience*, 9:259–270(12), 2000.

D. T. Dexter, F. R. Wells, A. J. Lee, F. Agid, Y. Agid, P. Jenner, and C. D. Marsden. Increased nigral iron content and alterations in other metal ions occurring in brain in Parkinson's disease. *Journal of Neurochemistry*, 52(6):1830–1836, 2006.

G. Di Giovanni, V. Di Matteo, and E. Esposito. *Birth, life and death of dopaminergic neurons in the substantia nigra*, volume 73. Springer, 2009.

D. DiFrancesco and D. Noble. A model of cardiac electrical activity incorporating ionic pumps and concentration changes. *Philosophical Transactions of the Royal Society B: Biological Sciences*, 307:353–398, Jan 1985.

Brian S. Donahue and R.F. Abercrombie. Free diffusion coefficient of ionic calcium in cytoplasm. *Cell Calcium*, 8(6):437 – 448, 1987. ISSN 0143-4160.

C. G. Drake. Arteriovenous malformations of the brain. *New England Journal of Medicine*, 309(5):308–310, 1983.

G. Drion, L. Massotte, R. Sepulchre, and V. Seutin. How modeling can reconcile apparently discrepant experimental results: The case of pacemaking in dopaminergic neurons. *PLOS Computational Biology*, 7(5):e1002050, 05 2011. doi: 10.1371/journal.pcbi.1002050.

Y. Du, Y. Nomura, Z. Liu, Z. Y. Huang, and K. Dong. Functional expression of an arachnid sodium channel reveals residues responsible for tetrodotoxin resistance in invertebrate sodium channels. *Journal of Biological Chemistry*, 284(49):33869–33875, 2009.

M. R. Duchen. Contributions of mitochondria to animal physiology: from homeostatic sensor to calcium signalling and cell death. *The Journal of physiology*, 516(1):1–17, 1999.

M. R. Duchen, A. Verkhratsky, and S. Muallem. Mitochondria and calcium in health and disease. *Cell Calcium*, 44(1):1–5, 2008.

B. M. Dufty, L. R. Warner, S. T. Hou, S. X. Jiang, T. Gomez-Isla, K. M. Leenhouts, J. T. Oxford, M. B. Feany, E. Masliah, and T. T. Rohn. Calpain-cleavage of alpha-synuclein: connecting proteolytic processing to disease-linked aggregation. *The American Journal of Pathology*, 170:1725–1738, 2007.

J. A. Egea, E. Balsa-Canto, M. S. G. García, and J. R. Banga. Dynamic optimization of nonlinear processes with an enhanced scatter search method. *Industrial & Engineering Chemistry Research*, 48(9):4388–4401, 2009.

B. Eisenberg. Ionic channels in biological membranes: natural nanotubes. *Accounts of Chemical Research*, 31(3):117–124, 1998.

L. P. Endresen, K. Hall, J. S. Hoye, and J. Myrheim. A theory for the membrane potential of living cells. *European Biophysics Journal*, 29:90–103, 2000.

A. R. Esteves, D. M. Arduino, R. H. Swerdlow, C. R. Oliveira, and S. M. Cardoso. Dysfunctional mitochondria uphold calpain activation: contribution to Parkinson's disease pathology. *Neurobiology of Disease*, 37:723–730, 2010.

H. Eyring. The activated complex in chemical reactions. *The Journal of Chemical Physics*, 3:107, 1935.

S. Fahn. Does levodopa slow or hasten the rate of progression of Parkinson's disease? *Journal of Neurology*, 252 Suppl 4:IV37–IV42, 2005.

J. H. Fallon and R. Y. Moore. Catecholamine innervation of the basal forebrain IV. topography of the dopamine projection to the basal forebrain and neostriatum. *The Journal of Comparative Neurology*, 180(3):545–579, 1978.

J. H. Fallon, J. N. Riley, and R. Y. Moore. Substantia nigra dopamine neurons: separate populations project to neostriatum and allocortex. *Neuroscience letters*, 7(2):157–162, 1978.

M. J. Farrer. Genetics of Parkinson disease: paradigm shifts and future prospects. *Nature Reviews Genetics*, 7(4):306–318, 2006.

M. Fink and D. Noble. Markov models for ion channels: versatility versus identifiability and speed. *Philosophical Transactions of the Royal Society A: Mathematical, Physical and Engineering Sciences*, 367(1896):2161–2179, 2009.

G. Fiskum, A. Starkov, B. M. Polster, and C. Chinopoulos. Mitochondrial mechanisms of neural cell death and neuroprotective interventions in Parkinson's disease. *Annals of the New York Academy of Sciences*, 991(1):111–119, 2006.

R. C. Foehring, X. F. Zhang, J. C. F. Lee, and J. C. Callaway. Endogenous calcium buffering capacity of substantia nigral dopamine neurons. *Journal of Neurophysiology*, 102(4):2326, 2009.

J. F. Fohlmeister and R. F. Miller. Mechanisms by which cell geometry controls repetitive impulse firing in retinal ganglion cells. *Journal of Neurophysiology*, 78:1948–1964, 1997.

C. Foix and J. Nicolesco. *Les noyaux gris centraux et la région mésencéphalo-sous-optique: suivi d'un appendice sur l'anatomie pathologique de la maladie de Parkinson.* Massons, 1925.

R. F. Fox. Stochastic versions of the Hodgkin-Huxley equations. *Biophysical Journal*, 72(5):2068 – 2074, 1997.

F. Francis, M. R. García, and R. H. Middleton. Energetics of ion transport in dopaminergic substantia nigra neurons. In P. Wellstead and M. Cloutier, editors, *Systems Biology of Parkinson's Disease*, pages 81–109. Springer New York, 2012. ISBN 978-1-4614-3411-5.

Y. Fujioka, K. Hiroe, and S. Matsuoka. Regulation kinetics of Na^+ - Ca^{2+} exchange current in guinea-pig ventricular myocytes. *The Journal of Physiology*, 529(3):611–623, 2000.

P. G. Galloway, P. Mulvihill, and G. Perry. Filaments of Lewy bodies contain insoluble cytoskeletal elements. *American Journal of Pathology*, 140:809–822, 1992.

S. Gandhi, M. M. K Muqit, L. Stanyer, D. G. Healy, P. M. Abou-Sleiman, I. Hargreaves, S. Heales, M. Ganguly, L. Parsons, and A. J. Lees. PINK1 protein in normal human brain and Parkinson's disease. *Brain*, 129(7):1720–1731, 2006.

S. Gandhi, A. Wood-Kaczmar, Z. Yao, H. Plun-Favreau, E. Deas, K. Klupsch, J. Downward, D. S. Latchman, S. J. Tabrizi, and N. W. Wood. PINK1-associated Parkinson's disease is caused by neuronal vulnerability to calcium-induced cell death. *Molecular Cell*, 33(5):627–638, 2009.

H. M. Gao, P. T. Kotzbauer, K. Uryu, S. Leight, J. Q. Trojanowski, and V. M. Lee. Neuroinflammation and oxidation/nitration of alpha-synuclein linked to dopaminergic neurodegeneration. *The Journal of Neuroscience*, 28:7687–7698, 2008.

R. P. J. García. Prehistory of Parkinson's disease. *Neurologia*, 19(10):735–7, 2004.

L. J. Gentet, G. J. Stuart, and J. D. Clements. Direct measurement of specific membrane capacitance in neurons. *Biophysical Journal*, 79:314–320, Jul 2000.

I. M. Glynn and V. L. Lew. Synthesis of adenosine triphosphate at the expense of downhill cation movements in intact human red cells. *The Journal of Physiology*, 207(2):393–402, 1970.

M. Goedert. Alpha-synuclein and neurodegenerative diseases. *Nature Reviews Neuroscience*, 2(7):492–501, 2001.

C. G. Goetz, S. Fahn, P. Martinez-Martin, W. Poewe, C. Sampaio, G. T. Stebbins, M. B. Stern, B. C. Tilley, R. Dodel, and B. Dubois. Movement disorder society-sponsored revision of the unified Parkinson's disease rating scale (MDS-UPDRS): Process, format, and clinimetric testing plan. *Movement disorders*, 22(1):41–47, 2007.

A. L. Goldin. Diversity of mammalian voltage-gated sodium channels. *Annals of the New York Academy of Sciences*, 868(1):38–50, 1999.

D. E. Goldman. Potential, impedance, and rectification in membranes. *The Journal of General Physiology*, 27(1):37–60, 1943.

T. Gonzalez-Hernandez, I. Cruz-Muros, D. Afonso-Oramas, J. Salas-Hernandez, and J. Castro-Hernandez. Vulnerability of mesostriatal dopaminergic neurons in Parkinson's disease. *Frontiers in Neuroanatomy*, 4:140, 2010.

M. Gourie-Devi, M. G. Ramu, and B. S. Venkataram. Treatment of Parkinson's disease in 'Ayurveda'(ancient indian system of medicine): discussion paper. *Journal of the Royal Society of Medicine*, 84(8):491, 1991.

A. A. Grace and B. S. Bunney. Intracellular and extracellular electrophysiology of nigral dopaminergic neurons - 2. Action potential generating mechanisms and morphological correlates. *Neuroscience*, 10(2):317–331, 1983a.

A. A. Grace and B. S. Bunney. Intracellular and extracellular electrophysiology of nigral dopaminergic neurons - 1. Identification and characterization. *Neuroscience*, 10(2):301–315, 1983b.

A. A. Grace and B. S. Bunney. The control of firing pattern in nigral dopamine neurons: burst firing. *The Journal of Neuroscience*, 4(11):2877–2890, 1984a.

A. A. Grace and B. S. Bunney. The control of firing pattern in nigral dopamine neurons: single spike firing. *The Journal of Neuroscience*, 4(11):2866–2876, 1984b.

A. M. Graybiel. The basal ganglia: learning new tricks and loving it. *Current Opinion in Neurobiology*, 15(6):638–644, 2005.

J. G. Greene. Gene expression profiles of brain dopamine neurons and relevance to neuropsychiatric disease. *The Journal of Physiology*, 575(2):411–416, 2006.

J. G. Greene, R. Dingledine, and J. T. Greenamyre. Gene expression profiling of rat midbrain dopamine neurons: implications for selective vulnerability in Parkinsonism. *Neurobiology of Disease*, 18(1):19–31, 2005.

J. G. Greenfield and F. D. Bosanquet. The brain-stem lesions in Parkinsonism. *Journal of Neurology, Neurosurgery & Psychiatry*, 16(4):213–226, 1953.

B. Greten-Harrison, M. Polydoro, M. Morimoto-Tomita, L. Diao, A. M. Williams, E. H. Nie, S. Makani, N. Tian, P. E. Castillo, V. L. Buchman, and S. S. Chandra. alpha-Synuclein triple knockout mice reveal age-dependent neuronal dysfunction. *Proceedings of the National Academy of Sciences*, 107: 19573–19578, 2010.

S. Guan, Q. Lu, and K. Huang. A discussion about the DiFrancesco-Noble model. *Journal of Theoretical Biology*, 189(1):27–32, 1997.

J. N. Guzman, J. Sanchez-Padilla, C. S. Chan, and D. J. Surmeier. Robust Pacemaking in Substantia Nigra Dopaminergic Neurons. *The Journal of Neuroscience*, 29(35):11011–11019, 2009. doi: 10.1523/JNEUROSCI.2519-09.2009.

J. N. Guzman, J. Sanchez-Padilla, D. Wokosin, J. Kondapalli, E. Ilijic, P. T. Schumacker, and D. J. Surmeier. Oxidant stress evoked by pacemaking in dopaminergic neurons is attenuated by DJ-1. *Nature*, 468:696–700, 2010. doi: 10.1038/nature09536.

A. H. Hainsworth, J. Röper, R. Kapoor, and F. M. Ashcroft. Identification and electrophysiology of isolated pars compacta neurons from guinea-pig substantia nigra. *Neuroscience*, 43(1):81–93, 1991.

J. K. Hale and S. M. V. Lunel. *Introduction to functional differential equations*, volume 99. Springer, 1993.

P. Hänggi, P. Talkner, and M. Borkovec. Reaction-rate theory: fifty years after Kramers. *Reviews of Modern Physics*, 62(2):251, 1990.

J. Hardy, H. Cai, M. R. Cookson, K. Gwinn-Hardy, and A. Singleton. Genetics of Parkinson's disease and Parkinsonism. *Annals of Neurology*, 60(4):389–398, 2006.

N. C. Harris, C. Webb, and S. A. Greenfield. A possible pacemaker mechanism in pars compacta neurons of the guinea-pig substantia nigra revealed by various ion channel blocking agents. *Neuroscience*, 31(2):355–362, 1989.

T. Hayashi, R. Rizzuto, G. Hajnoczky, and T. P. Su. MAM: more than just a housekeeper. *Trends in Cell Biology*, 19(2):81–88, 2009.

T. Heimburg. Mechanical aspects of membrane thermodynamics. Estimation of the mechanical properties of lipid membranes close to the chain melting transition from calorimetry. *Biochimica et Biophysica Acta (BBA)-Biomembranes*, 1415(1):147–162, 1998.

T. Heimburg. Lipid ion channels. *Biophysical Chemistry*, 150(1-3):2 – 22, 2010a. ISSN 0301-4622. doi: DOI:10.1016/j.bpc.2010.02.018.

T. Heimburg. The physics of nerves. *arXiv preprint arXiv:1008.4279*, 2010b.

T. Heimburg and A. D. Jackson. On soliton propagation in biomembranes and nerves. *Proceedings of the National Academy of Sciences*, 102(28):9790–9795, 2005.

C. Henchcliffe and M. F. Beal. Mitochondrial biology and oxidative stress in Parkinson disease pathogenesis. *Nature Clinical Practice Neurology*, 4(11): 600–609, 2008.

M. A. Herrera-Valdez. Membranes with the same ion channel populations but different excitabilities. *PLOS One*, 7(4):e34636, 2012.

B. Hille. *Ion Channels of Excitable Membranes*. Sinauer Associates, Inc., 2001.

A. L. Hodgkin and A. F. Huxley. A quantitative description of membrane current and its application to conduction and excitation in nerve. *The Journal of Physiology*, 117(4):500–544, 1952.

A. M. Hofer, S. Curci, T. E. Machen, and I. Schulz. ATP regulates calcium leak from agonist-sensitive internal calcium stores. *The FASEB Journal*, 10(2):302–308, 1996.

J. J. M. Hoozemans, E. S. Van Haastert, P. Eikelenboom, R. A. I. De Vos, J. M. Rozemuller, and W. Scheper. Activation of the unfolded protein response in

Parkinson's disease. *Biochemical and Biophysical Research Communications*, 354(3):707–711, 2007.

R. A. Horn and C. R. Johnson. *Matrix Analysis*. Cambridge University Press, 1985.

M. Høyer-Hansen and M. Jäättelä. Connecting endoplasmic reticulum stress to autophagy by unfolded protein response and calcium. *Cell Death & Differentiation*, 14(9):1576–1582, 2007.

T. J. Hund, J. P. Kucera, N. F. Otani, and Y. Rudy. Ionic charge conservation and long-term steady state in the Luo-Rudy dynamic cell model. *Biophysical Journal*, 81:3324–3331, Dec 2001.

B. I. Hyland, J. N. J. Reynolds, J. Hay, C. G. Perk, and R. Miller. Firing modes of midbrain dopamine cells in the freely moving rat. *Neuroscience*, 114(2): 475–492, 2002.

O. Ibanez-Sandoval, L. Carrillo-Reid, E. Galarraga, D. Tapia, E. Mendoza, J. C. Gomora, J. Aceves, and J. Bargas. Bursting in substantia nigra pars reticulata neurons *In Vitro*: Possible relevance for Parkinson disease. *Journal of Neurophysiology*, 98(4):2311–2323, 2007. doi: 10.1152/jn.00620.2007.

S. Ikebe, M. Tanaka, K. Ohno, W. Sato, K. Hattori, T. Kondo, Y. Mizuno, and T. Ozawa. Increase of deleted mitochondrial DNA in the striatum in Parkinson's disease and senescence. *Biochemical and Biophysical Research Communications*, 170(3):1044, 1990.

S. Ikebe, M. Tanaka, and T. Ozawa. Point mutations of mitochondrial genome in Parkinson's disease. *Brain Research. Molecular Brain Research*, 28(2):281, 1995.

E. Ilijic, J. N. Guzman, and D. J. Surmeier. The L-type channel antagonist isradipine is neuroprotective in a mouse model of Parkinson's disease. *Neurobiology of Disease*, 43:364–371, Aug 2011.

K. J. Inglis, D. Chereau, E. F. Brigham, S. S. Chiou, S. Schobel, N. L. Frigon, M. Yu, R. J. Caccavello, S. Nelson, R. Motter, S. Wright, D. Chian, P. Santiago, F. Soriano, C. Ramos, K. Powell, J. M. Goldstein, M. Babcock, T. Yednock, F. Bard,

G. S. Basi, H. Sham, T. J. Chilcote, L. McConlogue, I. Griswold-Prenner, and J. P. Anderson. Polo-like kinase 2 (PLK2) phosphorylates alpha-synuclein at serine 129 in central nervous system. *Journal of Biological Chemistry*, 284: 2598–2602, 2009.

V. P. Ivanova, I. M. Makarov, T. E. Schäffer, and T. Heimburg. Analyzing heat capacity profiles of peptide-containing membranes: cluster formation of gramicidin A. *Biophysical Journal*, 84(4):2427–2439, 2003.

K. Iwasa, I. Tasaki, and R. C. Gibbons. Swelling of nerve fibers associated with action potentials. *Science*, 210(4467):338, 1980.

T. Iwatsubo, I. Nakano, K. Fukunaga, and E. Miyamoto. Ca2+/calmodulin-dependent protein kinase II immunoreactivity in Lewy bodies. *Acta Neuropathologica*, 82:159–163, 1991.

E. M. Izhikevich. *Dynamical systems in neuroscience: the geometry of excitability and bursting*. Computational neuroscience. MIT Press, 2007. ISBN 9780262090438.

J. Jankovic and A. S. Kapadia. Functional decline in Parkinson disease. *Archives of Neurology*, 58(10):1611, 2001.

M. G. Kaplitt, P. Leone, R. J. Samulski, X. Xiao, D. W. Pfaff, K. L. O'Malley, and M. J. During. Long-term gene expression and phenotypic correction using adeno-associated virus vectors in the mammalian brain. *Nature Genetics*, 8 (2):148–154, 1994.

M. Kappl, G. Nagel, and K. Hartung. Voltage and Ca(2+) dependence of pre-steady-state currents of the Na-Ca exchanger generated by Ca(2+) concentration jumps. *Biophysical Journal*, 81:2628–2638, Nov 2001.

J. Keener. Invariant manifold reductions for Markovian ion channel dynamics. *Journal of Mathematical Biology*, 58:447–457, 2009.

P. M. Keeney, J. Xie, R. A. Capaldi, and J. P. Bennett. Parkinson's disease brain mitochondrial complex I has oxidatively damaged subunits and is functionally impaired and misassembled. *The Journal of Neuroscience*, 26:5256–5264, 2006.

P. Kienker. Equivalence of Aggregated Markov Models of Ion-Channel Gating. *Proceedings of the Royal Society of London. B. Biological Sciences*, 236(1284): 269–309, 1989.

B. Kim and S. Matsuoka. Cytoplasmic Na+-dependent modulation of mitochondrial Ca2+ via electrogenic mitochondrial Na+–Ca2+ exchange. *The Journal of Physiology*, 586(6):1683–1697, 2008.

C. Kim and S. J. Lee. Controlling the mass action of α-synuclein in Parkinson's disease. *Journal of Neurochemistry*, 107(2):303–316, 2008.

J. H. Kim, J. M. Auerbach, J. A. Rodríguez-Gómez, I. Velasco, D. Gavin, N. Lumelsky, S. H. Lee, J. Nguyen, R. Sánchez-Pernaute, and K. Bankiewicz. Dopamine neurons derived from embryonic stem cells function in an animal model of Parkinson's disease. *Nature*, 418(6893):50–56, 2002.

T. D. Kim, S. R. Paik, C. H. Yang, and J. Kim. Structural changes in α-synuclein affect its chaperone-like activity *in vitro*. *Protein Science*, 9(12):2489–2496, 2000.

Y. Kirichok, G. Krapivinsky, and D. E. Clapham. The mitochondrial calcium uniporter is a highly selective ion channel. *Nature*, 427:360–364, 2004.

D. Kirik, L. E. Annett, C. Burger, N. Muzyczka, R. J. Mandel, and A. Björklund. Nigrostriatal α-synucleinopathy induced by viral vector-mediated overexpression of human α-synuclein: a new primate model of Parkinson's disease. *Proceedings of the National Academy of Sciences*, 100(5):2884–2889, 2003.

K. Kiselyov and S. Muallem. Mitochondrial Ca^{2+} homeostasis in lysosomal storage diseases. *Cell Calcium*, 44(1):103–111, 2008.

S. J. Kish, K. Shannak, and O. Hornykiewicz. Uneven pattern of dopamine loss in the striatum of patients with idiopathic Parkinson's disease. *New England Journal of Medicine*, 318(14):876–880, 1988.

T. Kitada, S. Asakawa, N. Hattori, H. Matsumine, Y. Yamamura, S. Minoshima, M. Yokochi, Y. Mizuno, and N. Shimizu. Mutations in the parkin gene cause autosomal recessive juvenile Parkinsonism. *Nature*, 392(6676):605–608, 1998.

R. Klink, A. de Kerchove d'Exaerde, M. Zoli, and J.P. Changeux. Molecular and physiological diversity of nicotinic acetylcholine receptors in the midbrain dopaminergic nuclei. *The Journal of Neuroscience*, 21(5):1452–1463, 2001.

K. J. Klos, J. E. Ahlskog, K. A. Josephs, H. Apaydin, J. E. Parisi, B. F. Boeve, M W DeLucia, and D. W. Dickson. α-synuclein pathology in the spinal cords of neurologically asymptomatic aged individuals. *Neurology*, 66(7):1100–1102, 2006.

L. W. Ko, H. H. Ko, W. L. Lin, J. G. Kulathingal, and S. H. Yen. Aggregates assembled from overexpression of wild-type alpha-synuclein are not toxic to human neuronal cells. *Journal of Neuropathology & Experimental Neurology*, 67:1084–1096, 2008.

A. O. Komendantov, O. G. Komendantova, S. W. Johnson, and C. C. Canavier. A modeling study suggests complementary roles for GABAA and NMDA receptors and the SK channel in regulating the firing pattern in midbrain dopamine neurons. *Journal of Neurophysiology*, 91(1):346–357, 2004.

J. H. Kordower, Y. Chu, R. A. Hauser, T. B. Freeman, and C. W. Olanow. Lewy body-like pathology in long-term embryonic nigral transplants in Parkinson's disease. *Nature Medicine*, 14:504–506, 2008.

A. Y. Kuznetsova, M. A. Huertas, A. S. Kuznetsov, C. A. Paladini, and C. C. Canavier. Regulation of firing frequency in a computational model of a midbrain dopaminergic neuron. *Journal of Computational Neuroscience*, 28(3): 389–403, 2010. ISSN 1573-6873.

S. Lammel, A. Hetzel, O. Häckel, I. Jones, B. Liss, and J. Roeper. Unique properties of mesoprefrontal neurons within a dual mesocorticolimbic dopamine system. *Neuron*, 57(5):760–773, 2008.

H. A. Lashuel, B. M. Petre, J. Wall, M. Simon, R. J. Nowak, T. Walz, and P. T. Lansbury. α-synuclein, especially the Parkinson's disease-associated mutants, forms pore-like annular and tubular protofibrils. *Journal of Molecular Biology*, 322(5):1089–1102, 2002.

P. Läuger and H. J. Apell. A microscopic model for the current-voltage behaviour of the Na, K-pump. *European Biophysics Journal*, 13(5):309–321, 1986.

M. Lavrentovich and S. Hemkin. A mathematical model of spontaneous calcium (II) oscillations in astrocytes. *Journal of Theoretical Biology*, 251(4):553–560, 2008.

V. L. Leathers and A. W. Norman. Evidence for calcium mediated conformational changes in calbindin-D28K (the vitamin D-induced calcium binding protein) interactions with chick intestinal brush border membrane alkaline phosphatase as studied via photoaffinity labeling techniques. *Journal of Cellular Biochemistry*, 52(2):243–252, 1993.

H. J. Lee, S. Y. Shin, C. Choi, Y. H. Lee, and S. J. Lee. Formation and removal of alpha-synuclein aggregates in cells exposed to mitochondrial inhibitors. *Journal of Biological Chemistry*, 277(7):5411–5417, 2002.

H. J. Lee, S. Patel, and S. J. Lee. Intravesicular localization and exocytosis of α-synuclein and its aggregates. *The Journal of Neuroscience*, 25(25):6016–6024, 2005.

F. Leighton and R. Rivest. Estimating a probability using finite memory. *IEEE Transactions on Information Theory*, 32(6), 1986.

T. G. Lesnick, S. Papapetropoulos, D. C. Mash, J. Ffrench-Mullen, L. Shehadeh, M. de Andrade, J. R. Henley, W. A. Rocca, J. E. Ahlskog, and D. M. Maraganore. A genomic pathway approach to a complex disease: Axon guidance and Parkinson disease. *PLoS Genetics*, 3(6):e98, 06 2007.

F. H. Lewy. Paralysis agitans. I. Pathologische anatomie. *Handbuch der neurologie*, 3:920–933, 1912.

J. Y. Li, E. Englund, J. L. Holton, D. Soulet, P. Hagell, A. J. Lees, T. Lashley, N. P. Quinn, S. Rehncrona, A. Bjorklund, H. Widner, T. Revesz, O. Lindvall, and P. Brundin. Lewy bodies in grafted neurons in subjects with Parkinson's disease suggest host-to-graft disease propagation. *Nature Medicine*, 14:501–503, 2008.

W. Li, C. Lesuisse, Y. Xu, J. C. Troncoso, D. L. Price, and M. K. Lee. Stabilization of α-synuclein protein with aging and familial Parkinson's disease-linked A53T mutation. *The Journal of Neuroscience*, 24(33):7400–7409, 2004.

J. Liao, H. Li, W. Zeng, D. B. Sauer, R. Belmares, and Y. Jiang. Structural insight into the ion-exchange mechanism of the sodium/calcium exchanger. *Science's STKE*, 335(6069):686, 2012.

L. S. Liebovitch. Testing fractal and markov models of ion channel kinetics. *Biophysical Journal*, 55(2):373 – 377, 1989. ISSN 0006-3495. doi: DOI:10.1016/S0006-3495(89)82815-2.

L. S. Liebovitch, J. Fischbarg, J. P. Koniarek, I. Todorova, and M. Wang. Fractal model of ion-channel kinetics. *Biochimica et Biophysica Acta*, 896(2):173–180, Jan 1987.

G. Liu, C. Zhang, J. Yin, X. Li, F. Cheng, Y. Li, H. Yang, K. Uéda, P. Chan, and S. Yu. α-Synuclein is differentially expressed in mitochondria from different rat brain regions and dose-dependently down-regulates complex I activity. *Neuroscience letters*, 454(3):187–192, 2009.

R. B. Lomax, C. Camello, F. Van Coppenolle, O. H. Petersen, and A. V. Tepikin. Basal and physiological Ca2+ leak from the endoplasmic reticulum of pancreatic acinar cells second messenger–activated channels and translocons. *Journal of Biological Chemistry*, 277(29):26479–26485, 2002.

J. Lotharius and P. Brundin. Pathogenesis of Parkinson's disease: dopamine, vesicles and alpha-synuclein. *Nature Reviews Neuroscience*, 3(12):932–942, 2002.

C. H. Luo and Y. Rudy. A dynamic model of the cardiac ventricular action potential. I. Simulations of ionic currents and concentration changes. *Circulation Research*, 74:1071–1096, Jun 1994.

K. L. Manchester. Free energy ATP hydrolysis and phosphorylation potential. *Biochemical Education*, 8(3):70–72, 1980. ISSN 1879-1468. doi: 10.1016/0307-4412(80)90043-6.

S. Manna, J. Banerjee, and S. Ghosh. Breathing of voltage dependent anion channel as revealed by the fractal property of its gating. *Physica A: Statistical Mechanics and its Applications*, 386(1):573–580, 2007.

M. Marhl, T. Haberichter, M. Brumen, and R. Heinrich. Complex calcium oscillations and the role of mitochondria and cytosolic proteins. *Biosystems*, 57 (2):75–86, Jul 2000.

L. J. Martin, Y. Pan, A. C. Price, W. Sterling, N. G. Copeland, N. A. Jenkins, D. L. Price, and M. K. Lee. Parkinson's disease α-synuclein transgenic mice develop neuronal mitochondrial degeneration and cell death. *The Journal of Neuroscience*, 26(1):41–50, 2006.

J. Martinez, I. Moeller, H. Erdjument-Bromage, P. Tempst, and B. Lauring. Parkinson's disease-associated α-synuclein is a calmodulin substrate. *Journal of Biological Chemistry*, 278(19):17379–17387, 2003.

M. S. Matell and W. H. Meck. Neuropsychological mechanisms of interval timing behavior. *Bioessays*, 22(1):94–103, 2000.

N. Matsuda and K. Tanaka. Does impairment of the ubiquitin-proteasome system or the autophagy-lysosome pathway predispose individuals to neurodegenerative disorders such as Parkinson's disease? *Journal of Alzheimer's Disease*, 19(1):1–9, 2010.

W. Matsuda, T. Furuta, K. C. Nakamura, H. Hioki, F. Fujiyama, R. Arai, and T. Kaneko. Single nigrostriatal dopaminergic neurons form widely spread and highly dense axonal arborizations in the neostriatum. *The Journal of Neuroscience*, 29:444–453, 2009.

S. Matsuoka, H. Jo, M. Kuzumoto, A. Takeuchi, R. Saito, and A. Noma. *Modeling Energetics of Ion Transport, Membrane Sensing and Systems Biology of the Heart*, pages 435–455. Wiley-VCH Verlag GmbH & Co. KGaA, 2007. ISBN 9783527621095. doi: 10.1002/9783527621095.ch13.

M. P. Mattson. Calcium and neurodegeneration. *Aging Cell*, 6(3):337–350, 2007.

M.P. Mattson and S.L. Chan. Neuronal and glial calcium signaling in Alzheimer's disease. *Cell Calcium*, 34(4-5):385–398, 2003.

P. L. McGeer and E. G. McGeer. Inflammation and neurodegeneration in Parkinson's disease. *Parkinsonism & related disorders*, 10:S3–S7, 2004.

K. S. McNaught, D. P. Perl, A. L. Brownell, and C. W. Olanow. Systemic exposure to proteasome inhibitors causes a progressive model of Parkinson's disease. *Annals of Neurology*, 56:149–162, 2004.

P. Mecocci, U. MacGarvey, A. E. Kaufman, D. Koontz, J. M. Shoffner, D. C. Wallace, and M. F. Beal. Oxidative damage to mitochondrial dna shows marked age-dependent increases in human brain. *Annals of neurology*, 34(4):609–616, 2004.

T. Meyer and L. Stryer. Calcium spiking. *Annual review of biophysics and biophysical chemistry*, 20(1):153–174, 1991.

L. S. Milescu, G. Akk, and F. Sachs. Maximum likelihood estimation of ion channel kinetics from macroscopic currents. *Biophysical Journal*, 88(4):2494–2515, 2005.

G. L. Millhauser, E. E. Salpeter, and R. E. Oswald. Diffusion models of ion-channel gating and the origin of power-law distributions from single-channel recording. *Proceedings of the National Academy of Sciences*, 85(5):1503–1507, 1988.

I. Mizuta, T. Tsunoda, W. Satake, Y. Nakabayashi, M. Watanabe, A. Takeda, K. Hasegawa, K. Nakashima, M. Yamamoto, and N. Hattori. Calbindin 1, fibroblast growth factor 20, and α-synuclein in sporadic Parkinson's disease. *Human Genetics*, 124(1):89–94, 2008.

H. Mogami, A. V. Tepikin, and O. H. Petersen. Termination of cytosolic Ca2+ signals: Ca2+ reuptake into intracellular stores is regulated by the free Ca2+ concentration in the store lumen. *The EMBO Journal*, 17(2):435–442, 1998.

L. Moran, D. Duke, M. Deprez, D. Dexter, R. Pearce, and M. Graeber. Whole genome expression profiling of the medial and lateral substantia nigra in Parkinson's disease. *Neurogenetics*, 7:1–11, 2006. ISSN 1364-6745. 10.1007/s10048-005-0020-2.

E. V. Mosharov, K. E. Larsen, E. Kanter, K. A. Phillips, K. Wilson, Y. Schmitz, D. E. Krantz, K. Kobayashi, R. H. Edwards, and D. Sulzer. Interplay between cytosolic dopamine, calcium, and α-synuclein causes selective death of substantia nigra neurons. *Neuron*, 62(2):218 – 229, 2009.

L. J. Mullins. A mechanism for Na/Ca transport. *The Journal of General Physiology*, 70(6):681–695, 1977.

L. J. Mullins. The generation of electric currents in cardiac fibers by Na/Ca exchange. *American Journal of Physiology-Cell Physiology*, 236(3):C103–C110, 1979.

U. V. Nagerl, D. Novo, I. Mody, and J. L. Vergara. Binding kinetics of calbindin-D(28k) determined by flash photolysis of caged Ca(2+). *Biophysical Journal*, 79:3009–3018, 2000.

R. G. Nair-Roberts, S. D. Chatelain-Badie, E. Benson, H. White-Cooper, J. P. Bolam, and M. A. Ungless. Stereological estimates of dopaminergic, gabaergic and glutamatergic neurons in the ventral tegmental area, substantia nigra and retrorubral field in the rat. *Neuroscience*, 152(4):1024–1031, 2008.

A. Nekouzadeh and Y. Rudy. Statistical properties of ion channel records. part II: Estimation from the macroscopic current. *Mathematical Biosciences*, 210 (1):315 – 334, 2007.

D. L. Nelson and M. M. Cox. *Lehninger: Principles of Biochemistry*. W.H. Freeman, 2004. ISBN 9780716743392.

D. G. Nicholls and S. J. Ferguson. *Bioenergetics 3*. Academic Press, 1992. ISBN 9780125181211.

E. Niggli and W. J. Lederer. Activation of Na-Ca exchange current by photolysis of "caged calcium". *Biophysical Journal*, 65:882–891, Aug 1993.

R. A. Nixon. The calpains in aging and aging-related diseases. *Ageing Research Reviews*, 2(4):407–418, 2003.

E. Oancea and T. Meyer. Protein kinase C as a molecular machine for decoding calcium and diacylglycerol signals. *Cell*, 95(3):307–318, 1998.

C. Oka, C. Y. Cha, and A. Noma. Characterization of the cardiac Na^+/K^+ pump by development of a comprehensive and mechanistic model. *Journal of Theoretical Biology*, 265(1):68–77, 2010.

World Health Organization. Death and DALY estimates for 2002 by cause for WHO member states. *World Health Organization*, 2004.

K. D. Osborn, A. Zaidi, A. Mandal, R. J. Urbauer, and C. K. Johnson. Single-molecule dynamics of the calcium-dependent activation of plasma-membrane Ca2+-ATPase by calmodulin. *Biophysical Journal*, 87:1892–1899, Sep 2004.

A. M. Oster and B. S. Gutkin. A reduced model of DA neuronal dynamics that displays quiescence, tonic firing and bursting. *Journal of Physiology*, 2011.

N. Ostrerova-Golts, L. Petrucelli, J. Hardy, J. M. Lee, M. Farer, and B. Wolozin. The A53T alpha-synuclein mutation increases iron-dependent aggregation and toxicity. *The Journal of Neuroscience*, 20:6048–6054, 2000.

C. E. Overton. *Studien über die Narkose: Zugleich ein Beitrag zur allgemeinen Pharmakologie*. Fischer, 1901.

M. Ozer. An improved non-linear thermodynamic model of voltage-dependent ionic currents. *Neuroreport*, 15(12):1953–7, 2004.

M. Ozer. A comparative analysis of linear, nonlinear and improved nonlinear thermodynamic models of voltage-dependent ion channel kinetics. *Physica A: Statistical Mechanics and its Applications*, 379(2):579 – 586, 2007.

D. Papahadjopoulos, K. Jacobson, S. Nir, and I. Isac. Phase transitions in phospholipid vesicles fluorescence polarization and permeability measurements concerning the effect of temperature and cholesterol. *Biochimica et Biophysica Acta (BBA)-Biomembranes*, 311(3):330–348, 1973.

A. B. Parekh. Ca2+ microdomains near plasma membrane Ca2+ channels: impact on cell function. *The Journal of Physiology*, 586(13):3043–3054, 2008.

M. K. Park, O. H. Petersen, and A. V. Tepikin. The endoplasmic reticulum as one continuous Ca2+ pool: visualization of rapid Ca2+ movements and equilibration. *The EMBO Journal*, 19(21):5729–5739, 2000.

J. Parkinson. *An essay on the shaking palsy*. Printed by Whittingham and Rowland for Sherwood, Neely, and Jones, 1817.

L. Parkkinen, T. Pirttilä, and I. Alafuzoff. Applicability of current staging/categorization of α-synuclein pathology and their clinical relevance. *Acta neuropathologica*, 115(4):399–407, 2008.

J. C. Patel, P. Witkovsky, M. V. Avshalumov, and M. E. Rice. Mobilization of calcium from intracellular stores facilitates somatodendritic dopamine release. *The Journal of Neuroscience*, 29(20):6568–6579, 2009.

M. J. Pelczar, E. C. S. Chan, and N. R. Krieg. *Microbiology : Application Based Approach*. McGraw-Hill Education (India) Pvt Limited, 1993. ISBN 9780070151475.

M. Picard, T. Taivassalo, D. Ritchie, K. J. Wright, M. M. Thomas, C. Romestaing, and R. T. Hepple. Mitochondrial structure and function are disrupted by standard isolation methods. *PLoS One*, 6(3):e18317, 2011.

C. Pifl, B. Plank, W. Wyskovsky, O. Bertel, G. Hellmann, and J. Suko. Calmodulin·(Ca2+)$_4$ is the active calmodulin-calcium species activating the calcium-, calmodulin-dependent protein kinase of cardiac sarcoplasmic reticulum in the regulation of the calcium pump. *Biochimica et Biophysica Acta (BBA)-Biomembranes*, 773(2):197–206, 1984.

H. X. Ping and P. D. Shepard. Apamin-sensitive Ca2+-activated K+ channels regulate pacemaker activity in nigral dopamine neurons. *Neuroreport*, 7(3): 809, 1996.

P. Pizzo and T. Pozzan. Mitochondria-endoplasmic reticulum choreography: structure and signaling dynamics. *Trends in Cell Biology*, 17(10):511–517, 2007.

C. Poignard, A. Silve, F. Campion, L. M. Mir, O. Saut, and L. Schwartz. Ion fluxes, transmembrane potential, and osmotic stabilization: a new dynamic electrophysiological model for eukaryotic cells. *European Biophysics Journal*, 40:235–246, 2011.

M. H. Polymeropoulos, C. Lavedan, E. Leroy, S. E. Ide, A. Dehejia, A. Dutra, B. Pike, H. Root, J. Rubenstein, R. Boyer, E. S. Stenroos, S. Chandrasekharappa, A. Athanassiadou, T. Papapetropoulos, W. G. Johnson, A. M.

Lazzarini, R. C. Duvoisin, G. Di Iorio, L. I. Golbe, and R. L. Nussbaum. Mutation in the alpha-synuclein gene identified in families with Parkinson's disease. *Science*, 276:2045–2047, 1997.

J. G. C. Ponard, A. A. Kondratyev, and J. P. Kucera. Mechanisms of intrinsic beating variability in cardiac cell cultures and model pacemaker networks. *Biophysical Journal*, 92(10):3734–3752, 2007.

A. C. Poole, R. E. Thomas, L. A. Andrews, H. M. McBride, A. J. Whitworth, and L. J. Pallanck. The PINkK1/Parkin pathway regulates mitochondrial morphology. *Proceedings of the National Academy of Sciences*, 105(5):1638–1643, 2008.

R. K. Pradhan, D. A. Beard, and R. K. Dash. A biophysically based mathematical model for the kinetics of mitochondrial Na+-Ca2+ antiporter. *Biophysical Journal*, 98(2):218–230, 2010.

A. Priyadarshi, S. A. Khuder, E. A. Schaub, and S. S. Priyadarshi. Environmental risk factors and Parkinson's disease: a metaanalysis. *Environmental Research*, 86(2):122–127, 2001.

A. Probst, A. Bloch, and M. Tolnay. New insights into the pathology of Parkinson's disease: does the peripheral autonomic system become central? *European Journal of Neurology*, 15 Suppl 1:1–4, 2008.

S. Przedborski and H. Ischiropoulos. Reactive oxygen and nitrogen species: weapons of neuronal destruction in models of Parkinson's disease. *Antioxidants & Redox Signaling*, 7(5-6):685–693, 2005.

M. Puopolo, E. Raviola, and B. P. Bean. Roles of Subthreshold Calcium Current and Sodium Current in Spontaneous Firing of Mouse Midbrain Dopamine Neurons. *The Journal of Neuroscience*, 27(3):645–656, 2007. doi: 10.1523/JNEUROSCI.4341-06.2007.

I. Putzier, P. H. M. Kullmann, J. P. Horn, and E. S. Levitan. Cav1.3 channel voltage dependence, not Ca2+ selectivity, drives pacemaker activity and amplifies bursts in nigral dopamine neurons. *The Journal of Neuroscience*, 29: 15414–9, 2009 Dec 9 2009.

A. Raffaello, D. De Stefani, and R. Rizzuto. The mitochondrial Ca^{2+} uniporter. *Cell Calcium*, 2012.

M. E. Raichle and D. A. Gusnard. Appraising the brain's energy budget. *Proceedings of the National Academy of Sciences*, 99(16):10237, 2002.

R. F. Rakowski, D. C. Gadsby, and P. De Weer. Voltage dependence of the Na/K pump. *Journal of Membrane Biology*, 155:105–112, 1997.

C. D. Richards, T. Shiroyama, and S. T. Kitai. Electrophysiological and immunocytochemical characterization of GABA and dopamine neurons in the substantia nigra of the rat. *Neuroscience*, 80(2):545–557, 1997.

J. M. Ritchie and R. D. Keynes. The production and absorption of heat associated with electrical activity in nerve and electric organ. *Quarterly Reviews of Biophysics*, 18(4):3, 1985.

B. Ritz, S. L. Rhodes, L. Qian, E. Schernhammer, J. H. Olsen, and S. Friis. L-type calcium channel blockers and Parkinson disease in Denmark. *Annals of Neurology*, 67(5):600–606, 2010.

G. Rudow, R. O'Brien, A. V. Savonenko, S. M. Resnick, A. B. Zonderman, O. Pletnikova, L. Marsh, T. M. Dawson, B. J. Crain, M. J. West, and J. C. Troncoso. Morphometry of the human substantia nigra in ageing and Parkinson's disease. *Acta Neuropathologica*, 115(4):461–470, 2008.

A. R. Saha, N. N. Ninkina, D. P. Hanger, B. H. Anderton, A. M. Davies, and V. L. Buchman. Induction of neuronal death by α-synuclein. *European Journal of Neuroscience*, 12(8):3073–3077, 2008.

B. Sakmann and E. Neher. *Single-channel recording*. Springer, 2009.

F. Sala and A. Hernández-Cruz. Calcium diffusion modeling in a spherical neuron. Relevance of buffering properties. *Biophysical Journal*, 57(2):313–324, 1990.

M. S. Sansom, F. G. Ball, C. J. Kerry, R. McGee, R. L. Ramsey, and P. N. Usherwood. Markov, fractal, diffusion, and related models of ion channel gating. A comparison with experimental data from two ion channels. *Biophysical Journal*, 56(6):1229 – 1243, 1989.

H. Sauer and W. H. Oertel. Progressive degeneration of nigrostriatal dopamine neurons following intrastriatal terminal lesions with 6-hydroxydopamine: a combined retrograde tracing and immunocytochemical study in the rat. *Neuroscience*, 59(2):401–415, 1994.

R. Savica, W. A. Rocca, and J. E. Ahlskog. When does Parkinson disease start? *Archives of Neurology*, 67(7):798, 2010.

R. Savica, B. R. Grossardt, J. H. Bower, J. E. Ahlskog, and W. A. Rocca. Risk factors for Parkinson's disease may differ in men and women: An exploratory study. *Hormones and Behavior*, 2012.

R. J. Sayer, C. I. Turnbull, and M. J. Hubbard. Calbindin 28kDa is specifically associated with extranuclear constituents of the dense particulate fraction. *Cell and Tissue Research*, 302(2):171–180, 2000.

A. H. Schapira. Mitochondria in the aetiology and pathogenesis of Parkinson's disease. *The Lancet Neurology*, 7:97–109, 2008.

A. H. Schapira, J. M. Cooper, D. Dexter, P. Jenner, J. B. Clark, and C. D. Marsden. Mitochondrial complex I deficiency in Parkinson's disease. *The Lancet*, 333 (8649):1269, 1989.

M. L. Schmidt, J. A. Martin, V. M. Y. Lee, and J. Q. Trojanowski. Convergence of lewy bodies and neurofibrillary tangles in amygdala neurons of Alzheimer's disease and Lewy body disorders. *Acta Neuropathologica*, 91(5):475–481, 1996.

A. Schneeberger, M. Mandler, F. Mattner, and W. Schmidt. Vaccination for Parkinson's disease. *Parkinsonism & Related Disorders*, 18:S11–S13, 2012.

S. G. Schultz. *Basic principles of membrane transport.* IUPAB biophysics series. Cambridge University Press, 1980. ISBN 9780521297622.

R. C. Schwyn and C. A. Fox. The primate substantia nigra: a Golgi and electron microscopic study. *Journal fur Hirnforschung*, 15(1):95, 1974.

M. Sedova and L. A. Blatter. Dynamic regulation of $[Ca^{2+}]_i$ by plasma membrane Ca(2+)-ATPase and Na^+/Ca^{2+} exchange during capacitative Ca^{2+} entry in bovine vascular endothelial cells. *Cell Calcium*, 25:333–343, May 1999.

R. Sharon, I. Bar-Joseph, M. P. Frosch, D. M. Walsh, J. A. Hamilton, and D. J. Selkoe. The formation of highly soluble oligomers of alpha-synuclein is regulated by fatty acids and enhanced in Parkinson's disease. *Neuron*, 37: 583–595, 2003.

T. B. Sherer, J. H. Kim, R. Betarbet, and J. T. Greenamyre. Subcutaneous rotenone exposure causes highly selective dopaminergic degeneration and α-synuclein aggregation. *Experimental Neurology*, 179(1):9–16, 2003.

C. Sherrington. *The integrative action of the nervous system.* CUP Archive, 1966.

H. Shimura, N. Hattori, S. Kubo, Y. Mizuno, S. Asakawa, S. Minoshima, N. Shimizu, K. Iwai, T. Chiba, and K. Tanaka. Familial Parkinson disease gene product, parkin, is a ubiquitin-protein ligase. *Nature Genetics*, 25(3): 302–305, 2000.

J. M. Shulman, P. L. De Jager, and M. B. Feany. Parkinson's disease: genetics and pathogenesis. *Annual Review of Pathology: Mechanisms of Disease*, 6:193–222, 2011.

C. W. Shults. Lewy bodies. *Proceedings of the National Academy of Sciences*, 103: 1661–1668, 2006.

N. R. Sibson, A. Dhankhar, G. F. Mason, D. L. Rothman, K. L. Behar, and R. G. Shulman. Stoichiometric coupling of brain glucose metabolism and glutamatergic neuronal activity. *Proceedings of the National Academy of Sciences*, 95(1):316, 1998.

N. L. Silva, C. M. Pechura, and J. L. Barker. Postnatal rat nigrostriatal dopaminergic neurons exhibit five types of potassium conductances. *Journal of Neurophysiology*, 64:262–272, 1990.

N. P. Smith and E. J. Crampin. Development of models of active ion transport for whole-cell modelling: cardiac sodium-potassium pump as a case study. *Progress in Biophysics and Molecular Biology*, 85:387–405, 2004.

J. M. Souza, B. I. Giasson, Q. Chen, V. M. Lee, and H. Ischiropoulos. Dityrosine cross-linking promotes formation of stable alpha -synuclein polymers. Implication of nitrative and oxidative stress in the pathogenesis of neurodegen-

erative synucleinopathies. *Journal of Biological Chemistry*, 275:18344–18349, 2000.

M. G. Spillantini, M. L. Schmidt, V. M. Lee, J. Q. Trojanowski, R. Jakes, and M. Goedert. Alpha-synuclein in Lewy bodies. *Nature*, 388:839–840, 1997.

A. A. Starkov. The molecular identity of the mitochondrial Ca2+ sequestration system. *FEBS Journal.*, 277:3652–3663, 2010.

D. Sterratt, B. Graham, A. Gillies, and D. Willshaw. *Principles of Computational Modelling in Neuroscience*. Cambridge Univ Pr, 2011.

A. F. Strassberg and L. J. DeFelice. Limitations of the Hodgkin-Huxley formalism: Effects of single channel kinetics on transmembrane voltage dynamics. *Neural Computation*, 5(6):843–855, 1993.

S. H. Strogatz. Nonlinear dynamics and chaos: with applications to physics, biology, chemistry, and engineering (studies in nonlinearity). 2001.

D. Sulzer. Multiple hit hypotheses for dopamine neuron loss in Parkinson's disease. *Trends in Neurosciences*, 30(5):244–250, 2007.

D. Sulzer and Y. Schmitz. Parkinson's disease: return of an old prime suspect. *Neuron*, 55(1):8–10, 2007.

D. J. Surmeier. Calcium, ageing, and neuronal vulnerability in Parkinson's disease. *The Lancet Neurology*, 6(10):933–938, 2007.

D.J. Surmeier, J.N. Mercer, and C.S. Chan. Autonomous pacemakers in the basal ganglia: who needs excitatory synapses anyway? *Current Opinion in Neurobiology*, 15(3):312–318, 2005.

N. R. Swerdlow and G. F. Koob. Dopamine, schizophrenia, mania, and depression: Toward a unified hypothesis of cortico-striato-pallido-thalamic function. *Behavioral and Brain Sciences*, 10:197–245, 1987.

J. Symersky, G. Lin, S. Li, S. Qiu, M. Carson, N. Schormann, and M. Luo. Structural genomics of Caenorhabditis elegans: Crystal structure of calmodulin. *Proteins: Structure, Function, and Bioinformatics*, 53(4):947–949, 2003.

M. R. Tadross, I. E. Dick, and D. T. Yue. Mechanism of local and global Ca2+ sensing by calmodulin in complex with a Ca2+ channel. *Cell*, 133:1228–1240, 2008.

M. Takada, Y. Kang, and M. Imanishi. Immunohistochemical localization of voltage-gated calcium channels in substantia nigra dopamine neurons. *European Journal of Neuroscience*, 13(4):757–762, 2001.

H. Takahashi, E. Ohama, S. Suzuki, Y. Horikawa, A. Ishikawa, T. Morita, S. Tsuji, and F. Ikuta. Familial juvenile Parkinsonism clinical and pathologic study in a family. *Neurology*, 44(3 Part 1):437–437, 1994.

J. M. Tepper. Handbook of basal ganglia structure and function. In H. Steiner and K.Y. Tseng, editors, *Handbook of Behavioral Neuroscience*, chapter Neurophysiology of Substantia Nigra Dopamine Neurons: Modulation by GABA. Elsevier/Academic Press, 2010.

J. M. Tepper, S. F. Sawyer, and P. M. Groves. Electrophysiologically identified nigral dopaminergic neurons intracellularly labeled with HRP: light-microscopic analysis. *The Journal of Neuroscience*, 7(9):2794–2806, 1987.

J. M. Tepper, L. P. Martin, and D. R. Anderson. GABAA receptor-mediated inhibition of rat substantia nigra dopaminergic neurons by pars reticulata projection neurons. *The Journal of Neuroscience*, 15(4):3092–3103, 1995.

D. R. Thal, K. Del Tredici, and H. Braak. Neurodegeneration in normal brain aging and disease. *Science of Aging Knowledge Environment*, 2004:pe26, 2004.

B. Thomas and M. F. Beal. Parkinson's disease. *Human Molecular Genetics*, 16 Spec No. 2:R183–194, Oct 2007.

S. Tiveci, A. Akın, T. Çakır, H. Saybaşılı, and K. Ülgen. Modelling of calcium dynamics in brain energy metabolism and Alzheimer's disease. *Computational Biology and Chemistry*, 29(2):151 – 162, 2005.

G. K. Tofaris, R. Layfield, and M. G. Spillantini. α-synuclein metabolism and aggregation is linked to ubiquitin-independent degradation by the proteasome. *FEBS letters*, 509(1):22–26, 2001.

V. N. Uversky, H. J. Lee, J. Li, A. L. Fink, and S. J. Lee. Stabilization of partially folded conformation during α-synuclein oligomerization in both purified and cytosolic preparations. *Journal of Biological Chemistry*, 276(47): 43495–43498, 2001a.

V. N. Uversky, J. Li, and A. L. Fink. Evidence for a partially folded intermediate in alpha-synuclein fibril formation. *Journal of Biological Chemistry*, 276(14): 10737–10744, Apr 2001b.

A. Varghese and L. M. Boland. Computing transient gating charge movement of voltage-dependent ion channels. *Journal of Computational Neuroscience*, 12(2):123–137, 2002.

A. Varghese and G. R. Sell. A conservation principle and its effect on the formulation of Na-Ca exchanger current in cardiac cells. *Journal of Theoretical Biology*, 189(1):33–40, 1997.

A. Verkhratsky and E. C. Toescu. Calcium and neuronal ageing. *Trends in Neurosciences*, 21:2–7, 1998.

S. W. Vetter and E. Leclerc. Novel aspects of calmodulin target recognition and activation. *European Journal of Biochemistry*, 270(3):404–414, 2003.

D. Viswanath. The Lindstedt–Poincarè technique as an algorithm for computing periodic orbits. *SIAM Review*, 43(3):478–495, 2001.

C. Vives-Bauza, C. Zhou, Y. Huang, M. Cui, R. L. A. de Vries, J. Kim, J. May, M. A. Tocilescu, W. Liu, and H. S. Ko. PINK1-dependent recruitment of Parkin to mitochondria in mitophagy. *Science Signalling*, 107(1):378, 2010.

M. J. Volles and P. T. Lansbury. Zeroing in on the pathogenic form of alpha-synuclein and its mechanism of neurotoxicity in Parkinson's disease. *Biochemistry*, 42(26):7871–7878, 2003.

K. Wakabayashi, K. Tanji, F. Mori, and H. Takahashi. The Lewy body in Parkinson's disease: Molecules implicated in the formation and degradation of α-synuclein aggregates. *Neuropathology*, 27(5):494–506, 2007.

E. Walter and L. Pronzato. *Identification of Parametric Models from Experimental Data*. Springer, 1997.

R. H. Wasserman, R. A. Corradino, and A. N. Taylor. Vitamin D-dependent calcium-binding protein. *Journal of Biological Chemistry*, 243(14):3978–3986, 1968.

A. Weihofen, K. J. Thomas, B. L. Ostaszewski, M. R. Cookson, and D. J. Selkoe. PINK1 forms a multiprotein complex with Miro and Milton, linking PINK1 function to mitochondrial trafficking. *Biochemistry*, 48(9):2045–2052, 2009.

K. Welch and J. Yuan. Alpha-synuclein oligomerization: a role for lipids? *Trends in Neurosciences*, 26:517–519, 2003.

P. Wellstead and M. Cloutier. An energy systems approach to Parkinson's disease. *Wiley Interdisciplinary Reviews. Systems Biology and Medicine*, 3:1–6, 2011.

P. Wellstead and M. Cloutier. Modelling and simulation of brain energy metabolism: Energy and Parkinson's disease. In P. Wellstead and M. Cloutier, editors, *Systems Biology of Parkinson's Disease*, pages 19–38. Springer New York, 2012. ISBN 978-1-4614-3411-5.

J. L. Werth and S. A. Thayer. Mitochondria buffer physiological calcium loads in cultured rat dorsal root ganglion neurons. *The Journal of Neuroscience*, 14 (1):348–356, 1994.

P. S. Whitton. Inflammation as a causative factor in the aetiology of Parkinson's disease. *British Journal of Pharmacology*, 150(8):963–976, 2009.

A. R. Willms, D. J. Baro, R. M. Harris-Warrick, and J. Guckenheimer. An improved parameter estimation method for Hodgkin-Huxley models. *Journal of Computational Neuroscience*, 6(2):145–168, 1999.

C. J. Wilson and J. C. Callaway. Coupled Oscillator Model of the Dopaminergic Neuron of the Substantia Nigra. *Journal of Neurophysiology*, 83(5):3084–3100, 2000.

D. E. Wingrove and T. E. Gunter. Kinetics of mitochondrial calcium transport.II. A kinetic description of the sodium-dependent calcium efflux mechanism of liver mitochondria and inhibition by ruthenium red and by tetraphenylphosphonium. *Journal of Biological Chemistry*, 261(32):15166–15171, 1986.

K. Wirdefeldt, H. O. Adami, P. Cole, D. Trichopoulos, and J. Mandel. Epidemiology and etiology of Parkinson's disease: a review of the evidence. *European Journal of Epidemiology*, 26:1–58, 2011.

J. A. Wolff, L. J. Fisher, L. Xu, H. A. Jinnah, P. J. Langlais, P. M. Iuvone, K. L. O'Malley, M. B. Rosenberg, S. Shimohama, and T. Friedmann. Grafting fibroblasts genetically modified to produce L-dopa in a rat model of Parkinson disease. *Proceedings of the National Academy of Sciences*, 86(22):9011–9014, 1989.

Inc. Wolfram Research. *Mathematica*. Wolfram Research, Inc., version 7.0 edition, 2008.

Z. K. Wszolek, R. F. Pfeiffer, Y. Tsuboi, R. J. Uitti, R. D. McComb, A. J. Stoessl, A. J. Strongosky, A. Zimprich, B. Müller-Myhsok, and M. J. Farrer. Autosomal dominant Parkinsonism associated with variable synuclein and tau pathology. *Neurology*, 62(9):1619–1622, 2004.

F. Wu, E. Y. Zhang, J. Zhang, R. J. Bache, and D. A. Beard. Phosphate metabolite concentrations and ATP hydrolysis potential in normal and ischaemic hearts. *The Journal of Physiology*, 586(17):4193–4208, 2008. doi: 10.1113/jphysiol.2008.154732.

F. Wuytack, L. Raeymaekers, and L. Missiaen. Molecular physiology of the SERCA and SPCA pumps. *Cell Calcium*, 32, 2002.

X. M. Xia, B. Fakler, A. Rivard, G. Wayman, T. Johnson-Pais, J. E. Keen, T. Ishii, B. Hirschberg, C. T. Bond, S. Lutsenko, J. Maylie, and J. P. Adelman. Mechanism of calcium gating in small-conductance calcium-activated potassium channels. *Nature*, 395:503–507, 1998.

W. Xu and D. Lipscombe. Neuronal cav1. 3α1 L-type channels activate at relatively hyperpolarized membrane potentials and are incompletely inhibited by dihydropyridines. *The Journal of Neuroscience*, 21(16):5944–5951, 2001.

T. Yamada, P. L. McGeer, K. G. Baimbridge, and E. G. McGeer. Relative sparing in Parkinson's disease of substantia nigra dopamine neurons containing calbindin-D28K. *Brain Research*, 526:303–307, 1990.

Y. Yang, S. Gehrke, Y. Imai, Z. Huang, Y. Ouyang, J. W. Wang, L. Yang, M. F. Beal, H. Vogel, and B. Lu. Mitochondrial pathology and muscle and dopaminergic neuron degeneration caused by inactivation of drosophila PINK1 is rescued by Parkin. *Proceedings of the National Academy of Sciences*, 103(28):10793–10798, 2006.

S. Yu, X. Li, G. Liu, J. Han, C. Zhang, Y. Li, S. Xu, C. Liu, Y. Gao, and H. Yang. Extensive nuclear localization of α-synuclein in normal rat brain neurons revealed by a novel monoclonal antibody. *Neuroscience*, 145(2):539–555, 2007.

M. Zhang, T. Tanaka, and M. Ikura. Calcium-induced conformational transition revealed by the solution structure of apo calmodulin. *Nature Structural & Molecular Biology*, 2(9):758–767, 1995.

W. Zhou, M. S. Hurlbert, J. Schaack, K. N. Prasad, and C. R. Freed. Overexpression of human α-synuclein causes dopamine neuron death in rat primary culture and immortalized mesencephalon-derived cells. *Brain Research*, 866 (1):33–43, 2000.

W. Zhou, M. Zhu, M. A. Wilson, G. A. Petsko, and A. L. Fink. The oxidation state of DJ-1 regulates its chaperone activity toward α-synuclein. *Journal of Molecular Biology*, 356(4):1036–1048, 2006.

W. Zhou, C. Long, A. L. Fink, and V. N. Uversky. Calbindin-D 28K acts as a calcium-dependent chaperone suppressing α-synuclein fibrillation *in vitro*. *Central European Journal of Biology*, 5(1):11–20, 2010.

A. Zimprich, S. Biskup, P. Leitner, P. Lichtner, M. Farrer, S. Lincoln, J. Kachergus, M. Hulihan, R. J. Uitti, and D. B. Calne. Mutations in *LRRK2* cause autosomal-dominant Parkinsonism with pleomorphic pathology. *Neuron*, 44 (4):601–607, 2004.

A. Zou, Z. Lin, M. Humble, C. D. Creech, P. K. Wagoner, D. Krafte, T. J. Jegla, and A. D. Wickenden. Distribution and functional properties of human KCNH8 (Elk1) potassium channels. *American Journal of Physiology - Cell Physiology*, 285(6):C1356–1366, 2003.